RESPONSE OF WELL FOUNDATIONS UNDER HORIZONTAL LOADS

A THESIS
submitted in fulfilment
of the requirements for the award of the Degree
of
DOCTOR OF PHILOSOPHY

by

SATISH CHANDRA SHARDA

SCHOOL OF RESEARCH AND TRAINING
IN EARTHQUAKE ENGINEERING
UNIVERSITY OF ROORKEE
ROORKEE, INDIA

SEPTEMBER, 1975

DEDICATED

TO

My Parents

Shri V I J E Y   K A R A N   S A R D A
                    Chartered Engineer

and

Smt B I M L A   D E V I   S A R D A

Certificate

Certified that the thesis entitled, *"Response of Well Foundations under Horizontal Loads,"* which is being submitted by Shri **SATISH CHANDRA SHARDA** in fulfilment of the requirements for the award of the degree of **DOCTOR OF PHILOSOPHY** in Earthquake Engineering of the University of Roorkee is a record of the student's own work carried out by him under our supervision and guidance. The matter embodied in this thesis has not been submitted for the award of any other degree or diploma.

This is to further certify that he has worked for a total period of 45 months, during October, 1970 to September, 1975, for preparing this thesis.

(Shamsher Prakash)
Professor of Civil Engineering
University of Roorkee
Roorkee

Dated September 24, 1975

(Anand Swarup Arya)
Professor and Head
School of Research and Training
in Earthquake Engineering
University of Roorkee
Roorkee

S Y N O P S I S

Well foundations of bridges are subjected to vertical
forces due to dead load of structure, live load of vehicles,
buoyancy pressures and vertical inertial forces due to earth-
quakes. They are subjected to horizontal forces caused by
action of vehicles, contraction or expansion effects of super-
structures and forces caused by water, wind, soils and earth-
quakes. Due to the combined action of these loads a well
undergoes rotation relative to the surrounding soil. The action
is resisted by normal and frictional reactive forces of the soil
acting on the side faces and the base of the well. The design
problem in well foundations subjected to the combined loads and
moments is to work out its safe depth of embedment in soil so
as to limit the horizontal and vertical movement at the bearing
level within safe range and provide adequate factor of safety
against failure.

A review of literature shows that the current method of
solving the well problem are based on Terzaghi's (1943) elastic
and plastic approaches to the analysis of rigid bulkheads and
on inference drawn from some model studies. None of the solutions,
however, takes into account the non-linear behaviour of the
soil. Frictional forces on sides and base are also not accounted
for in an adequate manner.

In this thesis, a theory has been developed for analy-
sing the lateral resistance of well foundations which takes
into account, the non-linear pressure versus displacement

characteristics of the soil on the sides as well as the base. The partial or full mobilisation of frictional force on the soil-well contact is also considered. The soil pressure at any depth z_1 below the general ground (scour) level is taken as follows:

$$p = m_h \, z_1^{\,n} \, y^r$$

where p is the soil pressure, m_h a non-linear coefficient of horizontal subgrade reaction and y the lateral displacement. The indices n and r are to be determined by tests. For non-cohesive soils $n = 1$.

To substantiate the theory, static lateral load tests were performed on small scale models of square wells embedded in dense sand. The following variables have been studied in the model tests.

i) Size of well model, 15 cm and 20 cm side

ii) Vertical load from zero to a value sufficient to over-come frictional resistance on side faces

iii) Depth of embedment

iv) Position and magnitude of lateral load

v) Friction coefficient on faces

vi) Stiffness of subgrade at base

vii) Sloping surcharge due to scour pit around the well

Pressure distribution and frictional force on faces and base were obtained with specially designed earth pressure cells and friction cells respectively. The extent of soil disturbed at ground level under failure condition of well has also been observed.

The tests have given the average values of m_h as .0674 to .0624 in kg. cm units and values of r as 0.55 to 0.65 for the dry sand having a density of 1.658 g/cm³.

The observed results have been compared with the theoretical values using these values of m_h and r and are found to have very good agreement with each other.

Dynamic behaviour of wells has also been studied by free vibration tests and cyclic lateral load tests on these models.

Besides the small scale laboratory models tested in prepared beds stated above, a field model of reinforced concrete, 1.5m x 1.5m in plan and 2.25m depth, was sunk in natural soil deposit and tested under the combined action of vertical and horizontal loads. Larger size cells were fitted on the sides and base for observing earth pressures and friction of cells for observing frictional resistance. Free vibration tests were also performed. Its behaviour has been found to be similar to that of laboratory models.

The following are the main conclusions from the study:

1. Lateral load resistance of a well increases with the increase in its size and depth of embedment, with the increase in vertical load or stiffness of subgrade at base and due to inclined surcharge above deepest scour level. This resistance decreases if the coefficient of friction is reduced.

2. Under increasing lateral load, the instantaneous point of rotation of well starts at the base level at a distance more than 0.5B from the axis of well and goes on shifting upwards

and towards the axis. At sufficiently large tilts its position comes between 0.05D to .25D above the base and at a distance between 0.1B to 0.2B from the axis of well where B is the width of well and D the depth of well.

3. The non-linear theory developed for analysing the lateral load resistance is very well coroborated by the model tests and could be used for design of well foundations in non-cohesive soil deposits, provided m_h and r are determined by tests for the soil.

ACKNOWLEDGEMENT

C O N T E N T S

LIST OF TABLES

LIST OF TABLES (CONTD.)

LIST OF FIGURES

N O T A T I O N S

Symbol	Description	Units
a	Radius of Pressure Cell Diaphragm	L
b	Width of X-section of Friction Cell Cantilever	L
B	Width of Foundation in the Direction of Lateral Load	L
C_Φ	Coefficient of Elastic Non-uniform Compression	
C	Point on axis of Well at Scour Level About Which Moments are Equilibriated	
d	Depth of X-section of Friction Cell Cantilever	L
d, d_2, d_3, d_4	Displacement in Dial Gauges	L
D	Depth of Foundation Below the Maximum Scour Level to The Bottom of Well	L
D_1	Depth of Point of Rotation Below Scour Level	L
D_2	Distance of Point of Rotation Above Bottom of Well. $D_2 = D - D_1$	L
D_z	Distance of Mid-point Between Two Vertical Dial-Gauges from Base of Well	L
E	Young's Modulus	FL^{-2}
f	Bending Stress in Friction Cell Cantilever	FL^{-2}
F_1	Friction Force Due to P_1	F
F_2	Friction Force Due to P_2	F
F_3	Vertical Frictional Force on Each Side Face	F
F_4	Frictional Force on Each Side Face Above Instantaneous Point of Rotation	F
F_5	Frictional Force on each Side Face Below Instantaneous Point of Rotation	F
F_B	Frictional Force at the Base	F

H	Distance of Force Q above scour level	L
I	Moment of Inertia of X-section of Friction Cell Cantilever	L^{-4}
k_v	Modulus of Subgrade Reaction of Base	FL^{-2-r}
K_o	Coefficient of Earth-pressure at Rest	
K_p	Coefficient of Passive Pressure	
l	Length of Friction Cell Cantilever	F
l_g	Strain Gauge Length	F
L	Length of Foundation Transverse to the Lateral Load	L
M_o	Applied Moment to the Well at Scour Level Causing Tilt of Well	FL
M_{F1}	Moment Due to F_1 About C	FL
M_{F2}	Moment Due to F_2 About C	FL
M_{F3}	Moment Due to F_3 About C	FL
M_{F4}	Moment Due to F_4 About C	FL
M_{F5}	Moment Due to F_5 About C	Fl
M_{P1}	Moment Due to P_1 About C	FL
M_{P2}	Moment Due to P_2 About C	FL
M_{RB}	Moment Due to Base Reaction R_B About C	FL
m_h	Coefficient of Non-Linear Subgrade Reaction Against Faces	FL^{-2-r-n}
N_1, N_2, N_3	Numerical Quantities Representing Integrals	
n	Index for Coordinate of Depth Measured Below Scour Level	
O	Instantaneous Point of Rotation of Well	
p	Horizontal Subgrade Reaction at Any Depth (D_1-z)	FL^{-2}

p_1	Base Pressure at the Toe of the Well Base	FL^{-2}
p_2	Base Pressure at the heel of well base	FL^{-2}
p_B	Vertical Subgrade Reaction	FL^{-2}
p_{Bi}	Pressure on the Base Due to Initial Settlement	FL^{-2}
p_c	Base Pressure at the Centre of Base	FL^{-2}
p_{max}	Maximum Lateral Pressure	FL^{-2}
p_x	Pressure on Base at Any Distance x From O	FL^{-2}
P_1	Total Soil Reaction Normal To Front Face When Well Tilts	FL^{-2}
P_2	Total Soil Reaction Normal To Rear Face When Well Tilts	FL^{-2}
q	Uniform Applied Pressure on Pressure Cell	FL^{-2}
Q	Applied Horizontal Load to the Well	
Q_s	Total Vertical Skin Friction of Well	F
Q_v	Vertical Load of Super Structure and Well	F
r	Index for Lateral Displacement y	
r'	Index Defining Non-Linearity of the Subgrade at Base	
R_B	Total Vertical Reaction at the Base	F
s	Positive Odd Integer >1, in Dynamic Case	
t	Thickness of pressure Cell Diaphragm	L
T	Concentrated Load at the Cantilever end in Friction Cell	F
w	Deflection of Free end of Cantilever in Friction Cell	L

w_{max}	Maximum Deflection at the Centre of Diaphragm of Pressure Cell	L
W	Self Weight of Well	F
W_B	Applied Vertical Load From Top of Structure to Bottom of Well	F
x	Horizontal coordinate measured from O	L
x_1	Distance of Front Face from O	L
x_2	Distance of Rear Face from O	L
$\bar{x}$	Distance of O from Axis of Well	L
y	Any lateral Displacement of Well	L
z	Vertical Coordinate Measured Above or Below the Point of Rotation of Well	L
z_1	Any Depth From Ground Level	L
α	Friction Mobilization Factor at Base	
β	Positive Constant in Characteristic Curve	
γ	Density of Soil; Submerged, Saturated, Moist or Dry as the Case may be	FL^{-3}
δ	Angle of Wall Friction	
Δ	Settlement of Base at any Point	L
Δ_i	Initial Settlement of Base	L
Δ_1	Total Settlement of Front Face Under Tilted Condition	L
Δ_2	Total Settlement of Rear Face Under Tilted Condition	L
Δ_c	Total Settlement at the Centre of the Base Under Tilted Condition	L
Δ_i	Initial Settlement Due to application of W_B	L
ϵ	Strain in Pressure Cell Diaphragm	

ς Damping Factor

Φ Angle of Internal Friction of Soil

θ Tilt of Well

μ_1 Friction Coefficient on Faces

μ_2 Friction Coefficient on Base

ν Poisson's Ration

C H A P T E R 1

INTRODUCTION

1.1 GENERAL

A typical well foundation is a prismatic massive structure cast in brick or stone masonry or reinforced cement concrete. It is sunk into the ground by excavation from within its shell so that it sinks of its own weight by overcoming friction on its faces. The wells are used in varying cross-sections such as circular, octagonal, double D, or any other shape with compartments. Most of the wells in India are circular in cross-section. Rectangular and square section wells with rounded corners are also many times used. For very major bridges, double D sections are also adopted. Thus the length to width ratio of a typical well usually varies from 1 to 3. They are sunk to safe depths below the maximum scour level, the net grip below this level being 1/3 to 1/2 of the depth of maximum scour below highest flood level (Fig. 1). A study of the embedment depths shows that these usually lie between one to three times the width or diameter of the well. The strata through which wells are sunk are almost always anisotropic and non-homogeneous. It is a common practice to found wells on a firm base such as dense sand stiff clay or rock. The soil surrounding a well contributes to resisting forces required for its stability under lateral loads.

1.2 FORCES ACTING ON A WELL FOUNDATION

Forces acting on a well are shown in Fig.2. The external vertical forces at base of well are due to:

(i) Dead load of super-structure, bearings and pier

(ii) Live load of traffic over the deck

(iii) Buoyant self weight of the well foundation and

(iv) Inertial force due to vertical acceleration due to earthquakes.

The external horizontal forces are due to:

(i) Braking and tractive action of vehicles

(ii) Thrust due to bending or arching of bridge structure on account of vertical loading

(iii) Shrinkage or expansion of girders due to temperature changes

(iv) Centrifugal action due to vehicles on curved bridges

(v) Pressure of flowing water against pier and well

(vi) Wind pressure on girders

(vii) Earth pressures on wells, piers and abutments; and

(viii) Inertial force due to horizontal acceleration of earthquakes.

The external forces are resisted by soil on the sides and base of the well. Under the action of these finite forces the well will rotate as a rigid body about an instantaneous point of rotation O, giving rise to the following resisting forces.

P_1, P_2 = Resultant horizontal forces acting on the front and rear faces of the well respectively

F_1, F_2 = Vertical frictional forces on front and rear faces of the well respectively

F_3 = Vertical frictional force on each side face

F_4, F_5 = Horizontal frictional forces on each side face above, and below the point of rotation respectively

R_B = Normal reaction force at the base and

F_B = Frictional force at the base.

The determination of the various resisting forces constitutes the problem of analysis of well foundations.

1.3 STATEMENT OF THE PROBLEM

The problem of well foundation usually emerges in the following two ways:

(i) The Problem of Design

The vertical and lateral loads are known, and the level of the top of well cap is fixed from other considerations. The problem is to determine the cross-section and embedment depth of the well with a suitable factor of safety for the particular soil conditions so that the movements of the pier at the bearing level would be within tolerable limits in both horizontal and vertical directions. In the finalisation of the cross-section of the well, some of the considerations are length of piers in cross-section, size and type of bucket used for excavation, etc. besides strength of masonry or concrete used in the shell and the bearing capacity of soil. The grip is usually determined from lateral load considerations.

(ii) The Problem of Analysis

If the size of well foundation, its embedment depth, the vertical load and the soil conditions are known and the permissible movement of the pier in vertical and horizontal direction is specified the problem is to determine the safe horizontal load the foundation can sustain under the specified

conditions.

1.4 AVAILABLE METHODS OF ANALYSIS

The wells are designed first for safety against scour by providing a minimum grip length below the maximum depth of scour on the basis of thumb rules (Indian Railways, 1941, 1963; Indian Roads Congress, 1937, 1956, 1958, 1971). Then the stability is checked against horizontal loads by using one of the available methods of elastic or plastic analysis.

The Indian Railways and the Indian Roads Congress have related the grip length, D, below the maximum scour level to the maximum depth of scour H_s, below the high flood level (Fig.2). The minimum ratio of D/H_s is specified as 1/2 by the Indian Railways and 1/3 by the Indian Roads Congress. This procedure though arbitrary is suitable against scour but, since it does not relate the grip length to soil properties, it may give over-safe or inadequate grip lengths in various soil conditions in the field so far as lateral loads are concerned.

At present the following two rational approaches are commonly used for analysing well foundations under lateral loads. (Indian Roads Congress, 1971).

1. The elastic or linear subgrade modulus approach.
2. The plastic or ultimate failure approach.

The elastic approach is based on Pender's (1947) work on well foundation and Terzaghi's (1943) analysis of rigid bulkheads under lateral loads by the concept of modulus of subgrade reaction. Analytical attempts by Banerjee and Gangopadhyay (1960)

and Ray (1967) belong to this catagory. The short-comings of the elastic approach as used hitherto are the following:

(i) The pressures are considered proportional to displacements and the subgrade modulus is taken varying linearly with depth. In actual behaviour the soils have a non-linear pressure displacement relationship and the modulus of horizontal subgrade reaction may be non-linear with depth. At the base also the pressures vary non-linearly with settlements (Terzaghi 1955). The assumptions of the elastic methods are likely to give oversafe designs in lower ranges of lateral loads and unsafe design in higher ranges of lateral loads.

(ii) Frictional forces on the side faces are not considered in the analyses in a satisfactory manner.

(iii) Safety of well foundation is considered only with respect to horizontal displacements while vertical settlements may be quite important due to eccentricity of heavy vertical loading during tilt resulting in further horizontal displacements at the bearing level.

In the plastic approach the well problem is treated in a similar manner as for lateral load capacity of rigid bulkheads proposed by Terzaghi (1943). Analysis of well foundation by Chowdhary (1967), Sankaran and Muthukrishniah (1969) and Kapoor (1971) fall in this catagory. The main limitation to the plastic approach is that when a conventional factor of safety of 2 or 3 is applied to the ultimate load as calculated by the method, it is not known whether the deformations associated with the working

load arrived at in this manner will be safe or unsafe in regard to the permissible displacements at the bridge bearing level. For proper use of this analysis, considerable judgment in choosing a factor of safety will, therefore, be required.

Thus it is seen that the two theories give the resistance or strength of well foundation under lateral loads at the two ends of the total load-deformation curve, one dealing with the initial stage and the other with the ultimate stage. The transition between the two is missing and can only be provided by a non-linear theory considering the curvi-linear behaviour of soil. The development of frictional forces with the gradually increasing tilt of well foundation under increasing lateral load adds another dimension to the analysis and must be considered for a realistic solution.

1.5 MODEL STUDIES

Model studies to observe behaviour of wells under lateral loads have been made by several authors. Model studies reported by Roscoe (1957), Ninan and Murthy (1964), Bhagat (1967), Muthukrishniah and Ninan (1968) and Sankaran and muthukrishniah (1969) and and Katti et al (1972) are of a restricted nature and throw some light on behaviour of models in a limited way. Kapoor's (1971) model studies, provide information about distribution of soil pressure on faces and base in dense, medium and loose sands. His studies give some idea about the effect of shape and size of models also. These, however, need confirmation in field.

Model tests have been mostly designed for ultimate loads and not much attention has been paid to study the behaviour

in the range of tilts and lateral loads which are smaller than the ultimate condition. Further no effort has been made to observe friction on the faces, sides and base of the wells. Dynamic tests on models have not been performed. Certain important conditions usually encountered in the field and which may be of considerable importance in adding to the stability, e.g. the effect of stiffness of the base such as provided by a rocky subgrade or a stiff clay, has not been studied. The effect of shape of scour pit around a well (Arya and Sharda, 1973) had also not been studied in the earlier models.

1.6 OBJECT AND SCOPE OF STUDY

The objects of this study are as follows:

(i) To observe the behaviour of well foundations by model tests at various stages of both vertical and horizontal loading. The relevent characteristics of the soil for use in a non-linear analytical solution, have also been determined from these tests.

(ii) To develop an analysis of well foundation, subjected to combined vertical and lateral load, which would take into account the non-linear pressure vs displacement relationship of the soil surrounding it, the non-linearity of coefficient of horizontal subgrade reaction with depth and also the effect of friction on the faces, so that the tilt of well could be estimated rationally under the action of lateral loads larger than the elastic stage of the well.

(iii) To verify the analysis. The main variables in the well foundation problem are the soil surrounding the well on its sides and base, size of cross-section of well in relation to its depth of embedment, the magnitude of vertical load and the magnitude and point of application of the net lateral load.

The soil surrounding a field well may be different on sides as well as below the base. For example, the subgrade at the base consists of clayey soil and the soil surrounding the sides may be sandy or vice-versa, or, the well may rest on a rigid subgrade such as a rock and the surrounding soil may be sandy or clayey. Thus innumerable combinations of soil on sides and base and varying strata on the sides themselves may occur. The total work is too-large for one thesis. Therefore, the study has been restricted here to wells surrounded by only one type of soil, which has been taken as non-cohesive and the work is mainly confined to dense sand for ease of achieving reproducible beds in the laboratory.

Two sizes of well models, 15 cm square section and 20 cm square section have been used in this study, the sizes were mainly determined by the consideration of testing facilities.

In order to study the effect of embedment in relation to size of well, two values of the ratio D/B were chosen as 1.5 and 2.0, which practically cover the majority of wells in the field.

For studying the effect of vertical loads on the behaviour of well foundation models subjected to the action of varying

lateral loading, the vertical load was varied from zero to about one-third of the ultimate vertical load capacity of the well. For 15 cm x 15 cm well, this load was about 131 kg. Other loads considered were 101 kg and 51 kg.

In the lateral load tests, the lateral load was increased from zero to the stage when the tilts became sufficiently large to over come friction on the sides and sufficient non-linearity developed in the pressures on the sides.

The point of application of lateral load above the scour level was changed from 0.5 to 2.0 times, the depth of embedment of model. The ratios often occur in the field in various bridges and may also occur in the same bridge depending upon the different conditions of scour in the river bed.

Effect of low and high friction on sides has also been studied for both sizes of models. Change in friction on sides may be caused in field wells due to soil conditions or loosening of soil around the well during construction.

The observations in the model tests include soil pressures through pressure cells on front and rear faces and the base of well, lateral and vertical displacements through dial gauges and friction on the sides and base through friction cells.

In addition to the above, the effects of some important aspects, which have not been studied earlier, such as, the effect of a comparatively stiffer subgrade below a well foundation with sand surrounding the well on its sides, and the effect of shape of scour pit around the well, on the lateral load capacity also

have been investigated to a small extent.

Some tests have also been performed to study the size of the extent of failure surface at the ground level when the lateral load has been increased right upto the ultimate stage.

Dynamic behaviour of well models has also been studied under free vibration, cyclic loading and repetitive lateral loads.

A single reinforced concrete field model of 1.5m square section embedded 2.25 m deep in the local silty sand ground, has also been tested to study its behaviour under the combined action of vertical and lateral loads. Pressure distribution on front and rear faces, and base have been studied for comparison with laboratory models. Attempt has also been made to study friction on faces and base of this field model. Dynamic behaviour of this model has been studied through free vibration tests.

CHAPTER 2

REVIEW OF LITERATURE

A review of literature pertaining to well foundation is given in this chapter. The subject matter has been generally arranged in chronological order.

Until almost the fourth decade of this century, the part played by the surrounding soil in the stability of well foundations was not recognised. Well foundations were simply massive prismatic bodies that were comparatively easy to construct under difficult soil conditions and could take heavy vertical loads when founded on a firm strata below a river bed. It was believed that the weight of foundation and base friction will be sufficient to counteract any lateral load also. Disastrous effects of scour which undermined well foundations during floods pointed to the fact that wells must be taken to sufficient depth below scour level, for safety during high floods. Friction during sinking was thought to be one of the major hurdles in well construction and every possible idea including a conical well foundation (Chambers 1945) was brought into practice for reducing or avoiding skin friction.

Gales (1917), suggested use of fixed grip lengths for well foundations in sandy soils for railway bridges. His recommendations based on observations of scour levels in rivers, suggested use of 15.25 m (50 ft) deep foundation for a discharge of 0.12 to 0.36 lac cumecs (2.5 to 7.5 lac cusecs),

16.75m (55 ft) for 0.36 to 0.72 lac cumecs (7.5 to   lac
cusecs) and 19.8 m (65 ft) for 0.72 to 0.97 lac cumecs (15 to
20 lac cusecs).

Lacey (1929) with his formula for the scour depth
below highest flood level (H.F.L.) brought rationality to the
grip length calculations as far as safety against scour was
concerned.

Graphs correlating grip length with highest known
flood level and deepest ascertainable scour was later proposed
by Spring.

Indian Railway code (1941) included Spring's recommen-
dations for grip length. Passive resistance offered by soil
against lateral load was excluded from designs. However,
Indian Railways Code (1963) made a provision of embedment
depth equal to 1/2 the maximum scour depth below H.F.L. This
code allowed discrete use of contribution towards resistance
offered to lateral forces by surrounding soil in a well founda-
tion. Indian Roads Congress (1971) made a provision of embed-
ment depth equal to 1/3 of the scour depth below HFL. It also
provided for the restricted use of resistance offered by soil
under conditions of laterally loaded well foundation.

Terzaghi (1943) suggested an ultimate bearing capacity
formula for pier foundations under vertical loads which included
the effects of skin friction and embedment. He recommended the
use of full value of mobilization of friction on vertical faces
because the pier could not sink into the ground before the

skin friction is fully effective. Terzaghi (1943) also suggested the use of his analysis for rigid bulkhead under lateral loads for analysing cable tower foundation blocks under lateral loads. He neglected the contribution of side friction on faces parallel to the plane of tilt as they would err on safe side. For a better approximation of the lateral load capacity, be advised inclusion of the base reaction and friction in calculations. Terzaghi's methods of designing of rigid bulkheads formed the basis of analysis of well foundations by many authors as reported later.

Pender (1947) probably was the first to analyse well foundations under lateral loads in detail. His idea was to obtain a suitable grip length of a well in sandy soil theoretically by including soil support in the formulation. He emphasized that the theoretical treatment of a heavy, rigid and large foundation must be different from those of light narrow and sometimes flexible posts or piles as given by Stobie (1930), Wolf (1933).

In his analysis Pender assumed the sandy soil around the well to behave as linear springs whose stiffness increased in a straight line manner with depth. The analysis was attempted with two possible types of deformations. In the first, a well was supposed to be a smooth and weightless body which always rotated about an axis above its base. The applied lateral forces and moments were balanced by horizontal subgrade reaction on front face and back face only. No base resistance was taken in this case. In the second case the well was considered as

heavy and rotating about the centroidal axis of the base. The lateral loads were resisted by base friction and the front face reaction. Simple equations based on statical equilibrium of forces and moments were solved with soil modulus obtained in terms of Rankine's passive and active earth pressure coefficients by using the concept of impending plastic condition at surface. Grip length was calculated by trial and error with different point of rotations to satisfy the three equations. In case of weightless piers point of rotation was obtained as 0.667 times the embedment depth (D) below the ground level with respect to lateral loads equilibrium conditions and as 0.75 D in moment equilibrium condition. He argued that resisting moment due to friction on front face should not be considered as it was likely to mobilize at larger tilts and by that time the well would rest on its sides. He suggested the friction on front face to be used in case of heavy wells. He pointed out that if design was done purely on base pressure eccentricity considerations, without accepting resistance offered by side pressures due to rotation, the edge pressures would always be very high.

As a corollary to the two cases above, Pender showed that the embedment depth might be reduced by 15% and 25% in case of lightand heavy wells respectively if the soil against the front face was allowed to go plastic to a certain depth of embedment. He was in favour of ignoring contribution of friction offered by faces parallel to the plane of tilt since length of a pier in cross-section was much larger than the

width and offered very large resistance compared with that offered by friction on sides.

Roscoe (1957) proposed a design for pier type foundations in sands, based on plastic theory. Frictional forces on front and rear faces were assumed to be acting in upward direction. Roscoe justified this on the basis of the fact that piers settle downwards. Several simplifying assumptions were made to solve the static equilibrium equations. Coefficient of passive earth pressures were taken to be same for front and rear faces. Tests on free piers 91.5 cm (3 ft) deep and 48 cm (16.5 inch) diameter showed that centres of rotation of all piers except one moved considerably during initial loading but remained steady after the peak moment had been achieved. In all cases they were above those expected from theory. Tests on 5.08 cm (2") square and 5.08 cm (2") diameter piers with 15.25 cm (6") and 22.8 cm (9") depths in sands showed that the round pier withstood moment of 0.93 and 0.91 times the capacity of square pier in the two cases of depths respectively. He also suggested an approximate method for obtaining ultimate capacities in soils having cohesion. He has reported failure surface obtained in his large model tests.

Lazard (1957) carried out tests on piers of 91.5 cm (3 ft) to 274.5 cm (9 ft) deep for an assessment of overturning moments in the limiting case. He concluded that at the limit stage the phenomenon is essentially of passive earth pressure and therefore formulae should take into account, configuration

of the ground, the direction of pull and in general all other factors which are likely to increase or decrease the passive earth-pressure.

Banerjee and Gangopadhyay (1960) derived equations for obtaining lateral load capacity of wells in sandy soils. Pender's concept about well foundation and the concept of modulus of subgrade reaction in the designing of bulkheads as given by Terzaghin (1943) was used. Their equations of equilibrium include friction on front and rear faces. It was assumed that horizontal subgrade reaction varied linearly with displacement and the modulus of subgrade reaction increased linearly with depth. Coulomb's coefficients of earth pressures were considered in solution to the problem. The equations could give maximum permissible lateral load by applying a suitable factor of safety for a permissible tilt at scour level provided that the size and depth of embedment of well, the vertical loads and the points of application of vertical and lateral loads were known. The properties of soil required for solution were angle of internal friction, angle of wall friction, Coulomb's earth pressure coefficients, density of soil and the ratio of the modulus of horizontal subgrade reaction to vertical subgrade reaction. The base pressures could be checked by the equations of equilibrium due to vertical forces and moments at the base by considering sinking in the initial stages. The authors suggested the use of modulii of subgrade reactions given by Terzaghi (1955) or to obtain them from direct field tests if possible.

Ninan and Murthy (1964), Ray (1967) and Murthy and Kapoor (1969), also preferred the two dimensional approach by Banerjee and Gangopadhyay with minor modicications. Ninan and Murthy proposed that side face friction with earth pressure at-rest acting on side faces should also be considered along-with other forces. Ray applied the approach to circular wells and rectangular wells suggesting use of Rankine's coefficients. Murthy and Kapoor proposed a simplification in the pressure distribution diagram from parabolic to trapezoidal for ease in calculations. Indian Roads Congress (1971) have also adopted this approach for checking the stability and base pressures of well foundations in sands under lateral loads.

This approach has been termed as elastic or subgrade reaction approach to the problem of stability of well founda-tion, subjected to lateral loads, since the soil is assumed to behave as linear elastic springs, throughout the course of well movement.

Balwant Rao and Muthuswamy (1963), Chowdhary (1967) and Sankaran and Muthukrishniah (1969),however,preferred to apply the ultimate load approach suggested by Terzaghi (1943) for rigid bulkheads and pole foundations. In this case total passive pressure is mobilized to a large depth on the front face and the passive pressure diagram assumes a simplified triangular shape. For obtaining the working load the ultimate lateral load is divided by a suitable factor of safety. The equations of equilibrium in this condition can be solved by

direct use of earth pressure coefficients and the grip length could be worked out.

Since this approach to the problem was applicable for bulkheads and was two-dimensional in nature, Chowdhary (1967) suggested that friction on sides and base and the base pressures should be included in the formulation of equations. Sankaran and Muthukrishniah (1969) proposed a formulation of problem by considering side friction and three dimensional nature of the problem based on a certain hypothesis regarding tilt at failure observed in model tests. According to them, the well always failed at about 3° tilt in the sand used for testing.

Menard (1963) suggested a pressure distribution which was trapezoidal in form showing some pressure value at the scour level unlike that by Terzaghi who considered the reaction at the scour/to be zero. Menard proposed the use of a non-linear relation between subgrade reaction and displacement which could be obtained in-situ by a special device known as Pressiometer.

Verma (1966) favoured Menard's approach to the well problem. However he felt that the results obtained by a "pressiometer" device should be correlated with the more common standard penetration values since standard penetration tests are quite popular. He has proposed the design procedure for wells using Standard Penetration values.

The various approaches which utilize the concept
of ultimate failure of soil surrounding the well are known
as the ultimate resistance approach for the well foundation
problem.

Many issues of major importance however needed clari-
fication before the elastic or the ultimate approach could be
accepted in practice. The main issues were regarding the
true behaviour of foundation under lateral load and the problem
of evaluation of data, especially on soil, required in the
computation of lateral load capacity by different approaches.
Experimental studies of the problem were therefore resorted
to by various investigators for clarifying these issues.

Laboratory model tests in sands were taken up by many
authors,(Ninan and Murthy 1964), Muthukrishniah and Ninan (1968),
Bhagat (1967), Sankaran and Muthukrishniah (1969), Katti et al
(1972),for investigating various aspects involved in the stabi-
lity of well foundation.

All have observed that (a) there is an axis of rotation,
about which the well rotates in the final stages of failure.
This axis always lies at a distance of 0.2 to 0.3 times the
depth of well above its base. The axis of rotation was observed
by Ninan and Murthy (1964), to be starting from centroidal axis
of the base and gradually shifting upwards as the base friction
is overcome. No translation of wells during tilt was observed
by them.

From experiments on uninstrumented models in sand they have also observed that (a) lateral load to deflection relation was a non-linear curve, (b) larger base width provided larger lateral resistance, (c) larger vertical loads increased lateral load capacity, and (d) under similar conditions of embedment and loading circular wells offered smaller lateral resistance than rectangular wells of length equal to diameter of circular wells.

Muthukrishniah and Ninan (1968) observed in their two-dimensional model test setup that the failure surface in sandy soil at ultimate condition was of a typical shape consisting of a pear shaped surface at the base, passive failure surface, at an angle of $(45 - \Phi/2)$ with horizontal, on the front and an active zone at the rear. A similar failure shape was reported by Biarez and Capella (1961) in their study of rotation of block foundations also.

Bhagat (1967), using instrumented models in saturated sands, observed that the pressure distribution on front face had resemblance to a parabola. The failure surface observed by the author resembled those obtained by Roscoe (1957) in field tests on pier models. This was different from the failure surface observed by Muthukrishniah and Ninan. Bhagat concluded from her tests that in the ultimate stage of tilt of a well, 50 % of the total moments resisted by it were due to normal pressure on the face and the remaining due to pressure at its base.

Sankaran and Muthukrishniah (1969) from their tests
on models in dense sand, in two-dimensional and three-dimensional
setups, observed that the magnitudes of coefficients of passive
earth-pressure as obtained from two-dimensional experiments
were much larger than the Rankine's values and that they were
even larger in a three-dimensional case. The magnitudes of
coefficient of passive earth-pressure were 24.7 and 16 in
three-dimensional and two-dimensional cases respectively. The
point of rotation was observed above the base for any magni-
tude of lateral load, an observation contrary to the one
reported by Murthy and Ninan (p. 19). They observed a unique
relationship between tilt and lateral load irrespective of the
vertical load, size of well and grip length and also found
that the failure always occured at 3° tilt of the axis of
well. The failure at 3° tilt was one of the assumptions made
by them in the formulation of equations treating the well
problem to be a three-dimensional one. The rupture surface
observed by them was the same as observed by Muthukrishniah
and Ninan (p. 20). They were of the opinion that the models
may not represent the true behaviour of a prototype well due
to non scaling of mobilisation of friction in sands.

Balwant Rao (1970) in his discussions on test on
model wells by Sankaran and Muthukrishniah (1969) indicated
the importance of the effect of combined vertical and lateral
loads and was of the opinion that the lateral loads applied to
cause failure in a model tests were being taken too high as
compared with vertical loads, to be of any significance in

actual well problems. Regarding the failure mechanism, he pointed out that side resistance might have little effect on base failure but base failure could accelerate side failure.

Banerjee (1970) in his discussions on model studies by Sankaran and Muthukrishniah (1969) pointed out that a 3° tilt as observed in model studies meant a large movement of the top of pier which would never be permitted for the safety of super-structure. One half degree tilt, at the most, might be permissible. The ratios of lateral load at failure to the vertical loads were too high in comparison with the ratio obtained in practice, which never exceeded 15 %. He proposed that this should be ascertained by tests whether at this ratio, there might be sliding at the base of a well foundation. It was his opinion that the behaviour of well must be studied at horizontal loads much smaller than the failure loads to find out a rational method of design.

Katti et al (1972), with the help of instrumented small scale and large scale model tests showed that (a) the pattern of distribution of pressure on base and faces for all conditions of embedment was similar, (b) the moment shared by base went on increasing with the tilt in a linear manner, (c) for the same tilt, the moment shared by the base decreased with increasing depth of embedment, and (d) the moment shared by base at failure was about 12 % for D/B ratio larger than 1.5, but was only 3.4 % for D/B ratio of 1.5. They concluded on the basis of test results that the modulus of subgrade reaction approach of Banerjee and Gangopadhyay (1960) was a

sound proposition for obtaining working lateral loads in well foundations.

On the evidence of results from experimental investigations, Indian Roads Congress (1971) have included an analysis of well foundation for ultimate loads. The equilibrium conditions assume a triangular pressure diagram of Terzaghi's bulkhead problem and base resistance along an arc of circle passing through the edges of the base. The centre of the failure arc has been assumed to lie at 0.2 times the depth of the embedment above the base on the axis of the well.

Kapoor (1971) made a study of the problem of well foundation with the help of instrumented and uninstrumented models, in dense, medium and loose sands. Embedment depths vertical loads, point of application of lateral loads, size and shape were among the parameters studied by him. He also used field models to verify the findings from the laboratory model tests. His main observations on various aspects of the behaviour of wells are as below.

(i) A large amount of tilt is required to mobilise the ultimate lateral resistance. The tilt ranges between 1 in 20 to 1 in 16 ($2^{o}52'$ and $3^{o}26'$ respectively) in circular models and 1 in 14 to 1 in 12 (4° to $4^{o}34'$ respectively) for square and rectangular models in dense to loose sands. The lateral load tilt relationship is non linear and the slopes are the same in the initial range of lateral loads for same factor of safety irrespective of shapes and relative density.

(ii) Lateral load capacity increases with increased vertical load upto a base reaction of 0.6 times the ultimate bearing capacity.

(iii) Circular wells offer lower resistance then the square or rectangular wells of same area.

(iv) Percentage of loads shared by vertical sides and base of well does not remain constant at all lateral load levels. With shallow depths base carries larger share of load and in deeper wells the passive resistance carries the major share.

(v) Loose soils resist lesser loads than the dense soils.

(vi) Point of rotation lies almost at the base upto about half the ultimate lateral load but shifts upwards with increasing load and remaining at 0.8 times the depth of well from the top, at failure loads.

(vii) Pressure distribution on front and rear faces is parabolic.

(viii) The pressure at the base is concave downwards being larger at the edges. Edge pressures increase at the toe and reduce at heel with increasing tilts, the heel looses contact with the base at higher loads.

(ix) Eccentricity of base reaction has a limiting value of B/3 for square and rectangular wells.

(x) Pressure to displacement relation is non-linear in sandy soils and the modulus of horizontal subgrade reaction

is a changing value depending upon displacement and width
of well.

(xi) Coefficients of passive and active earth
pressures are functions of angle of internal friction, magni-
tude and sign of well friction and depth to length ratio of
the well. These coefficients may vary from $2\frac{1}{2}$ times to $1\frac{1}{2}$
times the two-dimensional. Coulomb's values for dense sand
and loose sands respectively.

Kapoor has proposed three types of analysis for
lateral load stability of well foundation based on three
different approaches namely (i) Dimensional Analysis, (ii) Limit
state of equilibrium or Ultimate load analysis with respect to
ultimate failure of soil and (iii) subgrade modulus theory on
non-linear pressure to displacement relation.

In the Dimensional Analysis he reduced various varia-
bles influencing the behaviour of well foundations to non
dimensional forms using the principles of dimensional analysis
as applied to rigid poles (Kondner and Cunningham,1963).Explicit
functional relationships were established between the non-
dimensional parameters. These were used for computing safe
grip length from graphs. He concluded that properly controlled
model tests with judicious use of dimensional analysis can give
reliable solution to the well problem.

In the limit stage of equilibrium or the ultimate
load approach he assumed a triangular distribution of passive
pressure, effect of positive and negative wall friction angles

and three dimensional nature of problem with its effect on passive and active earth pressure coefficients. He used the work by Horn (1970) and Heukel et al (1965),for obtaining the values of three dimensional passive pressure coefficients.

In the subgrade modulus approach with non-linear pressure versus displacement relationship Kapoor obtained a cubic equation in terms of depth of embedment. He used a hyperbolic variation of subgrade modulus with displacement (Kondner and Zelasko, 1963) and a linear variation of the same with depth for calculating pressures on faces.Non-linearity of the subgrade below the base was not taken into account by him. He came to the conclusion that the concept of subgrade reaction should not be used indiscriminately because the pro-perties of soil and well surfaces are functions of the relative displacements.

In an analytical attempt Arya and Sharda (1973) showed that the contribution to resisting moments due to total friction on faces of a square well may be quite significant and may be of the order of 20 % of the total moments in the initial range of lateral loading. The share of moment by friction on side faces may be quite considerable. They also pointed out that neglecting the surcharge effect due to overburden of soil due to shape of scour above the maximum scour lever may err on the safe side by even 100 % in its contribution to resisting moments.

CHAPTER 3

ANALYSIS

3.1 GENERAL

The problem of well foundation under combined action of vertical and lateral loads is usually analysed by either the elastic approach or the plastic approach. The elastic approach gives a linear lateral load-deflection curve due to the soil stress-strain characteristics having been assumed linear. However observations on well models by various investigators clearly show the lateral load-deflection characteristics to be non-linear. This is because of the non-linear stress-strain behaviour of soil surrounding a well on its sides and base. This aspect of non-linear stress-strain characteristics of soil should be taken into account in any rational analytical study of the problem. The development of frictional forces with the gradually increasing tilt of well foundation adds another dimension to the analysis.

The analysis presented in this chapter has been developed to include the non-linearity of stiffness with displacement and also confinement of soil surrounding the faces. The non-linear behaviour of soil below the base is also included. For developing the expressions it was necessary to know the path traced by the instantaneous point of rotation. This has been observed by model tests and is reported in Chapter 8. Typical positions of instantaneous point of rotation for small and large tilts are shown in Fig. 3. The forces considered in the analysis are shown in Fig. 4. The analysis takes into account the frictional forces on faces and base.

3.2 ASSUMPTIONS

The following assumptions have been made in this analysis.

(1) Well is a prismatic body of uniform cross-section of width B and length L. With slight modification the analysis will be applicable to circular or double-D wells.

(2) It is embedded in a homogeneous soil mass to a depth D.

(3) The well is a rigid body as compared with its surrounding medium.

(4) Initially the well sinks vertically under the action of self weight and weight of the super-structure. Full skin friction is mobilized.

(5) Under the action of lateral forces and moments, the well executes a two-dimensional motion as a rigid body and rotates about an instantaneous point of rotation O.

(6) Soil reaction on faces at any depth $(D_1 - z)$ due to a displacement y is governed by the following non-linear relationship,

$$p = m_h (D_1 - z)^n y^r \qquad \qquad \ldots (1)$$

where p is the horizontal subgrade reaction, m_h is the coefficient of non-linear horizontal subgrade reaction and n and r are indices, defining the non-linearity. Quantities m_h, n and r are to be determined by tests.

(7) The vertical subgrade reaction due to a settlement Δ is given by a non-linear relationship

$$p_B = k_v \Delta^{r'} \qquad \qquad \ldots (2)$$

where p_B is the vertical subgrade reaction, k_v is a coefficient of non-linear vertical sub-grade reaction, r' is an index defining non-linearity. k_v and r' are to be determined by tests.

(8) Full friction is mobilized on side faces parallel to the direction of lateral load.

3.3 ANALYSIS

(a) When only the vertical load is acting on the well, the total vertical load of well and supported structure will be held in equilibrium by base reaction and skin friction on all four sides due to at rest earth-pressure varying linearly with depth. From Fig. 4, we therefore, get the equation,

$$W_B = Q_v + W = p_{Bi} \cdot B \cdot L + \mu_1 \gamma K_o (B + L) D^2 \qquad \ldots (3)$$

where,

W_B,   is the applied vertical load from top of structure to bottom of well

Q_v,   vertical load of super-structure on well

W,   self weight of the well

p_{Bi},   pressure on the base due to initial settlement

B,   width of the foundation in the direction of lateral load

L,   length of foundation transverse to the lateral load

μ_1,   friction coefficient on faces

γ,   density of soil

K_o,   coefficient of earth-pressure at rest

and D,   the depth of foundation below the maximum scour level to the bottom of well.

Whence equation 3 gives,

$$p_{Bi} = \frac{W_B - \mu_1 \Upsilon K_o \,(B+L)D^2}{B.L} \qquad ...(3a)$$

According to assumption 7

$$p_B = k_v \Delta^{r'} \qquad ...(2)$$

If initially $\Delta = \Delta_i$, where Δ_i is the initial settlement due to vertical load, then from equation 2.

$$p_{Bi} = k_v \Delta_i{}^r \qquad ... (4)$$

b) When lateral load is applied the forces as computed below will develop on the vertical faces and the base and cause moments about the point of reference C along the intersection of the axis of the well and the scour level.

Total soil reaction P_1

Refering to Fig. 4, let the instantaneous point of rotation for the well be O.

Let, z be the vertical coordinate from O,

x, the horizontal coordinate from O,

and y, the horizontal displacement from datum,

then

$$P_1 = L \int_0^{D_1} p \, dz \qquad ... (5)$$

Where, p is the horizontal soil reaction on a strip dz at any depth (D_1-z) along the length 'L' of the front face, D_1 is the depth of instantaneous point of rotation below the scour level.

Now as per assumption 6,

$$p = m_h \, (D_1 - z)^n \, y^r \qquad \qquad \dots (1)$$

Substituting the value of p from equation (1) and $y = z\theta$, where θ is tilt of well, in equation 5, we obtain,

$$P_1 = L \int_0^{D_1} m_h \, (D_1 - z)^n \, (z\theta)^r \, dz$$

$$= L \, m_h \, \theta^r \int_0^{D_1} (D_1 - z)^n \, z^r \, dz$$

or

$$P_1 = L \, m_h \, \theta^r \, D_1^{\,n} \int_0^{D_1} \left(1 - \frac{z}{D}\right)^n z^r \, dz \qquad \dots (5a)$$

The integral can be evaluated in terms of Gamma Function as below:

Let,

$$\frac{z}{D_1} = \psi$$

whence

$$z^r = D_1^{\,r} \, \psi^r$$

and

$$dz = D_1 \, d\psi$$

Also at $z = 0$, $\psi = 0$; at $z = D_1$, $\psi = 1$

Integrating we get,

$$\int_0^{D_1} z^n \left(1 - \frac{z}{D_1}\right)^r dz = \int_0^1 D_1^{\,r} \, \psi^r \, (1 - \psi)^n \, D_1 \, d\psi$$

$$= D_1^{\,r+1} \int_0^1 \psi^r \, (1 - \psi)^n \, d\psi$$

$$= D_1^{\,r+1} \, \frac{\sqrt{n+1} \, \sqrt{r+1}}{\sqrt{n+r+2}}$$

provided that, $(n+1) > 0$ and $(r+1) > 0$

Hence equation 5a takes the form,

$$P_1 = L \, m_h \theta^r D_1^{\,n+r+1} \; \frac{\sqrt{n+1} \; \sqrt{r+1}}{\sqrt{n+r+2}} \qquad \ldots (5b)$$

or

$$P_1 = L \, m_h \theta^r D_1^{\,n+r+1} \, N_1 \qquad \ldots (5c)$$

where,

$$N_1 = \frac{\sqrt{n+1} \; \sqrt{r+1}}{\sqrt{n+r+2}}$$

The force P_1 acts from right to left in Fig. 4.

Refering to Fig. 4, again, the moment M_{P1} of force P_1 about point C will be given by the equation.

$$M_{P1} = L \int_0^{D_1} p \, (D_1 - z) \, dz \qquad \ldots (6)$$

$$= L \int_0^{D_1} m_h \, (D_1 - z)^{n+1} \, (z\theta)^r \, dz$$

or

$$M_{P1} = L \, m_h \theta^r D_1^{\,n+1} \int_0^{D_1} (1 - \frac{z}{D_1})^{n+1} \, z^r \, dz \qquad \ldots (6a)$$

Integrating as in case of equation 5, using Gamma Function we get,

$$\int_0^{D_1} (1 - \frac{z}{D_1})^{n+1} \, z^r \, dz$$

$$= \int_0^1 (1 - \psi)^{n+1} \, \psi^r \, D_1^{\,r+1} \, d\psi$$

$$= D_1^{\,r+1} \; \frac{\sqrt{n+2} \; \sqrt{r+1}}{\sqrt{n+r+3}}$$

$$= D_1^{r+1} \frac{(n+1)}{(n+r+2)} \frac{\sqrt{n+1} \ \sqrt{r+1}}{\sqrt{n+r+2}}$$

$$= D_1^{r+1} \frac{(n+1)}{(n+r+2)} N_1$$

Hence

$$M_{P1} = L \ m_h \ \theta^r \ D_1^{n+r+2} \frac{(n+1)}{(n+r+2)} N_1 \qquad \qquad \text{... (6b)}$$

The moment acts in a clockwise direction with respect point C in Fig. 4.

Frictional force F_1

Frictional force F_1 acts on the front face of the well and is given by

$$F_1 = \mu_1 \ P_1 \qquad \qquad \text{... (7)}$$

The force acts upward as in Fig. 4. Its moment M_{F1} about the point C is

$$M_{F1} = \mu_1 \ P_1 \ \frac{B}{2} \qquad \qquad \text{... (8)}$$

The moment acts anticlockwise

Total soil reaction P_2

Force P_2 acts on the rear face as shown in Fig. 4.

Measuring z now below the instantaneous point of rotation O, the depth of strip dz will be (D_1+z) below scour level. Therefore,

$$P_2 = L \int_0^{D_2} p \ dz \qquad \qquad \text{... (9)}$$

$$= L \int_0^{D_2} m_h (D_1+z)^n (z\theta)^r dz$$

$$= L m_h \theta^r D_1^n \int_0^{D_2} (1+ \frac{z}{D_1})^n z^r dz \qquad \cdots (9a)$$

For evaluating the integral let

$$\frac{z}{D_1} = \psi$$

whence, $dz = D_1 d\psi$

and, for $z = 0$, $\psi = 0$; and for $z = D_2$, $\psi = D_2/D_1$

Therefore

$$P_2 = L n_h \theta^r D_1^{n+r+1} \int_0^{D_2/D_1} (1+\psi)^n \psi^r d\psi$$

let $N_2 = \int_0^{D_2/D_1} (1+\psi)^n \psi^r d\psi$

or

$$P_2 = L m_h \theta^r D_1^{n+r+1} N_2 \qquad \cdots (9b)$$

The force P_2 will act from left to right in Fig. 4. The Moment M_{P2} of the force P_2 about point C is given by,

$$M_{P2} = L \int_0^{D_2} m_h (D_1+z)^{n+1} (z\theta)^r dz \qquad \cdots (10)$$

$$= L m_h \theta^r D_1^{n+1} \int_0^{D_2} (1 + \frac{z}{D_1})^{n+1} z^r zd$$

$$= L m_h \theta^r D_1^{n+r+2} \int_0^{D_2/D_1} (1+\psi)^{n+1} \psi^r d\psi \qquad \cdots (10a)$$

or $\quad M_{P2} = L\, m_h\, \theta^r\, D_1^{n+r+2}\, N_3 \qquad\qquad \dots (10b)$

where

$$N_3 = \int_0^{D_2/D_1} (1+\psi)^{n+1}\, \psi^r\, d\psi$$

The moment M_{P2} acts anticlockwise with respect to reference point C in Fig. 4.

Frictional Force F_2

Frictional force F_2 acts on the rear face and is given by

$$F_2 = \mu_1\, P_2 \qquad\qquad \dots (11)$$

Direction F_2 will depend on the position of the instantaneous point of rotation O, whether it is to the left or to the right of the rear face

F_2 will act upward if $\bar{x}\,\theta > \dfrac{B\theta}{2}$, or, if $\bar{x} > B/2$

F_2 will act downward if $\bar{x}\,\theta < \dfrac{B\theta}{2}$, or, if $\bar{x} < B/2$

where, $\bar{x}$ is the distance of O from the axis of well.

The moment M_{F2} due to F_2 about C is

$$M_{F2} = \mu_1\, P_2 \cdot \frac{B}{2} \qquad\qquad \dots (12)$$

and will act anticlockwise if $\bar{x} > B/2$ and clockwise if $\bar{x} < B/2$ (Fig.4).

Effect of active pressure on face 1 is neglected

Frictional force F_3

Assuming that earth-pressure varies linearly with depth the vertical frictional force F_3 in Fig.4 on face 3, is given by

$$F_3 = \frac{1}{2} \mu_1 K_o \gamma BD^2 \qquad \qquad \dots (13)$$

It acts in the upward direction and its moment M_{F3} about C is zero.

Frictional Force F_4

F_4 acts in a horizontal direction on side face 3 and is given by

$$F_4 = \frac{1}{2} \mu_1 K_o \gamma BD^2 \qquad \qquad \dots (14)$$

and it acts from right to left in Fig. 4a. The moment M_{F4} due to F_4 about C is

$$M_{F4} = \frac{1}{2} \mu_1 K_o \gamma BD_1^2 \cdot \frac{2}{3} D_1$$

or

$$M_{F4} = \frac{1}{3} \mu_1 K_o \gamma BD_1^3 \qquad \qquad \dots (15)$$

The moment will act clockwise with respect to C.

Frictional Force F_5

F_5 acts in a horizontal direction on side face 3, below O and is given by

$$F_5 = \frac{1}{2} \mu_1 B K_o \gamma (D^2 - D_1^2) \qquad \qquad \dots (16)$$

The moment M_{F5} due to F_5 about C is

$$M_{F5} = \frac{1}{2} \mu_1 BK_o \gamma D^2 \cdot \frac{2}{3} D - \frac{1}{2} \mu_1 BK_o \gamma D_1^2 \cdot \frac{2}{3} D_1$$

$$= \frac{1}{3} \mu BK_o \gamma (D^3 - D_1^3) \qquad \qquad \dots (17)$$

The moment will be anticlockwise in Fig.4a.

Total base reaction R_B
_____

Force R_B acts normal to the base as shown in Fig.4.

The total vertical settlement Δ of any point on the base will be given by

$$\Delta = \Delta_i + x\theta$$

where, Δ_i is the total initial settlement and $x\theta$ is the additional settlement of a point at a distance x from O.

Refering to assumption 7, the pressure p_x at the point due to the total settlement Δ will be

$$p_x = k_v (\Delta_i + x\theta)^{r'} \qquad \qquad \dots (18)$$

The total reaction R_B at the base due to total settlement Δ will be

$$R_B = L \int_{x_2}^{x_1} p_x \, dx$$

or

$$R_B = L \, k_v \int_{x_2}^{x_1} (\Delta_i + x\theta)^{r'} \, dx \qquad \dots (19)$$

The settlements at the centre and two ends of the base are:

$$\Delta_c = \Delta_i + \overline{x}\theta , \quad \text{at the centre distance } \overline{x} \text{ from O}$$

$$\Delta_1 = \Delta_i + x_1\theta , \quad \text{at the toe distance } x_1 \text{ from O}$$

and

$$\Delta_2 = \Delta_i + x_2\theta , \quad \text{at the heel distance } x_2 \text{ from O}$$

where $\quad x_1 = \overline{x}\theta + B/2 \quad$ and $\quad x_2 = (\overline{x}\theta - \frac{B}{2})$

By substituting these values in equation 18, the corresponding

pressures at various points respectively will be,

$$p_c = k_v (\Delta_i + \bar{x}\theta)r' \quad \text{at centre}$$

$$p_1 = k_v (\Delta_i + x_1\theta)r' \quad \text{at toe}$$

$$p_2 = k_v (\Delta_i + x_2\theta) r' \quad \text{at heel}$$

R_B (Eqn. 19) can be evaluated by applying Simpson's rule with interval $B/2$ and coordinates x_1 and x_2 as shown in Fig. 4a, thus,

$$R_B = L k_v \int_{x_2}^{x_1} (\Delta_i + x\theta)^{r'} dx$$

$$= k_v \frac{BL}{6} \left[(\Delta_i + x_1\theta)^{r'} + 4(\Delta_i + \bar{x}\theta)^{r'} + (\Delta_1 + x_2\theta)^{r'} \right]$$

$$\cdots (20)$$

The force acts upwards.

Taking moments of pressure ordinates about C and summing up by Simpson's rule, the moment M_{RB} due to R_B is given by,

$$M_{RB} = \frac{k_v B.L}{6} \left[(\Delta_i + x_1\theta)^{r'} . \frac{B}{2} - (\Delta_i + x_2\theta)^{r'} . \frac{B}{2} \right]$$

$$= \frac{k_v B^2 L}{12} \left[(\Delta_1 + x_1\theta)^{r'} - (\Delta_1 + x_2\theta)^{r'} \right] \qquad \cdots (21)$$

Frictional force F_B

Force F_B acts at the base in Fig.4 and is given by

$$F_B = \mu_2 . R_B \qquad \cdots (22)$$

where, μ_2 is the coefficient of friction at the base,

If the distance of the instantaneous point of rotation

above the base $D_2 > 0$, F_B will act from left to right in Fig. 4a. If $D_2 = 0$, F_B will be determined by the equation of equilibrium of horizontal forces and must lie between $\pm \mu_2 R_B$. Its value will be as follows

$$F_B = (P_1 - P_2 + 2F_4 - 2F_5) - Q$$

If F_B works out positive it is acting to the right and if F_B is negative it is acting to the left in Fig. 4.

The moment M_{FB} due to F_B will be

$$M_{FB} = F_B \cdot D \qquad \qquad \dots (23)$$

and will be anticlockwise if F_B acts to the right.

Moment due to eccentricity of the vertical load Q_v is considered negligible.

3.4 EQUATIONS OF EQUILIBRIUM

For statical equilibrium of the well under the combined action of vertical and lateral loads the following conditions must be satisfied

    (i) Sum of all vertical forces must be zero i.e. $\sum V = 0$

    (ii) Sum of all horizontal forces must be zero i.e. $\sum H = 0$

and   (iii) Moment of all forces about a point C must be zero or $\sum M_C = 0$.

Considering all forces and their moments on the well in Fig. 4 and using (+) sign for forces acting left to right and (+) sign for anticlockwise moments. The equilibrium equations can be written thus,

For $\sum V = 0$,

$$W_B = Q_v + W = F_1 \pm F_2 + 2F_3 + R_B \qquad \ldots (24)$$

For $\sum H = 0$,

$$Q = P_1 - P_2 + 2F_4 - 2F_5 - F_B \qquad \ldots (25)$$

where Q is the lateral load applied at the point C.

And for $\sum M_C = 0$,

$$M_o = Q \cdot H = - M_{P1} + M_{F1} + M_{P2} \mp M_{F2} - 2M_{F4} + 2M_{F5} + M_{RB} + M_{FB} \qquad \ldots (26)$$

where H is the height of point of application of load above point C.

C H A P T E R 4

INSTRUMENTATION

4.1 GENERAL

Laboratory models and a field model of well founda-
tion were proposed to be tested under a combined action of
vertical and horizontal loads. Observation of distribution of
pressure and friction on faces and base of these well models
were thought necessary to develop an insight into the nature of
normal and frictional forces which affect the behaviour of a
well foundation. Since a well model is comparatively a rigid
structure, direct method of measuring the soil reaction was
used in the models by using boundary earth-pressure cells.
Friction cell was used for observing frictional forces.

A transducer which could measure normal pressure and
friction at the same point (Arthur and Roscoe 1961) would have
been ideal but it was not feasible under the prevailing condi-
tions.

4.2 BOUNDARY EARTH PRESSURE CELLS FOR USE IN LABORATORY MODELS

Choice of Cell

A deflecting diaphragm type earth-pressure cell was
chosen for its simple design and construction and convenience
of use in well models.

The primary aim in developing a cell to measure
pressures in granular materials is to produce a system that

gives linear calibration characteristics. Any departure from linearity is associated with stress distribution within the sand material. It has been shown by Trollope and Currie (1960), that provided the central deflection to diameter ratio of the diaphragm of the cell is restricted to less than 1:2000, a sensible linear calibration curve may be obtained. For deflection ratios in excess of this amount, the calibration curve takes the form of a convex curve owing to the effect of arching in the sand material over diaphragm. It was therefore decided to design the cells with deflection to diameter ratio of 1:2000 at maximum pressure.

It was desirable to use a cell of small diameter in order not to alter the characteristics of the face of model in which they are used. The base of smallest model was of square cross-section of 15 cm sides. For the 15 cm wide faces, a small cell with 3 cm diameter was possible with a 1.8 cm diaphragm. The diaphragm size of 1.8 cm diameter was decided since it would accommodate two resistance type electric strain gauges for working of cell with a half bridge. The smallest available gauges were Rohit KWR-1A with the following specifications:

Resistance	120 Ohms
Gauge factor	2.8 $\pm$ 1 %
Grid size	1.5 mm x 0.5 mm
Base size	8 mm x 4 mm

Range of Pressures

In designing a cell, the range of pressure must be known (WES 1955). In the present case, pressures were required to be measured on the faces and base of a 15 cm square model embedded in dense sand with maximum depth D to width B ratio of 2 and 20 cm square model with D/B ratio of 1.5. Both models were to be embedded upto a depth of 30 cm. The models were to represent prototype wells and were to be tested under vertical and lateral loads.

Current design practice for a field well (IRC 1971) subjected to combined action of vertical and lateral loads provides that the maximum pressure at the toe should not exceed the allowable bearing capacity of soil. It was thought proper to apply the same condition in model testing also in order to simulate behaviour of large field wells. Dense sand which was chosen as the soil medium for testing, has an ultimate bearing capacity of about 8 kg/cm^2. The safe vertical load that could be applied on this sand was about 4 kg/cm^2, because beyond this load the sand near the edge of the base will have a tendency to go plastic due to parabolic distribution of pressure caused by a rigid base on elastic soil. If in this condition of vertical loading, the foundation is made to tilt, the edge pressures would be higher thereby increasing the chances of plastic failure. It was decided to keep a factor of safety of 3 on 4 kg/cm^2 for tilted well. This provided a safe bearing pressure of about 1.5 kg/cm^2 at the edges. Since the cells could not have been fixed at the edge itself but would be sufficiently

inside the edge due to its size, a design pressure of 0.8 kg/cm² was thought sufficient for base pressure cells.

The design pressure for the face cells was fixed in the following manner. It was tentatively decided that the lateral loads and tilts will be kept below those required for ultimate failure in the horizontal direction, since the field wells can not be permitted to such large tilts as required to produce ultimate resistance. It was proper to use a factor of safety of 3 over the ultimate pressures on face, as was used for the base.

Assuming the well to rotate about the base the maximum passive pressure at failure would occur at about mid-height as in case of rigid bulkheads (Terzaghi 1943). In this case the maximum passive pressure, p_{max}, would occur at a depth z equal to about 15 cm and its magnitude will be

$$P_{max} = K_p \gamma z$$

where K_p is the coefficient of passive earth pressure, γ , the unit weight of sand. Assuming that the unit weight of dense sand would be about 1.65 g/cm³, the angle of internal friction $\Phi = 40°$ and the angle of wall friction $\delta = - \Phi/2$ will be achieved. We obtain the value of $K_p = 10.38$ from tables of passive earth-pressure values (Singh 1967).

Thus

$$P_{max} = 341 \text{ g/cm}^2$$

with a factor of safety of 3 the design pressure works out to be 114 g/cm². A design value of 150 g/cm² or 0.15 kg/cm² was

therefore adopted.

Design

For the purpose of design, diaphragm was treated as a thin circular plate fixed at its perimeter and subjected to a uniform surface load (WES 1955).

The following data were used in designing the thickness of diaphragm and working out the sentitivity of the transducer.

i) Design pressures (q_{max}) for (a) face cells = 0.15 kg/cm^2

(b) base cells = 0.8 kg/cm^2

ii) Ratio of deflection of centre to diameter under q_{max} = 1/2000

iii) Radius of diaphragm 'a'   = 0.9 cm

iv) Young's Modulus of diaphragm material 'E' (Berrylium copper)   = 1.34 x10^{6}kg/cm^2

v) Poisson's ratio of diaphragm material (ν) (Hetenyi, 1960)   = 0.355

vi) Length of grid of strain gauge   = 1.5 mm

vii) Sensitivity of strain recording instrument   = 1 μ - strain

Thickness of diaphragms

Maximum deflection w_{max} of the centre of the diaphragm due to a uniform pressure q_{max} when treated as a thin circular plate fixed at its perimeter is given by (Timoshenko and Woinowsky-Krieger 1959).

$$w_{max} = \frac{3}{16} \frac{q_{max}\ a^4 (1-\nu^2)}{Et^3}$$

where t is the thickness of diaphragm.

Since deflection to diameter ratio adopted for maximum
pressure is 1 in 2000,-

permissible deflection of diaphragm at the centre is

$$\frac{1.8}{2000} \quad = 0.9 \times 10^{-3} \text{ cm}$$

Thickness of diaphragm for face pressure cell

Since,

$$q_{max} \quad = 0.15 \text{ kg/cm}^2$$

Thickness 't' of the diaphragm worked out from the deflection
formula comes to 0.0238 cm. A diaphragm thickness of 0.23 mm
was adopted.

Thickness of diaphragm for base pressure cell

Since

$$q_{max} = 0.8 \text{ kg/cm}^2$$

$$t \quad = 0.414 \text{ mm}$$

A diaphragm thickness of 0.42 mm was adopted.

Sensitivity of the Cells

Sensitivity of cells can be worked out if the posi-
tioning of the gauges on the diaphragm and the sensitivity of
the strain recording instrument is known. The positioning of
the gauges is shown in Fig. 5(a). One gauge is placed on the
centre of the diaphragm and the other at a centre to centre
distance of about 0.75 mm from centre. The strain output can
be worked as follows.

The general equation of radial strain (ε_{a_1}) produced at any radial distance 'a_1' from the centre of a fixed circular plate of radius a acted upon by a uniform pressure (q), (Timoshenko and Woinowsky-Kreiger 1959), is

$$\varepsilon_{a_1} = \frac{3}{8} \cdot \frac{q\, a^2\, (1-\nu^2)}{Et^2} \cdot \left(1 - \frac{3\, a_1^2}{a^2} \right)$$

The radial strain curve is shown in Fig. 5(b).

Avergae strain (ε_{ac}) on the strain gauge located at the centre will be

$$\varepsilon_{ac} = \frac{2.98}{8} \cdot \frac{q\, a^2\, (1-\nu^2)}{E}$$

similarly average strain (ε_{ae}) produced by strain gauge located near periphery at a distance of 0.75 cm from centre will be

$$\varepsilon_{ae} = - \frac{3.24}{8} \cdot \frac{q\, a^2\, (1-\nu^2)}{Et^2}$$

Due to a half bridge circuit the total strain indicated will be

$$\varepsilon_{ac} + \varepsilon_{ae} = \frac{6.23}{8} \cdot \frac{q\, a^2\, (1-\nu^2)}{Et^2}$$

Equating this strain to the minimum recordable strain.

$$\frac{6.23}{8} \cdot \frac{q_{min}\, a^2\, (1-\nu^2)}{Et^2} = 1 \times 10^{-6}$$

or $q_{min} = \dfrac{8Et^2 \times 10^{-6}}{6.23\, a^2\, (1-\nu^2)}$

For face pressure cell sensitivity obtained is

1.37 g/cm²/microstrain

and for the base pressure cell sensitivity obtained is

4.16 g/cm²/microstrain.

Fabrication

Figures 5(a) and 6 show the details of a typical pressure cell. Circular brass casing of 3 cm outer diameter and 1.8 cm inner diameter was machined out of brass rod. Circular disc of 2 cm outer diameter and thickness equal to that of designed diaphragm was cut out from beryllium copper sheet. The disc was carefully soldered flush with one of the faces of the casing to form a 1.8 cm size diaphragm, by placing them in a peripheral slot of the same thickness and diameter as the disc. Gauges were carefully pasted with araldite and then connected in a half bridge circuit. A coating of araldite was applied over the gauges for water-proofing. The leads were taken out of a nipple provided in a threaded brass cap at the outer end of the cell casing. The leads were subsequently fixed in the nipple with araldite as a precaution against damage to the strain gauge connections due to any accidental disturbance to leads.

In all six cells were fabricated to have 0 to 0.15 kg/cm² pressure range. These are designated as cell B-1 to B-6. Two cells were prepared to have the range 0 to 0.8 kg/cm² and are designated as C-1 and C-2.

Calibration

Water pressure was used for calibrating the cells. The complete calibration assembly is shown in Fig. 7. It consists of a small calibration chamber, a water pump and a pressure measuring unit. The calibration chamber (Fig. 8) was machined out of brass rod. The base of the chamber has an opening to allow water and a bleeder hole to expell air. The cell can be pressed against a circular rubber seal on a peripheral offset in the chamber near its bottom with the help of a threaded cover at the top of chamber.

For calibration, the cell was put into the chamber with the lid pressing it against the rubber seal. The chamber was connected to water pump and manometer. The complete system was de-aired by operating water pump and bleeder holes in the chamber and the pore pressure apparatus. Water pressure was applied in suitable increments. Strain readings for each incremental loading and unloading of pressures were recorded by an SR - 4 strain indicator.

The water calibration curves for a typical C-type cell and B-type cell are shown in Figs. 9(a) and 9 (b). Calibration factors for various cells used are given in Table 1.

Precautions were taken that no leak occured in the calibration system during testing. Cells were subjected to a chebk if sustained load altered the characteristics of the diaphragm. No change was discernible.

4.3 FRICTION CELL

Friction cells were designed and fabricated for measuring friction on the faces and base of mild steel models and also for use in field model. The cells were designed to function in the range of 0 to 0.20 kg/cm² shear stress. The cells worked on the principle that strains produced at the fixed end of a cantilever are linearly proportional to the tangential force applied at its free end (Perry and Lissner 1962). The cells were designed to measure reversible force only in one direction.

Design of the Cell

An account of design of a cell that can measure friction has been given by Arthur and Roscoe (1961). It has been suggested that for a satisfactory performance of a friction cell deflection of the free end of the cantilever should not exceed .001 inch or .025 mm. This criteria was adopted in designing the cell.

Following several trials with the size of the cell, keeping in view the size of the model well which had a 20 cm wide face, and convenience of fabrication, an overall size of 47 mm x 47 mm x 69 mm was finally adopted (Fig. 10a). The cantilever length was fixed at 5.5 cm. The section of cantilever was designed in the following manner.

Cross-Section of the Cantilever

The deflection 'w' of the free end of a cantilever of length 'l' due to a concentrated load 'T', at its end

is given by

$$w = T l^3/3EI$$

where 'I' is the moment of inertia of the cross-section of the cantilever and 'E' the modulus of elasticity of its material. Design frictional force is 0.20 kg/cm^2 and the area of the sensitive face is 10 cm^2. Therefore the maximum force at the cantilever end due to this stress will be

$$T = 0.2 \times 10.0 = 2.0 \text{ kg}$$

Assuming that the cantilever will be made of aluminium (Arthur and Roscoe, 1961) and its $E = 7.1 \times 10^{-5}$ kg/cm^2 (Hetenyi, 1960), the expression for deflection becomes,

$$w = \frac{2 \times 5.5^3}{3 \times 7.1 \times 10^{-5} \times I}$$

Now since $w = .0025$ cm

we get, $\quad I = \dfrac{2 \times 5.5^3}{3 \times 7.1 \times 10^5 \times .0025} \text{ cm}^4$

Providing a width of 1.5 cm for convenience of pasting two gauges of 7.5 mm wide base, we have

$$I = \frac{1.5}{12} d^3 = \frac{2 \times 5.5^3}{3 \times 7.1 \times 10^3 \times .254}$$

giving $\quad d = 0.79$ cm

A cross-section of 1.5 cm x 0.8 cm was adopted.

Sensitivity of the Cell

Assuming that the cantilever in Fig. 10c is acted upon by a concentrated load 'T' at its end. The bending

moment 'M_A' is given by,

$$M_A = T \ (1 - l_g/2)$$

where ' 1 ' is the length of the cantilever and ' l_g' is the length of gauge.

Stress 'f' on the top and bottom fibres of a rectangular section 'b x d' due to 'M_A' is given by

$$f = \frac{M_A}{Z} = \frac{T \ (1 - l_g/2)}{bd^2 - 6}$$

$$Strain = \frac{6T \ (1 - l_g/2)}{E. bd^2}$$

Substituting $l = 5.5$ cm, $l_g = 1.0$ cm, $E = 7.1 \times 10^5$ kg/cm^2, $b = 1.5$ cm, $d = 0.8$ cm, we get,

$$Strain \ at \ A \ = 4.4 \times 10^{-6} \ T$$

Four strain gauges were located at positions as shown in section at A'A' of Fig 10a , Due to their connection in a full bridge circuit(Fig. 10b) they produce an augmented strain out put equal to 4 times the strain in a single gauge. The strain measuring instrument is sensitive upto 1 microstrain. Therefore the sensitivity can be worked out. Thus,

minimum recordable
strain $= 1.0 \times 10^{-6} = T_{min} \times 4.4 \times 10^{-6} \times 4$

or $T_{min} = 5.68$ gm

The dimensions of the face of free end of the cantilever are 3.16 x 3.16 cm or 10 cm^2 area. The minimum shear

stress recordable with the cantilever and the instrument is

$$f_s = 5.6/10$$
$$= 00.568 \text{ gm/cm}^2$$
$$= 0.568 \times 10^{-3} \text{ kg/cm}^2$$

Fabrication

The cell which is shown in Fig. 10a and Fig.11 consists of a cantilever 5.5 cm long with a cross-section of 1.5cm x 0.8 cm fixed to a square base of 5 cm x 5 cm x 1.4 cm size. Its free end is made to have a square face of area 10 sq cm. These sizes were machined out accurately on a milling machine from a single aluminium casting. The cantilever block is encased into a hollow square shape casing such that the square face at free-end leaves an all round gap of 1 mm width within the inner face of the casing for allowing deflection of the cantilever when acted upon by a frictional force. A thin rubber membrane is stretched to cover the entire working end of the assembly, including the gap, for checking entry of water or soil particles into the gap during fuctioning of the cell. The sand grains if allowed to enter the gap may cause obstruction to the deflection of cantilever at free-end. The membrane is held in place by a thin steel lining screwed to the perimeter of the casing-end and a thin square steel sheet covering the free-end of cantilever. The surfaces of the lining on the casing and the square sheet on the cantilever-end are in the same plane, and do not obstruct the functioning of cantilever in any way. The square steel sheet forms the face on which frictional force is received.

Four gauges of Mahavir-L-10 type having 120 ± 0.5 ohm resistance and gauge factor of $2.8 \pm 2\%$ and grid 10mm x 4 mm with 15 mm x 8 mm base, were used for measuring strains. One pair of gauges i.e. (t_1 and t_2) in Fig. 10a, was pasted symmetrically and parallel to the long axis of the cantilever on its broader face and as near as possible to the fixed end. The second pair of gauges i.e. c_1 and c_2, (Fig. 10a) was pasted on the opposite face on a mirror image of the first pair. The gauges were connected in a full bridge circuit, as shown in Fig. 10b to achieve the desired performance. When a tangential force 'T' is applied to the cantilever in a direction perpendicular to the plane of the pasted gauges, gauges t_1 and t_2 sense strains equal in magnitude and alike in sign producing a bridge output proportional to the force T. The output of the gauges c_1 and c_2 which are also subjected to strains equal in magnitude and alike in sign, but of opposite nature to that of gauges t_1 and t_2 will act to augment the bridge output of gauge t_1 and t_2. If on the other hand an axial load is applied all the four gauges will sense strains of same magnitude and same sign and will cancel in the wheatstone bridge to produce zero output. The temperature compensation is also effected in the same manner in the full bridge. If however, a horizontal force is applied at right angles but in the same plane as the force T, the strains produced in the four gauges are of same magnitude but of opposite signs in pairs t_1 and c_2 and t_2 and c_1. This enables to reduce the output of the bridge to zero.

Calibration of the Cell

The calibration arrangement used is shown in Fig.12. The cell was clamped horizontally in a vice with sensing width of the cantilever beam remaining horizontal. Tangential load was applied with slotted weights at the centre of cantilever - end in suitable incremental loading. The strains in the cantilever were measured, with a strain indicator, corresponding to each loading. The readings were obtained for both loading and unloading. Figure 10d, shows a typical calibration curve of a friction cell. The same method was employed to check the effect of forces in another tangential direction. It was found that no unbalance of bridge occured due to this type of loading.

In all, ten friction cells were prepared. These have been designated as F-1 to F-10. Calibration factors for these cells are given in Table 2.

4.4 BOUNDARY EARTH-PRESSURE CELLS FOR FIELD MODEL

Choice of Cell

Deflecting diaphragm type cell was chosen for its simple design, covenience in fabrication and fixing on the face and base of the model.

The size of the field model was tentatively decided to be a square section with 1.5 m sides. A cell with 9 cm overall diameter was found to be convenient for fabrication with available machinery as also for placing it on faces and base of the model during its construction. A,5 cm diameter, diaphragm was found suitable since it could accommodate two Mahavir K-5 strain gauges which were available locally. These gauges are of flat grid type

with a grid size of 6 mm x 1.5 mm. The resistance is 120 ohm an the gauge factor 2.84 ± 2%.

Range of pressures

It was desirable that the field model should be geo-metrically similar to the laboratory model. A 1.5 m x 1.5mx square section model with D/B ratio of 1.5 was found to be a practical size for construction and testing by making use of the existing facilities.

Pressure on face of the model

Preliminary investigation of site had shown that the soil at about half the depth of well i.e. at about 1.12 m depth was a silty sand with a dry density of 1.49 g/cm^3 and angle of internal friction equal to approximately 30°. The well under the action of lateral load would probably rotate at the base and the maximum passive pressure that will develop at about half the depth i.e. at 1.25 m depth on the front face under the soil con-ditions would be,

$$P_{max} = K_p \Upsilon z_1$$

where P_{max} is the maximum pressure at a depth z_1, Υ is the den-sity of soil in saturated condition and K_p, the coefficient of passive earthpressure.

Assuming that the maximum wall friction will be due to $\delta = \Phi/2$, K_p for $\Phi = 30^O$ is obtained as 4.78 (Singh 1967).

The well was proposed to be tested with soil in satura-ted condition to simulate typical site condition in a river bed. The density of the soil under saturated condition can be taken

about 2 g/cm^3 Therefore,

$$p_{max} = 4.78 \times 2 \times 0.112 \text{ kg/cm}^2$$
$$= 1.07 \text{ kg/cm}^2$$

Since the well was not planned to be subjected to failure in lateral direction, the maximum value of presuure likely to be achieved with a factor of safety of 3.0 with respect to p_{max} would be 0.357 kg/cm^2. It was therefore decided to have pressure cells of 0 to 0.35 kg/cm^2 range for use on the faces of the model.

Pressures on base

The soil at the depth of 2.25 m where the bottom of the well was to rest, was a fine grained soil of medium consistancy of N-value between 4-8. The safe bearing capacity for such soil may be taken as 1.5 kg/cm^2 (Singh 1967). Assuming that the maximum pressure would be obtained at the edge in the direction of tilt the safe bearing pressure with a factor of safety of 3.0 works out to 0.5 kg/cm^2. It was decided therefore to have pressure cells of 0 to 0.5 kg/cm^2 range for the base.

Design

For design purposes diaphragm was treated as a thin circular plate fixed at its perimeter subjected to a uniform surface load (WES Bulletin 1955).

Design criterion used in this case also was that the ratio of the deflection at centre to the diameter of the diaphragm should not exceed 1/2000 at maximum pressure.

Phosphor bronze was selected as the material for face

pressure cells and non-magnetic stainless steel for base pressure cells. Use of stainless steel pressure cells at the base was desirable due to conditions of higher pressures and proximity of the water table near the base. Stainless steel cells would have been desirable for use on faces also but could not be produced in large numbers mainly because of difficulty in machining the metal.

Thickness of the diaphragm

The following data was used to obtain the thickness of the diaphragms of phospher bronze and stainless steel cells.

Radius of diaphragm (a)　　= 2.5 m

Central deflection/diameter　= 1/2000

Design pressure (q_{max}) for

      (i) face cells　=0.35 kg/cm²

      (ii) base cells　= 0.50 kg/cm²

Modulus of Elasticity for

      (i) Phospher bronze　= 1×10^6 kg/cm²

      (ii) Stainless steel　= 2×10^6 kg/cm²
        (Hetenyi 1960)

Poisson's ratio (ν) for

      (i) Phospher bronze　= .355

      (ii)Stainless steel　= .305
        (Hetenyi 1960)

Using the above data and the equation for deflection at the centre of a circular plate fixed at its periphery and subjected to uniform load, the thickness of the diaphragm worked out as given below.

      (i) Phospher bronze cells,　t = .967 mm
        a thickness of 1 mm was adopted.

(ii) Stainless steel cells,　t = .863 mm
a thickness of 1 mm was adopted.

Sensitivity of the Cells

A half bridge circuit with two strain gauges of 5 mm grid length was to be used for measuring strains in the diaphragm. The positioning of the gauges is shown in Fig. 13. The centre of the gauge near the periphery works out to about 2 cm from the centre of the diaphragm.

Using the general equation of radial strain,produced at any radial distance from the centre of a fixed circular plate acted upon by a uniform pressure, the sensitivity of the cells can be worked out as below.

For Phosphor Bronze diaphragm

$$E = 1 \times 10^6 \text{ kg/cm}^2$$

$$\nu = 0.355$$

$$t = 0.1 \text{ cm}$$

$$a = 2.5 \text{ cm}$$

Strain produced at the centre i.e. at $a_1 = 0$,

$$\epsilon_{ac} = \frac{3}{8} \frac{q (a)^2 (1 - \nu^2)}{Et^2}$$

strain produced at 2 cm radial distance from centre,

$$\epsilon_{ae} = \frac{2.76}{8} \frac{qa^2 (1 - \nu^2)}{Et^2}$$

The total strain indicated will be,

$$\epsilon_{ac} + \epsilon_{ae} = \frac{5.78}{8} \frac{q a^2 (1 - \nu^2)}{Et^2}$$

Equating this strain to the minimum recordable strain,

$$\frac{5.78q}{8} \frac{a^2 (1 - \nu^2)}{Et^2} = 1 \times 10^{-6}$$

Therefore, sensitivity   = 2.53 x 10^{-3} kg/cm^2 per microstrain.

Similarly for stainless steel cells,

sensitivity = 5.16 x 10^{-3} kg/cm^2 per microstrain.

Fabrication

A typical field pressure cell is shown in Figs. 13 and 14. The cells were formed by machining out a 9 cm diameter casing from 100 mm diameter phospher bronze and non-magnetic stainless steel rods. A 5 cm diameter diaphragm of required thickness was machined coaxially out of the casing to form an integrated part of the cell. The back cover for the cell was made from 100 mm diameter aluminium rod. Phospher bronze cells were electroplated from outside to protect them from corrosion. Gauges were pasted in position as shown in figure 13. These were connected in a half bridge circuit as in case of small earth-pressure cells. The strain gauges and the cells were rendered water proof with araldite from all sides for under water use. The water proofing was tested by keeping a cell under water for 24 hours.

Calibration

The cells were calibrated under water pressure. A calibration chamber was fabricated as shown in Fig. 15. The complete calibration set up is shown in Fig. 16. Calibration was done in the same manner as for small laboratory earth-pressure cells (p. 49). Typical calibration curves of a phospher bronze cell and a stainless steel cell are shown in Figs. 17a and 17b, respectively.

In all 21 cells were fabricated for use in the field
model. Of these 12 were of phospher bronze and have been
designated as P-1 to P-12. The 9 stainless steel cells have
been designated as S-1 to S-9. The calibration factors for
these cells are given in Table 3.

C H A P T E R 5

MODEL TESTS

5.1 GENERAL

Response of large structures such as well foundations can best be observed in in-situ tests. But such tests are neither economical nor practicable if not impossible. Properly planned and controlled model tests can yield significant data. These tests are not only economical but also provide the flexibility of studying the effects of all significant variables. Results of these tests can be used advantageously to check the analytical methods proposed. Further they help in highlighting the effects of certain variables which need only be studied on field scale.

Information regarding the laboratory tests on models for observing the behaviour of well foundation are given in this chapter. This includes test facility, models, soil medium, tests and test procedures.

5.2 TEST APPARATUS AND MATERIALS

Test Facility

A model testing facility was constructed in the laboratory. This is shown in Fig. 18 and the dimensions of the same are given in Fig. 19. The rectangular tank which is 2.5 m x 1.25 m x 1.25 m deep, was constructed with 25 cm-thick masonry walls. The size of the tank chosen was such that its boundary would not interfere with the performance of the

largest well model during testing. A frame work above the
tank was used for operating a hopper for filling sand in the
tank from a fixed height by free fall technique. A platform
skirting the tank served as working space. A beam with a roller
on fixed end and a knife edge on the well top was used for
loading the model vertically by placing desired weights on the
beam. A flexible wire attached to the model and stretched hori-
zontally after passing over a smooth pulley provided the arran-
gement for lateral loading by placing slotted weights on a sus-
pended pan. The loading arrangement is shown schematically in
Fig. 20 and a close up view of the same is shown in Fig. 21.

Models of Well Foundation

Two sizes of models with 15 cm and 20 cm square base
were used in the investigation. These models alongwith the
positioning of pressure cells and friction cells are shown in
Fig. 22. The model with 15cm base was prepared hollow using
seasoned teak wood planks of 3 cm thickness. The model was
42 cm long to accommodate D/B ratios of 1.5 and 2. The top
of the model was provided with attachments for loading it in
vertical and horizontal direction. The model was finished with
sand paper and then finished with french-polish to obtain a
uniform surface. The front face and base of this model were
provided with pressure cells with their faces flush with model
surfaces. Model size with D/B = 2, satisfied the criteria for
rigidity in dense sand (Davisson and Prakash 1963).

The model with 20 cm base was also prepared in the
same manner as 15 cm size. This was used mainly to observe

effect of size on well behaviour. Another 20 cm size base
hollow steel model was also prepared using 7 mm thick mild
steel plates. This model was mainly for observing frictional
forces on the model with the help of friction cells. Friction
cell positions on the model are shown in Fig. 22.

Soil Medium

Sand was chosen as the soil medium for tests because
its behaviour tends to be relatively free of time effects. A
high degree of uniformity of material is considered desirable
in producing a test medium with uniform physical properties.
The choice of a dense sand was governed by,

(a) possibility of obtaining a reproducible uniform sand-bed
of large size in a comparatively short period than for a loose
or a medium sand, and

(b) possibility of conducting an adequate number of tests with
satisfactory reproducibility in a short period of time.

Ranipur sand in its natural state was found suitable
for this purpose. The sand consists of pure quartz grains of
subangular shape. The gradation curve is shown in Fig. 23.
Other properties of sand determined by standard procedure are:

Specific gravity of particles	2.684
γ_d (minimum)	1.480 g/cm^3
γ_d (maximum)	1.688 g/cm^3
e_{max}	0.818
e_{min}	0.600
D_{10} size	0.150 mm

Cu, uniformity coefficient   1.90

Angle of internal friction Φ(peak)   42.5°

Angle of internal friction Φ_u(ultimate)   33.4°

Density of test beds (γ_d)   1.658 $\pm$.005g/cm^3

Relative density of test beds   91.5%

Typical stress-strain curve for Ranipur sand is shown in Fig.I-A in the Appex. The grain shape and sizes of the sand used is shown in Fig. I-B also in the Appendix.

5.3   MODEL TESTS

To achieve the stated objectives of this investigation, tests of various types have been performed on the model wells in the laboratory.   These primarily include static lateral load tests on different sizes of wells, different embedment depths, different vertical loads, different friction condition on the sides and different stiffness at the base.   Besides, cyclic and repetitive lateral load and free vibration tests have also been performed. The various tests conducted on well models are listed in Table 4 to 12 wherein the various parameters combinations are detailed, including the positions of pressure and friction measuring cells. The method of performing these tests is described in detail in the following section.

5.4   TEST PROCEDURE

Placing of Sand and Control of Density

Methods commonly used for obtaining a uniform dense sand model are (a) vibration technique and (b) free fall technique. The vibration technique in which soil is first deposited in uniform thin layers and vibrated with a vibrator was not preferred since

it was likely to disturb the orientation of the model and could damage the transducers on models. In the free fall technique sand is made to fall from a fixed height under gravity through a slit or holes in a container. The free fall method was preferable as it was not likely to disturb the model.

A mild steel hopper mounted on four wheels was fabricated for preparing the sand-bed by free fall method (Figs.24 and 25). Its capacity of 0.228 m^3 was decided on the basis of convenience in operation. The length of hopper was equal to the width of test tank. A slit of 2.5 mm at the bottom of the hopper along its length provided the outlet for pouring sand into the tank. Several trial runs of hopper with different openings and different heights of fall of sand showed that an opening of 2.5 mm and a free fall of about 70 cm or more would provide a uniform dense sand-bed of a density 1.658 $\pm$ .005 g/cm^3 with relative density of 91.5%. The graph showing the relationship of height of fall and density is given in Fig. 26. It shows that the density of sand models so built is a unique function of the height of free fall of sand as long as other variables such as rate of flow remain the same. Similar trend was observed by Walker and Whitaker (1964) with a similar technique of deposition of sand. The uniformity of sand bed at different depths and location in the tank was checked with specially fabricated brass containers of 200 cc capacity.

The hopper was run manually on the frame as shown in Fig 25. It was observed that if it is run at a speed greater than about 20 cm/sec , the sand is disturbed at the end of the run. This was due to air trapped between the wall of the tank and the falling sheet of sand. Precaution was taken to run the hopper at a speed not more than 20 cm/sec.

Static Lateral Load Tests

A typical lateral load test was performed in the following manner.

Embedment of model

(i) Sand was deposited in horizontal layers of about 5 cm upto a premarked level in the tank.

(ii) The model, with its transducers connected to a strain measuring unit, was placed gently on carefully levelled sand bed in the middle of the tank and oriented with the help of two guide wires. Verticality of model was checked with a plumb-line and a sensitive level.

(iii) Sand deposition was resumed until desired embedment had be been achieved. The soil was levelled after the top of the model had been cleaned.

(iv)   A device consisting of a hollow wooden box of the size of the model was placed on top of model to avoid loose filling of soil around the model. Any sand falling within the cross section of the model was collected in this box. This box with sand was removed after embedment of the model.

(v)   Two dial gauges of least count 0.01 mm were placed along the vertical axis of the model to measure tilts and shifts in horizontal directions. Two more dial gauges were placed on top of the model to measure tilts and settlement of the model as is shown in Fig. 20.

Vertical Loading

(vi)   The loading beam was carefully laid in a horizontal position with its knife edge on top of model and the roller-end on parapet of the tank. Horizontality was checked with a sensitive level.

(vii)   Slotted weights were gently placed on the beam to achieve desired loading on the model.

Lateral Loading

(viii)   A flexible wire was hooked on to the loading frame at the desired H/B ratio on top of the model. The wire was kept horizontal by taking it over an adjustible smooth pulley. The vertical end of the wire was loaded with slotted weights to provide lateral loading to the model.

Sustained lateral loading was usually done in increments of 2 kg to 5 kg. Four to six increments were often used for achieving desired tilts and loads. The incremental load was less when vertical load was less, and was large for larger vertical loads. Lower increments were often applied towards the end of a test as a precaution against sudden pull-out of model from sand-bed.

Experimental Monitoring

Readings on the four dial gauges were noted, (i) initially, (ii) after application of vertical load, and (iii) after each increment of lateral load.

Readings were taken when no change in readings of the gauges was discernable. It usually took 3 to 5 minutes to achieve the stage after loading.

Strain measurements of transducers were made through an SR-4 strain indicator and a 39-point switch. The connections were never disturbed until the last of the test with a model has been performed. Strain readings were taken, (i) before and after placing model on sand-bed and (ii) after any change in vertical and lateral loading.

Strain readings due to change in loading were recorded after dial gauge readings had been taken.

The complete cycle of filling, testing and removal of sand from tank for the succeeding test usually took about $2\frac{1}{2}$ to 3 working days.

Tests on Models With Smooth Vertical Faces

Vertical faces of wooden models were made to work as smooth faces by interposing polythene sheets, of the size of the faces, between wall of the model and the sand. It had been found earlier from preliminary skin friction tests with vertical loading that when polythene is interposed between wood and dense sand the model slips under its own weight indicating the skin friction having been reduced considerably. The skin friction tests with and without polythene sheets were conducted in a test set-up as shown in Fig.20a. Figure 27 shows polythene sheets and fixtures used for holding them to model before embedment.

Cyclic and Repetitive Lateral Load Tests

Embedment of model and vertical loading was done in the same manner as for the static lateral load tests. For cyclic tests lateral loads were applied in the same manner as in case

of static load test with the difference that an increment was first applied to the right, then it was released. The same increment then was applied to the left by a similar arrangement. This was then released. Next higher increment was then applied to the right and then to the left after release. This process continued until four to five increments of loads had been applied.

For repetitive lateral load tests a similar procedure as for cyclic tests was adopted with lateral loads applied and released only in one direction.

No pressure cell or friction cell readings were taken in these tests.

Free Vibration Tests

In these tests the procedure for embedment models in sand and vertical loading was the same as for static load tests. No sustained lateral load was applied.

An acceleration pick-up was screwed to the front face of the embedded model for measuring vibrations. The pick-up was connected to an ink-writing oscillograph through an amplifier. For obtaining an acceleration vs time record of the vibrating model, a gentle tap was given on the axis of the model in the direction perpendicular to the face with pick-up and records of free vibration were obtained on the oscillograph.

C H A P T E R 6

TESTS ON FIELD MODEL

6.1 GENERAL

Tests on full scale foundations in the field would naturally yield most reliable results. But such tests in case of well foundations would be costly and unwieldy. In fact lateral loading will require special and costly arrangement. Therefore usually laboratory models of small size are used in most investigations. To get a feel of the response of wells in the field, a fairly large scale model of a well was made and tested in the field under various types of loading. The details of the model and the testing procedure adopted are described in this chapter.

6.2 TEST SITE

In the begining it was proposed to test a large model in a nearby river-bed. Preliminary investigations of probable sites selected raised doubts about the success of the test. A site was therefore selected within the Earthquake School premises. Frames for lateral loading upto 5 tonnes and structural test bed for its fixing were available in the structural testing laboratory. The well model was located out-side in the ground but near this laboratory.

The exploration of the soil at site indicated that it was predominantly silty sand (SM). A clay layer was present at a depth of 3.1 m and the water table was at 2.5 m. Top soil was hard and standard penetration tests (SPT) gave N-value of

16,17,7,8 at zero, 1m, 2m and 2.5m depths. The ground was flooded with water as it would be at the time of testing. Another SPT

showed N values to be 9,10,6,8 at zero,1,2 and 2.5 m depths respectively. Samples from depth of 1 m and 2 m showed a dry density of 1.49 g/cm^3. Undisturbed samples showed a Φ value of about 30° with negligible cohesion in a drained triaxial test. Soil Explorationdata is given in Fig.I-C in Appendix.

6.3 THE WELL MODEL

The dimensions and details of the field well model are given in Fig. 28. It is square in plan with 1.5 m x 1.5 m size base. It is 2.25 m deep thereby providing D/B ratio of 1.5 which is same as kept in a number of laboratory model tests. The well consists of a 20 cm wide and 25 cm deep curb with a cutting edge. The curb is of R.C.C. and the cutting edge is of mild steel angle. The four walls constituting the steining are 20 cm thick through out the depth of well. These were designed as reinforced concrete retaining walls. The plug at the bottom is 20 cm thick and was designed as a reinforced concrete slab. Two numbers 22 mm diameter foundation bolts are provided on top of the well.

The well was constructed by the typical field technique of excavation and sinking in the following manner.

i)   The cutting edge was made from 6.75 x 6.75 cm x 8 mm thick m.s. angle, in the shape of a square frame of outer dimension about 20 mm more than the outer dimension of the steining. Vertical reinforcement consisting of 10 mm rounds was welded to it at proper positions. Horizontal reinforcement

consisting of 10 mm rounds was bound in position. The curb was cast over the cutting edge by leaving an offset of about 10 mm on all sides.

ii)   The curb was cured suitably and was placed horizontally and oriented on the ground in-situ with a theodolite. A formwork consisting of two concentric square wooden shuttering boxes of the size of inner and outer periphery of the steining was fixed to the curb. A 20 cm thick, 65 cm high R.C.C. steining was cast above the curb with the help of the formwork. This formed the first lift of the well steining.

iii)   After casting the steining suitably the soil near the cutting edge was excavated carefully so that the steining gradually sank due to its own weight to about 9/10 of its full height. Precaution was taken not to allow the well to tilt during sinking.

iv)   Vertical reinforcement was welded in continuation to the ends of the reinforcement bars of previous stage and horizontal reinforcement was bound in position. The formwork was now fixed to the top of the first stage of steining. Concreting was done as in (ii) and sinking was effected as in (iii).

v)   The operations of casting the steining and sinking the well was terminated when a depth of embedment of 2.25 m was achieved.

vi)   The soil within the bounds of cutting edge was levelled and a 25 cm thick R.C.C. plug was laid.

Figure 29 shows the formwork and reinforcement before laying the curb. Figure 30 shows the curb with cutting edge

below it and reinforcement for first stage steining. Figure
31 shows the completed curb in position. The formwork for con-
creting the first stage of steining is shown in Fig. 32 and Fig.
33 shows welding of reinforcement for the third stage of stein-
ing.

6.4 INSTRUMENTATION

Field pressure cells and friction cells already described
in Chapter 4 were required to be fixed in various positions on
faces and base of well as shown in Fig. 35a.

The usual method of fixing pressure cells on the face
of a retaining wall or base of a footing is either to embed
them in masonry or concrete with their sensitive faces flush
with the surface, or fix them with their sensitive faces pro-
jecting on the surface. The advantage of the embedment tech-
nique is that the sensitive face is flush with the surface
which is desirable for good results but the disadvantage is
that it is difficult to retrieve the cells either for repairs
or for use in other tests. The advantage of fixing the cells
on surface is that these cells possibly could be retrieved after
the test is over but the disadvantage is that the projection is
not desirable for good results.

In the present case the cells were fixed by an arrange-
ment in which the cells could be placed with their sensitive
faces flush with the surface and also could be retrieved easily
when required. The arrangement is shown in Fig. 35b. 'A' is a
mild steel pipe 100 mm inner diameter and 20 cm long. A^1 is
an 8 mm thick mild steel square plate with sides slightly

longer than 100 mm. This plate has a machined opening of appropriate shape to accommodate either a pressure cell or a friction cell with its sensitive face flush with plate's outer face. This plate is welded to one of the ends of 'A'. The transducers can be fixed to 'A^1' or removed from it from the open end of 'A'. The pipe assembly is placed between the inner and outer formwork before concreting is done, as shown in Fig. 35c. For this, plate A^1 is screwed to the outer shuttering from within the pipe A. The pipe assembly gets embedded when concreting is done. The screws holding the pipe assembly with the outer shuttering, are accessible after the inner shuttering is removed. The opening thus formed in the concrete steining can now accommodate transducers by operating from inside the well.

Desired number of pipe fixtures were embedded in walls and bottom plug for fixing pressure cells and friction cells at various locations indicated in Fig 35a. Transducers on faces were put in position before sinking operation was under-taken. The transducers at bottom were placed after the concreting of the plug, along with the pipe fixtures, has been done. The leads of the transducers were taken to a strain measuring unit through plastic tubes with one of their ends fixed to the nozzle of the transducer. The space left in the pipe after fixing the cells was filled with grease as a precaution against any leakage of water into the well through these pipes.

Figure 34 shows the pipes with plates welded to it for pressure cells and friction cells.

Figure 36 shows the pipes with their plates screwed to the outer formwork before the first stage of concreting. Figure 37 shows the rear face of the well with openings for fixing cells in the first stage of well construction. Figure 38 shows the cells in position on rear face and side face.

Figure 39 shows the leads of the cells shown in position in Fig 38. Figure 40 shows the arrangement for positioning the cells in the bottom plug.

6.5 TESTS PERFORMED

Behaviour of the well was to be studied under static and dynamic conditions. Tests performed are indicated in Table 13. Since lateral load test under static condition was likely to disturb the soil around the well steining and the base, it was decided to perform such test first which would cause least disturbance in the soil. Various tests were therefore performed in the following order.

i)   Vertical load test

ii) Free vibration tests, and

iii) Lateral load tests.

The vertical load test (no. 118) was thought necessary for obtaining the characteristics of vertical subgrade reaction of soil on which the well was founded. Free vibration tests (Test Nos 119 to 123) were performed, to study the natural frequency and damping characteristics of thewell foundation under different loading and ground conditions. Lateral load tests Nos. 124 and 125) were performed (i) to obtain lateral load vs tilt, D_2/D vs tilt and $\bar{x}/B$ vs tilt relationships as in case of laboratory

models and (ii) to obtain presuures and friction on faces and base as in case of laboratory tests. Test No. 125 was performed under the same condition of embedment and loading as Test No.124, to see the effect of disturbance on well caused by a previous loading.

6.6 TESTING PEOCEDURE

Vertical Load Test

The well was loaded vertically with sand bags and concrete blocks of known weights. The incremental loads applied were 2.25 tonnes, 4.25 tonnes and 6.75 tonnes. Settlement corresponding to each load increment was noted with four dial gauges of .01mm least count. These dial gauges were positioned near four corners of the top of well. The dial gauges were supported on datum beams fixed to massive concrete blocks at some distance from the well steining so that the datum was not affected by possible settlement of nearby ground due to loading. Readings were taken only when no change in dial gauge reading was discernible. Readings, were taken by unloading the well in the reverse order of loading.

Free Vibration Tests

Horizontal free vibration tests were performed. Three acceleration pick-ups one near the top, another near mid depth of well and the third near the bottom plug, where fixed to the inner face of the rear wall of the well steining. These were connected to three inkwriting pen recorders with amplifier for obtaining vibration records. The well was set on free vibration by hitting the top of well with a hammer. Records were

obtained with only the self weight of the well acting and with 2.25 tonne and 4.25 tonne superimposed vertical loads. Free vibration tests were performed under two types of ground conditions.

i) With soil surrounding the well in its natural state of very low moisture content.

ii) With soil surrounding the well in almost saturated state by flooding the ground for a week.

A view of the free vibration test in progress is shown in Fig. 41.

Lateral Load Tests

The test set up is shown schematically in Fig. 42. The 5 tonne loading frame fixed on the well was 3.5m high and was made of angles and channels. It was fixed on top of well with the help of 8 foundation bolts embedded in the four walls at the top. The dial gauges in the vertical direction and horizontal directions were supported on datum beams which had their support at a suitable distance from the sides of the well to ensure least disturbance to the datum beam at the time of loading the well. A 4m high, 5 tonne reaction frame was fixed on the structural test bed, at a distance of about 15 m from the well axis. The lateral loading was provided by a horizontal steel cable of 12 mm dia. One of its ends was clamped to the loading tower at top of the well at a height of 3.375m above the ground so as to give an H/D = 1.5, and the other end was connected to a loading beam in the 5 tonne reaction tower with a lever ratio of 1:5. A

5-tonne tension proving ring was provided in series with the cable to record the applied lateral load. Pressure cells and friction cells were connected through long leads to an SR-4 indicator through a 39-point switch.

The ground was flooded with water for a week before testing and was kept flooded during testing also. A 6 tonnes superimposed vertical load was applied on top of the well with concrete blocks and sand bags of known weights. Lateral load was applied in suitable increments by the loading beam. The loading beam was always kept in a horizontal position by adjusting the levelling arrangement. Dial gauge readings were taken before and after loading. Readings were noted only ehen no change in reading was discernible. Strain readings were taken before and after loading. Strain readings were always taken after the dial gauge readings have been recorded.

Figure 43 shows the reaction frame on structural test bed with loading beam and other arrangements for static lateral load test. Figure 44 shows the loaded well for lateral load test.

C H A P T E R 7

PRESENTATION OF TEST DATA

7.1 VARIABLES AND THEIR RANGE

The main variables in the problem of well foundation are the soil surrounding the well on its sides and base, the size of cross-section, the depth of embedment in relation to its size, the magnitude of vertical load and the magnitude and point of application of the net lateral load. Friction on sides and shape of scour pit around the well are also other important variables.

The soil surrounding a field well may be different on sides as well as below the base. For example, the subgrade at the base may consist of clayey soil and the soil surrounding the sides may be sandy or vice-versa, or, the well may rest on a stiff subgrade such as a rock or stiff clay and the surrounding soil may be sandy or clayey. Thus innumerable combinations of soil on sides and base and varying strata on the sides themselves may occur. To cover up all the cases in a single attempt will be an impossible job. Therefore the study has been restricted to wells surrounded by only non-cohesive soil in case of laboratory tests. An attempt has also been made to see the effect of a stiff subgrade below the base of a well surrounded by dense sand on its sides. A large well model has been tested in the field to compare its behaviour with laboratory models.

Dense sand was used as the soil medium for testing the well models in the laboratory mainly because it was possible to obtain a reproducible uniform sand bed of large size in a comparatively short period than for a loose soil and also it was

possible to conduct an adequate number of tests with satisfactory reproducibility in a short period of time.

Two sizes of well model, 15 cm square section and 20 cm square section, were adopted for performing various tests in the laboratory. The sizes were mainly determined by the consideration of testing facilities. The field well model size was 1.5 m square cross-section and was chosen by the consideration of ease of working from within the well.

The effect of embedment in relation to the size of the well in the laboratory tests wea studied with two values of D/B ratio. These were 1.5 and 2.0. These values practically cover the majority of wells in the field. The field well model was tested for D/B ratio of 1.5.

For studying the effect of vertical loads on the behaviour of well foundation, models were subjected to the action of varying lateral loading of such magnitude as would cause the soil to strain beyond the linear range. The vertical load was varied from zero to about one-third of the ultimate vertical load capacity of the laboratory well under eccentric loading. For 15cm x 15cm well, this load was about 131 kg. Other loads considered were 101 kg and 51 kg and were chosen as the loads which are larger than the vertical skin friction that could be carried by the well. Zero vertical load was chosen to observe the behaviour of the well for the cases when the well is entirely held in position by skin friction on its sides. The field model was tested with 6 Tonnes of vertical load superimposed on it. This was expected to cause a vertical pressure of about one-third the ultimate vertical

loading capacity of the well.

The point of application of lateral load above the scour level was changed from 0.5 to 2.0 times the depth of embedment of laboratory models. Expressed in terms of width of well B, the H/B ratio was varied from 0.75 to 4. H/B ratios of 2.25, 3 and 4 may often occur in the field in various bridges during floods where as the ratios 0.75 to 2 may be occuring during low water conditions under a bridge. H/B ratio for the field model was 2.25.

Friction on sides of a well may be different in field due to various soil conditions or due to disturbance of soil around a well during construction. Therefore it was decided to study two conditions of friction on sides, namely, a high friction condition such as may be caused by a dense sand against a well steining and a low friction condition as may be caused by loose sand or loosening of soil around a well and the lubricating effect of water between a well steining and the soil in which the well is embedded.

Effect of friction was observed in the laboratory models by simulating a high friction condition and a low friction condition on the vertical face of the model. High friction condition was obtained by embedding the model in dense sand with the sand directly in contact with-the walls, where as the low friction condition was created by inter-posing polythene sheets between the model walls and the surrounding dense sand.

The field model was tested for lateral loading in a condition when the surrounding soil was flooded by water for at least one week.

In order to study the effect of a stiffer subgrade at the base of a well on its lateral load capacity, a 3 cm thick wooden plank, made of same quality of wood as the well, was used to simulate a stiffer base than obtained by a dense sand.

Thus the range of variables adopted for studying the responsible of wells through laboratory model tests and the field model tests may be summarized as follows:

(a) For Model Tests in Laboratory

Sl.No.	Variable	Symbol	Values Used
1.	Size of well	B X B	i) 15cm x 15cm ii) 20cm x 20cm
2.	Depth of embedment	D/B	2, and 1.5
3.	Vertical load	Q_v	131, 101 and 51 kg and zero
4.	Position of lateral load	H/B	0.75, 1, 1.5, 2, 2.25, 3 and 4
5.	Friction	-	High friction and low friction on all sides and low friction on two side faces.
6.	Base stiffness	-	Well resting on wooden plank and well resting on dense sand

(b) For Field Model Tests

S.No.	Variable	Symbol	Value used
1.	Size of well	B x B	1.5m x 1.5m
2.	Depth of embedment	D/B	1.5
3.	Vertical load	Q_v	6 Tonnes
4.	Position of lateral load	H/B	2.25
5.	Friction	-	Natural ground flooded with water.

Some miscellaneous tests were also performed. These tests were :

(i)   to study the extent of disturbance around a well to ultimate lateral load

(ii)   measurement of friction on faces and base of a well and

(iii)   to study the effect of sloping scourpit surcharge on lateral load capacity

(iv)   to study the dynamic behaviour of wells.

In all these tests also the variables stated in the previous paragraphs were used.

7.2 TESTS PERFORMED

To cover the effects of various parameters on the behaviour of well foundations, a total of 117 tests on small scale laboratory models and 8 tests on a large scale field model were carried out. For convenience of reference the parameter combinations used in each test have been serially presented in Tables 4 to 13, which also show, in sketch form, the direction of lateral loading and position of pressure and friction cells on the models. The main contents of the Tables 4 to 13 are described below.

Table 4. Static lateral load tests on 15 cm square section wooden model with D/B = 1.5. The variables considered are, vertical load 131,101 and 501 kg, H/B ratio equal to 3.0 and 2.25 and rough and smooth side faces. (Number of tests -10).

Table 5. Static lateral load tests on 15 cm square section wooden model with D/B = 2. The variables considered

are, vertical load 131 kg, 101 kg, 51 kg and zero, H/B ratio
equal to 4.0, 3.0, 2.0 and 1.0 and rough and smooth side faces.
(Number of tests - 18).

Table 6. Static lateral load tests on 15 cm square base
wooden model with D/B = 2. The variables considered are verti-
cal loads of 101 kg and 51 kg, H/B ratios equal to 4.0, 3.0, 2.0
and 1.0, and rough and smooth side faces, with the base resting
on a plank to simulate a stiffer strata. (Number of tests - 8).

Table 7. Static lateral load tests on 20 cm square base
wooden model with D/B = 1.5 and 2. Other variables considered
are, vertical load 131 kg, and zero, H/B ratios of 4.0, 3.0, 2.25,
2.0 and 1.5 and rough and smooth side faces. (Number of tests - 9).

Table 8. Static lateral load tests on 20 cm square
section mild steel model to observe friction on sides and base.
Variable being, D/B = 1.5 and 2, vertical load 131 kg, 56 kg and
zero, H/B ratios 4.00, 3.0C and 2.25. With scour pit surface
inclined to 15° with horizontal in one test. (Number of tests-13).

Table 9. Cyclic and Repetitive lateral load tests on
15 cm and 20 cm square wells of wood and 20 cm square well of
mild steel. The parameter for 15 cm well being D/B = 3, and
H/B = 3.0, with variable vertical loads of 131 kg, 101 kg and
zero and rough and smooth side faces. For 20 cm well, the para-
meters were D/B = 1.5 and H/B = 3.0, with variable vertical loads
of 156 kg, 131 kg and 56 kg.(Number of tests - 10).

Table 10. Free vibration tests on 15 cm and 20 cm models
for D/B ratios of 1.5 and 2, vertical loads of 131 kg 101 kg,

71 kg, 56 kg, 51 kg, 31 kg and zero and rough and smooth side faces. (Number of tests - 32).

Table 11. Skin friction tests on 15 cm and 20 cm wells with vertical loading only and with rough and smooth side faces (Number of tests - 7).

Table 12. Tests for observing failure pattern on ground level under ultimate lateral load, with 15 cm and 20 cm models oriented in different position with respect to lateral load direction. (Number of tests - 10).

Table 13. Tests on field model with 1.5 m square section reinforced concrete walls, D/B ratio equal to 1.5 and H/B ratio equal to 2.25, tests performed being vertical load test, free vibration tests and lateral load tests. (Number of tests - 8).

7.3 OBSERVATIONS FROM LATERAL LOAD TESTS ON 15 CM MODEL RESTING ON DENSE SAND

Test data obtained from lateral load tests on 15 cm model resting on dense sand subgrade has generally been presented in the form of graphs as given below.

i) Lateral pressure distribution on front and rear faces with depth along their vertical axes for increasing lateral loads. These were required for observing lateral pressure distribution pattern on faces and also to work out lateral pressure displacement relationships and their parameters.

ii) Pressure distribution along the centroidal axis of the base for increasing lateral loads. These were required to see only the pressure distribution at the base with tilt.

iii) Lateral load versus tilt (Q vs θ) curves. These were required for comparison of effect of different variables on the lateral load capacity of a well.

iv) Ratio of distance of instantaneous point of rotation above the base and the depth of embedment versus tilt i.e. D_2/D vs θ curve, and

v) Ratio of distance of instantaneous point of rotation from the well axis and the width of the well versus tilt i.e. $\bar{x}/B$ vs θ curve.

The last two curves were required to study the position of instantaneous point of rotation so that response of a well may be understood to develop a suitable theory.

The method of obtaining the above curves from observations is explained below.

Lateral Pressure Distribution with Depth

Five earth-pressure cells were provided on one face of the vertical axis of the well model at regular intervals from the base. With D/B ratio of 1.5, only four cells were embedded in sand and with D/B ratio of 2.0, all the five cells were embedded. When the face with earth pressure cell was oriented in the direction of lateral load it formed the front face. When it was oriented in the opposite direction to the lateral load it served as the rear face.

After the required embedment of the model, when the lateral load was applied, the cells at various depths showed change in strain readings with respect to their readings before embedment

due to soil reaction against their diaphragms. This difference
of strain in a pressure cell was multiplied by the calibration
factor of the cell to obtain the lateral pressure at the posi-
tion of the pressure cell with depth. Thus four pressure read-
ings corresponding to four pressure cells in the case of D/B
= 1.5 and five pressure readings corresponding to D/B = 2 for
any increment of lateral loading were obtained, in various tests.
These pressures at various depths in a test for a lateral load
have been plotted along the x-axis in a graph with y-axis as the
depth of embedment. The points at various depths were joined by
a smooth curve, to obtain the lateral pressure distribution with
depth corresponding to changing lateral loads.

The lateral pressure distribution curve shown in Fig.45a
was obtained from observations recorded in Test No. 1 for a 15 cm
well with embedment depth of 22.5 cm and D/B of 1.5. The vertical
load was 131 kg and lateral loads of 5 kg, 10 kg, 15 kg, 19.5 kg
and 23.5 kg were applied. The key sketch shows the orientation
of the earth-pressure cells with respect to lateral loading
direction.

In majority of the tests the lateral pressure distribution
with depth were recorded for front face only. However in a few
tests, pressures on the rear face were also recorded to get an
idea of the likely pressure that may develop on this face. All
the lateral pressure distribution curves with depth,for different
tests performed,are shown in Figs. 47a, 49a, 52a, 54a, 56a, 58a,60a,
62a, 64a, 66a, 68a, 71a, 73a, 75a, 77a, 80a, 83a and 85a.

Polythene sheet was used on the vertical faces of well

(Figs.51,70,82 respectively)

model in Test nos.5,16, 25 and / to study the effect of friction

on the face. Therefore in these cases, the pressure distribution

could not be recorded.

Pressure distribution for Test Nos. 21 and 23 have also

not been shown since these could not be recorded due to distur-

bance from external source and disorder in the strain recording

instrument respectively.

The pressure distribution curves are found to be curvili-

near. Similar distribution has been observed by Kapoor (1971)

also. It is seen that the point of zero pressure on the face

tends to shift upwards with the increase in lateral load.

Pressure Distribution Along the Centroidal Axis of the Base

Three pressure cells were provided along the centroidal

axis of the base for recording base pressures. In Fig. 45b, the

pressure distribution along the centroidal axis obtained from

Test No. 1 has been plotted. The pressure cell positions are

shown in the index sketch. Since the pressure cells could only

be fixed at some distance from the edge of the base, and the pressures

recorded at these points only, the pressure distribution curves

have been extrapolated to the edges. All the base pressure

distribution curves for different tests performed are shown in

Figs.   47b, 49b, 51a, 52b, 54b, 56b, 58b, 60b, 62b, 64b,66b,

68b, 70a, 71b, 73b, 75b, 77b, 80b, 82a, 83b and 85b.

Pressure cells at the base were of varying stiffnesses

and were arranged for obtaining pressures when the vertical face

with cells was oriented in the direction of lateral load. The
orientation of well in Test Nos. 3, 8, 19 and 26/was in the $^{(Figs.47,54,73 \text{ and } 82 \text{ respectively})}$
opposite direction and therefore base pressures were not recorded
for these tests.

Pressure distribution at the base is found to be convex
in almost all tests. It is observed that pressure tends to in-
crease rapidly at the toe of base of model and decreases at the
heel with increasing tilts. The convexity of pressure distribution
tends to decrease with increasing tilt. The convex pressure dis-
tribution may be due to greater confinment near the centre of the
base. Pressure distribution at the base have been observed to be
concave by Kapoor (1971). A convex pressure distribution though
has been observed by Chae et al (1965) under circular footings.

Lateral Load - Tilt Relationships

Two dial gauges were placed at fixed distance along the
vertical axis of the well and two on the horizontal top of the
well model to record displacements in the horizontal and vertical
directions respectively. Tilt angle 'θ' in radians was calculated
from the set of readings obtained from vertical and horizontal
dial gauges. Tilt was obtained by dividing the difference in
dial gauge readings, by the distance between the two dial gauges.
The average value of θ obtained from the horizontal and vertical
dial gauge readings was used for plotting the lateral load-tilt
relationship.

In Fig. 46a the lateral load vs tilt curve for Test No.1
has been plotted. The index sketch in the figure indicates the

test conditions. All lateral load vs tilt curves for different tests performed have been shown in Figs 46a, 48a, 50a, 51b,53a, 55a, 57a, 59a, 61a, 63a, 65a, 67a, 69a, 70b, 72a, 74a, 76a,78a, 79a, 81a, 82b, 84a and 86a.

In Fig. 48a, two sets of data for Q vs θ curves obtained from Test Nos 2 and 3 with identical conditions of embedment and loadingm have been plotted. These are shown by dots and circles. The closeness of the two sets of points is indicative of good reproducibility of data. Figure 55a shows the reproducibility of test data of identical Test Nos. 7 and 8, Fig. 74a for Test Nos. 18 and 19 and Fig. 82b for Test Nos. 25 and 26.

Instantaneous Point of Rotation with Tilt

When a lateral load is applied the well rotates about an instantaneous point of rotation. This point is defined by D_2/D and $\bar{x}/B$ in the vertical and horizontal planes respectively with the centroid of the base as the origin. D_2 is the vertical coordinate above or below the base of the well and $\bar{x}$ is the horizontal coordinate either to the left or to the right of the vertical axis of the well.

$$D_2 = D_z - \frac{d_1 + d_2}{2\theta}$$

where, d_1 and d_2 are the displacements observed intthe upper and the lower dial gauges and D_z is the distance of the mid-point between the two dial gauges from the base of well.

$\bar{x}$ was determined from the readings of the horizontally positioned dial gauges as given below.

$$\bar{x} = \frac{d_3 + d_4}{2\theta}$$

where d_3 and d_4 are the displacements observed in the front and rear dial gauges respectively.

The position of the instantaneous point of rotation was obtained from D_2 and $\bar{x}$ determined for each lateral load level. In Figs. 46b and 46c the coordinates of instantaneous point of rotation (D_2/D and $\bar{x}/B$) with θ have been plotted at different lateral loads in Test No. 1. The index sketch in the figure shows the test conditions. The initial settlemtnt Δ_i observed after application of vertical load is also indicated in the figure. Similar curves for different tests performed are shown in Fig. 46b,c, 48b,c, 50b,c, 51c,d, 53b,c, 55b,c, 57b,c, 59b,c, 61b,c, 63b,c, 65b,c, 67b,c, 69b,c, 70c,d, 72b,c, 74b,c, 76b,c, 78b,c, 79b,c, 81b,c, 82c,d, 84b,c and 86b,c.

Reproducibility of data has been shown in Figs. 48b,c 55b,c, 74b,c, and 82c,d.

7.4 OBSERVATIONS FROM LATERAL LOAD TESTS ON 15 CM MODELS RESTING ON PLANK

One of the aims of the study was to observe the effect of a stiff subgrade below the base of a well, on the lateral load capacity. Stiff subgrade was simulated by placing a 3cm thick 50cm wide and 100 cm long wooden plank on dense sand. The well was made to rest on this plank and then the sand was poured by rainfall method as in all other tests. The various combinations of variables in this series were so selected that the results could be compared directly with those of a well resting on dense sand. Tests performed for different combinations of variables

are given in Table 6. the details of which are listed briefly on page 85. In this series of tests, lateral load-tilt relationships only were studied in Figs. 87a to 87d, Q vs θ have been plotted, for Test Noss 29 to 32 and in Figs 88a to 88d for Test Nos. 33 to 36. Test condition are indicated by the index sketch in the figures.

7.5 OBSERVATIONS FROM LATERAL LOAD TESTS ON 20 CM WOODEN MODEL

Lateral load tests on 20 cm square base wooden models were performed mainly to study the effect of size on the lateral load capacity of wells under similar conditions of embedment and loading as for 15cm wells. Tests performed with different combinations of variables are given in Table 7 (p.176). The details of which are listed briefly on page 85. Lateral load-tilt relationships for this series of tests are plotted in Figs 91a to 91i. The test conditions are indicated by the index sketch in the figure.

In this series another data which was observed in two typical tests i.e. Test Nos.37 and 40 was the pressure distribution on front and rear faces simultaneously and has been plotted in Figs 89 and 90 respectively.

7.6 OBSERVATIONS FROM LATERAL LOAD TESTS ON 20 CM SQUARE MILD STEEL MODEL

Tests on 20 cm mild steel model were performed mainly with the objective of observing friction and its mobilization on front and rear faces, side face and base of a well under static lateral load under different loading conditions. The effect of

the sloping surcharge, which is often caused due to scour around a well during a flood, on the lateral load capacity was also observed by this model with two tests.

Friction cells had been prepared to observe friction on the sides and base of a well. Friction cells and their sensitive faces were made of steel. If these were to be put on 20 cm square wooden model, the size of which only could accommodate these cells, the sensitive faces of the cells and the face of the well would have made some difference due to difference in surface properties of the two materials. It was therefore appropriate to make a mild steel model of 20 cm square section for measuring friction.

In all seven tests were performed for observing friction on front and rear faces of the model and six tests for observing friction on its side face and base. All the tests with their test conditions are given in Table 8 on p. 177 and are also detailed briefly on page 85.

Friction on front and rear faces was to be observed in either upward or downward direction. When the model with friction cell had been embedded to the required depth and lateral load applied, the model tilted and friction was mobilized on its front and rear faces. This was recorded in terms of strains through friction cells. The change in the direction of strain was an indication of the direction of friction force on the sensitive face of the cell.

Figure 92 shows the data on friction, plotted in terms of shear stress with depth on front and rear faces of well,

obtained from Test Nos 46 and 47. In both these tests which were identical except for the orientation of cells, D/B was 1.5 and H/B,3.0. The vertical load Q_v was 131 kg. The index sketch in the figure shows the orientation of faces with cells. The shear stresses on front face are shown by firm lines and those on rear face by dashed lines. The lateral load level is also indicated on these curves. The sign convention that has been followed for indicating the direction of friction on either faces is positive friction upward and negative downward.

Figure 93 shows shear stress with depth on front and rear faces for Test Nos. 48 and 49. These tests were also performed with Q_v = 131 kg and D/B = 1.5 but H/B was changed to 2.25 other conditions are given in the index sketch in the figure.

Figure 94 contains the shear stress distribution only on front face of 20 cm mild steel model. The data was obtained from Test No. 50. The vertical load applied in this test was only 56 kg as compared with Q_v=131 kg in Test No. 46. D/B was 1.5 and H/B = 3.0. The index sketch in the figure gives details of positioning of friction cells and direction of loading as also other relevent details.

In Fig. 95 shear stress distribution on front face is plotted for Test No. 51. In this test Q_v was zero, D/B = 1.5 and H/B = 2.25. Other details are indicated in the index sketch.

Figure 96 shows the shear stress distribution on front face of 20 cm mild steel model for Test No. 52. This test was performed to see the effect of sloping surcharge due to scour pit around a well during flood. In this test also Q_v was zero,

D/B = 1.5 and H/B = 2.25. But the ground sloped at 15° with the horizontal to simulate the scour pit. The index sketch in the figure shows the test conditions.

Lateral load vs tilt relationship were also obtained from Test Nos. 51 and 52 to compare the cases of ground with and without scour pit. The comparison has been shown in Fig. 132 on P. 300.

In Test No. 53 of Table 8 on page 177 the friction cells had been mounted on the side face and the base to study mobilization of friction on these surfaces with displacement. In Fig. 97a, friction on three cells F-4, F-5 and F-6 (see index sketch) has been plotted against absolute displacement of the cell itself, which was computed by multiplying the vertical distance between the instantaneous point of rotation and the centroid of the sensitive face of cell with the tilt of the well. Friction in cells F-4 and F-6 is oriented in opposite direction and friction on cell F-5 is erretic. This shows that the instantaneous point of rotation lies between F-4 and F-5 and may be closer to cell F-5. Figure 97b shows the shear stress vs displacement of cells F-9 and F-10 located at the base as shown in the index sketch. In this figure while the friction at the toe of the well increases throuhout, the same at the heel shows a reverse trend after initial stages of loading.

In Fig 98a and b shear stress on side face vs displacement of cells and shear stress on base vs the displacement respectively are shown for Test No. 54. The test conditions are shown in the index sketch.

While Figs. 99a and b show the shear stress vs displacement of cells for side face and base respectively for Test No. 55 in which Q_v was 56 kg with D/B = 1.5 and H/B = 3.0, Figs 100a and b show the shear stress vs displacement relationship for Test No. 56 in which the only change from the previous case was that of H/B being 2.25 instead of 3.0.

Figures 101a and b contain the shear stress vs displacement observed on side face and base respectively of 20 cm mild steel model in Test No. 57. The D/B ratio was 1.5 and H/B = 3.0. No vertical load was applied on top. The index sketch explains the testing conditions.

In Figs 102a and b, the shear stress vs displacement of cells observed on side face and base respectively are shown also for Q_v = 0 and D/B = 1.5 but H/B in this case is 2.25.

7.7 OBSERVATIONS FROM CYCLIC AND REPETITIVE LATERAL LOAD TESTS ON 15CM AND 20 CM MODELS

Seven cyclic lateral load tests and three repetitive lateral load tests were performed on 15 cm and 20 cm wooden and steel wells to study the equivalent viscous damping characteristics of wells when they are subjected to large displacements under dynamic conditions.

All the cyclic and repetitive tests with their embedment and loading conditions are given in Table 9 p. 179 and are also briefly detailed on p. 85.

The data for tests on the wells has been plotted in the form of lateral load vs displacement at ground level. The

displacements were obtained by multiplying the distance of the ground level from the instantaneous point of rotation with the tilt.

In cyclic tests two-directional loading was applied and a complete hysteretic loop was obtained. The load level in every successive cycle was increased.

Figure 130 is for Test no. 58. the key sketch gives details of embedment and loading.

Data for other cyclic load tests (Test Nos 60 to 65) is plotted in Figs. 104 to 109. The test conditions of embedment and loading are explained in the index sketches in each of these figures.

In repetitive tests, the loading was only in one direction and with successive cycle, the lateral load level was increased.

Figure 110 is a plot of Q vs displacement at ground level for Test No. 66. For other tests (Test Nos. 67 and 68) in this series Q vs displacements at ground level are plotted in Figs 111 and 112. The test conditions are given in each of the figures.

7.8 OBSERVATIONS FROM FREE VIBRATION TESTS ON 15 CM AND 20 CM WELLS

Free vibration tests on 15 cm and 20 cm wells were performed to study the various parameters influencing the vibrational characteristics of a well.

Information about tests performed is given in Table 10

p. 180 and also briefly indicated on pp. 85 - 86

Observations in the free vibration tests were in the form of acceleration vs time record. Since a large number of tests were performed only a few representative records have been included in this report. The data from other records have been tabulated in the form of natural frequencies (f_n) and damping factors (ζ).

Figure 113, shows the acceleration vs time records corresponding to Test Nos 69 to 78 on 15 cm well under different conditions of embedment and loading explained for each record with the help of the index sketch in the figure. The natural frequency and the damping factors for these tests have been tabulated in Table 14 , p. 186.

Natural frequency "f_n" was determined from the records by counting the number of cycles in a specified time and the damping factor " ζ " was obtained by the logarithmic decrement method (Thomson 1964).

7.9 OBSERVATIONS FROM VERTICAL LOAD TESTS FOR SKIN FRICTION ON FACES OF 15 CM AND 20 CM MODELS

The effect of different friction condition on the res- ponse of wells under lateral loading was to be studied. Wells were tested under high and low friction conditions. Wells with sand directly against their faces were treated as having high fric- tion condition and were termed as wells with rough faces. When polythene sheets of the size of the faces of well were inter- posed between the walls of the well and surrounding sand it was expected to create low friction condition and the face in

this condition were termed as smooth.

To assess the performances of rough and smooth faces quantitatively, vertical load tests were performed on 15 cm and 20 cm wells.

In this series of tests the well was so embedded in sand that its base remained a clear 2 cm above the subgrade sand-bed so that it was totally held by friction (see Chapter 5 p. 69). Vertical load was applied in suitable increments and the corresponding displacements were measured.

In Fig. 114a, the load-displacement curves are plotted for 15 cm x 15 cm base wooden well. Curve 'A' shows the load-displacement plot of the well when its embedment depth was 22.5 cm or D/B = 1.5. Curve 'B' is for embedment depth of 30 cm or D/B = 2.0. In both of these cases the sand surrounding the well rested directly against the well face and so the test was with all faces being rough.

Curve 'C' in Fig. 114a is load-displacement plot for the case when all faces were treated 'smooth' by interposing the polythene sheets between well faces and surrounding sand. The test conditions are explained in the index sketch.

Figure 114b, shows the plots of load vs displacement for 20 cm wooden and mild steel wells. While curves D,E and F are for the wooden well, curve G is for the mild steel well.

7.10   OBSERVATION FOR FAILURE IN SOIL AT
         ULTIMATE LOAD

It was felt that it will be useful to find out the
extent to which the soil mass surrounding a well is affected
due to lateral loading, since this could give helpful ideas
about planning of test facility in future. One of the method
to achieve this aim was to study the soil-failure zones when
failure load is applied. In case of wells there would be active
and passive zones shown on the ground level of the sand bed
when ultimate lateral load is applied.

In all ten tests   on 15 cm and 20 cm wells were con-
ducted to study the extent of failure under different condition
of embedment, loading and orientation of wells. The details
of these tests are given in Table 12 and are also briefly
reported on p. 86.

When the ultimate lateral load was applied to a well the
soil surrounding the well was disturbed showing shell-like out
crop, typical of a passive failure zone, against the front face
in the direction of lateral load and a shell-like depression
against the opposite face (rear face) typical of an active
failure zone. No disturbance was observed against the faces
parallel to the direction of loading.

Figure 115 shows the typical failure of soil at ground
level in the form of shell-like passive failure out crop in the
front and the active failure depression at the back of well,
For Test No. 111, performed on 15 cm well, with its base resting
on a plank, with $D/B = 2$, $Q_v = 56$ kg and $H/B = 1$.

Figure 116a, shows the dimensions in plan od the failure zones at the ground level, with reference to the initial position of well at zero tilt for Test No. 108, which was performed on 15 cm well with $D/B = 2$, $H/B = 2$, and vertical load equal to zero. Failure load in this case was found to be 21 kg. These values are indicated by the side of the figure. The plus sign shows a raised out crop where as minus sign shows a depression in soil bed.

For convenience of comparison ratios L_p/x_p and L_a/x_a of the failure zones have been shown in Table 15. L_p and x_p are the dimensions of the passive failure out crop at its extremities in the direction parallel to the face and at right angles to it respectively as shown in Fig. 116a. L_a and x_a are the dimensions of the active failure depression at its extremeties in the two directions.

Figures 116b,c and d, show the failure zones for test nos. 109, 100 and 111. The test conditions and failure loads are mentioned in each case in the figure.

In Figs. 117a and c the failure zones are plotted for 15 cm well and 20 cm well respectively for the condition shown against each case.

In Fig. 117b, the failure zones are plotted for a case of the well of diamond cross-section. This was performed on 15 cm well with the lateral load applied in line with one of its diagonals. The values L_p; x_p, L_a and k_a have been taken from the diagonal in this case as is evident from the figure. Other test conditions and failure loads are shown near the

diagram.

In Figs. 118a and b, plots of failure zones are given for 20 cm well for various conditions as shown adjacent to each diagram. These correspond to Test Nos. 115, 116 and 117.

In Fig. 118 c, the ground was sloping at 15° to the horizontal. The plus zone beyond the active zone shown with a minus sign was caused as a result of excessive lateral load even after the plus zone in front of the well had been formed.

The ratios L_p/x_p and L_a/x_a for all tests in this series have been tabulated in Table 15.

7.11 OBSERVATIONS FROM TESTS ON FIELD MODEL WELL

Tests were performed on a large reinforced concrete 1.5m x 1.5m x 2.25m deep instrumented field model well. Details of tests performed are given in Table 13 on page 185 and are also briefly detailed on page 86.

Vertical Load Tests

Figure 119 shows the base pressure vs settlement curve, for both loading and unloading conditions of the well in Test No. 118. The vertical loads were applied in three increments of 2.25 Tonne, 4.5 Tonne and 6.75 Tonne for obtaining base pressures of 1, 2 and 3 T/m^2 respectively. The settlement was taken as the average value of settlements measured for each loading with four dial gauges placed on four corners of the well. The index sketch in the figure shows the test conditions.

Free Vibration Tests

The data of free vibration tests on field model is presented in Figs. 120a to 120e in the form of acceleration vs time records for horizontal vibrations imparted to the well. Figure 120a which corresponds to Test No. 119, shows the acceleration-time record for horizontal vibration of the well when no vertical load was superimposed on it and the surrounding ground was in its natural condition of low moisture content.

Figures 120b and c are the free vibration records for the natural ground condition for superimposed vertical loads of 2.25 Tonnes and 4.25 Tonnes respectively. Figures 120d and e are the horizontal free vibration records of the well when ground had been flooded with water to saturate the soil. The vertical superimposed loads applied in the two cases were 4.25 Tonne and 2.25 Tonne respectively.

Lateral Load Tests

In Fig. 121a is plotted the lateral load versus tilt, in Fig. 121b. D_2/D versus tilt and in Fig. 121c $\bar{x}/B$ versus tilt for Test No. 124. This test was performed tith $Q_v = 6.0$ Tonne, $D/B = 1.5$ and $H/B = 2.25$ soil was in a flooded condition. Lateral load increments of 400 kg, 808 kg, 1228 kg, 1675 kg and 2010 kg were applied. No further load was applied since the well started tilting very fast. The test conditions are explained in the index sketch. Figure 122a shows the lateral load versus tilt plot, from Test No. 125 performed on the well under same conditions of embedment and loading as in Test No. 124. This test was performed to observe the response of well after the well has been previously

disturbed by a previous lateral load. Figures 122b and c are the plots of D_2/D versus tilt and $\overline{x}/B$ versus tilt for Test No. 125.

In the lateral load tests on field well model, pressure cells were placed along the central axis of the front and rear faces as well as in a direction perpendicular to the axes for recording pressures with tilting of well. Pressure cells were placed at the base also in the direction of load and perpendicular to it for recording pressures at the base. Friction cells were also placed at various positions on faces and base. The positions of various cells is shown in Fig. 35.

In Fig. 123a, lateral pressures on front and rear faces and on Fig. 123b, base pressure along the centroidal axis of the well in Test No. 124 have been plotted. Test conditions are shown in the index sketch.

Figure 124a shows pressure distribution across the front face at 35 cm depth below the ground level. Figure 124b, is the pressure distribution on the frontface at 100 cm below the ground level for the well. Figure 124c gives the pressure distribution across the rearface at a depth of 205 cm below ground level.

Figure 124d shows the pressure distribution at the base at a distance of 35 cm from the toe in a direction perpendicular to the lateral load.

In Fig. 125, the data obtained from friction cells on front and rear faces (Fig.35) has been presented in the form of curves

shear stress distribution with depth along the vertical axes
of the faces. The shear stress were calculated from strains
observed in the friction cell. The plotting has been done
exactly in the same manner as explained in Section 7.6 . Test
conditions are shown in the index sketch in the figure itself.

C H A P T E R 8

INTERPRETATION AND DISCUSSIONS

8.1 INTRODUCTION

The data obtained from all the laboratory tests have been interpreted in this Chapter.

The testing facility including instrumentation and reproducibility of test data have been discussed first.

The effect of (i) vertical load (ii) depth of embedment (iii) position of lateral load (iv) size of well (v) friction on sides (vi) base stiffness and (vii) shape of scour pit on the response : vis-a-vis lateral load capacity of the well have been discussed in a general way.

The instantaneous point of rotation and its shift during application of lateral load and consequent tilt has been described on the basis of model tests. Also the coefficient of earth pressure at rest have been computed from observed friction on sides. Values of parameters m_h, n, r, k_v, r' required in theoretical computations by the theory developed in Chapter 3 have been worked out. The numerical data thus obtained and the effect of each variable listed above has been used to compute the lateral load carrying capacity of the models.

The procedure of computation using the theoretical equation is explained and analytical results are compared with experimental results.

The mechanics of development of frictional forces on the sides and base of wells and development and extent of the rupture in the soil at failure lateral loads have been discussed.

Dynamic tests on well model have been discussed in a general way.

The behaviour of the Field model well under static and dynamic loads have also been discussed.

8.2 TESTING FACILITY AND REPRODUCIBILITY OF TEST

The testing facility consisting of the test tank, sand material, sand raining device and loading arrangements have served the purpose well for which they were adopted. This is evident by the following facts.

i) It was possible to deposit the soil medium accurately with a density of $1.658 \pm .005$ g/cm^3.

ii) The size of the test tank was large enough not to interfere with the performance of the model during testing. This is evident from the dimensions of the failure outcrop for the largest model shown in Figs. 117 and 118.

iii) Polythene sheet as a material for reducing skin friction has been quite successful as is evident from the fact that coefficient of friction was reduced from 0.66 to approximately 0.2 as shown in Table 17. Previous workers (Kapoor 1971) were not able to reduce the friction of faces successfully.

iv) Friction cells which were designed and fabricated for measuring friction on faces and base have behaved excellently.

This is evident from the consistency and reproducibility of shear stress-displacement diagrams shown in Figs. 97, 98 etc.

v) A satisfactory reproducibility was obtained as is evident from Q vs θ, D2/D vs θ and $\bar{x}$/B vs θ, curves in Figs. 48, 55, 74 and 82 obtained from Test Nos. 2 and 3, 7 and 8, 18 and 19, 25 and 26, with identical embedment and loading conditions.

8.3 EFFECT OF VARIABLES
Vertical Load

Effect of magnitude of vertical load on lateral has been investigated on 15 cm x 15 cm wooden model. Figure 126a contains plots of lateral load versus tilt for this well with D/B = 1.5 and H/B = 2.25. The vertical loads are 131 kg, 101 kg and 51 kg. This data corresponds to test Nos. 1, 6 and 10 presented in Figs. 46a, 53a and 59a respectively.

It is observed from these plots that the effect of increased vertical load on the well is to reduce the tilt and thus impart greater stability to it in the range of tilts and variables studied.

Similar data has been plotted in Figs. 126b,c,d,e and f for different cases taken from figure numbers marked on each of the curves. The test conditions are also indicated in each figure. All these figures also show that the effect of increased vertical, with other conditions remaining same, is to impart greater stability to well.

In a well, the superimposed vertical load is shared by skin friction and bearing at the base initially. Once the skin

friction is mobilized additional vertical load is transferred to base which generates resistance to tilt under lateral load. The total skin friction on the sides due to vertical load here for 22.5 cm depth of the 15 cm well,is of the order of 21 kg(p.189). Hence additional vertical load beyond 21 kg gives rise to increased friction at the base of the well. This behaviour has been substantiated by the theory developed in Chapter 3 and computation made on p. 138.

Effect of depth of Embedment

Effect of depth of embedment on lateral load capacity has been investigated through 15 cm square base wooden model. Figure 127a, contains plots of lateral load versus tilt for this well with with H/B at 3 and vertical load of 131 kg. The depths of embedment are 22.5 cm and 30 cm i.e. D/B = 1.5 and 2. The data corresponds to Test Nos. 3 and 13 presented in Figs. 48a and 63a respectively. Figure 127b contains the plots of lateral load versus tilt for Test Nos. 7 and 18 presented in Figs 55a and 74a respectively.

In both of these figures it can be observed that increased depth of embedment increases the lateral load capacity. The reason for this behaviour is that larger depths involve larger vertical surface area which allow larger normal and frictional resisting forces when compared with those due to lesser depth of embedment involving lesser surface area.

It was shown above that the 15 cm well with 22.5cm depth could have a skin friction of about 21 kg. The same well with 30 cm depth has a skin friction of about 31.5 kg (Table 16)

p. 189). Thus the well with 30 cm depth will transfer lesser vertical load due to greater skin friction for an equal amount of vertical loads applied to the two cases. It is interesting to note that the resistance increases despite reduction in the base pressure due to greater skin friction in case of deeper wells. This goes to show that vertical surface area plays a dominant role in the lateral load capacity of a well. Also it follows directly from the above observation that if the base pressures were the same after overcoming the total skin friction due to vertical loads deeper wells would offer more resistance than the shallower wells for the same tilt.

The exact numerical effect of the depth of embedment on the lateral load capacity of the well has been developed in Chapter 3 in Eqn. 25. The data obtained from the tests corresponding to Fig. 127 has been analysed on the basis of this theory and this behaviour has been substantiated in numerical terms (p. 138).

Also in Figs. 127a and b the ratios of lateral loads for the two cases of depth considered i.e. cases $D/B = 2$ and $D/B = 1.5$ for various tilts have been shown by the dashed line. The ratio at a tilt was obtained by dividing ordinate AB by AC shown in Fig. 127a. It is seen that this ratio remains almost constant throughout the range of tilts obtained. The average value of the ratios for lateral loads in both the Figs. 127a and b works out to 1.38. The depth ratios in two cases with $D = 30$ cm and 22.5 cm is 1.33. Thus the lateral load capacity appears to be almost in the same ratio as the ratio of depth of embedment.

other factors remaining constant. However this conclusion needs
further verification on larger number of models with different
values of parameters.

Effect of position of lateral load

Effect of moments on well foundation has been studied
by comparing lever arms of the lateral loads with respect to the
scour level.

In Fig. 128a two plots of lateral loads vs tilt are
given. Both the plots are for 15 cm well model with embedment
depth of 22.5 cm or $D/B = 1.5$ and the vertical load $Q = 131$ kg
The upper plot is for a smaller lever arm of $H/B = 2.25$ and has
been plotted from Fig. 46 a for Test No. 1. The lower plot
is for a lever arm $H/B = 3$ and has been plotted from Fig.48a
for Test No. 2. The lerer arm and the figure numbers from which
these plots are taken are marked on each of the curves. The embed-
ment and loading is also indicated in the figure.

It is clearly seen from the comparison that for the same
lateral load,larger lever arms produce large tilts or that the
higher point of application of lateral loads reduces the lateral
load capacity of a well for the same tilt. In other words increa-
sing the applied moment,for given values of lateral load,increases
the tilt of the well.

Figures 128b, c and d show the plots of lateral load vs
tilt for 15 cm well resting on sand for comparison of lever arm
effects under different conditions of embedment and loading. The
plots have been taken from various figure numbers indicated on

each of the plots. The lever arm ratios are also mentioned. Figures 128e and f show the plots of lateral load vs tilt for 15 cm well resting on plank for comparison of the lever arm effects under different conditions of embedment and loading. The figure numbers from which these plots are taken as also the lever arm ratio with width of well is indicated on each of the curves. The embedment condition and the loads applied are also shown in each figure. From all these figures also it is seen that increasing moments for given values of lateral load increases the tilt of well. This conclusion has also been substantiated in numerical terms (p. 138) for well resting on sand.

Effect of Size of Well

The effect of size of well on lateral load capacity of a well has been investigated by testing 15 cm and 20 cm square base wooden models. Figure 129a contains plots of lateral load vs tilt for these wells for $D/B = 1.5$, $H/B = 2.25$ and vertical load $Q_v = 131$ kg. The data corresponds to Test No. 1 and Fig. 46a for 15 cm well and Test No. 37 and Fig 91a for 20 cm well.

It is observed from these plots that the lateral load capacity of well is increased with an increase in the size of the well base.

The plots of lateral load vs tilt of Figs. 129b, c and d also show the same trend. These plots are taken from the figure numbers indicated on each curve.

The reason for the observed behaviour can be attributed to the fact that larger size involves larger area on sides which are responsible for offering more horizontal and frictional

resistance thereby increasing the lateral load capaicty.

It is interesting to note here also, that the lateral load resistance increases despite reduction in base pressure due to greater skin friction owing to larger area in case of larger size of wells (Table 16 p.189). This again goes to show that vertical surface area plays a dominant role in the lateral load capacity of wells and confirms the observation made on p. 110.

Also it follows from the above observation that if the base pressureswere the same after overcoming the total skin friction due to vertical loads, larger sizes of wells will offer more resistance than the smaller sizes and hence will be more stable.

The ratios of the lateral loads for wells of larger size to that for the smaller size for a given tilt as well as ratio Q/B for both sizes have also been plotted in each of the Fig.129a to d.

It is seen that in Figs. 129a and b the ratios of lateral load through/is constant with an average of about 1.33 the result
out
that Q/B values for B = 20 cm and 15 coincide in both the figures. However in Figs. 129c and d Q/B values do not coincide beeause lateral loads ratios are found to be about 1.6 and 2.1 in the two cases respectively. It appears that in case of wells with D/B ratios larger than 1.5, wider wells have the advantage of resisting more lateral loads and also the height of application of lateral load has a marked effect on the capacity.

Effect of Friction

Effect of friction on vertical faces of a well on lateral load capacity has been investigated on 15 cm as well as 20 cm

wooden models. Figure 130a contains three plots of lateral load versus tilt for the 15 cm well with D/B = 1.5, H/B = 2.25 and Q_v = 131 kg. These plots of lateral load vs tilt are for three different cases of friction on sides of the well. The first case corresponding to Test No. 1 and reported in Fig. 46a is of high friction on all faces (RR), and is shown by firm line. The second is that of low friction on all faces (SS) produced by polythene sheet in Test No. 5 reported in Fig. 51b and is shown by dashed line and the third is for low friction on side faces parallel to lateral load direction and high friction on front and rear faces (SR) as indicated in Fig.50a corresponding to Test No. 4 and is shown by dash-dot line.

Figures 130b, c and d also contain lateral load vs tilt plots from tests on 15 cm models for investigating the effects of friction. The figure numbers from which these curves have been taken are marked on each curve for reference. To distinguish the different cases of friction the curves have been drawn with different lines as indicated by the legend in Fig. 130.

Figures 130e and f have been obtained from tests on 20 cm models. The details of test condition and figure reference for the curves are given in each figure.

It is clearly seen from these figures that for the same tilt, lateral load resisted by a well having low friction on all faces is considerably lower than that resisted by a well having high friction on all faces and the lateral load resisted by wells with only two side faces with low friction lies in between the two preceeding cases.

The lateral load ratios of well with high friction on all sides to the two cases of low friction plotted in Figs. 130a to f show in general that contribution of friction to lateral load capacity is some what larger in the initial stage of loading and becomes almost constant as the tilt increases. This may be attributed to the larger magnitude of mobilized friction in the initial stages of deformation.

Considering the average friction at a tilt of 5×10^{-3} radians when the lateral load ratios appear to be stabilised, the ratios of lateral loads for wells with high friction on all faces to the lateral loads for wells with low friction on two side faces only in cases of Fig. 130e and f is 1.04 and 1.25 respectively. The ratios in Figs. 130a, c and d for this case lie between these values. The significant parameter change in Figs 130e and f is the value of vertical load which changes from the maximum of 131 kg to zero. Thus the contribution of friction of the two sides seems to be relatively more when the vertical load is lower than the vertical skin friction resisted by a well.

Arya and Sharda (1973) have shown the contribution of friction on side faces of a square well to be about 20%. The contribution in the test envelopes this value. The lateral load range in these tests is on account of several combinations of parameters and the low percent contribution in some cases is due to the fact that the side friction could not be made zero, nor very definite by the method of testing.

Effect of Stiffness of Subgrade at the base

The effect of stiffness of subgrade below a well has been investigated by using 15 cm wooden model. Figure 131a has the

plots of lateral load versus tilt for this well with D/B = 2, H/B = 4 and Q_v = 101 kg. The curve with firm line is taken from Fig. 87. Corresponding to Test No. 29 in which well was placed on a plank simulating a stiffer subgrade than obtained by dense sand. The dotted curve is from Fig. 72a corresponding to Test No. 17 in which well was resting on dense sand.

It can be observed from the comparison of the two curve of Fig. 131a that higher, stiffness of subgrade at base improves the lateral load capacity of the well. The vertical load applied in this case was 101 kg and the skin friction due to vertical load is about 21 kg, thus sufficiently large load is transferred to the subgrade. The increase in lateral load capacity in case of plank as subgrade may be due to higher coefficient of friction and better elastic properties of the subgrade.

Figure 131b contains four plots of lateral load versus tilt curves for observing the effect of stiffness of subgrade when vertical load applied is 51 kg which is close to the skin friction of 21 kg for this well than the 101 kg load in case of Fig. 131a. The figure numbers from which the curves have been taken are given on each curve and the test conditions are also indicated.

It is observed from these curves that the improvement in the lateral load capacity is only marginal as compared with the case where Q_v was 101 kg. This shows that stiffness of subgrade does not play an important role in the lateral load resistance if the vertical loads are nearer the value of skin friction sustained by well. This may be due to the fact that although the vertical load

is higher than the total skin friction that can be taken by the well the mobilization of skin friction is less due to stiffness of the subgrade which does not permit sufficient movement for its mobilization owing to a smaller load.

Effect of Shape of Scour Pit Around a Well

The effect of shape of scour pit has been studied using 20 cm x 20 cm steel model. In Fig. 132a two lateral load versus tilt curves are given. The upper one is obtained from lateral load test from Test No. 52 which was performed with D/B = 1.5, H/B = 2.25 and Q_v = 0 with a sloping surchage of 15° simulating a scour pit around a well during flood condition. The lower curve has been obtained from Test No. 51 in which also the D/B was 1.5, H/B was 2.25 and Q_v was zero, but the ground level in this case was horizontal or the surcharge angle was zero, the test conditions are also indicated by index sketches in the figure. By taking the vertical load zero the effect of base has been eliminated. It is seen from the comparison of these curves that the shape of scour pit with 15° slope tends to increase the lateral load capacity considerably.

A comparison of lateral load ratios at various tilt values of the two curves is also shown. It is seen that the lateral load ratio is higher initially and tends to become constant as the tilt increases. The increase in the lateral load capacity is about 15% at larger tilts. Theoretical calculations (Arya and Sharda 1973) had shown in case of square wells that a 15° slope of scour around a well could increase the lateral load capacity by more than 100% against that given by a horizontal scour level

at the ultimate load in plastic analysis with coefficient of wall friction $\delta = 0$. The reason for large difference in the values is not known and needs further detailed investigation on this aspect of well problem.

8.4 INSTANTANEOUS POINT OF ROTATION OF WELL DURING TILTING

The position of instantaneous point of rotation in a well foundation subjected to lateral load has been a topic of observation in almost all model tests by research workers. The importance of the location of the instantaneous point of rotation is due to the fact that the direction of a number of forces on a well and the magnitudes of their moments are decided by its position. In the available literature the position of the instantaneous point of rotation has been described mostly along the vertical axis of a well. Its position in the horizontal direction with the axis of well as reference has found little attention. The continuous shifting of instantaneous point of rotation from zero tilt to a tilt where sufficient non-linearity has been achieved for a well was required to be studied under various loading and embedment conditions to develop a suitable analysis.

The position of instantaneous point of rotation with tilt has been studied with 15 cm square well resting on and surrounded by dense sand. Figures 48b and c contain the plots of D_2/D versus tilt and $\bar{x}/B$ versus tilt respectively. D_2 is the ordinate and $\bar{x}$ is the abscissa of the instantaneous point of rotation with centroid of the base of well as the origin. The index sketch shows these positions in two dimension in the figure. These plots

correspond to Test No. 2 and 3 which were performed on 15 cm well with D/B = 1.5, H/B = 3.0 and Q_v = 131 kg. The skin friction was about 21 kg for this depth of embedment and hence this well can be considered as a heavy well as the vertical load transfered to the base in excess of friction will be almost 111 kg.

From D_2/D versus tilt curve in Fig. 48b it is seen that in the first instance D_2 starts from below the base of the well and then rises to be between the base and .05 D above the base in the range of tilts used.

From $\overline{x}/B$ versus tilt curve in Fig 48c it is seen that the instantaneous point of rotation starts at a horizontal distance to the left beyond the heel i.e. 0.6B from the axis of the well and at subsequent tilts it tends to become fixed at a distance of about 0.15B from the axis of the well.

Further Figs. 59b and c show the plots of D_2/D versus tilt and $\overline{x}/D$ vs tilt for Test No. 10 which was performed on 15 cm model with D/B = 1.5, H/B = 2.25. The vertical load in this test was 51 kg so that this well may be considered as a light well as compared with the well having Q_v = 131 kg. The D_2/D vs tilt curve in Fig. 59b shows that in the first instance D_2 starts from below the base and then shifts to base and finally to a position about .09 D above the origin. The $\overline{x}/B$ vs tilt curve in Fig.59c shows that $\overline{x}$ $\overline{x}$ starts from much beyond 0.5 B from the origin and tends to become fixed at about .10B to the left of the axis of well. Figure 133 contains plots of D_2/D vs tilt and $\overline{x}/B$ vs tilt obtained from Test series on 15 cm wooden well with D/B = 1.5 (Table 4). Figure 133a contains the D_2/D vs tilt

plots of all tests in this series with vertical load of 131 kg.
These correspond to Figs. 46b, 48b, 50b and 51c with reference to
Test Nos. 1, 2 and 3, 4 and 5. $\overline{x}/B$ vs tilt for the same set of
tests are contained in Fig. 133b and are plotted from Figs. 46c,
48c, 50c, and 51d. Figures 133c and d contain all plots of D_2/D
vs tilt and $\overline{x}/B$ tilt respectively for this series for vertical
load of 101 kg. The figure number reference for each curve is
indicated on the curve. Figures 133e and f are replotted D_2/D vs
tilt and $\overline{x}/B$ vs tilt curves from Figs. 59b and c for convenience
of reference.

It is interesting to note from these curves that they show
a definite trend of instantaneous point of rotation with tilt.
The instantaneous point of rotation lies close to the base ($D_2 = 0$)
in case of well with highiest vertical load of 131 kg (Fig. 133a).
For smaller vertical loads of 101 kg and 51 kg, D_2 lies between
0.05 D to 0.20 D from the base (Figs. 133b and c). In the ini-
tial stages though all wells of $D/B = 1.5$ as is the case in this
series show a tendency to translate in the direction of lateral
load as indicated by D_2/D starting from a negative value.

The trend of $\overline{x}/B$ vs tilt curves in Figs 133b, d and f
is more or less the same. The point of rotation starts somewhere
beyond 0.5B to the left of well axis (toward the heel) and tends to
stabilize between 0.1 B to 0.15 B from well axis. The trend of
the $\overline{x}/B$ vs tilt curve in this series of tests is indicative of
settlement during tilting of well. The settlement rate is higher
during initial lateral loading causing small tilts and is smaller
at higher tilts due to higher loading. The settlement is probably

due to the fact that with the application of lateral load the
shifting of the base results in disturbance/re-setting of struc-
tural arrangement of the soil particles of the subgrade.

In Figs. 134a to h the coordinates of the instantaneous
point of rotation with tilt have been plotted for all tests in
test series on 15 cm wooden model with depth of embedment of
30 cm i.e. $D/B = 2$ (Table 5). Figure 134a contains the
plots of D_2/D versus θ, curves taken from Figs 61b, 63b, 65b,
67b, 69b, 70c, and are for a vertical load of 131 kg. These
correspond to Test Nos 11 to 16. The plots of $\bar{x}/B$ versus θ for
these tests which are taken from Figs. 61c, 63c, 65c, 67c, 69c
and 70d are plotted in Fig. 134b. Figure 134c, e and g contain
the plots of D_2/D versus θ for various remaining tests in this
test series and Figs. 134d, f and h contain the plots of $\bar{x}/B$
versus θ of these tests respectively. The figure numbers from which
each curve has been plotted is marked on each of the curves. The
vertical load values for which these plots have been made are
also marked in each figure.

It can be seen from D_2/D vs θ curves in Figs. 134a, c, e
and g that the coordinate D_2 of the instantaneous point of
rotation starts from near the base at smaller tilts and than tends
to stabilize between 0.15 D to .25 D at larger tilts. It is
interesting to note that in the wells with $D/B = 2$. Carrying the
heaviest load $Q_v = 131$ kg (Fig. 134a), the instantaneous point
of rotation stabilizes at a higher level than observed for
$Q_v = 131$ kg for $D/B = 1.5$. This is probably due to the reason
that in the former case the depth of embedment is large and s the

skin friction is of the order of 30 kg where as in the latter case it is only 21 kg. The load transfered to the base, therefore, is lesser in the deeper well and which results in its behaving as a lighter well.

The trend of $\overline{x}/B$ vs tilt curves for vertical loads of 131 kg, 101 kg and 51 kg (Figs 134b, d and f) appears to be similar. The $\overline{x}$ coordinate of the instantaneous point of rotation appears to be starting at a distance greater than 0.5 B from the axis of well and then tries to stabilize at about 0.1B from the axis. These results are similar to those obtained with Q_v = 131 kg, 101 kg and 51 kg for 15 cm wells with D/B = 1.5. Thus the wells with heavier loads than the/skin friction, show a tendency to settle with tilting.

The trend of $\overline{x}/B$ vs tilt curve for Q_v = 0 as shown in Fig. 134h however is different. It shows that the well has a tendency to lift off as the tilt is increased. This is indicated by the points lying below the x-axis.

8.5 COMPARISON OF EXPERIMENTAL AND ANALYTICAL VALUES
Evaluation of non-linear Parameters

In the theory presented in Chapter 3, the normal forces P_1 and P_2 on the front and the rear faces respectively are obtained by integrating the horizontal soil reaction on these faces. The horizontal soil reaction is given by

$$p = m_h \, (D_1 - z)^n \, y^r \qquad \qquad \ldots \, (1)$$

where p is the horizontal soil reaction at a depth $(D_1 - z)$ due to a displacement y (Fig. 4), m_h is a modulus of non-linear

horizontal soil reaction and n and r are indices of non-linearity.

To evaluate p, the values of m_h , n and r must be known. These values can be evaluated from the experimental data as follows.

The Eqn. (1) can also be written in the form

$$p = k_h \, y^r \qquad \qquad \dots (1a)$$

where k_h is the coefficient of non-linear horizontal soil reaction at a depth (D_1-z). Comparing the Eqn. (1) and (1a) we see that

$$k_h = m_h \, (D_1-z)^n \qquad \qquad \dots (1b)$$

Taking logarithm of both sides of Eqn (1a) we get

$$Log \, p \; = \; \log k_h + r \log y$$

Thus if the best fit of a non-linear p-y curve is plotted on a logarithmic scale, k_h and r will be given by the intercept and slope of the curve respectively. Similarly from Eqn. (1b), k_h vs (D_1-z) from various tests when plotted on a logarithmic scale will yield the m_h and n as the intercept and slope of the best fit. The procedure adopted for deriving m_h , n and r from the observed data is described below.

Figure 135a shows a pressure "p" vs displacement 'y' plot for various depths $z_1 = (D_1-z)$ points have been obtained from the curvilinear pressure vs depth diagrams of Figs. 45, 47, 49, 52, 54, 56 and 58,   corresponding to Test Nos 1, 2, 4, 6, 7, 9 and 10 in Table 4. Displacement y, at a depth z_1 was calculated from observed points of rotation D_2 and the tilt θ.

Figures 135a and 135b are the p vs y plots for z_1 = 3 cm and 6 cm respectively. It is seen in both the figures that all the points can be approximately bounded by an upper and a lower bound p-y curve. Similarly Fig. 136a shows the upper bound and lower bound p-y curves for z_1 = 9 cm for the above case. When plotted on logarithmic scale as described earlier values of m_h, r and n are obtained for the tests given in Tables 4 and 5. These values are shown below, as also are the equations obtained between pressure and displacement

COMPUTED VALUES OF COEFFICIENT m_h AND INDICES r AND n

Sl. No.	Reference to Tests	m_h in kg and cm units		r	n
		Upper bound	Lower bound		
1	Table 4	.0781	.0568	0.55	1
2	Table 5	.0714	.0535	0.65	1

Upper bound

$$p = .0781 \, z_1 y^{0.55} \qquad \text{for tests of Table 4}$$

$$p = .0714 \, z_1 y^{0.65} \qquad \text{for tests of Table 5}$$

Lower bound

$$p = .0568 \, z_1 y^{0.55} \qquad \text{for tests of Table 4}$$

$$p = .0535 \, z_1 y^{0.65} \qquad \text{for tests of Table 5}$$

In these equations p is in kg/cm², z_1 in cm and y also in cm.

The values m_h, r and n shown in the preceding table are due to the non-linear horizontal soil reaction as shown by the pressure-displacement relationship in Figs. 135a, b and 136a. The values of 'r' obtained for dense sand in laboratory are 0.55 and 0.65. Kubo (1965) has obtained a value r = 0.5 for dense sands.

The value of 'n' has been found to be 1. This is due to the fact that the soil is sandy. Terzaghi (1955) has also suggested this value for sandy soils.

From non-linear p-y relationship obtained in model tests in Figs. 135a, b and 136a for Test Nos. 1 to 10, it is possible to work out an equivalent elastic soil stiffness parameter by considering a secant modulus at an appropriate displacement, Then a direct comparison with the values suggested by Terzaghi (1955) is possible. In dense, sands, the displacement required to achieve passive failure is about 4% of the depth of wall (Rowe and Peaker, 1965). In the case of wells in these studies displacement at the ground level would be 4 % of the distance of the point of rotation from the ground level D_1. It can be seen that in model Test Nos. 1 to 10 the point of rotation lies approximately at a distance of 0.1 D from the base (Fig. 133). The displacement required for failure in Test Nos. 1 to 10, is obtained by substituting D = 22.5 cm thus

Depth of point of rotation   =   0.9 D

                                  =   20.25 cm

Displacement at ground level
at 4 % of 20.25 cm   =   0.8 cm

Displacement required for failure at the depth for which the p-y curves are plotted (z_1 = 3 cm) i.e. distance of 17.25 cm from point of rotation, will therefore be 6.9 mm.

Terzaghi's values of n_h ($m_h = n_h/z$) have been calculated for piles 30.4 cm (1 ft) wide with linear relationship of p-y at half the utilmate load. The ultimate displacement is likely to be 6.9 mm in Fig. 135a of the p-y relations for z_1 = 3 cm. Assuming that half the ultimate load occurs at about 1/3 the displacement i.e. 2.3 mm, the value of k_h can be worked out by extending the p-y curve to 2.3 mm and obtaining the slope of the line passing through this point on the curve and origin for both the upper bound and lower bound curves. The curves extended to 2.3 mm have been shown by dashed lines and the straight line relationship by chain dotted lines in Fig. 135a. The values of k_h for upper bound and lower bound curves work out to .348 and .522 kg/cm^3 for the linear case. Assuming a straight line variation of k_h with depth z_1, we obtain m_h = 0.116 and 0.174 kg/cm^4 for upper bound and lower bound k_h values respectively. The average value works out to 0.145 kg/cm^4. Terzaghi has given a value of n_h, which is equal to m_h x B, as 56 T/ft^3 for 1 ft wide pile in dense sand (1T = 2000 lb). This gives us an n_h value of 1.75 kg/cm^3 and m_h = 0.058 kg/cm^4. Thus values of m_h obtained from the Tests are about /2.5 times the values given by Terzaghi. The difference in Terzaghi's and experimental values may be due to difference in density of sands, which has been taken as 1.6 g/cm^3 by Terzaghi for his calculation of n_h and in our case it is 1.658 g/cm^3. Further, Terzaghi's values have been worked out with

the help of piletest where skin friction in vertical direction is not likely to be mobilized, whereas in wells the skin friction is fully mobilized. Another reason for the increase may be the selection of half value of ultimate load which has been taken approximately as being the load at 1/3 the ultimate displacement.

Thus n_h values by Terzaghi (1955) are quite conservative and are likely to err on the safer side when used for analysing well foundation as is prevelent code practice (I.R.C. 1971).

From the foregoing discussion it appears therefore that the current practice (I.R.C. 1971) of usijg elastic approach for analysing well foundation with Terzaghi's values of n_h is a safe practice and would err on safer side even if no factor of safety is given.

Evaluation of Coefficient of Friction on Faces and Base

For calculating the frictional forces F_1, F_2, F_3, F_4 and F_5 on faces and F_B on the base of the well, the coefficient of friction μ_1 and μ_2 are required. Curve A of Fig. 114a shows that the 15 cm x-section square well with embedment depth $D = 22.5$ cm develops a maximum skin friction of 21 kg at about 1.1 mm displacement inclusive of the self weight of the well ($W = 6.5$ kg). It is evident that any vertical load Q_v greater than 21 kg is likely to mobilize full vertical friction on all faces with the slightest movement. The maximum value of angle of friction along the faces can be taken as the ultimate value of angle of friction since the interlocking between the particles will decrease to the point where continuous shear deformation can

continue without further volume change (Lambe and Whitman, 1973).
The ultimate value of angle of internal friction for the dense
sand used is 33.4^O and hence coefficient of friction can be taken
as Tan 33.4^O or 0.66. Since particles of sand are likely to
move along with well near its face, the coefficient of wall fric-
tion to be used will be the same as coefficient of friction for
sand.

Coefficient of friction 'μ_2' at the base can also be
taken as 0.66 since the base will also have tendency to slide on
sand, when lateral load is applied.

Evaluation Coefficient of Earth Pressure at Rest

The coefficient of earth pressure at rest 'K_O' is
required for calculating the frictional forces F_3, F_4 and F_5 in
the analysis. Since vertical load tests for skin friction are
available (Fig. 114) and the coefficient of friction for the face
is $\mu_1 = 0.66$, it is only proper to work out coefficient of earth
pressure at rest 'K_O' indirectly from these values as these
will be more relevent to the actual test conditions.

Assuming a triangular distribution of at-rest earth-
pressure with depth, the total skin friction Q_S for a rectangu-
lar well is given by the equation

$$Q_S = \mu_1 K_O \Upsilon (L + B) D^2$$

where μ_1, is the coefficient of friction on face, K_O is the
coefficient of earth pressure at rest, Υ the density of sand, L
the length of front/rear face, B the width of side faces and D
the depth of embedment. Curve A of Fig. 114a shows that for the

well with B = L = 15 cm, D = 22.5 cm, and soil density
= 1.658 g/cm³, the maximum skin friction observed is 21 kg.
Thus substituting Q_s = 21 kg, the values of B, L, D and Y, as
given above and μ_1 = 0.66, in the equation for Q_s we get
K_o = 1.265. Formula given by Jaky (1944) for coefficient of
earth pressure at rest K_o = 1 - SinΦ gives us a value of K_o
= 0.320 with Φ_{peak} = 42.5°. The actual K_o value is much
higher than Jaky's value. This may be due to the fact that the
sinking of well through dense sand causes dialatory pressures.

Values of K_o as calculated from curves A, B, D, F
and G of Fig. 114, for various sizes and embedment depth of
models are given in Table 16.

Evaluation of Coefficient of Friction of Faces with Polythene Sheet

Skin friction was reduced with the help of polythene
sheets. The coefficient of friction for this case has been worked
out indirectly as follows. In Figure 114a, curve C has been
obtained from the vertical load test for skin friction on model
with polythene sheet on it. It is seen that the well jsut slips
on its own weight (6.5 kg). Thus skin friction for this case
may be taken as Q_s = 6.5 kg. Assuming that the coefficient of
earth pressure at rest for this case where B = L = 15 cm, D=22.5
cm and Y = 1.658 g/cm³ will be same as for the curve A i.e. K_o
= 1.265 as above, the value of coefficient of friction, for this
case can be worked out from the formula $Q_s = \mu_1 \ K_o \ Y \ (L+B)D^2$.
For this case the value works out to be K_o = .205. The value

of coefficient of friction worked out in this manner for 15 cm
and 20 cm square wells with polythene sheets for various depths
are given in Table 17. In computations for cases of wells with
polythene sheets the average value of coefficient of friction
used has been 0.195 (Table 18). ..

Non-linearity index r' for the subgrade at Base

For calculating the reaction R_B at the base by Eqn.20
in Chapter 3, the contact pressures are to be evaluated. The
subgrade reaction at the base is assumed to be

$$p_B = k_v . \Delta^{r'}$$

... (2)

where p_B is the vertical subgrade reaction of soil at the base,
k_v the modulus of vertical subgrade reaction, Δ, the vertical
displacement and r' an index defining non-linearity.

In all the tests the vertical load transmitted to the
base is considerably smaller in magnitude than the ultimate load
for the dense sand used. Even at the maximum tilt applied in
various tests the pressure at the toe may not exceed the ultimate
bearing pressure due to the sand being dense and confined. This
is also evident from the pressure values indicated in the base
pressure distribution curves of Fig. 45b where by extrapolation
the toe pressure is not likely to exceed about 0.7 kg/cm² while
the safe bearing capacity is about 4 kg/cm². It is therefore
assumed that the pressure settlement relationship will remain
linear and hence the value of r' can be assumed as unity. In all
the calculation thus n has been taken as 1.

Procedure for Computing Lateral Loads

The following procedure has been adopted for calculating lateral loads in a model test for the verification of the analysis presented in Chapter 3. Notation and Eqn. numbers used here are the same as in Chapter 3.

In Chapter 3 it is established that :

For the condition $\sum V = 0$

$$W_B = F_1 \pm F_2 + 2F_3 + R_B \qquad \qquad \dots (24)$$

Where,

$$W_B = Q_v + W \qquad \qquad \dots (3)$$

$$F_1 = \mu_1 P_1 = \mu_1 L m_h \theta^r D_1^{n+r+1} N_1 \qquad \dots (7)$$

$$N_1 = \frac{\sqrt{n+1} \ \sqrt{r+1}}{\sqrt{n+r+2}}$$

$$F_2 = \mu_1 P_2 = \mu_1 L m_h \theta^r D_1^{n+r+1} N_2 \qquad \dots (11)$$

$$N_2 = \int_0^{D_2/D_1} (1 + \psi)^n \psi^r \, d\psi$$

Whence by Simpson's rule

$$N_2 = \frac{D_2}{6D_1} \left[(1 + \frac{D_2}{D_1})^n \ (\frac{D_2}{D_1})^r + 4 \ (1 + \frac{D_2}{2D_1})^n \ (\frac{D_2}{2D_1})^r \right]$$

$$F_3 = \frac{1}{2} \ u_1 \ k_o \ \gamma \ BD^2 \qquad \qquad \dots (13)$$

$$R_B = k_v \frac{B.L}{6} \left[(\Delta_i + x_1\theta)^{r'} + 4 \ (\Delta_i + \overline{x}\theta)^{r'} + (\Delta_i + x_2\theta)^{r'} \right]$$

$$\dots (20)$$

$$x_1 = \bar{x} + B/2$$

$$x_2 = \bar{x} - B/2$$

For the condition $\sum H = 0$,

$$Q = P_1 - P_2 + 2F_4 - 2F_5 - F_B \qquad \qquad \dots (25)$$

Where,

$$P_1 = Lm_h\ \theta^r\ D_1^{n+r+1}\ N_1 \qquad \qquad \dots (5c)$$

$$P_2 = Lm_h\ \theta^r\ D_1^{n+r+1}\ N_2 \qquad \qquad \dots (9b)$$

$$F_4 = \frac{1}{2}\ \mu_1 K_o\ \Upsilon\ BD_1^2 \qquad \qquad \dots (14)$$

$$F_5 = \frac{1}{2}\ \mu_1\ K_o\Upsilon\ B(D^2 - D_1^2) \qquad \qquad \dots (15)$$

$$F_B = \mu_2\ R_B \qquad \qquad \dots (22)$$

For the condition $\sum M$ about $C = 0$,

$$M_o = -M_{P1} + M_{P2} + M_{F1} \mp M_{F2} - 2\ M_{F4} + 2M_{F5} + M_{RB} + M_{FB}$$
$$\dots (26)$$

Where,

$$M_o = Q.\ H$$

$$M_{P1} = Lm_h\ \theta^r\ D_1^{n+r+2}\ N_1\ \ \frac{(n+1)}{(n+r+2)} \qquad \qquad \dots (6b)$$

$$M_{P2} = Lm_h\ \theta^r\ D_1^{n+r+2}\ N_3 \qquad \qquad \dots (10b)$$

$$N_3 = \int^{D_2/D_1} (1+\psi)^n\ \psi^{r+1}\ d\psi$$

or by Simpson's rule

$$N_3 = \frac{D_2}{6D_1}\left[(1 + \frac{D_2}{D_1})^n\ (\frac{D_2}{D_1})^{r+1} + 4\ (1 + \frac{D_2}{2D_1})^n .\ (\frac{D_2}{2D_1})^{r+1} \right.$$

$$M_{F1} = F_1 \cdot B/2 = \mu_1 P_1 \cdot B/2 \qquad \cdots (8)$$

$$M_{F2} = F_2 \cdot B/2 = \mu_1 P_2 \cdot B/2 \qquad \cdots (12)$$

$$M_{F4} = \frac{1}{3} \mu_1 K_o \Upsilon BD_1^3 \qquad \cdots (15)$$

$$M_{F5} = \frac{1}{3} \mu_1 K_o \Upsilon B (D^3 - D_1^3) \qquad \cdots (17)$$

$$M_{FB} = F_B \cdot D \qquad \cdots (23)$$

$$M_{RB} = k_v \frac{B^2 L}{12} \left[(\Delta_i + x_1 \theta)^{r'} - (\Delta_i + x_2 \theta)^{r^1} \right] \qquad \cdots (21)$$

For any solution to be correct all the three equations of statical equilibrium must be satisfied simultaneously.

The position of instantaneous point of rotation has been defined by D_2 as vertical coordinate and $\overline{x}$ as the horizontal coordinate with respect to centroid of the base (p.119). The computations were made by taking observed value of $\overline{x}$ into account and assuming a value of D_2 which would satisfy statical equilibrium conditions.

The following steps describe the computational process adopted.

Step 1:

To start with, the vertical distance D_2 of position of point of rotation was assumed to be zero, i.e. the point of rotation was assumed to lie on the base of well.

Step 2 :

Base reaction R_B was calculated from Eqn 24, by substituting the values of Q_v, W, μ_1, B, L, m_h, n, r, D, K_o and γ and a velue of θ taken from a test with assumed value of D_2 as zero.

Step 3 :

k_v was now computed from Eqn. 20, by substituting the values of B, L, Δ_i, x_1, x_2, $\overline{x}$ and r' of the test. Δ_i was known to be the settlement due to vertical load and x_1, x_2 were calculated from observed values of $\overline{x}$ for the θ value taken in step 2. Here k_v, the modulus of subgrade reaction is a coefficient for uniform loading condition at the base, while the loading condition at the base of the well results in non-uniform pressure condition. Therefore the corresponding modulus needs be used in our analysis. No literature is available on this aspect.

However, Barkan (1962) has suggested ratios which relate coefficient of elastic non-uniform compression (C_ϕ), to the coefficient of elastic uniform compression in case of saturated fine sands. The ratios lie between 1.92 to 2.30 for various areas of footings. Since no values are available for the test conditions included in this study a ratio of 2.30 has been assumed for dense sands in dry condition in these computations. And k_v' has been used in the analysis instead of k_v.

Therefore

$$k_v' = 2.3 \, k_v$$

Step 4 :

F_B was substituted from Eqn. 25 in the moment Eqn. 26 and Q was computed from the resulting moment equation by substituting R_B from step 2 and k_v' from step 3.

Step 5 :

F_B was now computed from Eqn. 25 by substituting the value of Q from step 5. If the mobilization factor, α, at the base is defined by

$$\alpha = \frac{(P_1 - P_2 + 2F_4 - 2F_5) - Q}{F_B}$$

the equilibrium Eqn. 25 needs be satisfied for

$$-1 < \alpha < 1$$

for physical compatibility, $|\alpha| \leq 1$

In case $D_2 = 0$, Eqn. 25 can be satisfied for $|\alpha| \leq 1$ only. If α turns out to be greater than 1, it means that our assumption of $D_2 = 0$ needs modification.

A value of $D_2 > 0$ is now assumed. This will result in some movement of the base. If the sand is assumed to have a rigid plastic behaviour in tests for development of friction at the the base, the value of α should be equal to unity for any value of $D_2 > 0$. Hence the value of D_2 corresponding to $\alpha = 1$ will result in the final solution of the problem.

The method of computing the lateral loads is explained with a numerical example in Appendix.

Comparison of Observed and Computed
Loads and Displacements

Figure 137a shows the points of comparison between measured and computed lateral loads for Test No. 1 which was performed on 15 cm well with $Q_v = 131$ kg, $D/B = 1.5$ and $H/B = 3.0$. Table 4 gives other details. The dark points show the comparison for upper bound m_h values and the squares show the comparison for lower bound m_h values. Figures 137b to f show the comparison of measured and computed lateral loads for Test Nos. 2, 3, 4, 5 and 6. Details of test conditions and Figure reference are given in Table 4. Figure 138a shows the comparison of observed lateral load vs displacement at ground level and the computed lateral loads vs computed displacement at ground level, for Test No. 1. Displacement at ground level was obtained by multiplying the vertical distance between the ground level and the instantaneous point of rotation with tilt θ. The firm curve joining the triangular points is the observed load-displacement curve. The dark circle represent points of computed lateral load displacement for upper bound m_h values and the squares represent the point for lower bound m_h values.

Figures 138b to f show the comparison of measured and computed lateral load vs displacement at ground level (scour level) curves for Test Nos 2, 3, 4, 5 and 6. Details of Test condition and figure references are given in Table 4. The measured and the computed values of lateral loads, and lateral load vs displacement at scour level for different tests for upper and lower bound m_h values have been compared in different figures as tabulated below. Reference to Tables for details of

these tests is also indicated.

Test No.	Table Ref	Comparison of Lateral Loads	Lateral load vs displacement
1 to 6	4	Fig. .137	Fig. 138
7 to 10	4	Fig. 139	Fig. 140
11 to 14	5	Fig. 141	Fig. 142
15 to 20	5	Fig. 143	Fig. 144
23 to 26	5	Fig. 145	Fig. 146

Computation for Tests with zero vertical loads have not been attempted since they are not covered by the theoretical analysis in which skin friction is assumed to be fully mobilized. Figure 147a shows the plots of all the points of comparison between measured and computed lateral loads for 15 cm well with $D/B = 1.5$ and $Q_v = 131$ kg. The bars show the spread of points plotted from Fig. 137a, b, c, d and e for upper and lower values of m_h. The flared lines in Fig. 147a show approximately the trend of computed lateral loads as compared with measured loads. The exact comparison indicated by the $45°$ line lies between the two bounding values . Thus the average value of the computed Q from upper and lower m_h value will lie very close to the exact solution. The average computed value will be slightly to the line. It is indicated upper side of the exact solution/ from the trend that the theory predicts lower values of lateral loads than the actual. Figure 147b shows the plots of all the points of comparison between measured and computed lateral loads for 15 cm well with $D/B = 1.5$ and $Q_v = 101$ kg. In this case the trend appears to be that the theory predicts higher values of lateral loads than the actual

ones. In Fig. 147c and d plots of all the points of comparison between measured and computed lateral loads for 15 cm well with $D/B = 2$ and $Q_V = 131$ kg and 101 kg respectively have been plotted from Figs. 141 and 143.

It is interesting to note that except for Fig. 147a the trend in all the other three figures is that the theory predicts values on the higher side of the actual values of lateral load inspite of the fact that $Q_V = 131$ kg for the plots of Figs. 147a and 147c. This may be due to the reason that due to greater depths in case of Fig. 147c the skin friction is of the order of 30 kg where as it is only about 21 kg for Fig. 147a. Thus the well of Fig. 147c is lighter as compared with that for Fig. 147a. This is also the case with Figs. 147b, and d.

Therefore it can be concluded that for heavier well the theory predicts lateral loads on the lower side of the actual values and on the ⟨higher⟩ side for lighter wells. From Figs. 145a, b, c and d which show the comparison of observed and computed lateral load for $Q_V = 51$ kg for $D/B = 2$ of the 15 cm well also confirms this trend. Figs 145 c and d are however conspicuous by the fact that computed loads are on very much higher side than the measured ones. The reason for this may be that the values of m_h, used for all computation, may be on the higher side of the actual ones in case of smooth faces

8.6 DEVELOPMENT OF FRICTION ON WALLS AND BASE OF WELL

Pressures on faces and base of well models have been observed by some authors (Kapoor 1971) in their studies but friction and its development at different spots on faces and

base of a well model have not been observed so far/and its deve-
lopment on faces and base of well models were observed with frie-
tions cells on 20 cm mild steel model.

Friction on Front and Rear Face

Figures 92 and 93 show the magnitudes of frictional
forces and their direction as obtained from Test Nos. 46, 47
and Test Nos. 48, 49 respectively on 20 cm mild steel well. In
each case, the vertical load of 131 kg was applied beforehand.
The friction values were measured for various values of lateral
load Q. The frictional force on front face is drawn in the
figures by firm lines and on the rear face by dashed lines. As
a convention, shear stress diagrams to the right of the vertical
axis indicate upward direction of the frictional force on a face
and those to the left downward direction. It can be seen that
large frictional force acts on front and rear faces of a well
when lateral load is applied. The direction of the frictional
force is upward on the front face and its distribution is curvi-
linear with depth. However, in case of rear face the direction
of frictional force is seen to be downward in the case of well
with H/B = 3 (see Fig. 92) and upward in well with H/B = 2.25,
(see Fig. 93). This is indicative of upward movement of rear
face under large overturning moment of H/B = 3. More data is,
however, required to draw any conclusion regarding direction of
friction near the base on the rear face. The figures however
conclusively point to the fact that frictional forces do act on
front and rear faces and they increase with increasing lateral
load. Their distribution being curvilinear with depth seems to

be in conformity with the observation of lateral pressures on front face also being curvilinear as seen earlier, since frictional force is a product of normal pressure and the coefficient of friction.

Figures 94 and 95 show the distribution of frictional force indicated as shear stress with depth on front face for wells with a smaller vertical load (Q_v = 56 kg) and no vertical load (Q_v = O) respectively. It can be seen that the distribution of shear stress, again, is curvilinear and is in conformity with lateral pressures.

Figure 96 shows the distribution of frictional force with depth on front face in case of Test No. 52 with sloping surcharge. Friction on rear face were not obtained. Here also a curvilinear distribution of frictional forces is seen on faces. It is also observed from Figs. 92 to 94, which are for wells with heavier loads, that the peak point of the curvilinear distribution is at a greater depth than for those with no vertical loads as shown in Figs. 95 and 96. As seen earlier, the point of rotation of the well carrying larger vertical loads is near the base and shifts upwards with decreasing vertical load. Correspondingly, the point of maximum lateral earth pressure on front face also shifts upwards with decrease in vertical load. The observed friction distribution is qualitatively in line with the lateral pressure distribution.

Friction on Side Face

Figures 97a, 98a, 99a, 100a, 101a and 102a, show the mobilization of horizontal friction on side face of a well model.

It is observed that as the lateral load is increased the friction is fully mobilized in the portion nearer to the ground as indicated by curve F-4 in these figures whereas it is only partly mobilized at lower levels. Also, the direction of frictional force is opposite to the direction of lateral force in the portion near the ground level (see curve F-4) whereas it is generally in the same direction as the applied force in the portion close to the base of the well. This suggests that the well moves in the direction of lateral load at its upper portion and opposite to it in the lower portion. It is also seen that frictional stresses recorded by cells F-5 and F-6 show somewhat erratic variation with lateral load. This may be due to changing positions of the point of rotation with the increasing load and adjustment of soil particles during the movement of the well. The maximum value of frictional stress mobilised at location of cell F-4 in various tests is given below.

Test No	Figure No.	Maximum Shear Stress kg/cm²	Test No.	Figure No.	Maximum shear stress kg/cm²
53	97(a)	0.0202	56	100(a)	.0164
54	98(a)	0.0202	57	101(a)	.0144
55	99(a)	0.0202	58	102(a)	.0122

Thus we obtain a maximum value of frictional stress of .0202 kg/cm² and minimum value of .0122 kg/cm². Now shear stress is equal to coefficient of friction times the normal stress, knowing the frictional stress, normal stress could be computed if coefficient of friction is known. The movement observed in the

model in these cases may be taken as that for the ultimate condition in a direct shear box test when the interlocking between the soil particles has decreased to the point where shear deformation can continue without further volume change. Lambe and Whitman (1973) suggest that in case of smooth surfaces such as in case of sand sliding against unrusted steel, the friction angle is most likely equal to Φ_u for the sand. Considering our case to be similar and considering the Φ_u value in the case of Ranipur sand as 33.4° we get coefficient of friction as 0.66 and thus we obtain from maximum and minimum shear stress values as:

Maximum normal stress = 0.3060 kg/cm²

Minimum normal stress = 0.1850 kg/cm²

This can be taken as earth pressure atrest at a depth of 7.5 cm from ground level i.e. the depth of centre of cell F-4.

We know that earth pressure at rest $p = k_o \gamma z_1$ where K_o is the coefficient of earth pressure at rest, γ is the unit weight of soil and z the depth of the point, under consideration, from the ground level . Now substituting $\gamma = 1.658$ g/cm³, $z_1 = 7.5$ cm and the values of maximum, and minimum normal pressures respectively in the above equation we obtain K_o as below

Normal pressure (p) kg/cm²	$K_o = p/\gamma z_1$	Remarks
0.3060	2.460	Maximum value
0.1850	1.465	Minimum value

The coefficient of earth pressures at rest, in case of dense sand used in the tests, as worked out from skin friction on side faces (Table 16) ranges from 0.875 to 1.84 and ranges from 1.465 to 2.460 as obtained from friction cell readings and calculated in this section. This variation in the value of K_o can be attributed to the fact that the values have been derived from various model wells and under different loading conditions. It is likely that the skin friction developed changes the steess conditions in the soil in the vicinity of the well faces thereby leading to varying lateral pressures. It is felt that these aspects should be further investigated using stress measurement in the soil. However, it will be readily noticed that the values of k_o are more than that suggested by Jaky (1944) which works out to 0.325 with $\Phi = 42.5^o$. Mackey and Kirk (1967) have reported $K_o = 3.42$ in dense sands. It is therefore appropriate to believe that the coefficient of earthpressure at rest is affected by the relative movement of structure without lateral displacement and the soil. It appears therefore that at rest pressure which decides the frictional forces F_3, F_4 and F_5 Eqns. 13, 14, 16 of Chapter 3 is an important factor and adds to the resisting forces.

Friction at the Base

Curves F-9 and F-10 of Figs. 97a, 98a, 99a, 100a, 101a and 102a represent the mobilization of friction at the base of well near the toe and the heel respectively. The location of the curve above the x-axis (displacement) is indicative of frictional force being in the same direction as the lateral load whereas points below the displacement axis represent friction in the opposite

direction. It is seen that in all these cases the friction near the toe (curve F-10) is in the same direction as the lateral load. The friction near the heel (curve F-9) for cases where greater vertical load is transferred to the base (Figs. 97b, 98b and 99b) is first mobilized in the same direction as that for the toe and then it starts reducing to zero. In fact the curves F-10 and F-9 are seen to coincide in the initial stages of tilts. This suggests that in the initial stages the mobilization throughout the base is uniform and as the tilt increases the heel has a tendency of a lifting up accompanied by a reduction in normal pressure whereas the toe pressure goes on increasing thereby increasing the friction with its movement. The horizontality of the curve at the end suggests that full frictional force is mobilized near the base of toe at a displacement of/about 1.1 to 1.2 mm. The drooping of curve F-9 to that below the displacement axis suggests that probably there are some unknown and erratic soil movements as the soil gets disturbed due to rotation. Figures 101b and 102b which are for zero vertical loads show that the friction near the heel is directed in the opposite direction to that near the toe. This again may be due to erratic movement of soil particles when the soil at the base is disturbed by lift off of the heel with rotation in this case.

Comparison of Friction mobilization with Direct Shear Curve

In Fig. 148 the mobilization curves F-4 of side face and F-10 of base of Figs. 97a and b and Figs. 98a and b respectively and curves F-4 of Figs./100a, 101a and 102a have been
99a,

compared with that from Direct Shear test. The percentage
mobilization of friction was calculated by dividing the fric-
tional resistance at any displcaement by the ultimate frictional
resistance. It is interesting to note that the mobilization
curves of side face and base follow the trend of mobilization
curve obtained from Direct Shear test. The mobilization curves
of side face and base are steeper than $\angle$ that of Direct Shear test mobi-
lization curve and the full mobilization is achieved at a lesser
displacement of about 1.2 mm as against 1.5 mm of the direct shear.
The difference in mobilization curves may be attributed to
different confining conditions in various cases.

8.7 RUPTURE IN SOIL AROUND A WELL

Figures 116, 117 and 118 show the failure outcrops that
is caused in the surrounding soil of a well when maximum lateral
load is applied. The shell shaped heaving to the right of the
well is due to passive failure caused by the rotational displcaement
of the front face. The small closed curves to the left of the
section of well are outlines of hollows formed due to active
failure in sand caused by rotational displacement of the rear
face. However in Fig. 118a, a larger shell shaped heaving
beyond the depression is seen. This is caused by pushing out
of the soil near the heel due to excessive rotation of well. It
is interesting to note that the soil adjoining the side faces
does not seem to be affected in all the figures except Fig.117b.
In this figure, which is represntative of a diamond shaped cross
section of well, the outcrops for passive and active zones start
from the two ends of the diagonal.

Figure 115 shows a photograph of a typical failure out-crop obtained in test No. 111. In Figs. 116a, b, and c, and 118b, and c, extra outcrops are observed within the outer most passive outcrop. This may be due to the fact that the dense soil nearer the ground level dialates faster due to low confining pressure. Thus the passive failure appears to be a progressive phenomenon in these cases.

From the outcrop of passive zones and active zones of all these figures except Fig. 117b for the case of diamond section well, it appears that there is little effect of various embedment conditions and loading on the failure outcrops. It also suggests that resistance from soil around the well at ultimate lateral load is provided mainly by the layers near the ground.

The maximum distance of passive zone outcrop from the front face, x_p, its maximum width (L_p) parallel to length of the frontface L, and the maximum distance of active zone depression from rear face x_a, and its width L_a have been worked out in terms of the length of the front and rear face L, $\angle$ The distances in Table 15. x_p, L_p, x_a, L_a are indicated in Fig. 116a. For the diamond shaped x-section well also, these values have been worked out by taking the distance x_p and x_a from the diagonal perpendicular to the direction of lateral load. It is noted that the maximum distance to which a passive zone outcrop extends is x_p = 1.2L to 1.266L. and its width is L_p = 1.468L to 1.6L. The values for active zone are x_a = 0.389L to .0633L and L_a = 1.0L to 1.2L. For the diamond cross section these values work out to x_p = 1.41L, L_p = 2.12L, x_a = 1.07L and L_a = 1.225L. Here L is

the projected length of the faces along the diagonal as shown in Fig. 117b.

8.8 DYNAMIC RESPONSE

Free Vibration Tests

Free vibration tests were carried out on 15cm and 20cm wells to get an insight into the following:- (a) the resistance of the soil medium to deformation when the well vibrates, (b) the damping in the system and (c) the total mass including the virtual mass of soil participating in vibrations.

Some typical records of free vibrations of wells are shown in Fig. 113. These are for 15 cm well model. From the records of free vibration test on wells the natural frequency and the damping factors have been computed (p. 99) and are tabulated in Table 14.

It has been observed from these results that when the vertical load on the well exceeds the frictional resistance of the sides, the natural frequency as well as damping value get reduced. The reduction of frequency is due to decrease of lateral stiffness after friction is fully mobilised. For instance higher frequency is observed in natural frequency column No. 5 of Table 14 for Test Nos. 71, 74, 78, 81, 84, 88, 92, 96 and 100. For cases when the loads are greater than the skin resistance further increase in loads would cause higher stressing of the soil below the well and so in addition to the non-linearity in the soil, it is also likely that larger soil mass would be participating in vibration, both factors leading to

smaller natural frequencies as observed in Table 14 column 5 for Test Nos. 69, 70, 72, 73, 75 to 77, 79, 80, 82, 83, 85 to 87, 89 to 91, 93 to 95, and 97 to 99.

Also when the loads on the well are smaller than the total skin resistance, the damping forces would be due to the side soil as well as the soil below the base of the well. But once the extra damping force from the side is removed due to the application of larger vertical loads the damping in the system reduces as observed in Table 14 column 6 for Test Nos. 69, 70, 72, 73, 75 to 77, 79, 80, 82, 83, 85 to 87, 89 to 91, 93 to 95 and 97 to 99.

Therefore it can be concluded on the basis of these studies that, as the wells are not in general held wholly by skin friction, the soil below the base would contribute substantially to the dynamic response of wells.

The values of natural frequencies and damping factors in Table 14 show that the damping factors in case of wells held by friction only in dense sand lie between 11.50 and 23% with an average value of 18.42 %. In case of wells carrying heavier loads than the skin friction, the damping factors lie between 5.34 and 16.4% with an average value of 10.5 %.

Cyclic and Repetitive Lateral Load Tests

Figures 103 to 112 clearly show that the response under all conditions of loading, embedment and friction is a hysteretic systems of non-linear nature. The loops are not well defined in the initial stages in a few cases. This may be due to readjustment of soil around the well causing erratic movement of

the model. As the displacement increases the loops are well defined and a skeleton curve through the peak points can be distinctly drawn. The loops show that considerable energy is dissipated when cyclic motion is imparted to a model. They also show that the tilt once acquired due to lateral loading becomes permanent and there is very little elastic rebound.

Hudson (1965) has shown that by equating the energy loss per cycle in a hysteretic system to the energy loss per cycle in the corresponding small amplitude linear system an equivalent viscous damping coefficient (ξ_{eq})can be defined which will permit accurate calculations of the maximum amplitude of resonant vibrations in hysteretic systems which are strongly non-linear. Back bone or the characteristic curve in a non-linear hysteretic system has been described by Jennings (1963) by the following equation

$$\frac{x}{x_y} = \frac{Q}{Q_y} + \beta \left(\frac{Q}{Q_y} \right)^s \qquad \qquad \cdots (27)$$

where x = displacement of structure

x_y = characteristics displacement

Q = restoring force

Q_y = characteristic force

β = positive constant

s = positive odd integer greater than one

Using Jenning's Eqn. 27, Hudson (1965) has given the equation for equivalent viscous damping of the system as

$$\xi_{eq} = \frac{\frac{2\beta}{\pi} \left(\frac{s-1}{s+1} \right) \left(\frac{Q_m}{Q_y} \right)^{s-1}}{\left[1 + \beta \left(\frac{Q_m}{Q_y} \right)^{s-1} \right]^2} \qquad \qquad \cdots (28)$$

where Q_m is the maximum force for the maximum displacement. To find the values of s and β that gives the best fit between Eqn. 27 and experimental data, a logarithmic plot is made of the departure from linearity of the deflection (x) versus the applied force Q. From Eqn. 27 it is seen that the logarithm of the departure from linearity is $\log \beta + s \log (Q/Qy)$. Thus β and s are the intercept and slope of the strainght line which fits best the data of this logarithm plot.

Table 18 shows various data and the values of ξ_{eq} obtained from the hysteretic curves of Figs. 103 to 112 by using the method explained above. The portion of the characteristic curve above the origin $\angle$ only was used for calculation as a matter of convenience. The method of calculation of β and s and other values involved in the Eqns. 27 and 28 is shown in Figs. 149a,b, and c. From Table 18 it is observed that for high yield ratios ie x_m/x_y 10.80 to 20,equivalent viscous damping is between 6.43 % to 4.26%. And for yield ratios between 2.81 to 9.35 equivalent viscous friction is beteeen 7.08% to 8.83%. These results more or less compare with the findings of Hudson (1960).

8.9 PRACTICAL APPLICATION OF THE ANALYSIS

In Chapter 3, the three equations of statical equilibrium are given for solving the well foundation problem under lateral loads. Both the design problem and the analysis problem (Chapter 1) can be reduced to three unknown quantities and the same can be solved by the equations of equilibrium.

The problem of analysis is simple to solve since the depth

depth D of well is known and the three unknowns $\bar{x}, D_2$ and the lateral load Q can be computed by satisfying the equations as given in the analysis in Chapter 3.

The problem of design also can be solved by these equations however difficulty will arise in that the solution will have to be obtained by trial and error since the term D will appear with higher powers.

The main difficulty in solving a practical problem will however be in obtaining the soil coefficient and indices defining non-linearity of soil in situ since these are not/available. Methods will have to be developed to get these values if the analysis is to be applied to field problems.

readily

8.10 FIELD WELL MODEL

Response of the Field Model

The general behavioural pattern of the field model has been studied with reference to the relationships of lateral load and instantaneous point of rotation with angle of tilt. Figure 121a shows the lateral load versus tilt plot when the field model was tested for the first time corresponding to Test No. 124. The test conditions are given in the index sketch. It is seen that the lateral load versus tilt relationship is non-linear, similar to the trend observed in laboratory models. The rate of increase of tilt is higher at higher loads. The last point on the curve corresponds to a lateral load of 2010 kg and a tilt of 123×10^{-5} radians. At this stage the well tended to tilt too rapidly and the testing was stopped so as to carry out other tests also. In the same figure the point A_o shows unloading state when

lateral load was completely removed except that due to self weight of loading beam. The initial tilt corresponding to the self weight of the loading beam was about 8×10^{-5} radians but the final is about 87×10^{-5} radians. This suggests that well has not returned back to its original position. This is possibly due to the fact that displacement required to mobilize friction is not recoverable.

Figure 122a shows the lateral load vs tilt plotted for Test No. 125 which was performed after but otherwise under same conditions as Test No. 124. The curve therefore will start at the position A_0 of Fig. 121a. It is seen that the general trend of the curve is same as that in Fig. 121a except that the well has now taken slightly more lateral load and has tilted to a lesser extent before it started slipping. This increase in load may be due to the fact that stiffness of the surrounding soil has improved due to first loading on the well in Test No. 124. It may therefore be infered that a well will acquire an irrecoverable tilt, once it is disturbed due to lateral load causing some movement at the base and also that the lateral load capacity is not oaffected   an initial tilt.

Figure 121b shows the coordinates of the instantaneous point of rotation with tilt observed in Test Nos. 124, in terms of D_2/D. It is seen that the vertical coordinate D_2 starts from a point above the base in the initial stages and then stabilizes at $0.3D$. This may be due to initial readjustment of soil surrounding the well and the soil conditions being non-homogeneous.

Figure 121c shows the plot of horizontal coordinate $\bar{x}/B$ with tilt. It is seen that the point of rotation starts beyond 0.5B from the axis of well and gradually tends to stabilize at 0.18 B. This trend is similar to that observed in laboratory models. This shows that there is settlement initlally when lateral load is applied.

Figure 122b, and c are the plots of D_2/D vs tilt and $\bar{x}/B$ vs tilt respectively for Test No. 125. From Fig.122b it is seen that the point of rotation starts at the base and tends to stabilize between 0.05D to 0.2D. This observation is similar to those observed in laboratory models. This however is different from observation in Fig. 121b where the point of rotation starts from above the base. The sliping in the direction of the lateral load in the initial stages in Fig. 122b may be to the permanent tilt of base acquired in the direction of lateral load due to the loading in Test No. 124.

From Fig. 122c it is seen that the trend of the horizontal coordinate of the instantaneous point of rotation is almost same as observed in Fig. 121c, the only change being that settlements are comparatively lesser. This may be due to the reason that the soil may have become stiffer due to earlier loading in Test No. 124.

Thus briefly it can be said that there is a similarity in the performance of small and large model of well as far as ins- tantaneous point of rotation is concerned. Also the base friction in large models $\underset{\diagup}{\overset{\text{may be}}{}}$ mobilized at a much smaller tilt than in laboratory model. This may be due to the reason that mobilization

of shear force requires an absolute movement approximately given
by displacements in a direct shear box and therefore larger wells
which have greater depths require smaller tilts for displacement
for mobilization
required /at the base as compared with small wells if point of
rotation is at same relative distance from the base.

Figure 123a shows the lateral pressure distribution on
front and rear faces in Test No. 124. The pressures near the
ground level are larger and near mid depth very small. Again,
they are larger near the base. This may be due to the fact that
the soil near the ground level and near the base level is stiff
as borne out by the N_{spt} performed at site Appendix (Fig.I-C).
The pressure distribution with depth qualitatively shows a trend
which is similar to that observed in smaller models. However
since the soil around the well is not uniform it may not be
proper to use these curves for obtaining the non-linear equation
for solving this problem analytically.

Figure 123b shows the base pressures along the centroidal
axis for Test No. 124. The base pressures appear to be concave
upward and are seen to be increasing at the toe of the base and
decreasing at its heel with increasing lateral loads and conse-
quent tilts.

Figures 124a to d show pressure distribution on faces and
base in a horizontal direction at right angles to the direction of
Some
lateral load. The pressure distribution appearsto be convex in /cases
and convex in others.

Figure 125 shows the distribution of frictional force in terms of shear stress with depth for Test No. 124. It is seen that the distribution is similar to those observed in laboratory model tests and frictional forces act in an upward direction on front face as well as on the rear face.

Free Vibration Tests

The purpose of these tests was to ensure whether the well could be treated as a single or two degree freedom system and also to find out damping characteristic. The free vibration records (Fig.120) shows probable presence of higher modes and are not indicative of purely sinusoidal motion. This may be due to variation of soil properties around the well, the loading arrangements etc and hence only very general conclusions can be drawn. It seems that the first natural frequency for the H/B ratio of 2.25 lies in the neighbourhood of 15 H_z and that the damping factor around 7 to 15 % (Table 19). These are fairly well corroborated by the model tests also.

Observed and Computed Lateral Loads

Although it was not possible to get the non-linear stiffness equation for soil in field model test, lateral loads have been computed from the theoretical equation by taking some data of field test and some by judgement.

From field test the following data is available

$B = L = 1.5$ m $\qquad$ $D = 2.25$ m

$H = 3.375$ $\qquad$ $Q_V = 6$ Tonne

$W = 6.5$ Tonne $\qquad$ $\Delta_i = 10.7 \times 10^{-2}$ cm

$\Phi = 30^{\circ}$

and the values of $\bar{x}$ for various tilts are (Fig. 121c).

θ (rad)	$\bar{x}$ (cm)
13×10^{-5}	0.65 B
22×10^{-5}	0.49 B
22×10^{-5}	0.49 B
40.5×10^{-5}	0.36 B
72×10^{-5}	0.27 B
123×10^{-5}	0.18 B

Since the soil was in a flooded state and in loose condition around the well due to excavation, We may assume $\gamma = 1.6 g/cm^3$ and coefficient of wall friction $\mu_1 = \tan \delta - \tan (\frac{2}{3} \Phi)$ = $\tan 20^o = 0.36$. Also coefficient of friction at base/can be assumed as $\mu_2 = 0.36$. K_o can be obtained by the Jaky's Eqn. as $(1 - \sin \Phi) = 0.5$ for $\Phi = 30^o$.

Using the data above and the values of $n = 1$, $r = 0.5$ and $r' = 1$ (Fig. 119) it has been possible to compute lateral loads, for different assumed/values of m_h, as in case of laboratory model tests with modification factor for coefficient of subgrade reaction as 1.2. Computed values are compared with the observed ones in the table on next page.

It is seen that the observed values of Q lie between those computed by $m_h = .0032$ kg-cm units and $m_h = .0064$ (kg-cm units). Thus the correct value of m_h must lie between these two values. These m_h values are about 1/9 to 1/15 of those observed in model test in dense sand. This may be due to the reason/that the soil in field was a medium saturated sand which

COMPARISON OF OBSERVED AND COMPUTED VALUES OF
FIELD MODEL WELL FOR TEST No. 124

Obs. No.	$10^{-5} \theta$ rad	OBSERVED Q(kg)	Computed Q (kg)	
			$m_h = .0032$	$m_h = .0064$
1	13	400	718.43	954.73
2	22	808	886.83	1183.23
3	40.5	1228	1167.33	1518.39
4	72	1675	1531.89	1912.75
5	123	2010	2089.07	2552.36

could have a m_h value much lower than the dense sand as has
been observed by Terzaghi/also in his n_h values of soils of
varying densities.
(1955)

C H A P T E R 9

CONCLUSIONS AND SUGGESTION FOR FURTHER RESEARCH

9.1 CONCLUSIONS

Based on the analytical and experimental study reported in the previous chapters, following conclusions may be drawn.

1. A theory for analysing well foundations which takes into account the non-linear behaviour of soil on sides and base has been successfully developed and varified in case of square-models embedded in homogeneous dense sand.

2. The instantaneous point of rotation starts at the base at a distance more than 0.5B from axis of well and stabilizes between .05 D to .25D above the base and at a distance of between .1B to .2B from the axis.

3. It has been observed and substantiated by computations that the lateral load capacity of well increases with increase in vertical load, depth, and size and decreases with larger moments under same lateral loads.

4. Lateral load capacity of a well decreases when side faces have low friction. The lateral load capacity in a square well may decrease by about 28 % when all of its faces are having low friction.

5. Lateral load capacity is augmented with an increase in the stiffness of the subgrade and also with an inclined sur-charge at ground level, as in case of scour pit around a well.

6. Lateral pressure distribution with depth on the front and rear vertical face is curvilinear. The normal pressure distribution along the centroidal axis for the base may be taken as convex downward.

7. Friction on front face with depth is curvilinear and acts in the upward direction. Friction on the rear face may act in either upward or downward direction depending on the embedment and moment conditions.

8. Friction on side faces mobilizes with increasing tilt. Friction is fully mobilized upto about half the distance of the point of rotation below ground level. Friction is mobilized only partly in the vicinity of the point of rotation. Friction on the side faces above the point of rotation acts in the direction opposite to the lateral force. Friction below the point of rotation acts in the direction of lateral force.

9. Friction at the base is mobilized gradually. Full friction is mobilized when the base has moved by an amount approximately required for full mobilization in a direct shear box. The friction in the rear half of the base gradually dies out with increasing tilt.

10. The maximum distance to which the soil against the front face is affected at failure under horizontal load in a well is about 1.25 times the width of the face. The soil adjacent to the side face does not fail at any stage of the tilt of well.

11. Damping factor is high for a well having vertical load smaller than the skin friction and is low when loads are higher.

9.2   SUGGESTIONS FOR FURTHER RESEARCH

The determination of lateral load resistance of well foundation is a complex problem. Investigations reported in this work have contributed only to some extent to the understanding of the problem. Laboratory and field model test have shown encouraging results. The Instrumentation has also been found to be useful. Small models have the limitation of space for using adequate number of transducers. It is therefore suggested that larger models may be used with adequate number of instruments to get maximum data about pressure and friction. The work can be extended to medium sands, silty sands, saturated silty sands and clays and combination of different subgrades at the base and surrounding soils.

Wells of the size of the field model are conveniently made. Large artificial sand beds can be used to test these wells in a more familiear condition of soil deposits. Tests should be performed on circular and double - D swells also.

It would be preferable to have transducers which serve both as a pressure cell and a friction cell to obtain pressure and friction force at a point simultaneously.

Effort may be directed to obtain non-linear coefficients of field soils.

Since many of the well foundations are located in active seismic areas, detailed experimental and analytical investigation of the dynamics of such foundations should be undertaken. Stress measurements within the soil is felt necessary for a physical understanding of the mechanism involved.

REFERENCES

1. Arthur, J.R.F., and Roscoe, K.H., (1961), "An Earthpressure Cell for the Measurement of Normal, and Shear Stresses", Civil Engineering and Public Works Review, Vol. 56, No.659, pp. 765-770.

2. Arya, A.S., and Sharda, S.C., (1974), "Lateral Load Resistance of Well Foundations", Bridge and Structural Engineer, Vol. 4, No. 3, Sept. 1974.

3. Balwant Rao, B., (1970), Discussions on "Wells Subjected to Horizontal Forces - A Model Study" by Sankaran and Muthukrishniah (1969), Journal of The Indian Roads Congress, Vol. XXXII-4, p. 740.

4. Balwant Rao, B., and Muthuswamy, C., (1963), "Considerations in the Design and Sinking of Well Foundations for Bridge Piers", Journal of the Indian Roads Congress, Vol. XXVII-3.

5. Banerjee, A., (1970), Discussions on "Wells Subjected to Horizontal Forces - A Model Study" by Sankaran and Muthukrishniah (1969), Jnl. of the Indian Roads Congress, Vol. XXXII - 4, p. 744.

6. Banerjee, A., and Gangopadhyay, S., (1960), "Study on the Stability of Well Foundations for Major Bridges", Jnl. of the Indian Roads Congress, Paper No. 226, Vol. XXV, part 2, pp. 163-184.

7. Barkan, D.D., (1962), "Dynamics of Bases and Foundations", Mc Graw-Hill Book Company, Inc., New York, p. 33.

8. Bhagat, S., (1967), "Well Foundations for Concrete Bridges", International Symposium on Concrete Bridge Design", ACI Publication SP-23, p. 763.

9. Biarez, J., and Capelle, J.F., (1961), "Contribution to the Study of the Rotation of Foundations and the Observation of the Rotation of Block of Foundations", Proceedings of the Fifth International Conference on Soil Mechanics and Foundation Engineering, Vol. II, pp. 367-371

10. Chae, Y.S., Hall, J.R. and Richart, F.E.,(1965), "Dynamic Pressure Distribution Beneath a Vibrating Footing", Proceeding of the Sixth International Conference on Soil Mechanics and Foundation Engineering, Vol. II, p. 24.

11. Chambers, J., (1945), "The Design and Construction of the Purnabhava Bridge", Jnl. of The Indian Roads Congress, Paper No. 103, Vol. X-1.

12. Chowdhary, R.N.,(1967), "Design of Well Foundations for Eccentric Loads", Jnl. of Indian SNational Society of Soil Mechanics and Foundation Engineering, Vol. 6, No.4, p. 413.

13. Davisson, M.T., and Prakash, S., (1963), "A Review of Soil-Pole Behaviour", Highway Research Board Bulletin.

14. Gales, R.R., (1917), "The Hardinge Bridge over the Lower Ganges at Sara", Minutes of the Proceedings of the Institution of Civil Engineers U.K., Vol. CCV, Part I, p. 18.

15. Heuckel, S., Kwasmewski, J., and Baran, L., (1965), "Distribution of Passive Earth Pressures on the Surface of a Square Vertical Plate Embedded in Soil", Proceeding of the Sixth International Conference on Soil Mechanics and Foundation Engineering, Canada, Vol. II, p. 381.

16. Hetenyi, M.,(1960), "Hand Book of Experimental Stress Analysis", John Wiley and Sons, Inc., New York, p. 6.

17. Horn, A.,(1970), "Sohlreibung Und Raumlicher Erdwiderstand bei Massiven Grunungen in Nichtbindigem Boden", Institut fur Verkehrswarserbau, Graundbau Und Boden Mechanik, Technische Hochschule, Aachen, W. Germany.

18. Hudson, D.E., (1965), "Equivalent Viscous Friction For Hysteretic Systems with Earthquake like Excitations", Third World Conference on Earthquake Engineering, New Zealand, Vol. II, p. II-185.

19. Indian Railways,(1941), "Pier and Abutment Code", Railway Board, Ministry of Railways, Government of India.

20. Indian Railways,(1963), "Standard Bridge Substructure Code", Railway Board, Ministry of Railways, Government of India.

21. Indian Roads Congress,(1937, 1956, 1958), "Standard Specifications and Code of Practice for Road Bridges in India", Indian Roads Congress, New Delhi, India.

22. Indian Roads Congress, (1971), "Recommendations of the Sub-Committee of IRC for Calculating the Side Resistance of Wells", Indian Roads Congress, New Delhi, India.

23. Jaky, J.,(1944), "The Coefficient of Earth Pressure at Rest", Journal of the Society of Hungarian Architects and Engineers, pp. 355-358.

24. Jennings, Paul, C.,(1963), "Response of Simple Yielding Structures to Earthquake Excitation", Ph.D. Thesis, California Institute of Technology, OPasadena, California.

25. Kapoor, R., (1971), "Lateral Stability Analysis of Well Foundations", Ph.D. Thesis, Deptt. of Civil Engineering, University of Roorkee, Roorkee.

26. Katti, R.K., Deokule, S.D, and Vyas, J.N., (1972), "Soil Structure Inter- tion of Well Foundations, Model Studies", Indian Geotechnical Journal, Vol.2, No.1, pp. 41-53.

27. Kondner, R.L., and Cunningham, (1963), "Lateral Stability of Rigid Poles Partially Embedded in Sand", HRB Record No. 39, Highway Research Board, Washington, USA, p. 49.

28. Kondner, R.L. and Zelasko,(1963), "A Hyperbolic Stress-Strain Relation for sands", Proc. 2nd Pan American Conference Soil Mechanics and Foundation Engineering, Vol.1, p. 289.

29. Kubo, K.,(1965), "Experimental Study of the Behaviour of Laterally Loaded Piles", Proc. VI International Conference of S.M. and F.E. Montreal, Vol. 12, pp. 275-279,

30. Lacey, G.,(1929), "Stable Channels in Alluvium", Minutes of the Proceedings of the Institution of Civil Engineers, U.K., Vol. 229, Part I.

31. Lambe, T.W. and Whitman, R.V.,(1973), "Soil Mechanics, Wiley Eastern Private Limited, New Delhi, Ch. 11, pp. 144-145.

32. Lazard, A.,(1957), "Limit of Overturning Moment of Isolated Foundations", Proceeding, IV Int. Conf. on Soil Mechanics and Foundation Engineering, London, Vol 1, pp, 349-354.

33. Mackey, R.D. and Kirk, D.P.,(1967), "At Rest Active and Passive Earth Pressures", Proceedings of the Southeast Asian Regional Conference on Soil Engineering, p. 184.

34. Menard, L.,(1963), "Calcul de la Force Portanleds Foundations Sur la base des resultates des enais Prenionetriques", Sols Soils, V.2, No. 5,6,pp. 9-32.

35. Murthy, V.N.S. and Kapur, C.,(1968), "Lateral Stability Analysis of Caisson Foundations", Acta Technica Academice Scientiarum, Hungaricae, Tonus 64 (1-2), pp. 173-181.

36. Muthukrishniah, K., and Ninan, P.K.,(1968), "Experimental Studies on the Rotation of Deep Rigid Foundation Models Subjected to Vertical and Horizontal Loads", Jnl. Indian National Society of Soil Mechanics and Foundation Engineering, Vol.7, No. 2.

37. Ninan, P.K. and Murthy, V.N.S.,(1964), "Experimental Studies on the Stability of Well Foundations for Bridges in Sands", Jnl. of Indian National Society of Soil Mechanics and Foundation Engineering, Vol. 3, p. 307.

38. Pender, E.B.,(1947), "The Lateral Support Afforded to Pier Founded on Sand", Jnl. of Institution of Engineers, Australia, Vol. 19, No. 7.

39. Perry, C.C. and Lissner, H.R.,(1962), "The Strain Gage Primer", Second Edition, Mc Graw Hill Book Company, Inc, New York, p. 235.

40. Ray, K.C.,(1976), "Well Foundations", Cement and Concrete, Jan-March 1967.

41. Roscoe, K.H.,(1957), "A Comparison of Tied and Free Pier Foundation", Proc. IV, Int. Conf. on Soil Mechanics and Foundation Engineering, London, Vol. I, pp. 419-423.

42. Rowe, P.W. and Peaker, K.,(1965), "Pas ive Earth Pressure Measurements", Geotechnique 15, No. 1, p. 57.

43. Sankaran, K.S, and Muthukrishniah Y.K.,(1969), "Well subjected to Horizontal Forces a Model Study", Jnl. of Indian Roads Congress, Vol. XXXII, p. 51.

44. Sharaishi, S.,(1960), "Resistance of Foundation Ground Against Overturning Forces", II World Conference on Earthquake Engineering Vol. 1, pp. 249.

45. Shultze, E. and Horn, A.,(1967), "The Base Friction for Horizontally Loaded Footings in Sand and Gravel", Geotechnique, December 1967.

46. Singh, A.,(1967), "Soil Engineering in Theory and Practice", Asian Publishing House, Bomyay, p. 454.

47. Spring, F.J., "River Training and Control on the Guide Bank System", Technical Paper No. 153, Railway Board, Ministry of Railway, Government of India.

48. Stobie, J.,(1930), "Pole Footings", Jnl. Institution of Engineers, Australia, Vol. 2, p. 58.

49. Terzaghi, K.,(1943), "Theoretical Soil Mechanics", John Wiley and Sons, Inc., New York.

50. Terzaghi K.,(1955), "Evaluation of Coefficient of Subgrade Reaction", Geotechnique, Vol. V, No. 4, pp. 297-326.

51. Thomson, W.T.,(1964), "Mechanical Vibrations", George Allen and Unwin Limited, London, Second edition 1964, p. 53.

52. Timoshenko, S. and S. Woinowsky-Krieger, S.,(1959), "Theory of Plates and Shells", McGraw Hill Book Company Inc., International Students Edition, pp. 55-56.

53. Trollope, D.H. and Currie, D.T.,(1960), "Small Embedded Earth Pressure Cells, Their Design and Calibration", III Australia-New Zealand Conference on Soil Mechanics and Foundation Engineering, pp. 145-151.

54. Trollope, D.H., and Lee, I.K.,(1957), "The Performance of a Laboratory Earth Pressure Cell", Australian Journal of Applied Science 8, pp. 84-87.

55. Verma, S.,(1966), "Design of Wells against Horizontal Forces", Jnl. of Indian Roads Congress, Vol. XXIX-4, p. 627.

56. Walker, B.P. and Whitakar, T., (1967), "An Apparatus for
     Forming Uniform Beds of Sand for Model Foundation Tests",
     Geotechnique 17, 161-167.

57. Waterways Experiment Station Bulletin No. 40, (1955),
     "Pressure Cells for Field Use", Corps of Engineering, U.S.
     Army, Vicksburg, Mississippi, U.S.A., p. 3.

58. Wolf, C.V.,(1933), "Members Wholly or Partly Burried and
     Subjected to Lateral Forces", Concrete and Construction
     Engineering, Vol. 28, No. 11.

TABLE 1

CALIBRATION FACTORS OF LABORATORY EARTH-PRESSURE CELLS

Sl. No.	CELL	Calibration factor kg/cm^2/micro-strain	Sl. No.	CELL	Calibration factor kg/cm^2/micro-strain
1	B-1	0.99×10^{-3}	5	B-5	1.091×10^{-3}
2	B-2	1.09×10^{-3}	6	B-6	1.10×10^{-3}
3	B-3	1.09×10^{-3}	7	C-1	4.09×10^{-3}
4	B-4	1.10×10^{-3}	8	C-2	2.36×10^{-3}

TABLE 2

CALIBRATION FACTORS FOR FRICTION CELLS

Sl. No.	CELL	Calibration factor kg/cm^2/microstrain
1	F-1	0.792×10^{-3}
2	F-2	0.823×10^{-3}
3	F-3	0.823×10^{-3}
4	F-4	0.823×10^{-3}
5	F-5	0.891×10^{-3}
6	F-6	0.713×10^{-3}
7	F-7	0.668×10^{-3}
8	F-8	0.763×10^{-3}
9	F-9	0.713×10^{-3}
10	F-10	0.763×10^{-3}

TABLE 3

CALIBRATION FACTORS FOR FIELD EARTH PRESSURE-CELLS

Sl. No.	Cell	Calibration factor kg/cm²microstrain
1	P-1	2.36×10^{-3}
2	P-2	1.54×10^{-3}
3	P-3	2.00×10^{-3}
4	P-4	3.30×10^{-3}
5	P-5	2.50×10^{-3}
6	P-6	2.00×10^{-3}
7	P-7	2.00×10^{-3}
8	P-8	1.82×10^{-3}
9	P-9	2.20×10^{-3}
10	P-10	2.20×10^{-3}
11	P-11	2.00×10^{-3}
12	P-12	2.20×10^{-3}
13	S-1	4.50×10^{-3}
14	S-2	6.60×10^{-3}
15	S-3	5.00×10^{-3}
16	S-4	6.60×10^{-3}
17	S-5	5.00×10^{-3}
18	S-6	6.60×10^{-3}
19	S-7	5.70×10^{-3}
20	S-8	5.70×10^{-3}
21	S-9	5.50×10^{-3}

TABLE 4

STATIC LATERAL LOAD TESTS ON 15 cm SQUARE WELL; D/B=1.5

B =15 cm; Base on sand

D= 22.5 cm; Embedment in sand

H_V =42.5

W, Self weight of well= 6.5 kg
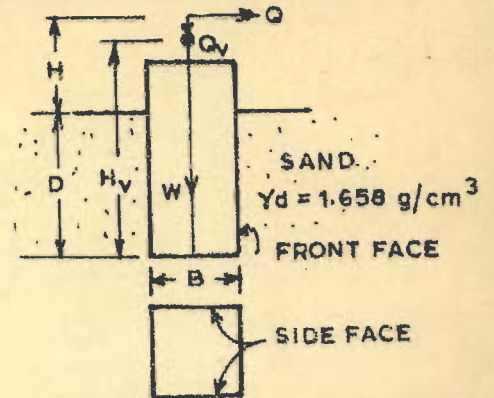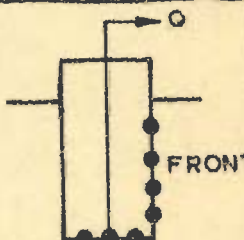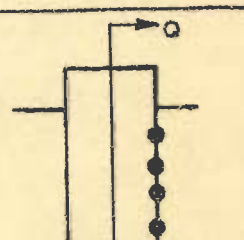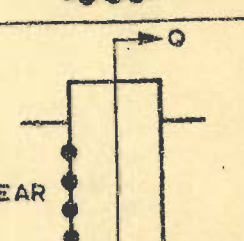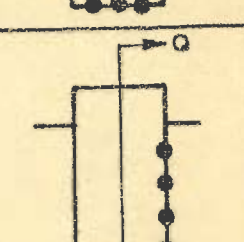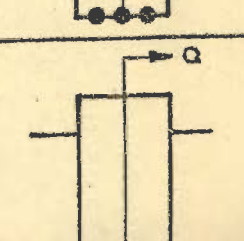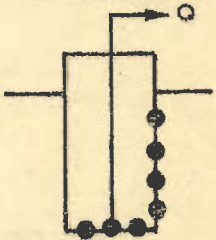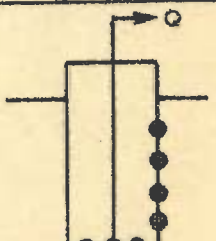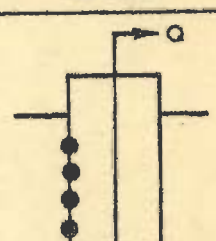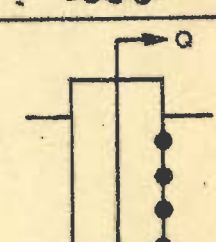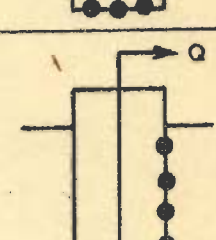
TEST NO. (1)	Q_v (kg) (2)	H/B (3)	FRICTION CONDITION		LOCATION OF PRESSURE CELLS (6)	FIG. REF. (7)
			FRONT AND REAR FACES (4)	SIDE FACES (5)		
1	131	2.25	R	R		45,46
2	131	3.00	R	R		47,48
3	131	2	R	R		47,48
4	131	2.25	R	S		49,50
5	131	2.25	S	S		51

TABLE 4 (contd.)

(1)	(2)	(3)	(4)	(5)	(6)	(7)
6	101	2.25	R	R		52,53
7	101	3	R	R		54,55
8	101	3	R	R		54,55
9	101	3	R	S		56,57
10	51	2.25	R	R		58,59

R = Rough face; sand against wood

S = Smooth face; sand against polythene
sheet on face

TABLE 5

STATIC LATERAL LOAD TESTS ON 15 cm SQUARE WELL; D/B = 2

B = 15 cm, Base on sand
D = 30 cm Embedment in sand
H_V = 42.5 cm
W = 6.5 kg
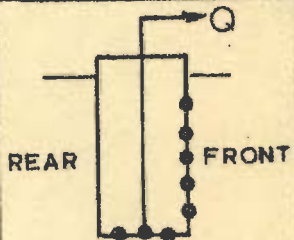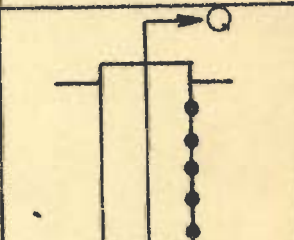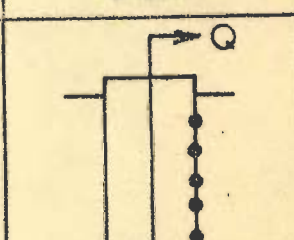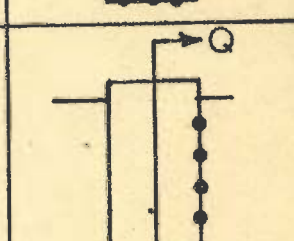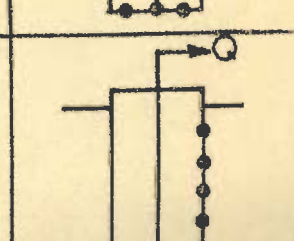
TEST NO. (1)	Q_V (kg) (2)	H/B (3)	FRICTION CONDITION		LOCATION OF PRESSURE CELLS (6)	FIG. REF. (7)
			FRONT AND REAR FACES (4)	SIDE FACES (5)		
11	131	4	R	R		60,61
12	131	3	R	R		62,63
13	131	2	R	R		64,65
14	131	1	R	R		66,67
15	131	3	R	S		68,69

TABLE 5 (contd)
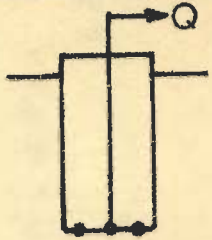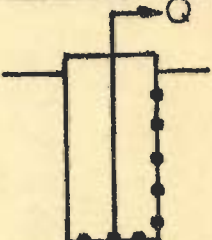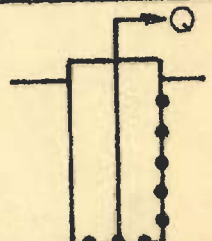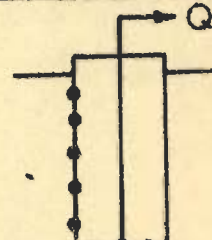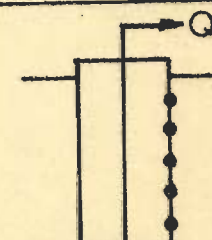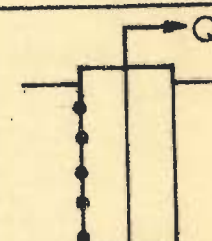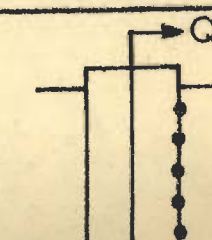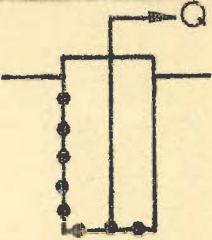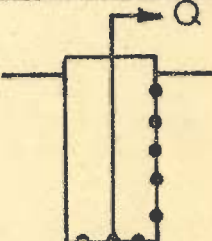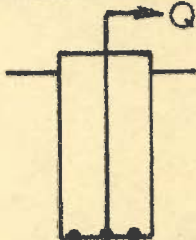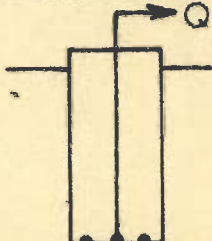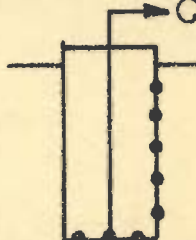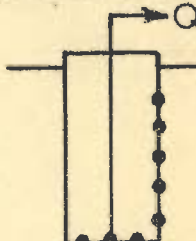
(1)	(2)	(3)	(4)	(5)	(6)	(7)
16	131	3	S	S		70
17	101	4	R	R		71,72
18	101	3	R	R		73,74
19	101	3	R	R		73,74
20	101	3	R	S		75,76
21	101	3	R	S		—
22	51	4	R	R		77,78

TABLE 5 (contd.)

(1)	(2)	(3)	(4)	(5)	(6)	(7)
23	51	.3	R	R		79
24	51	3	R	S		80,81
25	51	3	S	S		82
26	51	3	S	S		82
27	O	4	R	R		83,84
28	O	3	R	R		85,86

R = Rough face; sand against load
S = Smooth face; sand against polythene sheet on face

TABLE 6

STATIC LATERAL LOAD TEST ON 15 CM SQUARE WELL WITH BASE ON PLANK

B = 15 CM; BASE ON PLANK

D = 30 CM; EMBEDMENT IN SAND

H_V = 42.5 CM

W = 6.5 Kg

$\gamma_d = 1.658 \, g/cm^3$
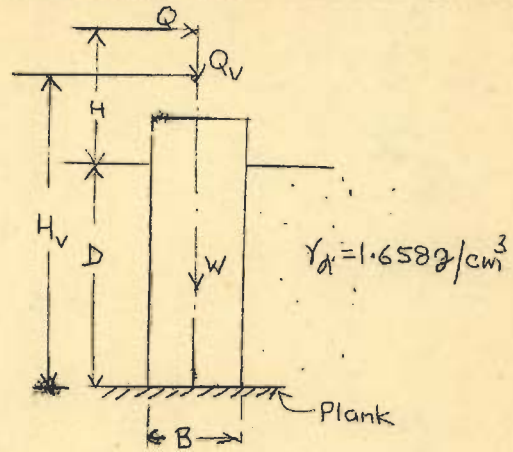
Test No.	Q_V kg	H/B	FRICTION CONDITION		Figs. Ref.
			Front and Rear faces	Side Faces	
29	101	4	R	R	87a
30	101	2	R	R	87b
31	101	1	R	R	87c
32	51	4	R	S	87d
33	51	4	R	R	88a
34	51	3	R	R	88b
35	51	2	R	R	88c
36	51	1	R	R	88d

R = Rough face; Sand against wood

S = Smooth face; Sand against polythene sheet placed on wood

TABLE 7

STATIC LATERAL LOAD TESTS ON 20 CM SQUARE WELL

B = 20 CM ; BASE ON SAND

H_V = 57 CM

W = 12 Kg; WOODEN WELL

EMBEDMENT IN SAND

$Y_d = 1.658 \, g/cm^3$
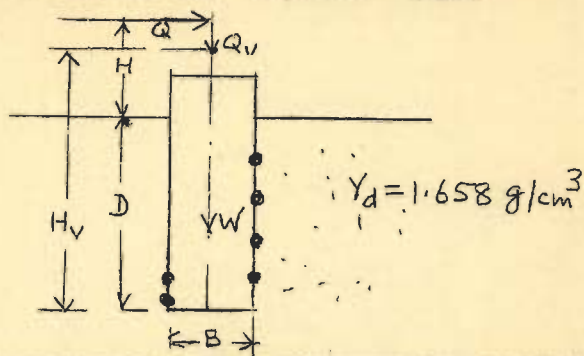
Test No.	D/B	Q_V (Kg)	H/B	FRICTION CONDITION Front and Rear faces	Side Faces	Fig. Ref.
37	1.5	131	2.25	R	R	89,91a
38	1.5	131	2.25	R	R	91b
39	1.5	131	2.25	S	S	91c
40	1.5	0	2.25	R	R	90,91d
41	2	131	2	R	R	91c
42	2	131	2	R	R	91f
43	2	0	4	R	R	91g
44	2	0	4	R	S	91h
45	2	0	2	R	R	91i

R = Rough face; Sand against wood

S = Smooth face; Sand against polythene sheet on wood

TABLE 8

STATIC LATERAL LOAD TESTS ON 20 cm SQUARE MILD STEEL WELL

B = 20 cm, Bottom on sand: D = 30 cm; Embedment in sand

H_V = 57 cm ,   W = 32 kg
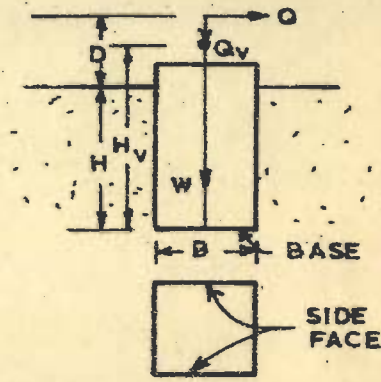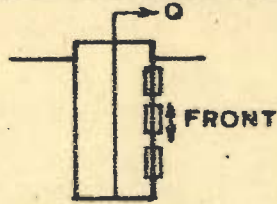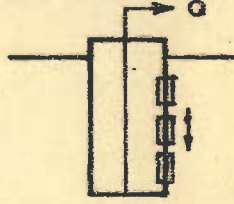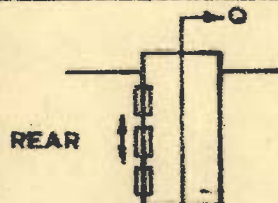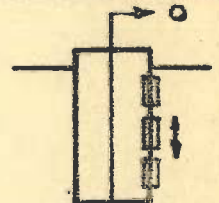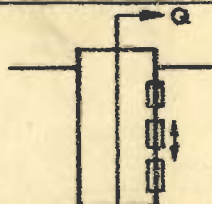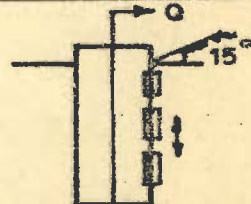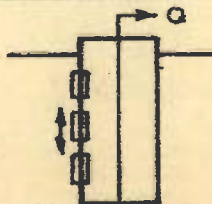
TEST NO. (1)	Q_V (kg) (2)	H/B (3)	LOCATION OF FRICTION CELLS (4)	FIG. REF. (5)	TEST NO. (1)	Q_V (kg) (2)	H/D (3)	LOCATION OF FRICTION CELLS (4)	FIG. REF. (5)
46	131	3	FRONT	92	50	56	3		94
47	131	3	REAR	92	51	0	2.25		95
48	131	2.25		93	52	0	2.25	15°	96
49	131	2.25		93					

↕ DIRECTION OF FRICTION MEASUREMENT IN ALL CELLS IN MODEL

▯ FRICTION CELL LOCATION ON FRONT AND REAR FACES

TABLE 8 (contd)

(1)	(2)	(3)	(4)	(5)	(1)	(2)	(3)	(4)	(5)
53	131	3		97	56	56	2.25		100
54	131	2.25		98	57	0	3		101
55	56	3		99	58	0	2.25		102

BASE PLAN

BASE PLAN

→ DIRECTION OF FRICTION MEASUREMENT IN ALL CELLS OF A MODEL

□ FRICTION CELL LOCATION ON SIDE FACE

▭ FRICTION CELL LOCATION ON BASE

TABLE 9

CYCLIC AND REPITITIVE LATERAL LOAD TESTS

A = TEST ON 15 CM WELL

B = 15 cm; D = 30 cm; H = 45 cm; D/B = 2; H/B = 3.0;
H_V = 42.5 cm; W = 6.5 Kg.

Test No.	Nature of loading	Q_V Kg	FRICTION CONDITION Front and Rear Faces	Side Faces	Fig. Ref.
59	Cylic	131	R	R	103
60	Cyclic	131	R	S	104
61	Cyclic	131	S	S	105
62	Cyclic	131	S	S	106
63	Cyclic	0	R	R	107

$\gamma_d = 1.658$ g/cm³
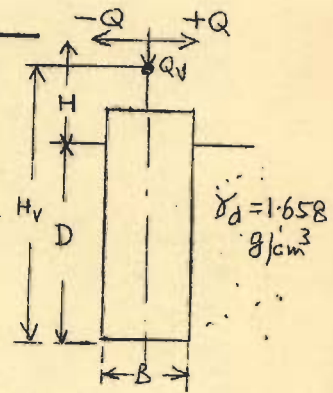
(B) TESTS ON 20 CM WELL

B = 20 cm; D = 30 cm; H = 60 cm; D/B=1.5;
H/B = 3; H_V = 57 cm

64ff	Cyclic	131	R	R	108	
65+	Cyclic	131	R	R	109	ff Wooden model
66+	Repititive	156	R	R	110	W = 12 kg
67+	Repititive	131	R	R	111	+ Mild steel model W = 32 kg
68+	Repititive	56	R	R	112	

R = Rough faces; S = Smooth faces

TABLE 10

FREE VIBRATION TESTS ON LABORATORY MODELS

(A) TESTS ON 15 CM WELL

B = 15 cm; H_v = 42 cm;

W = 6.5 Kg
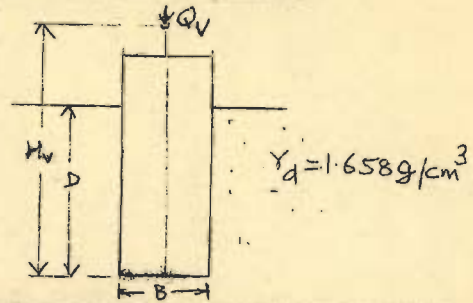
$Y_d = 1.658 g/cm^3$

Test No.	D/B	Q_v Kg	FRICTION CONDITION Front and Rear Faces	Side Faces	Figs. Ref.
69	1.5	101	R	R	113a
70	1.5	51	R	R	113b
71	1.5	0	R	R	113c
72	1.5	101	S	S	113d
73	1.5	51	S	S	113c
74	1.5	0	S	S	113e
75	2	131	S	S	117g
76	2	101	S	S	113h
77	2	51	S	S	113i
78	2	0	S	S	113j

TABLE 10 (CONTD.)
FREE VIBRATION TESTS

(B) TESTS ON 20 CM SQUARE M.S. WELL

B = 20 CM; H_v = 57 CM; W = 32 KG

Test No.	D/B	Q_v (kg)	FRICTION CONDITION Front and Rear Faces	Side Faces
79	1.5		R	R
80	1.5		R	R
81	1.5		R	R
82	2		R	R
83	2		R	R
84	2		R	R

(C) TESTS ON 20 CM SQUARE WOODEN WELL
B = 20 CM; H_v = 57; W = 12 Kg

Test No.	D/B	Q_v (kg)	Front and Rear Faces	Side Faces
85	1.5	131	R	R
86	1.5	71	R	R
87	1.5	31	R	R
88	1.5	0	R	R
89	1.5	131	S	S

TABLE 10 (CONTD.)
FREE VIBRATION TESTS

(C) TESTS ON 20 CM SQUARE WOODEN WELL (Contd)

$B = 20$ CM. $H_v = 57$; $W = 12$ Kg

Test No	D/B	Q_v (Kg)	FRICTION CONDITION Front and Rear Faces	Side Faces
90	1.5	71	S	S
91	1.5	31	S	S
92	1.5	0	S	S
93	2	131	R	R
94	2	71	R	R
95	2	31	R	R
96	2	0	R	R
97	2	131	S	S
98	2	71	S	S
99	2	31	S	S
100	2	0	S	S

R = Rough Face; Sand Against wood or Mild Steel

S = Smooth Face; Sand Against Polythene Placed on Wood

TABLE 11

SKIN FRICTION TESTS WITH VERTICAL LOADING

All Tests in Dense Sand
of $\gamma_d = 1.658$ g/cm³
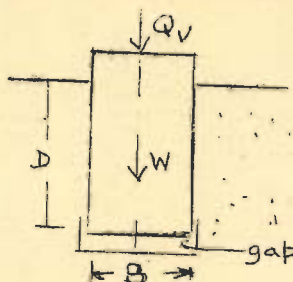
Test No.	Model	Cross-section BxL(cm)	Weight of well W(kg)	Depth of Embed-ment D(cm)	Depth to width ratio D/B	Condition of Faces	Figs Ref
101	Wooden	15x15	6.5	22.5	1.5	R	114a
102	Wooden	15x15	6.5	30	2	R	114a
103	Wooden	15x15	6.5	30	2	S	114a
104	Wooden	20x20	12	30	1.5	R	114b
105	Wooden	20x20	12	30	1.5	S	114b
106	Wooden	20x20	12	40	2	R	114b
107	Mild Steel	20x20	32	30	1.5	R	114b

R = Rough Face; Sand Against Wood

S = Smooth Face; Sand Against Polythene Sheet on Wood

TABLE 12

TESTS FOR FAILURE OUTCROP ON GROUND DUE TO LATERAL LOADING

$\gamma_d = 1.658\,g/cm^3$
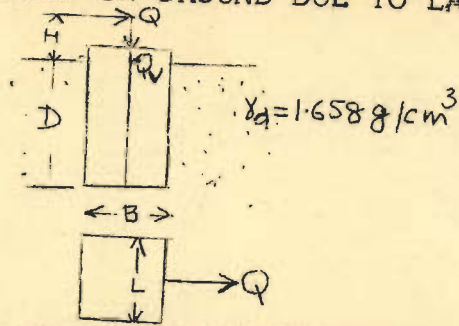
Test No.	Model size B×L(cm)	D/B	H/B	Q_v (kg)	Horizontal load at Failure Q_v(kg)	Orientation of model in Plan	Figs. Ref.
108	15x15	2	2	0	22	→Q	116a
109[+]	15x15	2	1	0	28.5	→Q	116b
110	15x15	1.5	1.5	0	16.75	→Q	116c
111[+]	15x15	2	1	51	43	→Q	115, 116d
112	15x15	2	3	0	13.5	→Q	117a
113	15x15	2	3	0	14.5	→Q	117b
114	20x20	1.5	2.25	0	33	→Q	117c
115	20x20	1.5	2.25	131	44.5	→Q	118a
116	20x20	1.5	2.25	0	32	→Q	118b
117[++]	20x20	1.5	2.25	0	38	→Q	118c

+ Base on Plank

++ Ground sloping at 15° from horizontal

TABLE 13

TESTS ON FIELD MODEL

B = 1.5 m

D = 2.25 m

D/B = 1.5

W = 6.5 Tonne
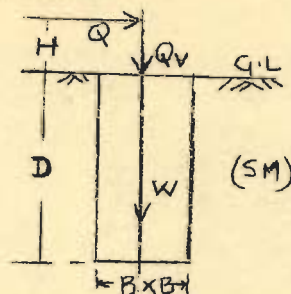
Test No.	Type of Test	Q_v (Tonne)	Other conditions	Fig. Ref.
118	Vertical load Test	-	Surrounding soil in natural state. Load increments of 2.25, 4.25 and 6.75 tonne	119
119	Free Vibration Test	0	Surrounding soil in natural state (Low moisture content)	120a
120	Free vibration Test	2.25	Surrounding soil in natural state (Low moisture content)	120b
121	Free vibration Test	4.25	Surrounding soil in natural state (Low moisture content)	120c
122	Free vibration Test	4.25	Surrounding ground in flooded condition	120d
123	Free vibration Test	2.25	Surrounding soil in flooded condition	120e
	Lateral load Test	6.0	Surrounding soil in saturated condition H = 3.375m; H/B = 2.25	121,123 124 and 125
125	Lateral load Test	6.0	Surrounding soil in saturated condition H = 3.375m; H/B = 2.25	122

TABLE 14

NATURAL FREQUENCY AND DAMPING FACTORS OF LABORATORY WELL MODELS

(A) Free Vibration Tests on 15 cm Base Wooden Models

Test No.	D/B	Q_v (kg)	Friction on faces	Natural Frequency (f_n) (cycles/sec)	Damping Factor (ξ) %
69	1.5	101	R	13	9.00
70	1.5	51	R	15.25	7.47
71	1.5	0	R	27	20.4
72	1.5	101	S	13.9	11.0
73	1.5	51	S	15.65	9.1
74	1.5	0	S	48	22.3
75	2	131	S	15.65	6.77
76	2	101	S	12	8.11
77	2	51	S	16	11.0
78	2	0	S	52	11.5

(B) Free Vibration Tests on 20cm Base Mild Steel Model

Test No.	D/B	Q_v (kg)	Friction on faces	Natural Frequency (f_n) (cycles/sec)	Damping Factor (ξ) %
79	1.5	131	R	13.91	11
80	1.5	56	R	25	13.8
81	1.5	0	R	54.8	18.75
82	2	131	R	25	16.4
83	2	56	R	33.4	11
84	2	0	R	62.5	19.2

R = Rough Face; sand against wood

S = Smooth Face; sand against polythene on wood.

TABLE 14 (CONTD.)

(C) Free Vibration Test on 20 cm Base Wooden Model

Test No.	D/B	Q_V (Kg)	Friction on face	Natural Frequency (cycles/sec)	Damping Factor of ξ %
85	1.5	131	R	12.5	7.48
86	1.5	71	R	15.65	5.34
87	1.5	31	R	25.0	9.32
88	1.5	0	R	62.5	17.5
89	1.5	131	S	10.4	14.6
90	1.5	71	S	13.9	9.1
91	1.5	31	S	20.8	16.4
92	1.5	0	S	62.5	23.0
93	2	131	R	25.0	11.0
94	2	71	R	17.85	6.42
95	2	31	R	29.8	10.3
96	2	0	R	50	13.8
97	2	131	S	12.5	12.4
98	2	71	S	17.85	13.6
99	2	131	S	12.5	11.0
100	2	0	S	62.5	20.8

R = Rough Face; Sand against wood

S = Smooth Face; Sand against Polythene on wood.

TABLE 15

FAILURE OUT CROP AROUND WELLS AT MAXIMUM LATERAL LOAD

Test No.	Figure No.	Passive Zone		Active Zone	
		x_p/L	L_p/L	x_a/L	L_a/L
108	115a	1.266	1.465	0.566	1.165
109	115b	1.200	1.533	0.633	1.200
110	115c	1.200	1.468	0.500	1.000
111	115d	1.200	1.468	0.600	1.000
112	117a	1.266	1.465	0.500	1.000
113	117b	1.41	2.120	1.075	1.225
114	117c	1.200	1.500	0.550	1.000
115	118a	1.200	1.500	0.550	1.000
116	118b	1.250	1.500	0.389	1.000
117	118c	1.200	1.600	0.450	1.000

TABLE 16

EXPERIMENTAL VALUES OF COEFFICIENT OF EARTH PRESSURE AT REST

Test No.	Fig. No.	Curve	Model Size L (cm)	B (cm)	Embedment Depth D(cm)	Maximum Skin Friction Q_s(kg.)	K_o	Remarks
101	114a	A	15	15	22.5	21	1.265	Wooden Model
102	114a	B	15	15	30	31.5	1.135	Wooden Model
104	114b	D	20	20	30	42	1.07	Wooden Model
106	114b	F	20	20	40	60	0.875	Wooden Model
107	114b	G	20	20	30	70	1.84	Mild Steel Model

TABLE 17

COEFFICIENT OF FRICTION FOR MODELS WITH POLYTHENE SHEET (FIG.114)

Model size	D (cm)	Q_s (kg)	K_o	Coefficient of skin friction	Average skin friction
15x15	22.5	6.5	1.265	.265	
15x15	30.0	6.5	1.135	.146	
20x20	30.0	12	0.761	.263	0.195
20x20	40.0	12	0.700	.168	

TABLE 18

CYCLIC AND REPITITIVE LATERAL LOAD TEST DATA AND EQUIVALENT VISCOUS FRICTION

Test No.	Fig. No.	D/B	Q_v (kg)	Friction on face	Q_y (kg)	x_y (mm)	$\dfrac{Q_m}{Q_y}$	$\dfrac{x_m}{x_y}$	α	s	Damping factor %	Remarks
59	103	2	131	R	7	.20	2.5	6.30	0.26	3	7.54	15cm Model
60	104	2	131	R	6	.12	2.92	8.06	0.165	3	8.83	15cm Model
61	105	2	131	S	8	.40	2.175	4.175	0.20	3	7.93	15cm Model
62	106	2	101	S	6	.16	2.5	5.63	0.20	3	7.84	15cm Model
63	107	2	0	R	4.5	.15	2.67	11.3	0.40	3	6.15	15cm Model
64	108	1.5	131	R	10	.16	2	2.81	0.125	3	7.08	20cm Wooden Model
65	109	1.5	131	R	12	.14	2.5	9.35	0.300	3	7.82	20cm Mild steel Model
66	110	1.5	156	R	12	.12	2.92	17.45	0.500	3	4.90	20cm Wooden Model
67	111	1.5	131	R	12	.20	2.92	10.80	0.300	3	6.43	20cm Wooden Model
68	112	1.5	56	R	8	.08	2.75	20.00	0.700	3	4.26	20cm Wooden Model

R = Rough Face, Sand against wood

S = Smooth face, Sand against polythese on wood

TABLE 19

RESULTS OF FREE VIBRATION TESTS ON FIELD MODEL

Test No.	Figure No.	Q_v (Tonne)	Surrounding soil condition	Natural Frequency cycles/ sec.	Damping Factor β %
119	120a	0	Natural	13.78	9.07
120	120b	2.25	Natural	15.12	15.15
121	120c	4.25	Natural	16.65	7.2
122	120d	4.25	Saturated	17.85	15.25
123	120e	2.25	Saturated	18.15	7.2

Axis of
well | Bearing level

H.F.L.

Normal depth of scour

Maximum
scour depth

Pier

Top plug

Well cap

Normal river
bed level
under highest floo

Well

Max. scour level

Embedment depth
D

Sand
filling

Bottom plug

Well curb
Cutting edge

Base

Width
B

Sectional elevation

Length = L

B
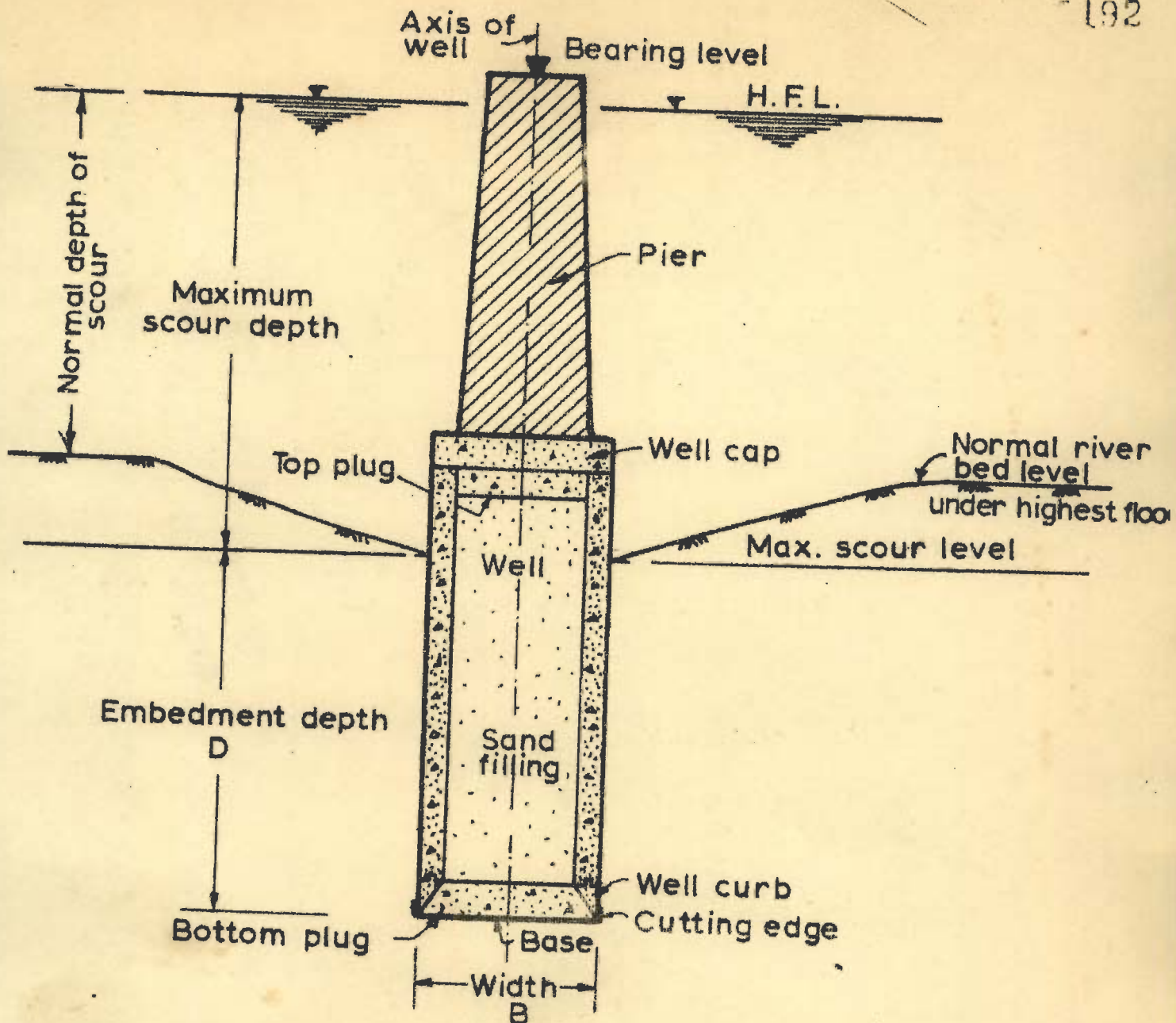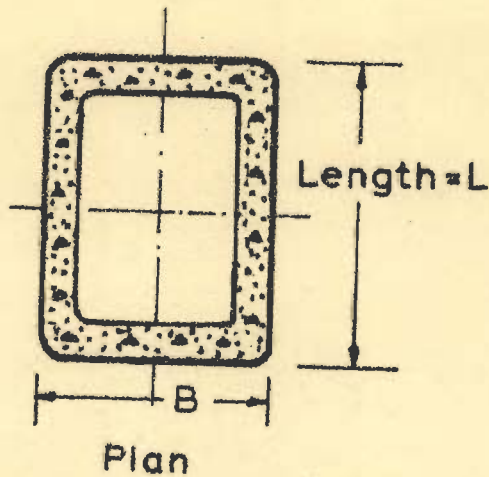
Plan

FIG. 1 – A WELL FOUNDATION

FIG. 2 _ FORCES ACTING ON A WELL FOUNDATION

Scour level

M_o

Q_v

Q

Base before loading

Base after vertical loading

Point of rotation
O ●

Δi

X

Base after vertical and horizontal loading

a_ At smaller tilts

Scour

Q_v

M_o

Q

level

D

Point of rotation

D_1

$\bar{x}$

Δi

D_2
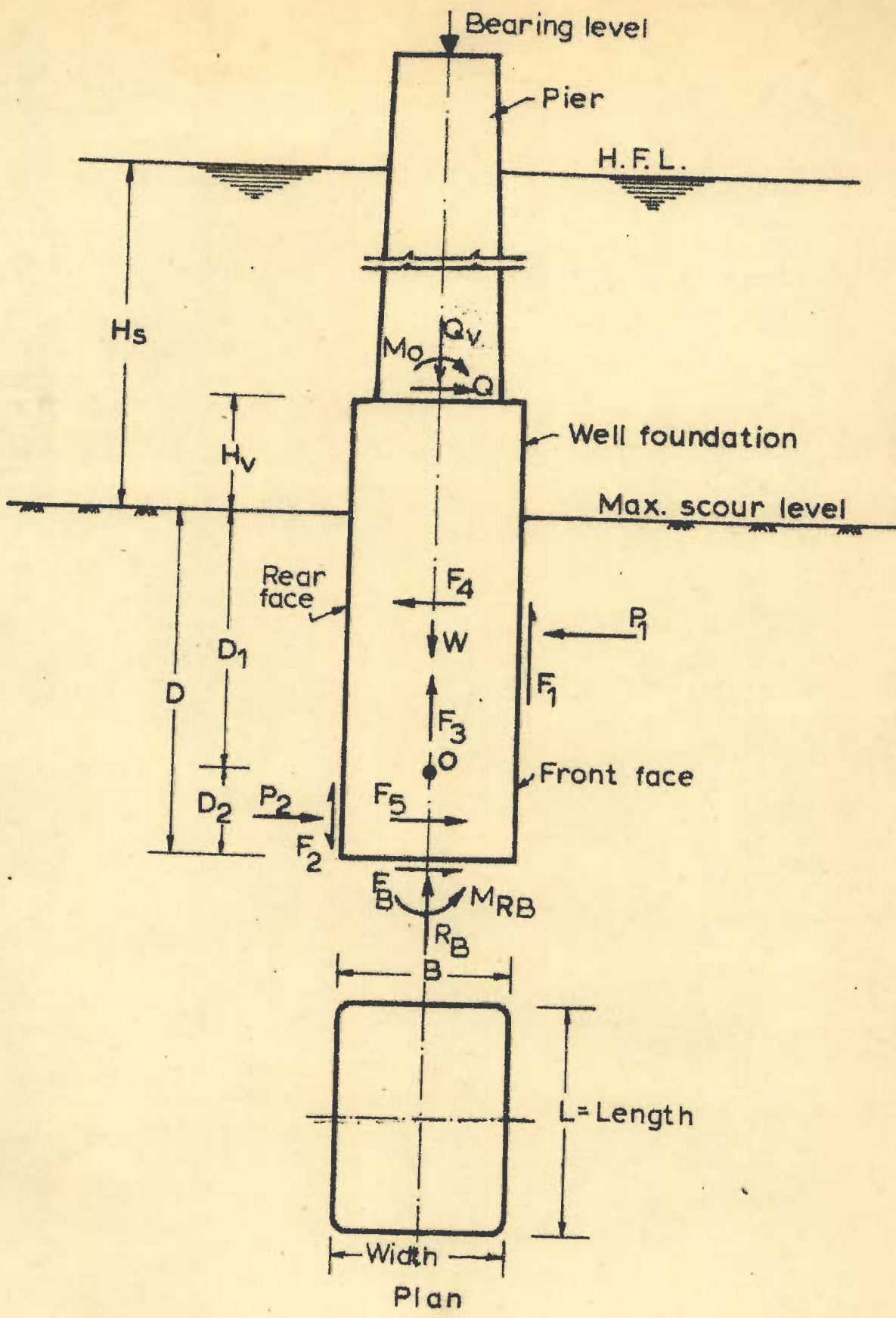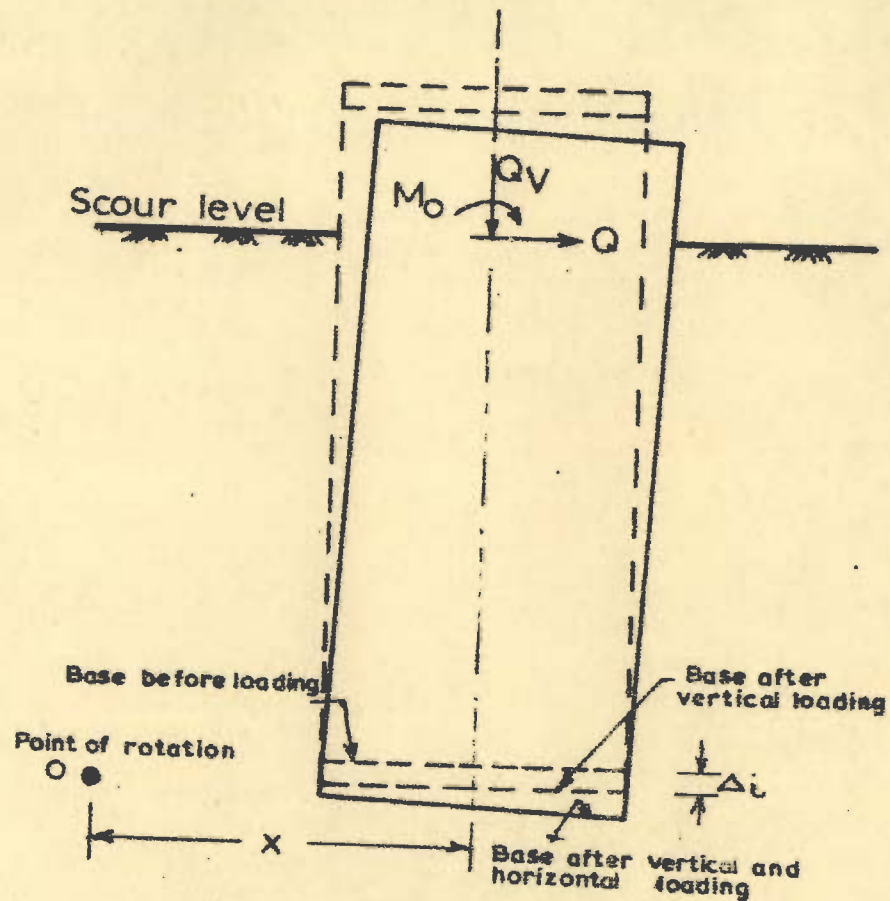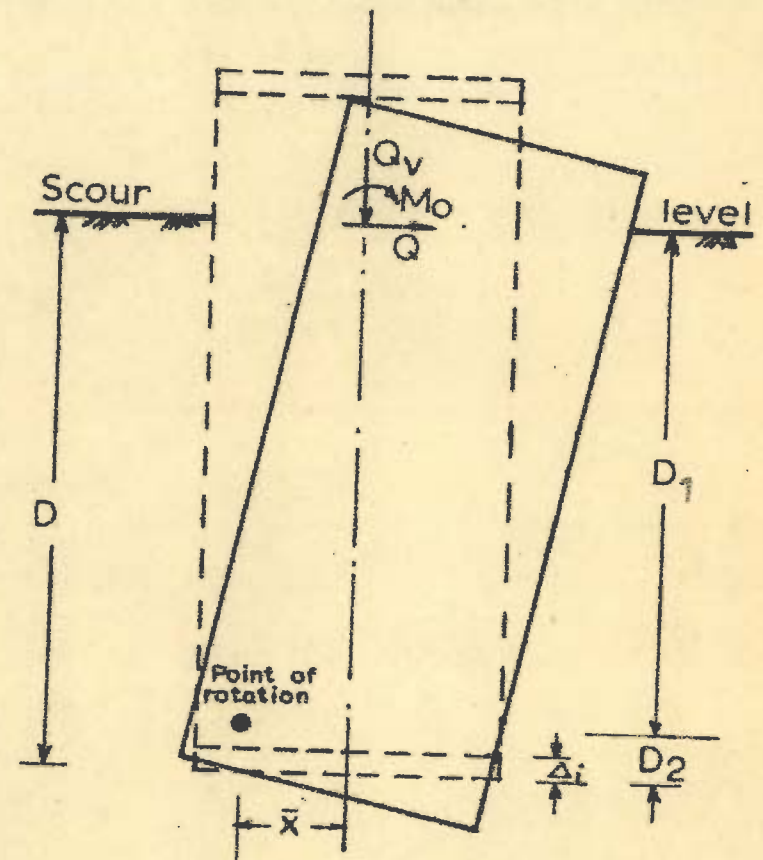
b_ At larger tilts

FIG. 3 _OBSERVED BEHAVIOUR OF WELL FOUNDATION MODELS
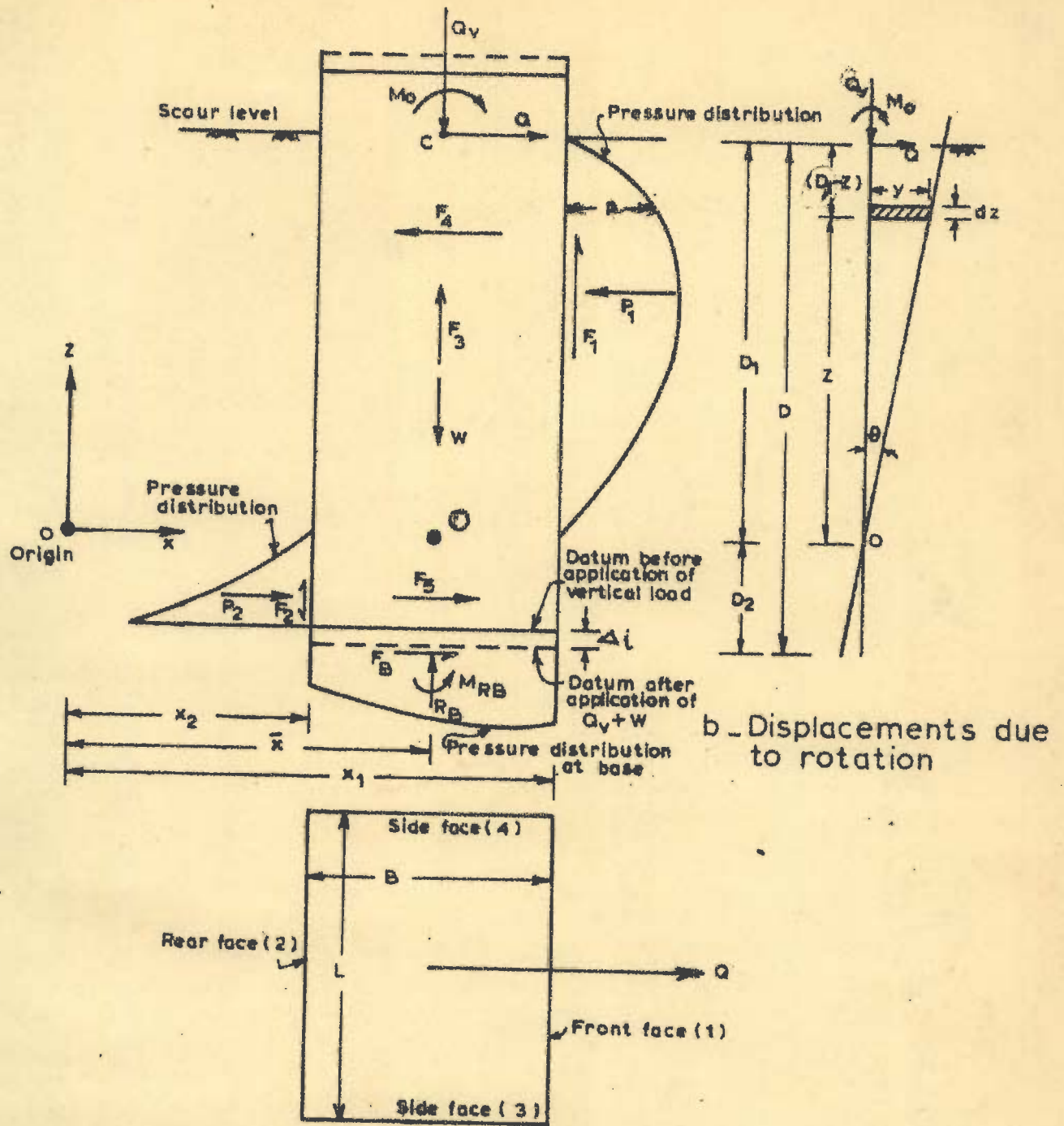
a – Elevation and plan of a well

b – Displacements due to rotation

FIG. 4 – FORCES CONSIDERED IN THE ANALYSIS

View A'A'　　　　Section AA
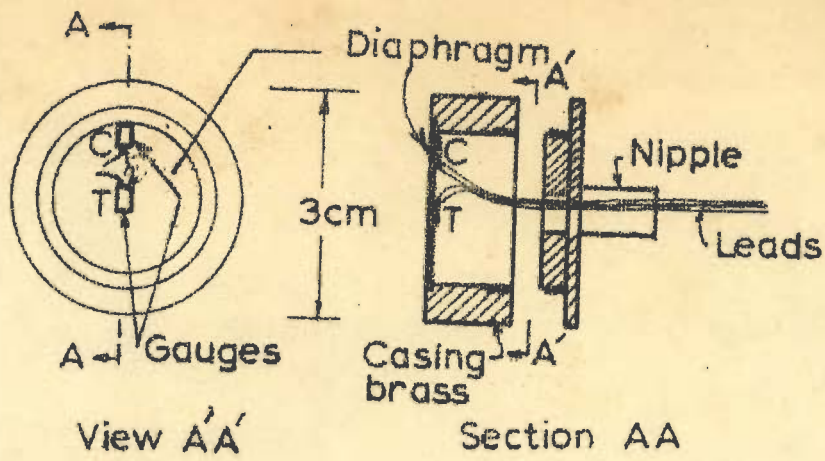
a—Boundary earth pressure cell for use in laboratory models

$\epsilon_r = \frac{3}{8} \frac{q a^2 (1-\nu^2)}{E t^2}$

Radial strain

0.578

Straingauge location (-ve strain)

$\epsilon_r = \frac{3}{4} \frac{q a^2 (1-\nu^2)}{E t^2}$

Direction of uniform pressure

c— Half bridge circuit

(+ve strain)

O　　　r/a →　　1.0

Diameter of diaphragm
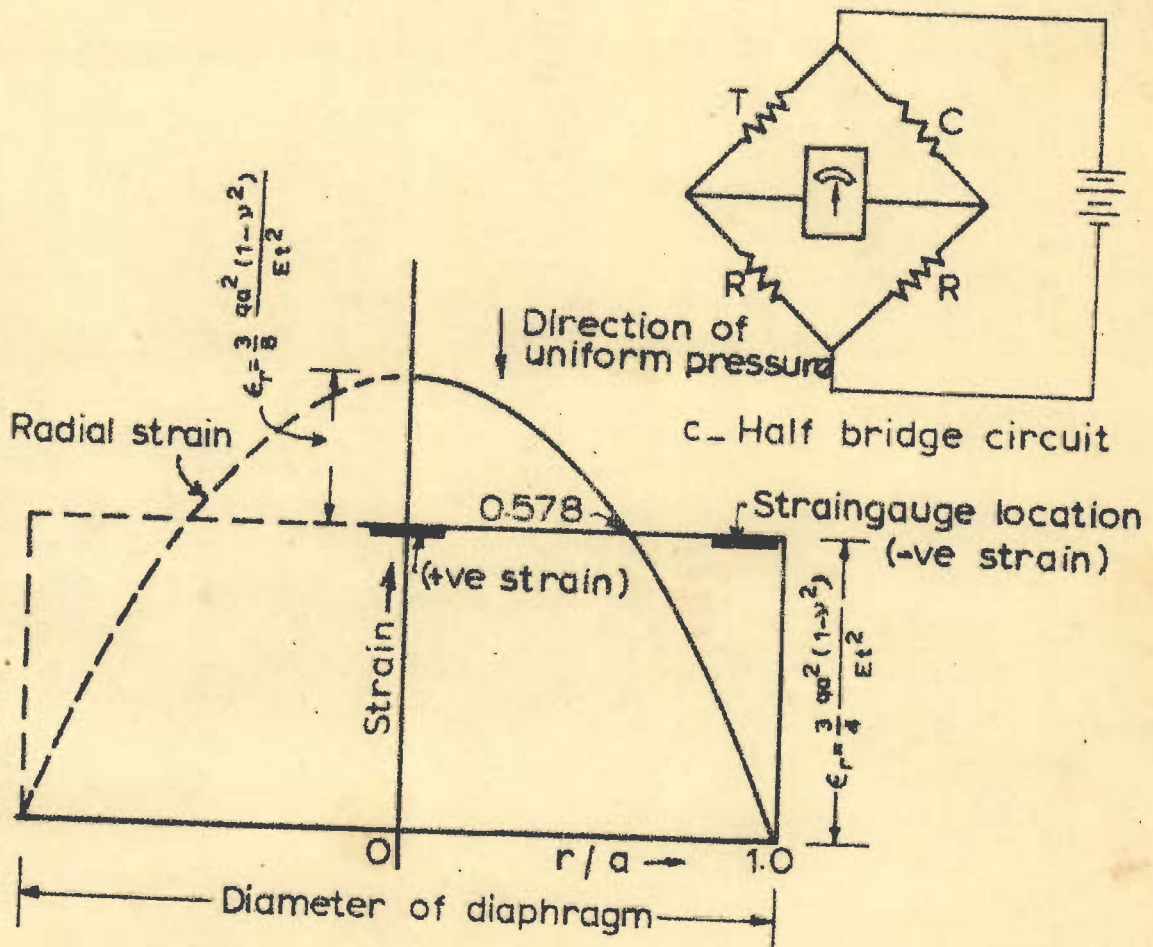
b—Distribution of radial strain on uniformly loaded circular diapragm with clamped edges.

FIG. 5 — BOUNDARY EARTH-PRESSURE CELL AND DESIGN PRINCIPLE

FIG. 6 – Earth-pressure Cell for
Laboratory Wells
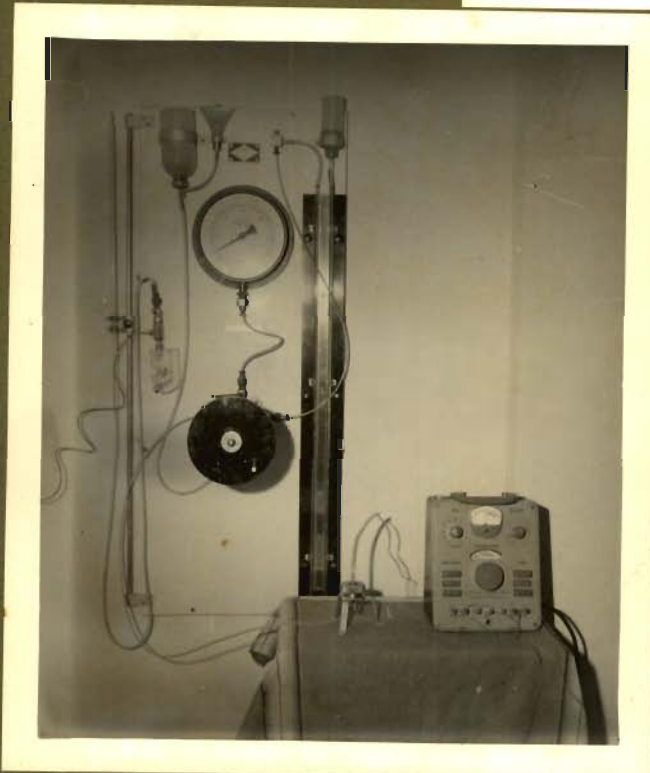
FIG. 7 – Calibration Apparatus
Earth-pressure Cell

FIG. 8 – Calibration Chamber
Earth-pressure Cell
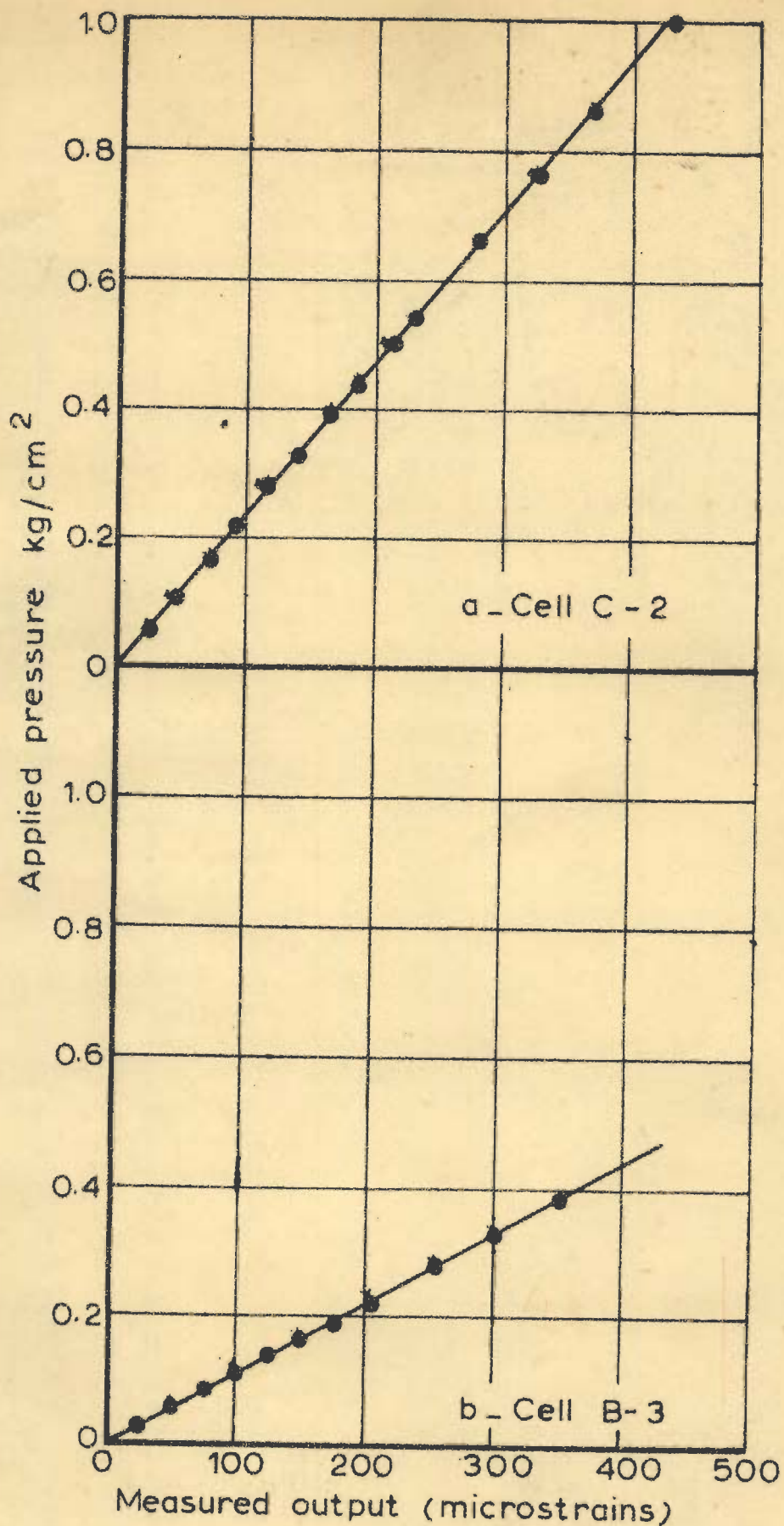
FIG. 9 _ TYPICAL CALIBRATION CURVES FOR LABORATORY
EARTH PRESSURE CELLS
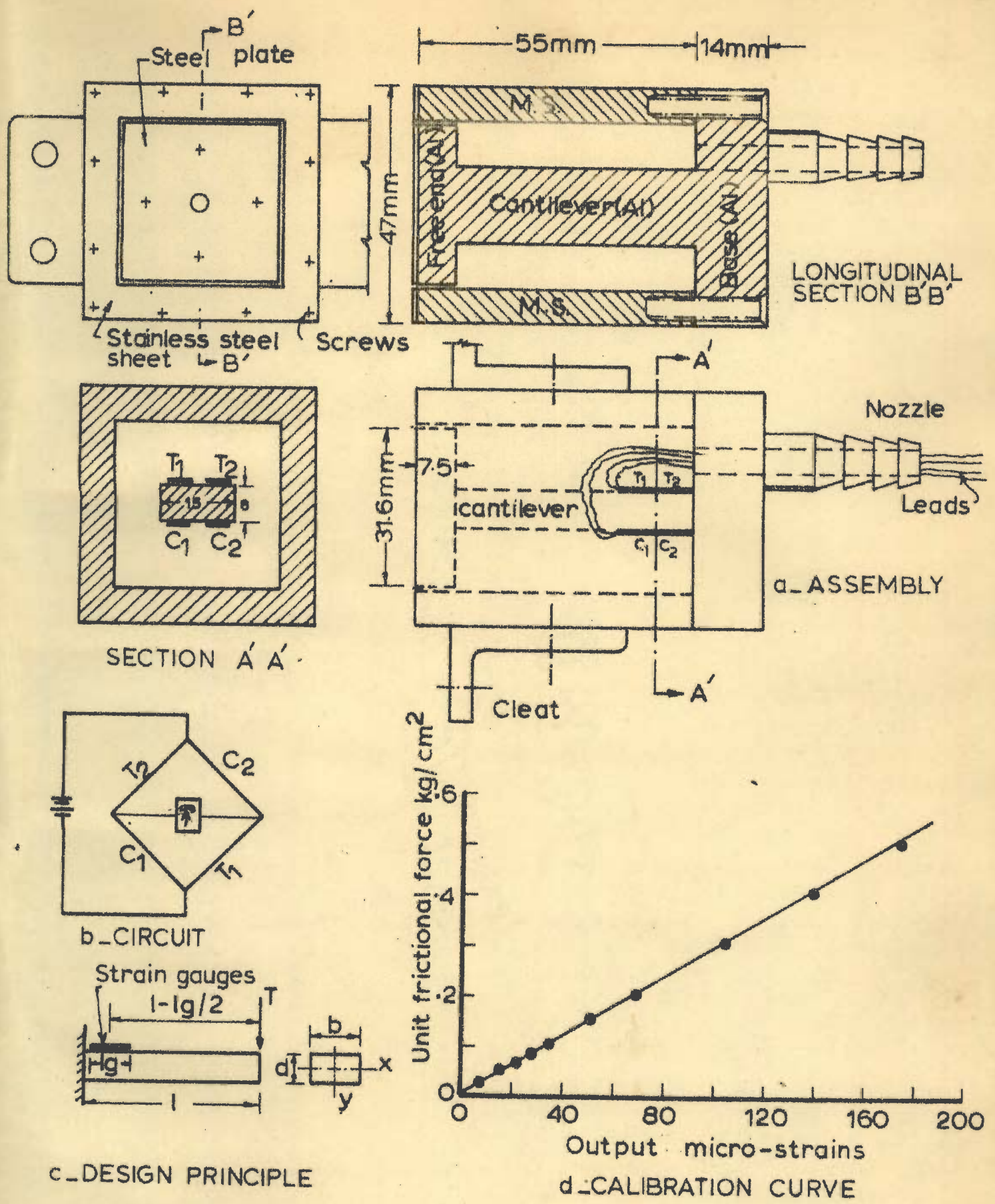
FIG. 10 _ FRICTION CELL
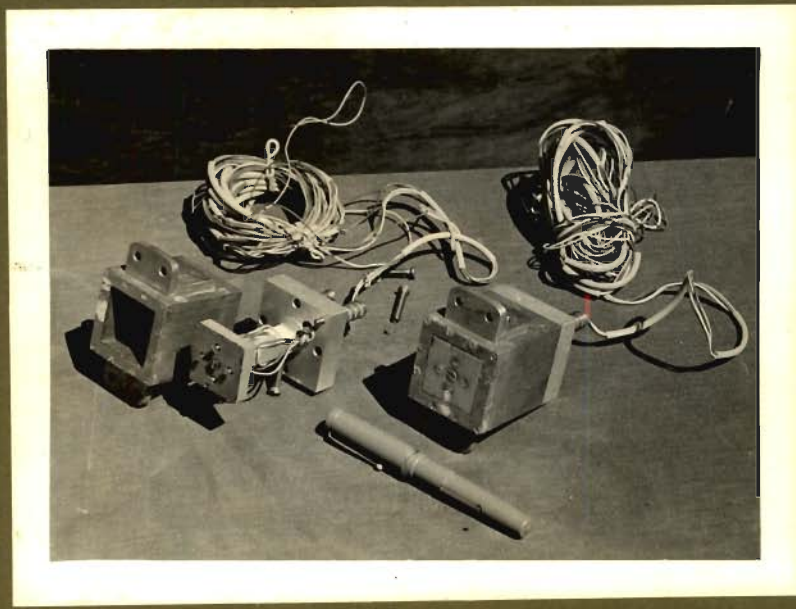
FIG.11- Friction Cell
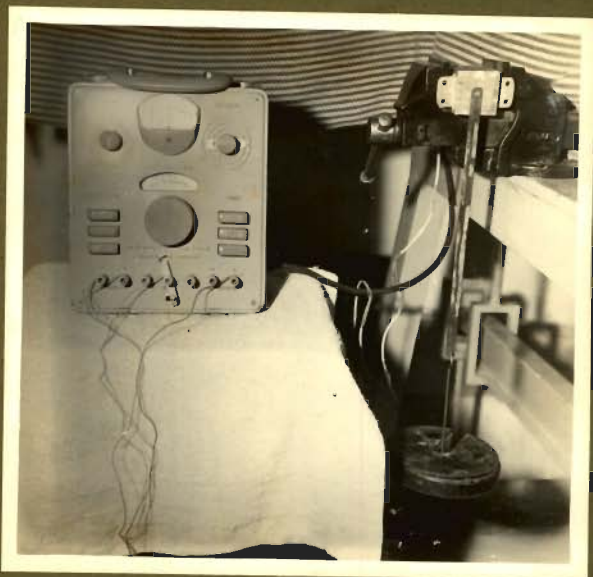
FIG.12- Calibration Apparatus
Friction Cell
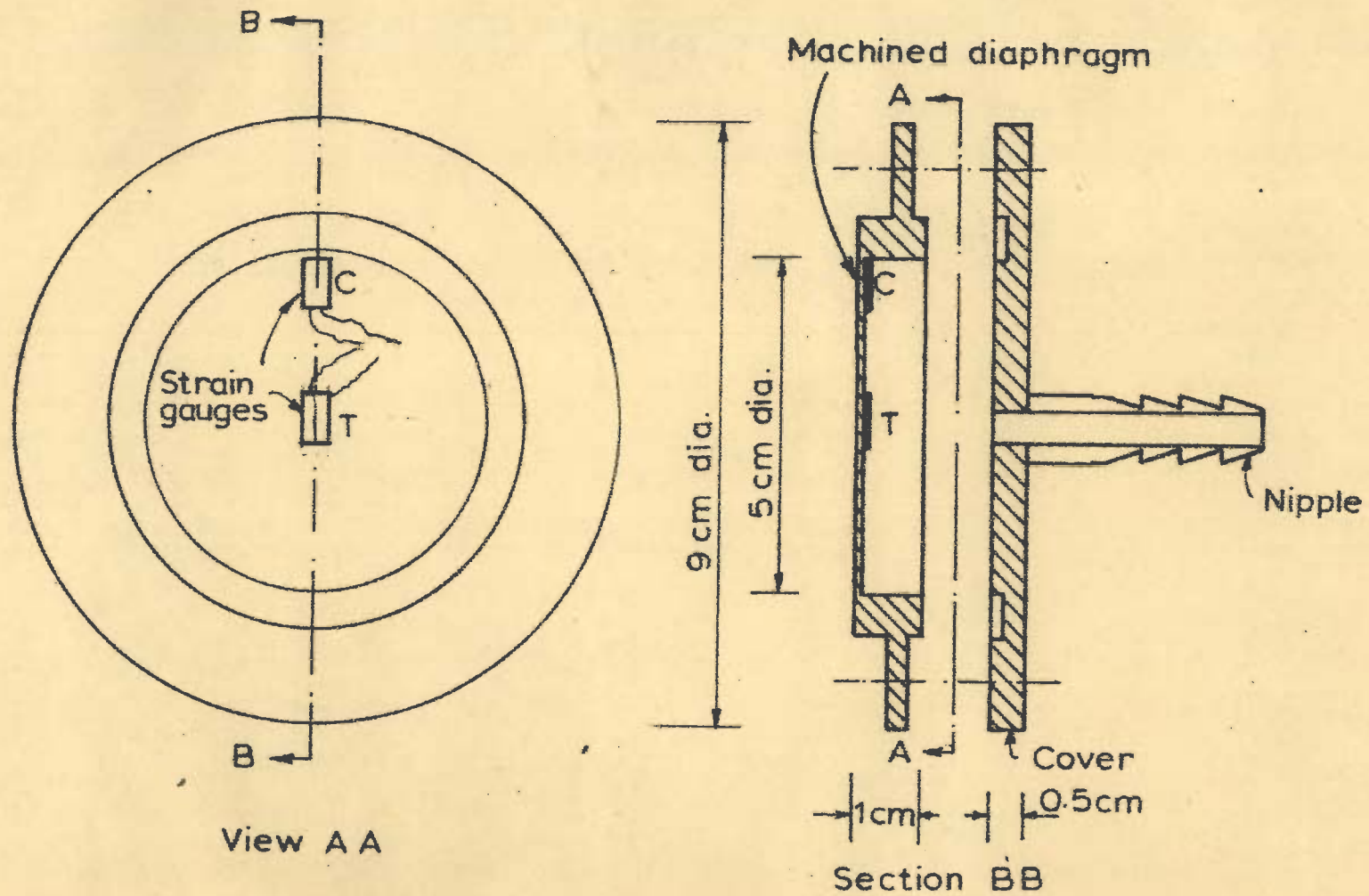
FIG. 13 – BOUNDARY EARTH-PRESSURE CELL FOR FIELD WELL MODEL
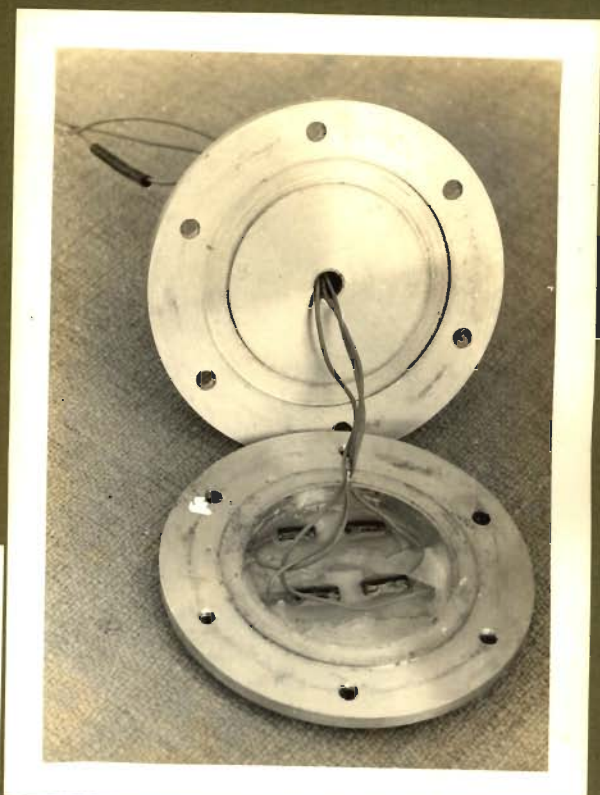
FIG.14- Earth-pressure Cell For
Field Well Model

FIG.15- Calibration Chamber
Field Pressure Cell

FIG.16- Calibration Apparatus
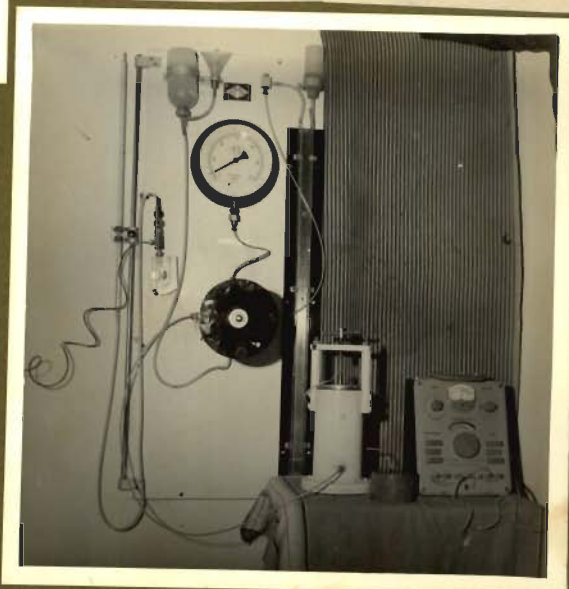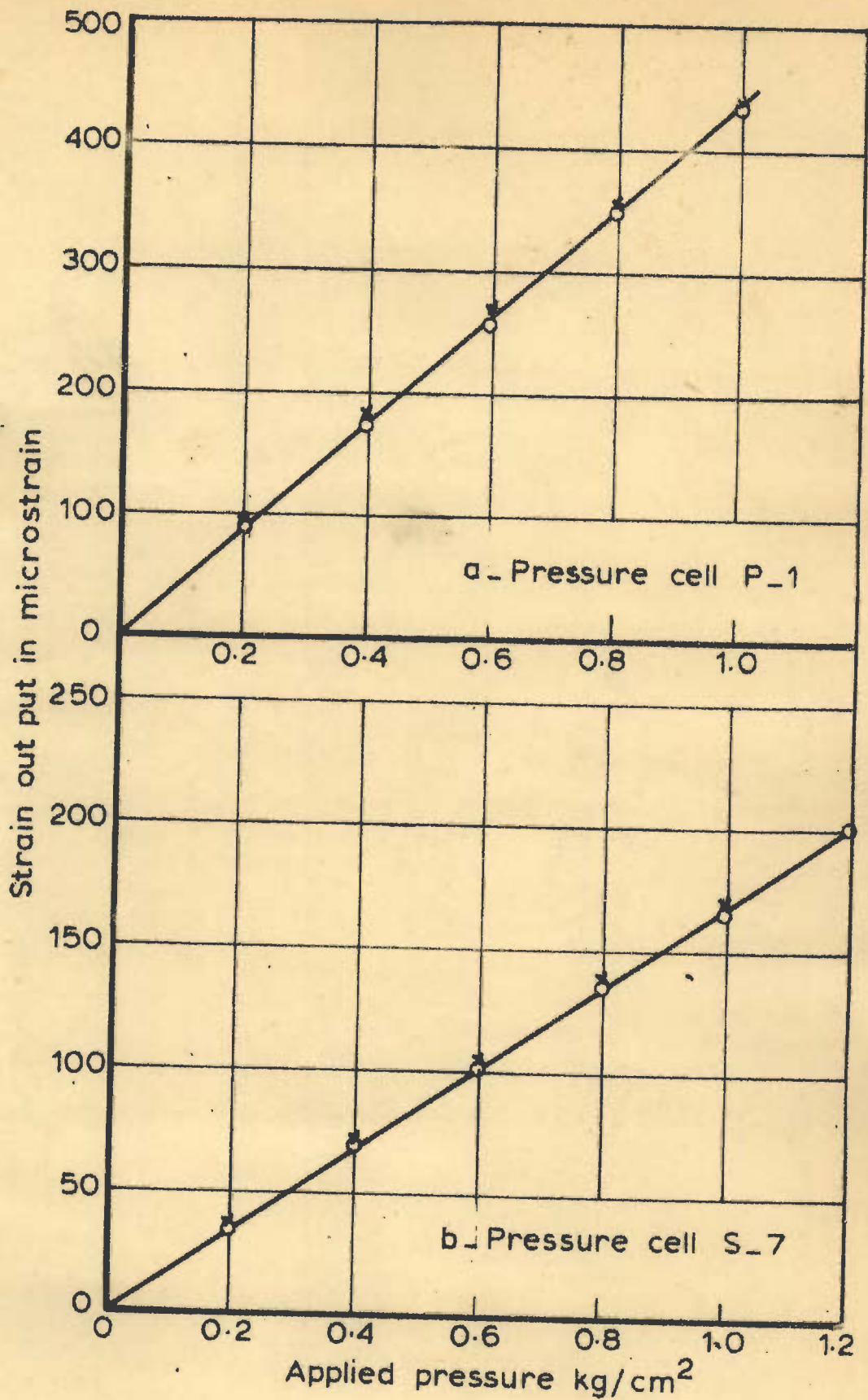
FIG. 17 _ TYPICAL CALIBRATION CURVES OF FIELD
PRESSURE CELLS
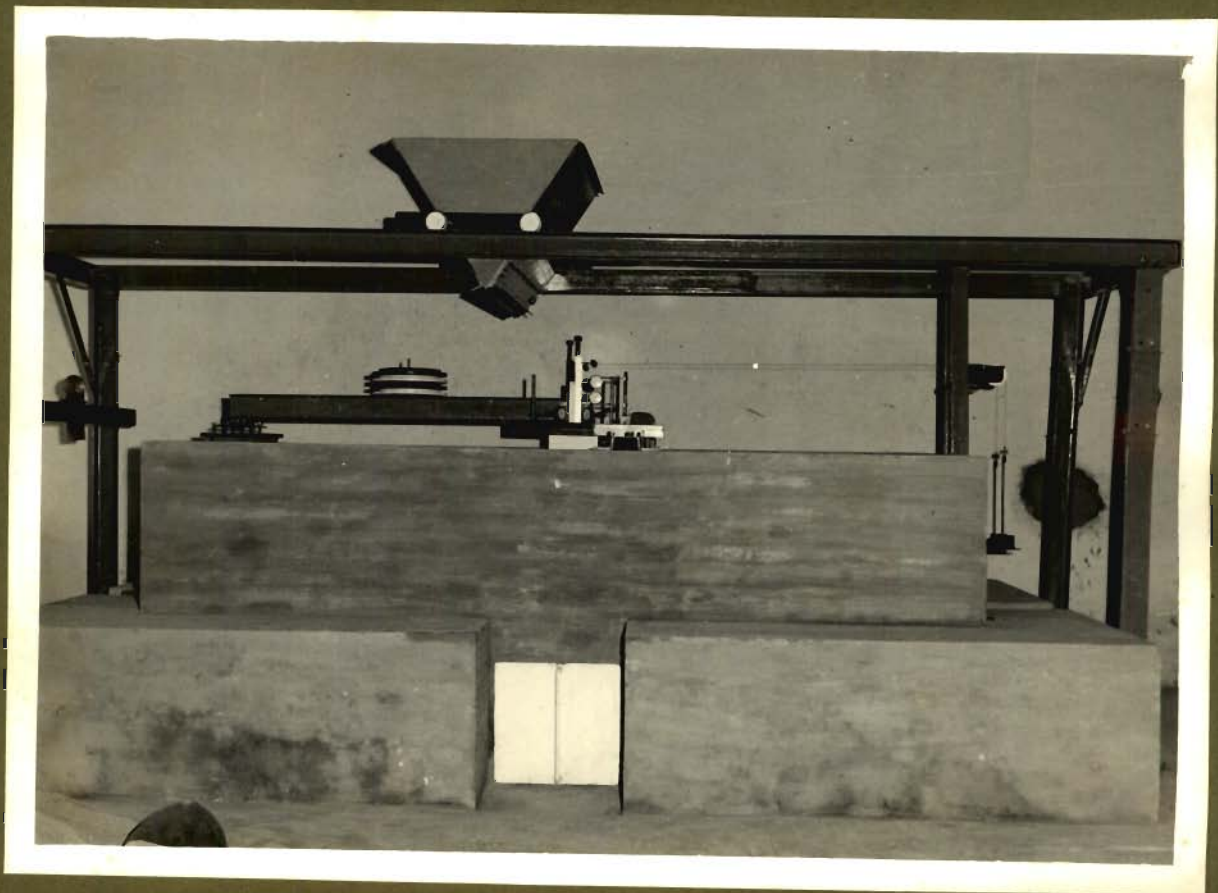
FIG.18- Laboratory Model Testing
Facility
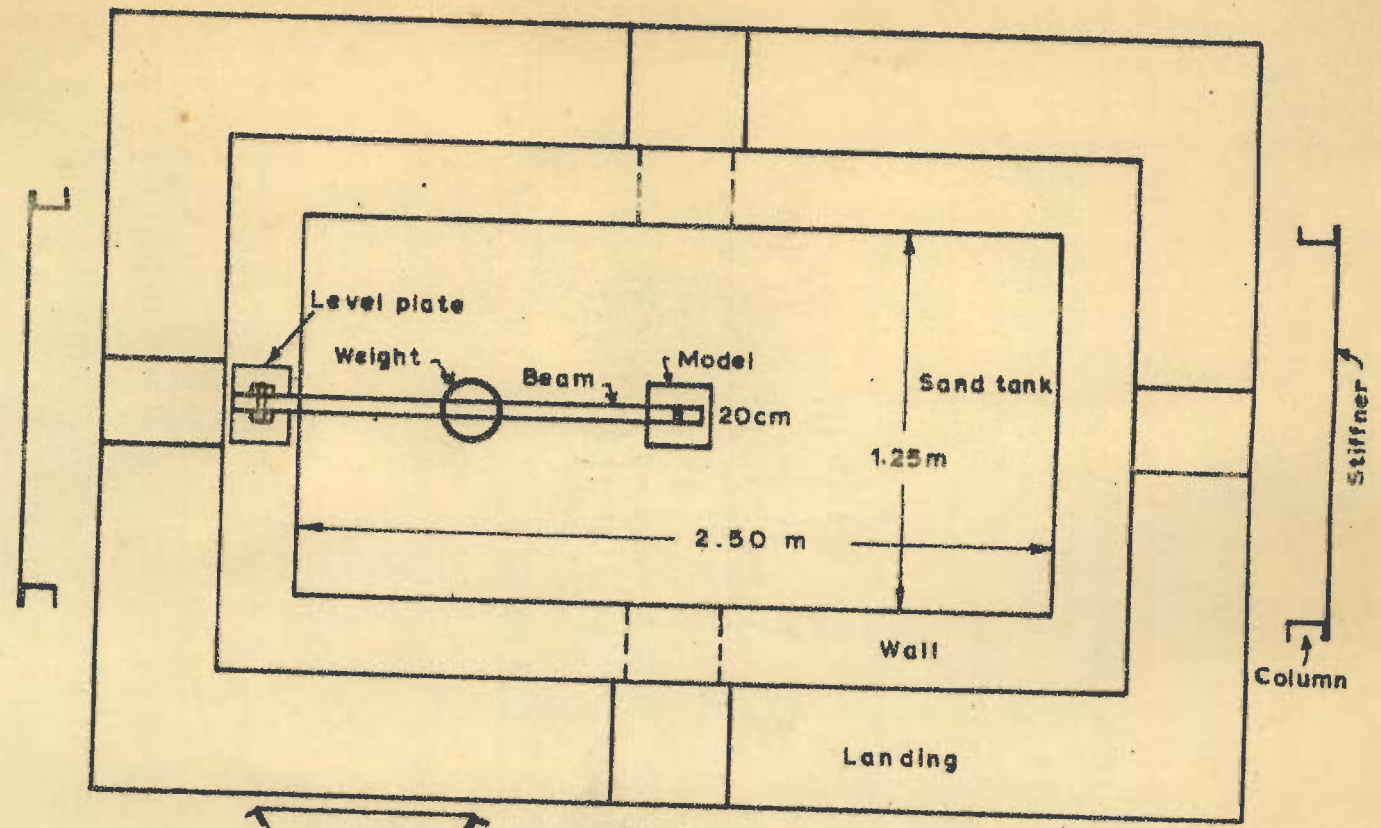
Plan
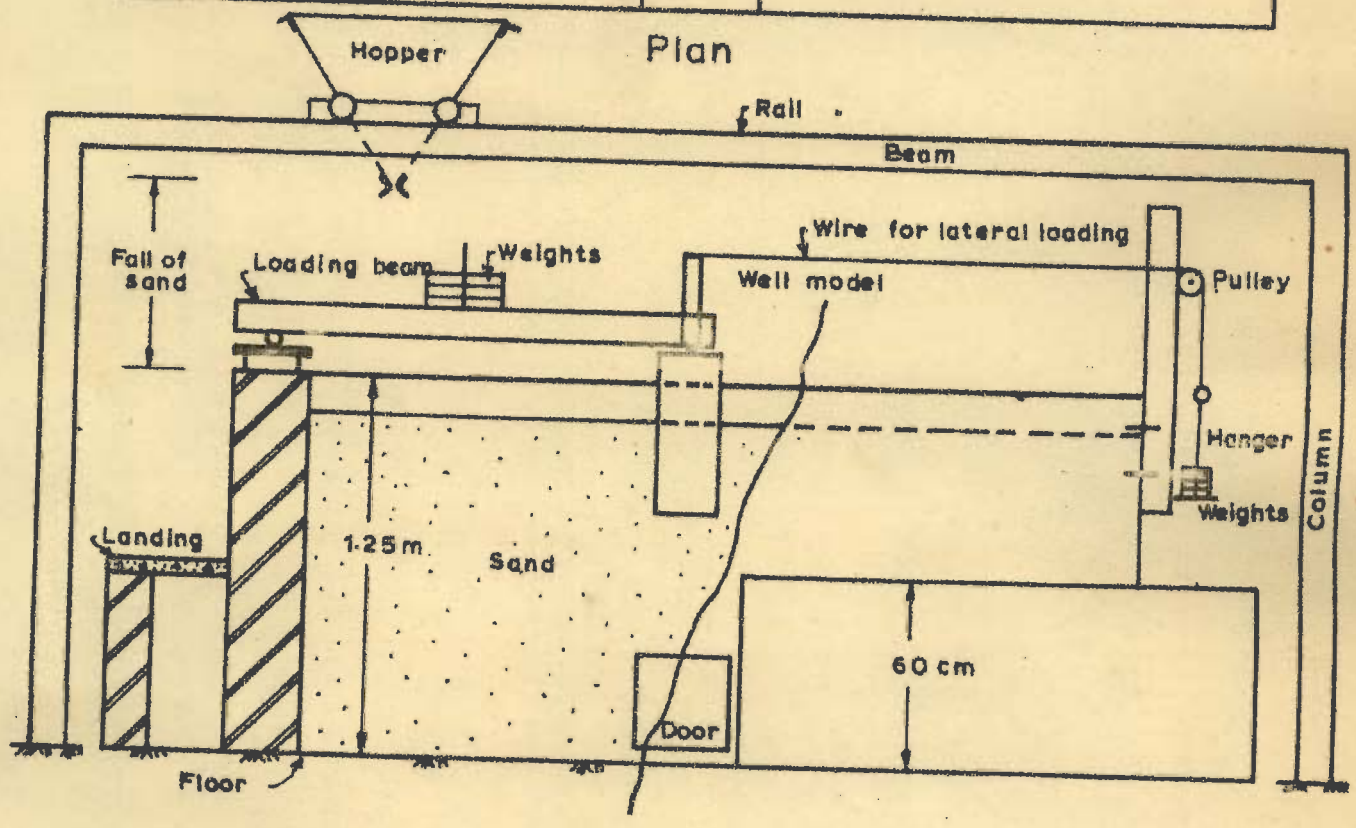
Half longitudinal sectional elevation

FIG. 19 _ LABORATORY MODEL TESTING FACILITY
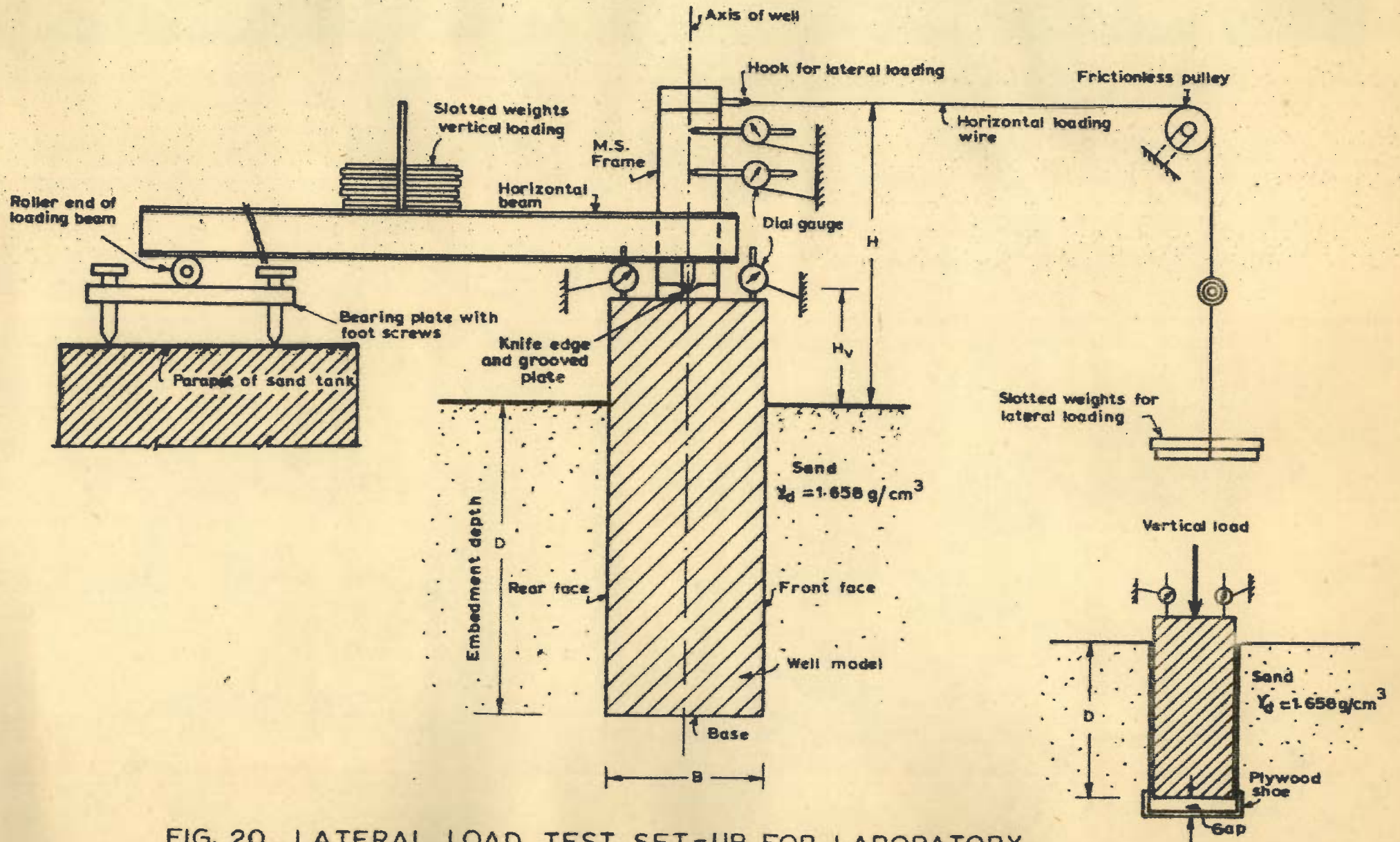
FIG. 20 - LATERAL LOAD TEST SET-UP FOR LABORATORY WELL MODELS

a - SKIN FRICTION TEST SETUP

FIG.21- Test Set up-A view

Angle for dial gauge reading

Frame for loading

Front

Front

Back

Side face

Front

B-1

B-2

B-3

B-4

B-5

B-1 +

B-2 +

B-3 +

B-4 +

B-5 +

B-6 +

F-3

F-4

F-5

F-6

F-1

F-2

F-3

F-4

41.5

57

15

20

15

20

B-6 +

C-1 +

C-2 +

Front face

F-9   F-10

5   5

Direction of measurement of frictional force

All dimensions in cm

a_Wooden models with pressure cells

b_Mildsteel model with friction cells
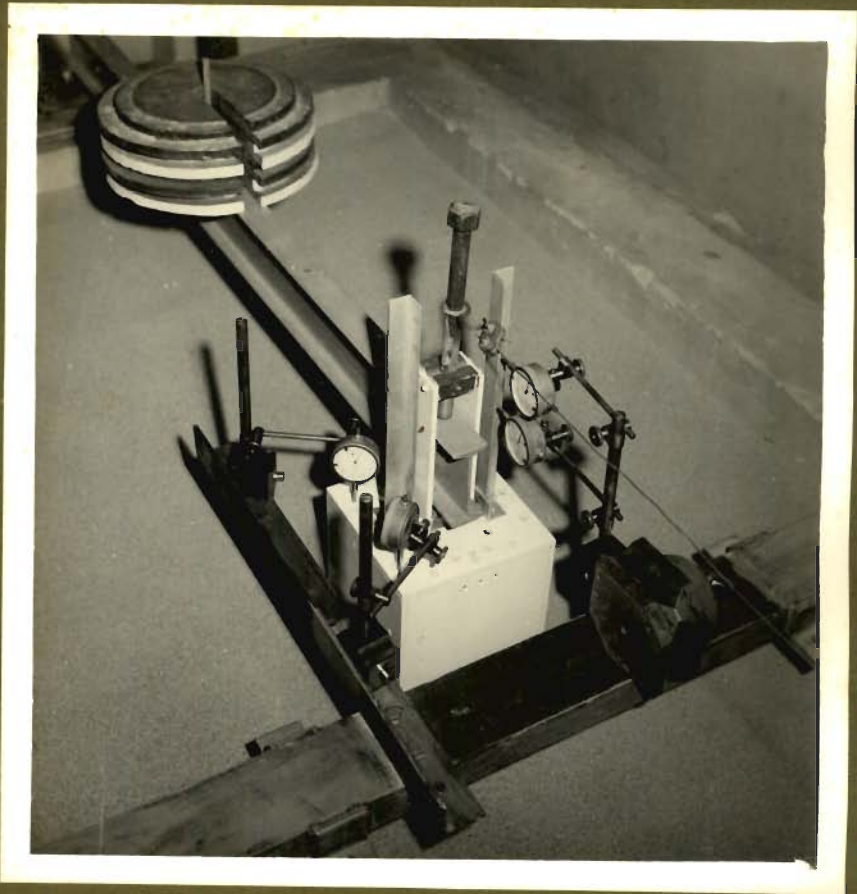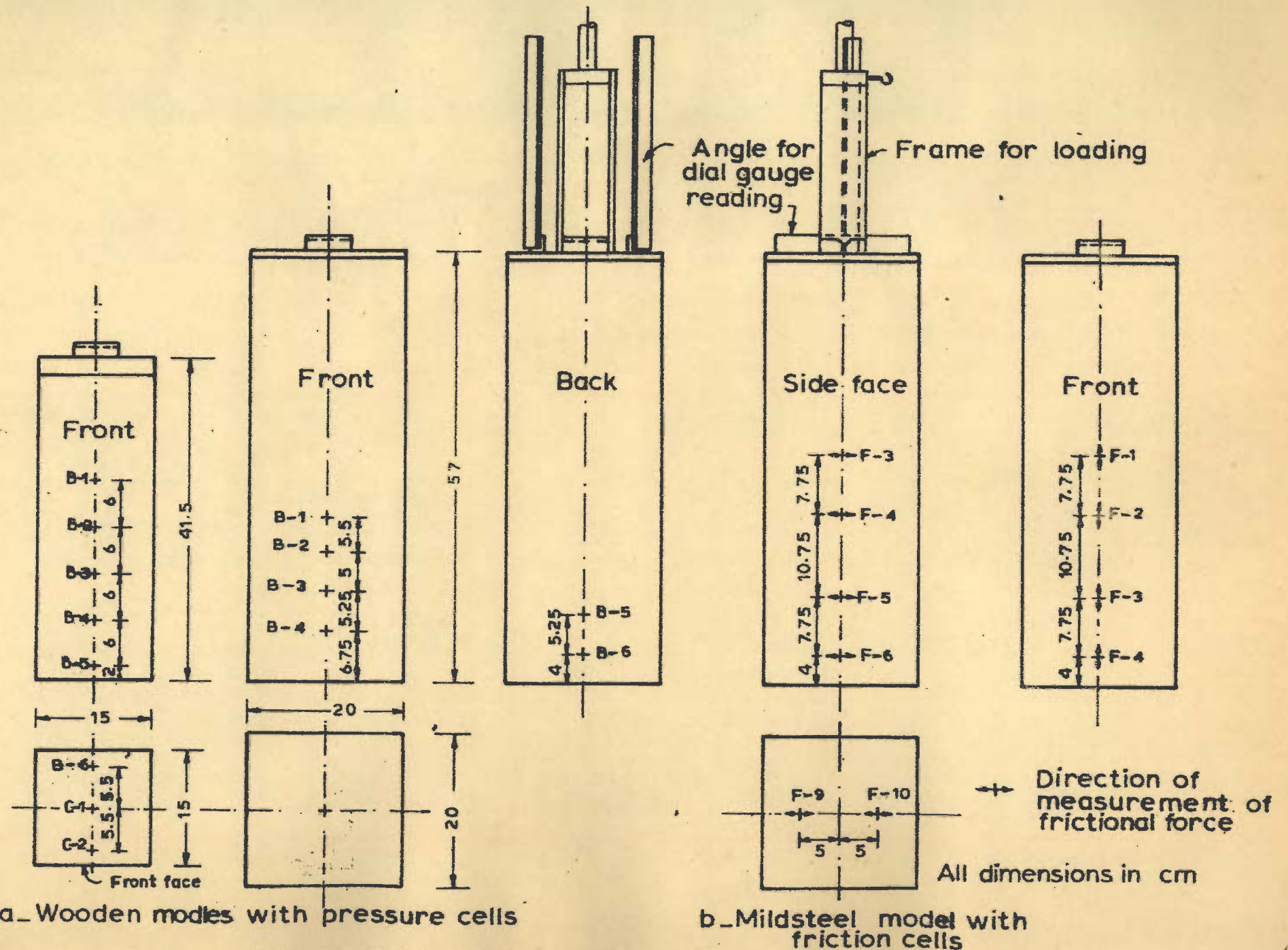
FIG. 22 _ DIFFERENT LABORATORY MODELS WITH CELLS
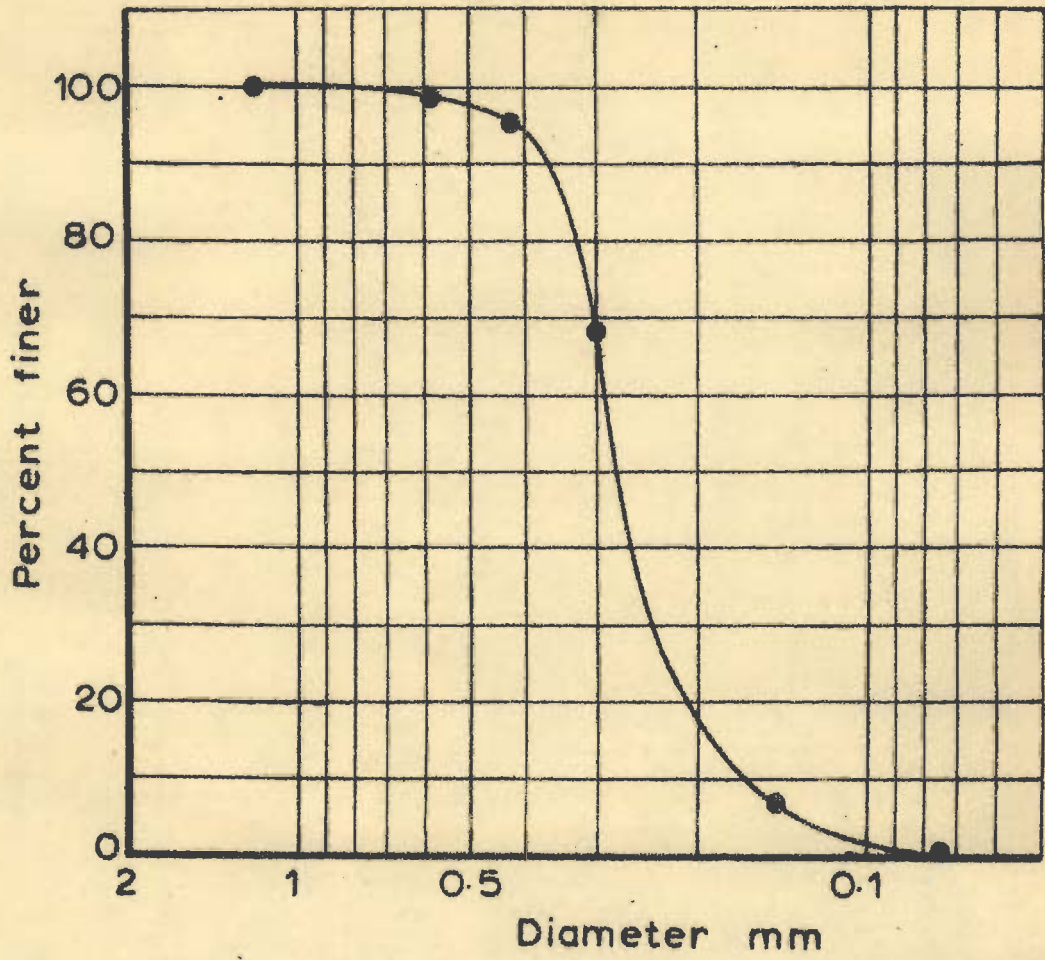
FIG. 23 _ GRAIN SIZE DISTRIBUTION CURVE
(RANIPUR SAND)
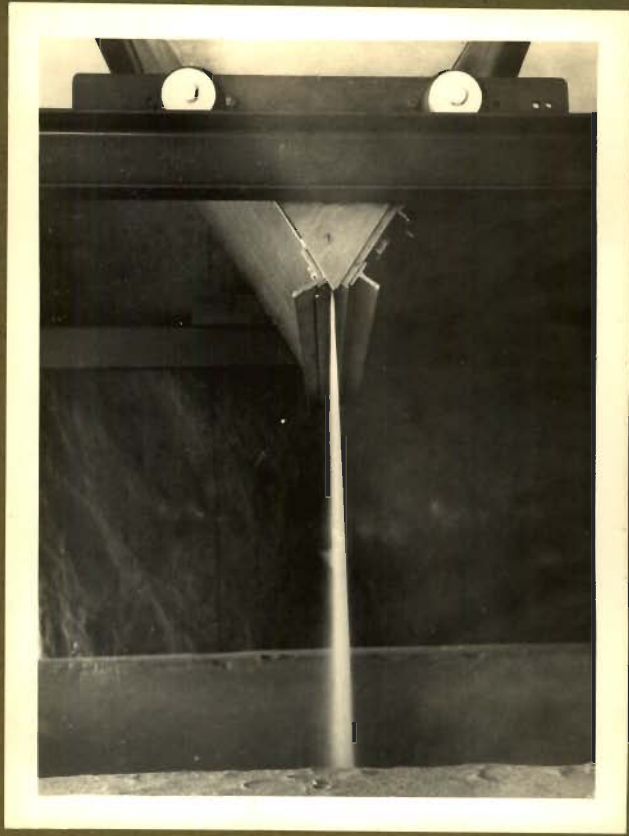
FIG.24- Hopper and Free Fall of Sand
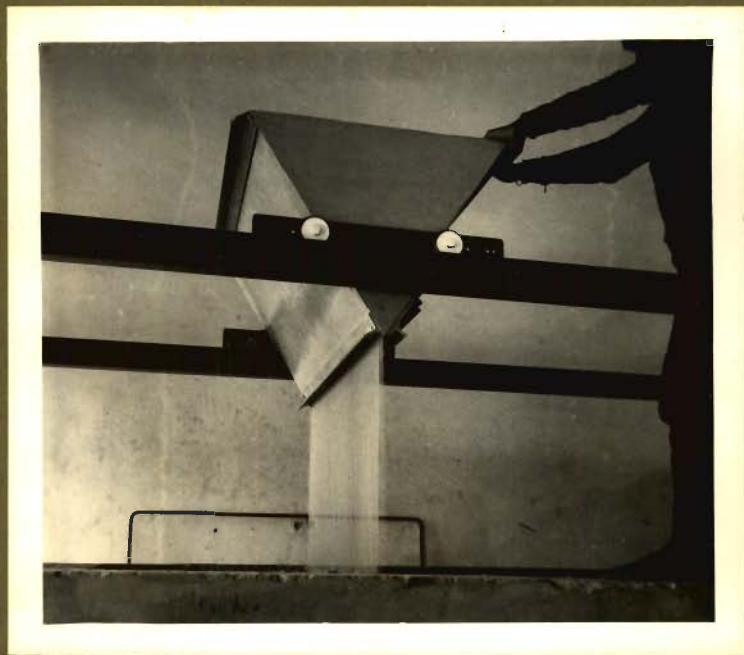
FIG.25-Mannual Operation of Hopper
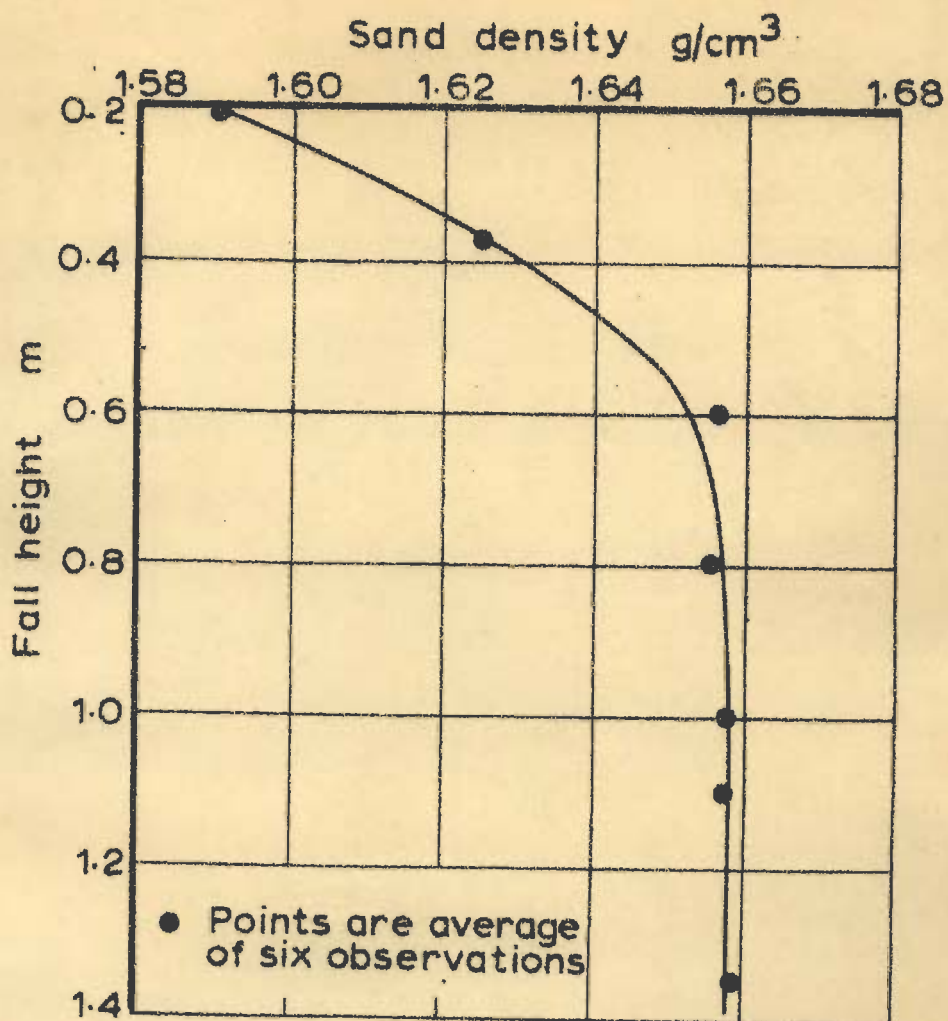
Sand density g/cm³

a – Fall of sand vs sand density
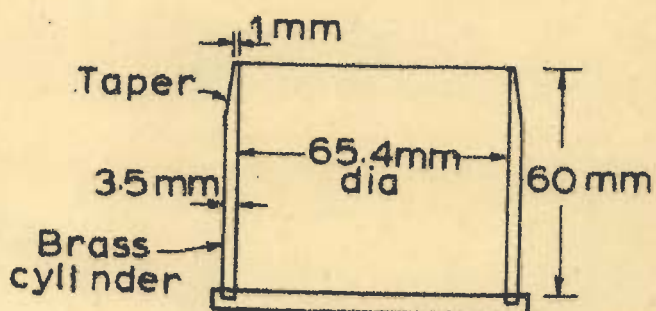
b – Container for density measurement
(half full size)

FIG. 26 – SAND DENSITY WITH FALL OF SAND
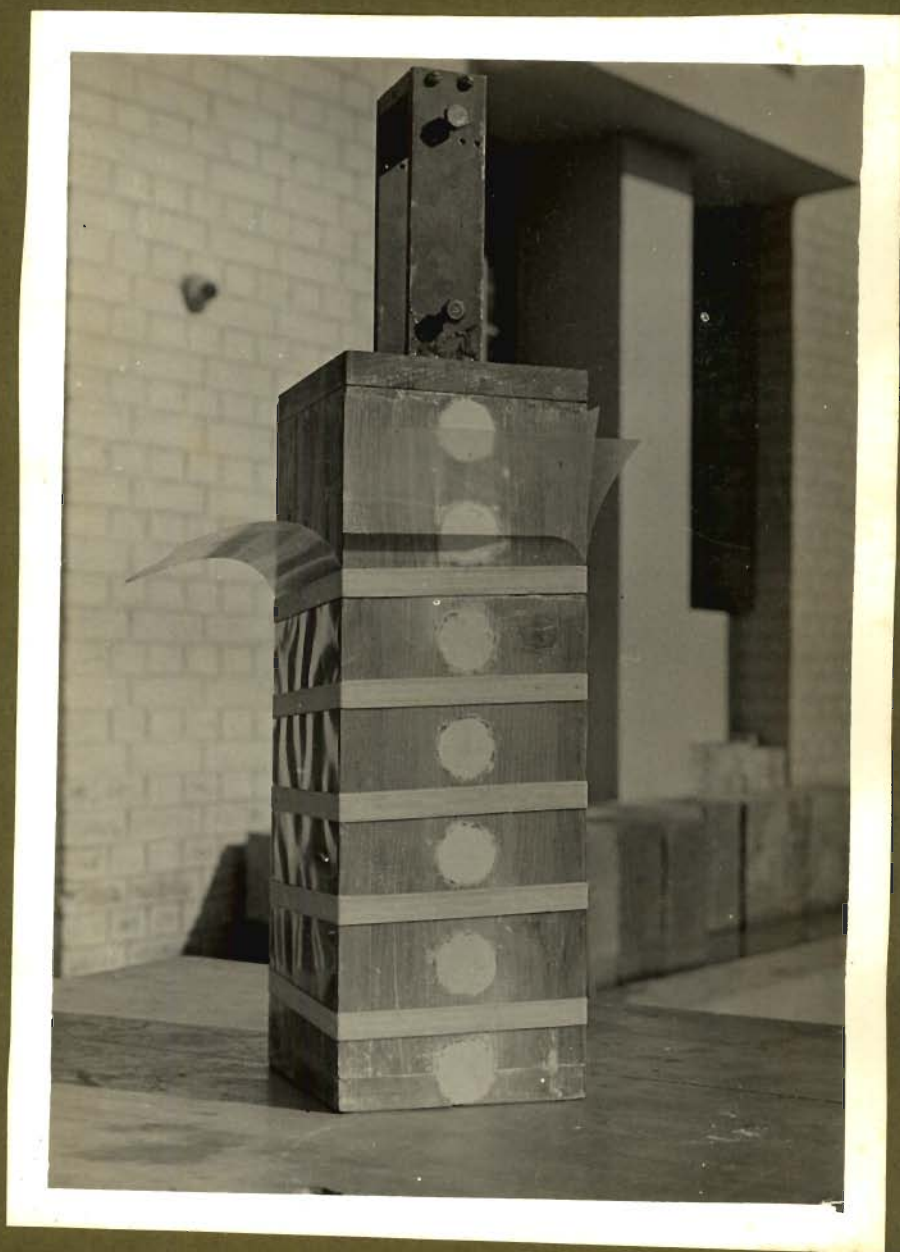
FIG.27-Polythene Sheets on Well Model

Section at BB

22mm ∅ foundation bolts

40cm

A — A

20 cm

35

10 mm dia horizontal reinforcement

10 mm dia vertical reinforcement

35

Cement concrete (1:2:4)

6 nos. 10 mm ∅ @ 40 cm c/c

2.25m

25

Steining

25

20

10mm Horizontal

20

25cm R.C.C PLUG

10

Anchors 10 mm ∅ 3in each row @ 35 cm c/c

Section at AA

1.5 m

10 mm dia vertical reinforcement

1.5m

10 mm dia

20cm

B — B

55 cm

Curb details

10 mm ∅ vertical reinforcement

Cement concrete (1:1·5:3)

10 mm ∅ horizontal reinforcement

10mm

M.S. Angle 6.75 cm x 6.75 x 0.8cm cutting edge

FIG. 28 _ DETAILS OF FIELD WELL MODEL

213
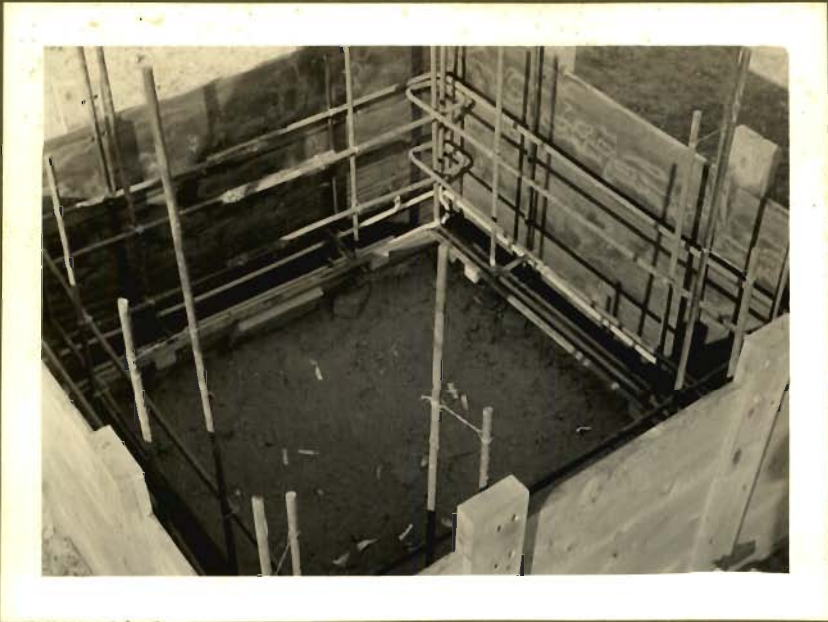
FIG.29-Form-work in Position
for Laying the Curb

FIG.30-The Concrete Curb and
the Cutting Edge
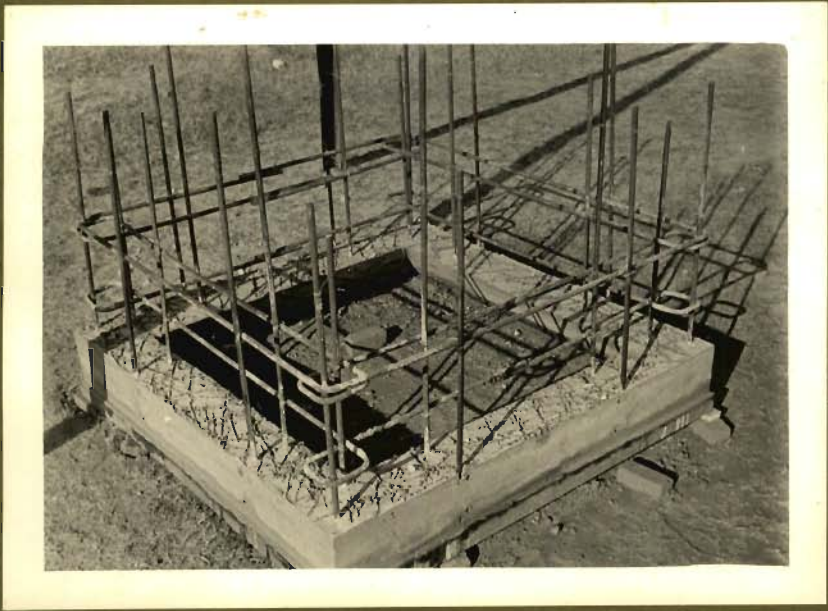
FIG.31-

-The Curb with Reinforcement
for First Stage of Steining

FIG.32-Form-work in Position For
First Stage of Steining

FIG.33-Welding Reinforcement for
Third Stage of Steining
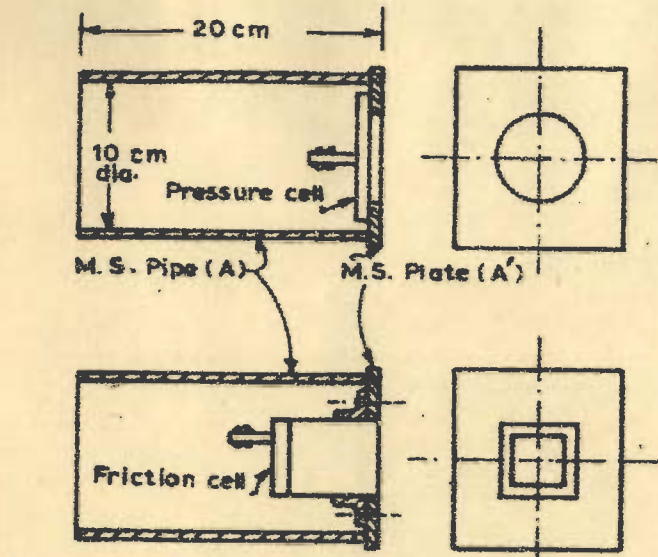
b - Fixture for pressure cell and friction cell
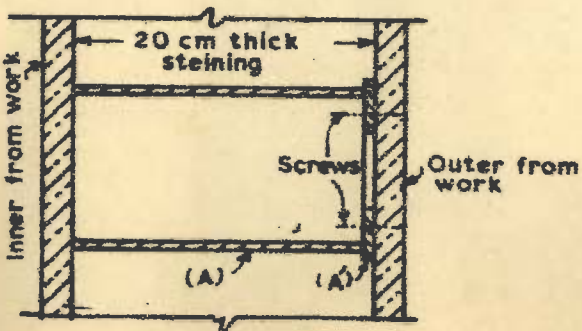
c - M. S. Pipe in position before concreting
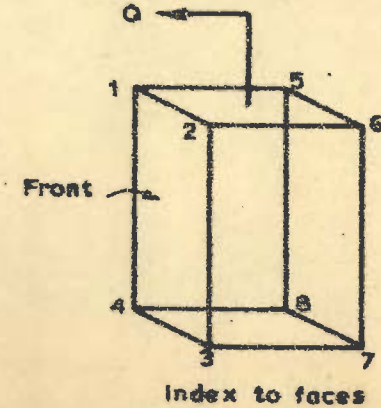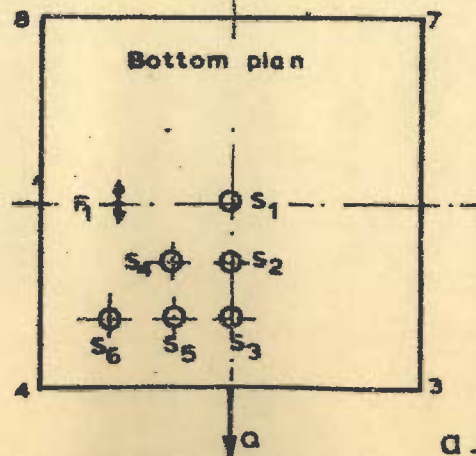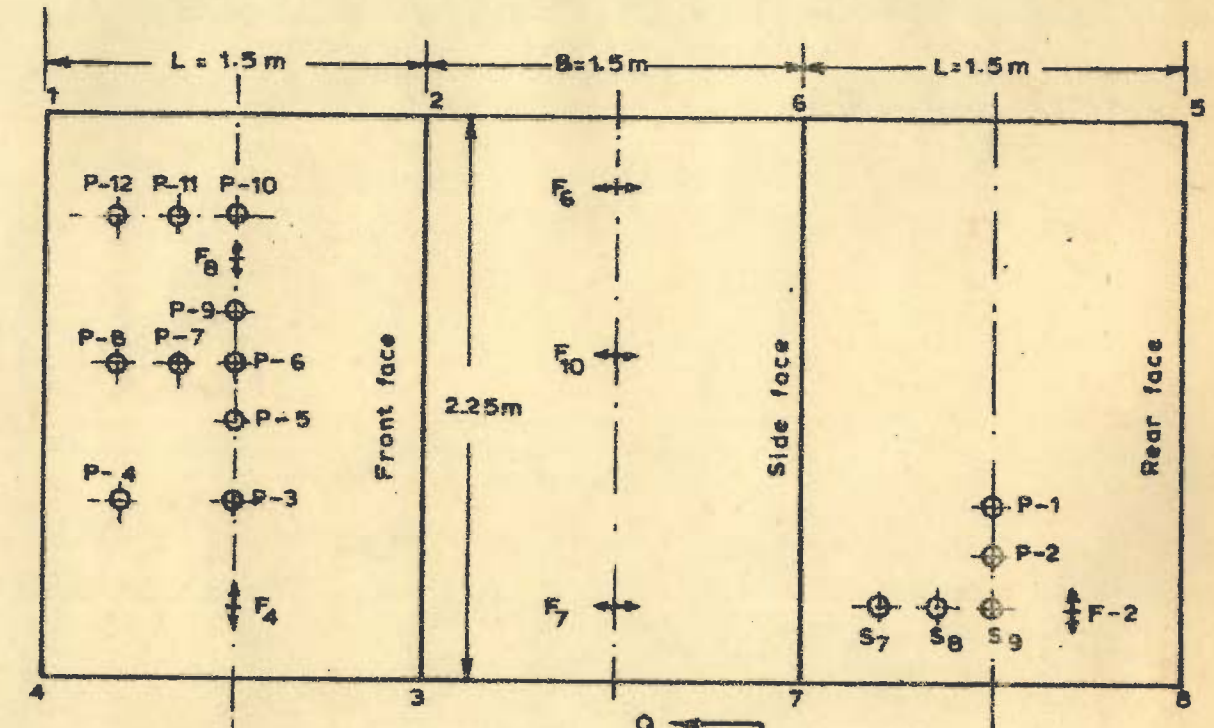
a - Arrangement of pressure cells and friction cells on face and base

FIG. 35 - INSTRUMENTATION IN FIELD WELL MODEL

216
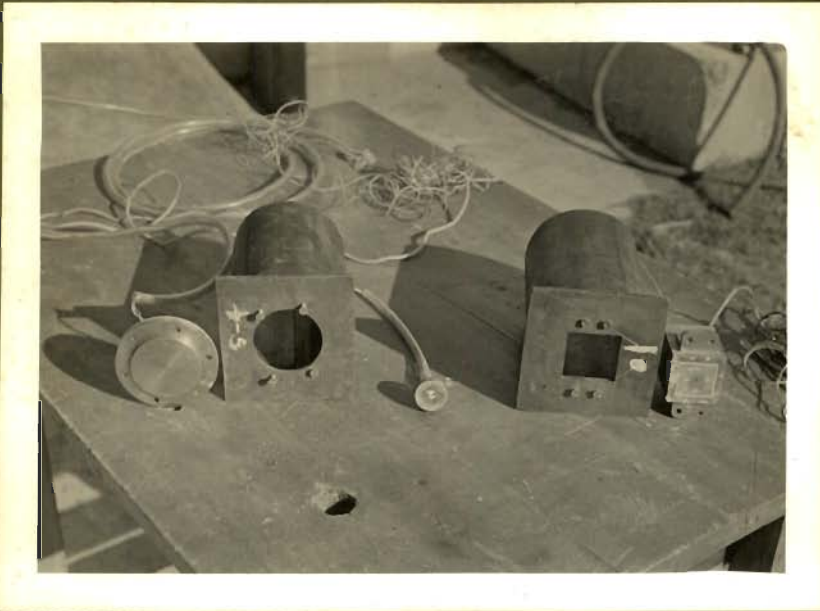
FIG.34-Pipes with Plates For
    Fixing Pressure Cells
    and Friction Cells

FIG.36-Pipes Screwed to
    Outer Formwork
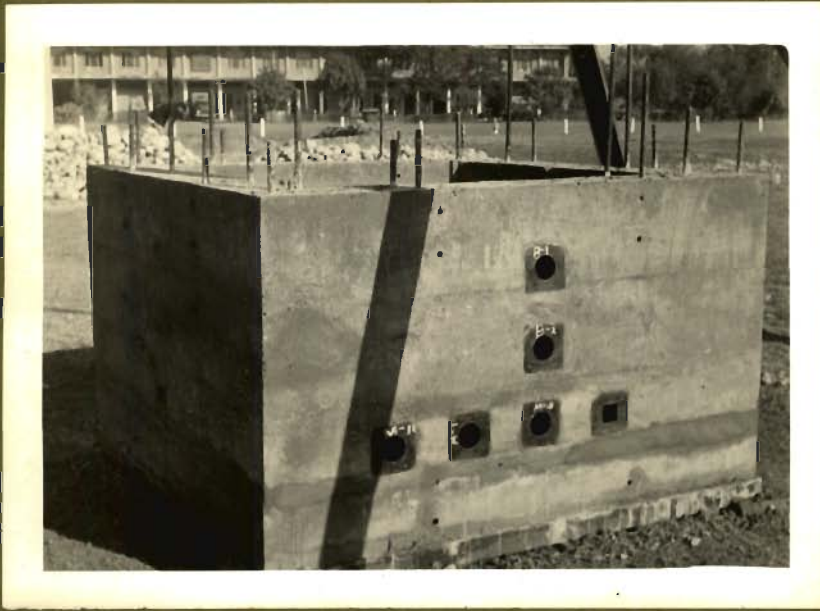
FIG.37-

-Openings for Fixing Cells
in the First Stage of
Well   Construction
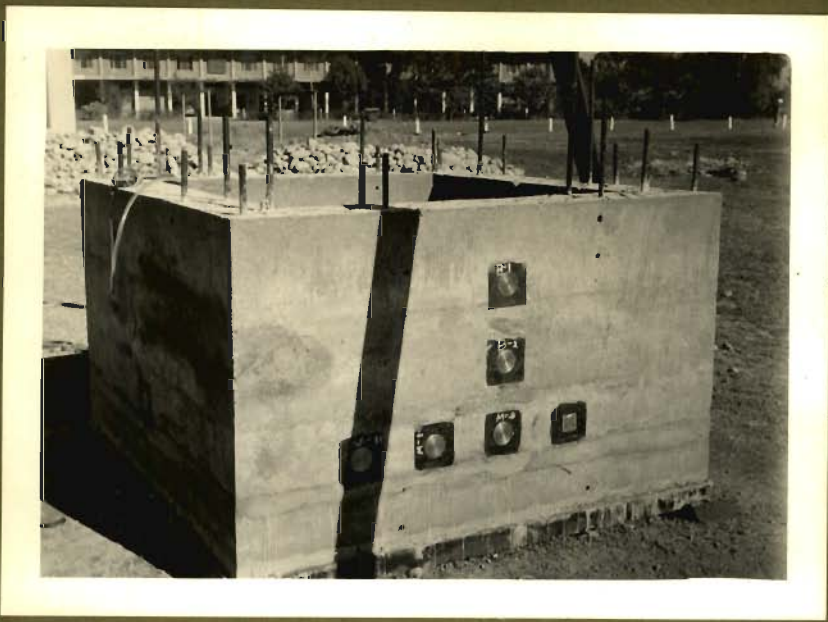
FIG.38-

-Pressure Cells and Friction
Cells in Position on Rear
Face and Side Face
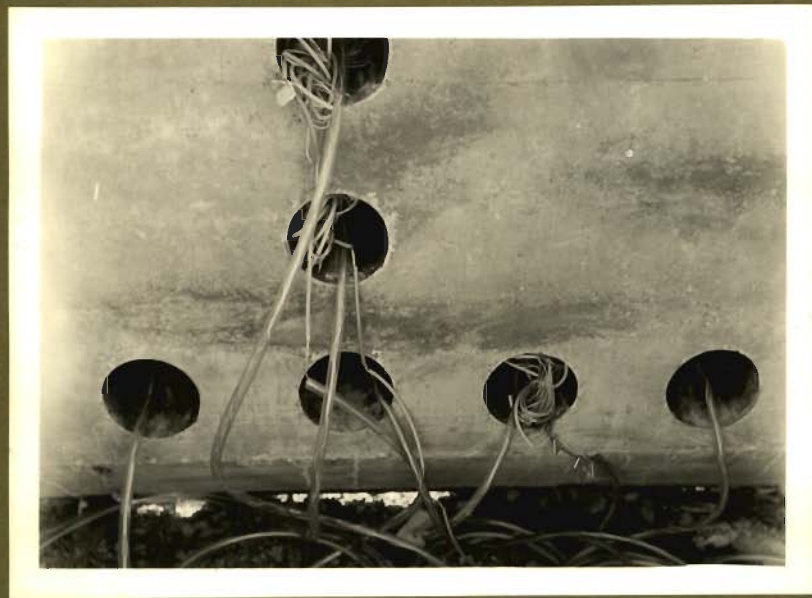
FIG.39-

-Leads of the Cells From
Inside the Well
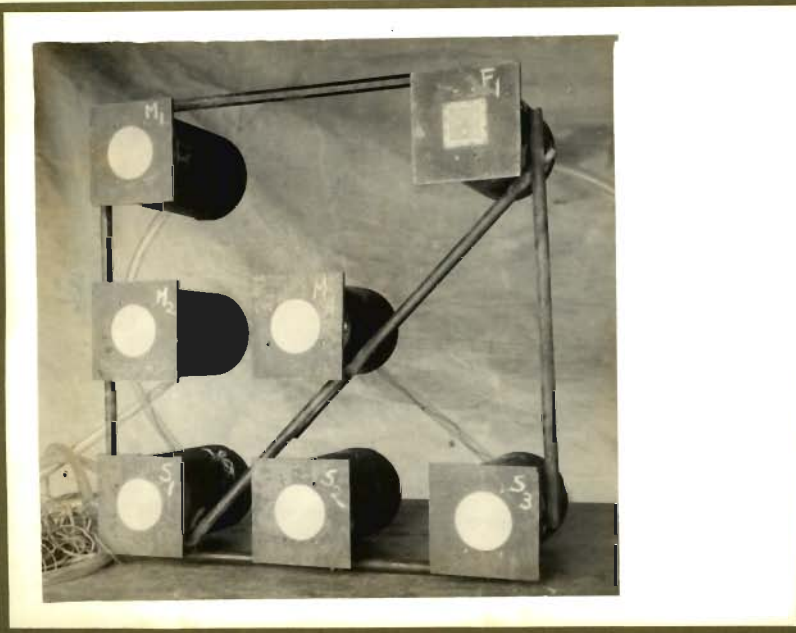
FIG.40-Cell Fixture for the
Bottom Plug

FIG.41-Free Vibration Test in Progress
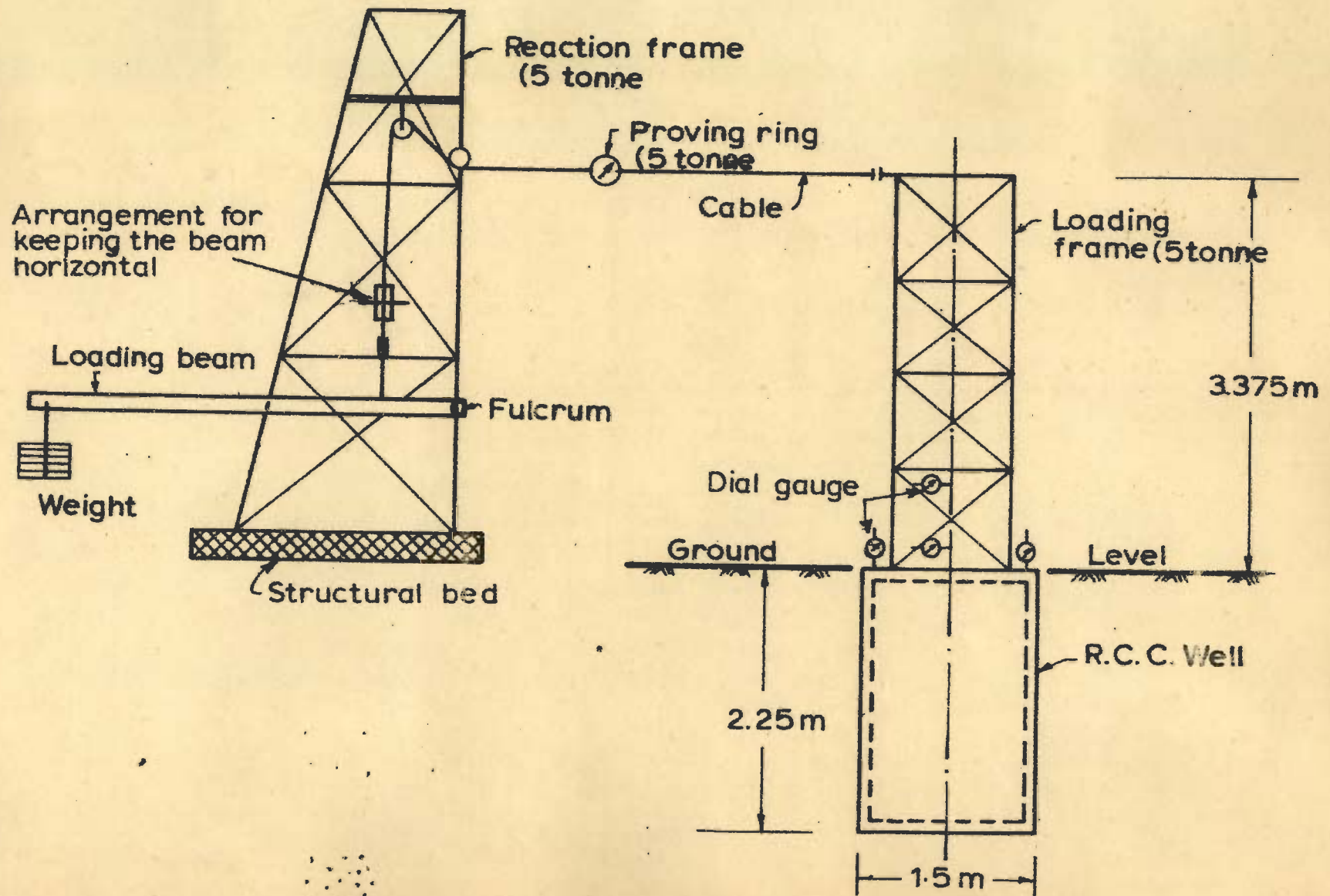
FIG. 42 _LATERAL LOAD TEST SETUP–FIELD MODEL

Reaction frame
(5 tonne

Proving ring
(5 tonne

Cable

Loading
frame (5 tonne

3.375 m

Arrangement for
keeping the beam
horizontal

Loading beam

Fulcrum

Dial gauge

Weight

Ground

Level

Structural bed

R.C.C. Well

2.25 m

1·5 m

FIG.43- 5-Tonne Reaction Frame With Loading Beam and Weights and Proving Ring

FIG.44- Field Well In-situ With Loading Frame, Loading Blocks, Datum Beams and Loading Cable
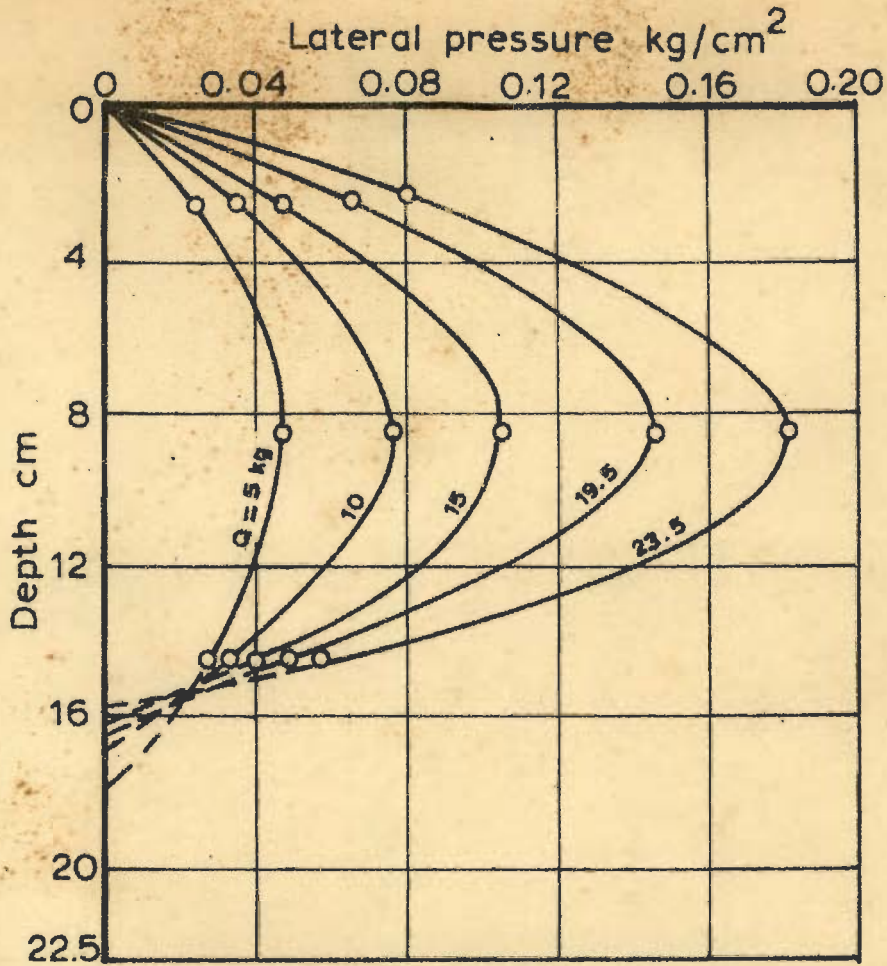
a _ Pressure distribution on front face vertical axis
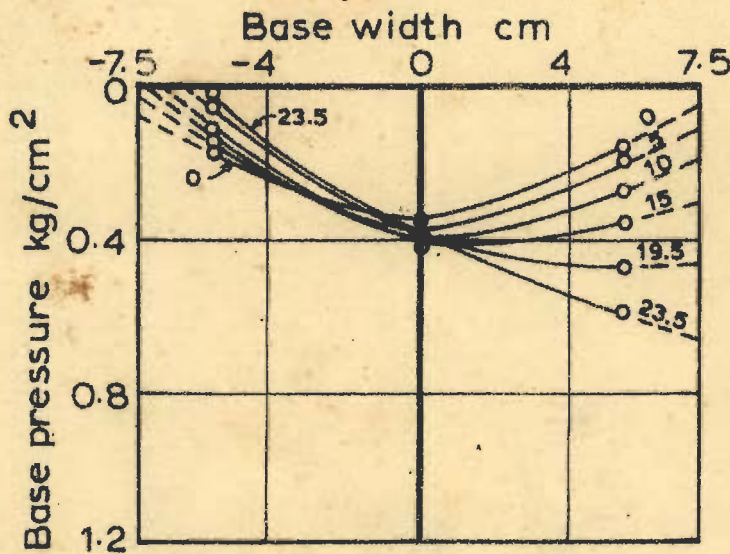
b _ Pressure distribution on centroidal axis of the base
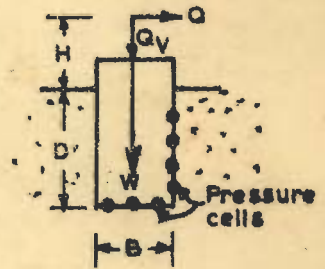
B = 15 cm, D = 22.5 cm
D/B = 1.5, H/B = 2.25
W = 6.5 kg
Q_V = 131 kg

FIG. 45 _ PRESSURE DISTRIBUTION ON FACE AND BASE
(Test no. 1)
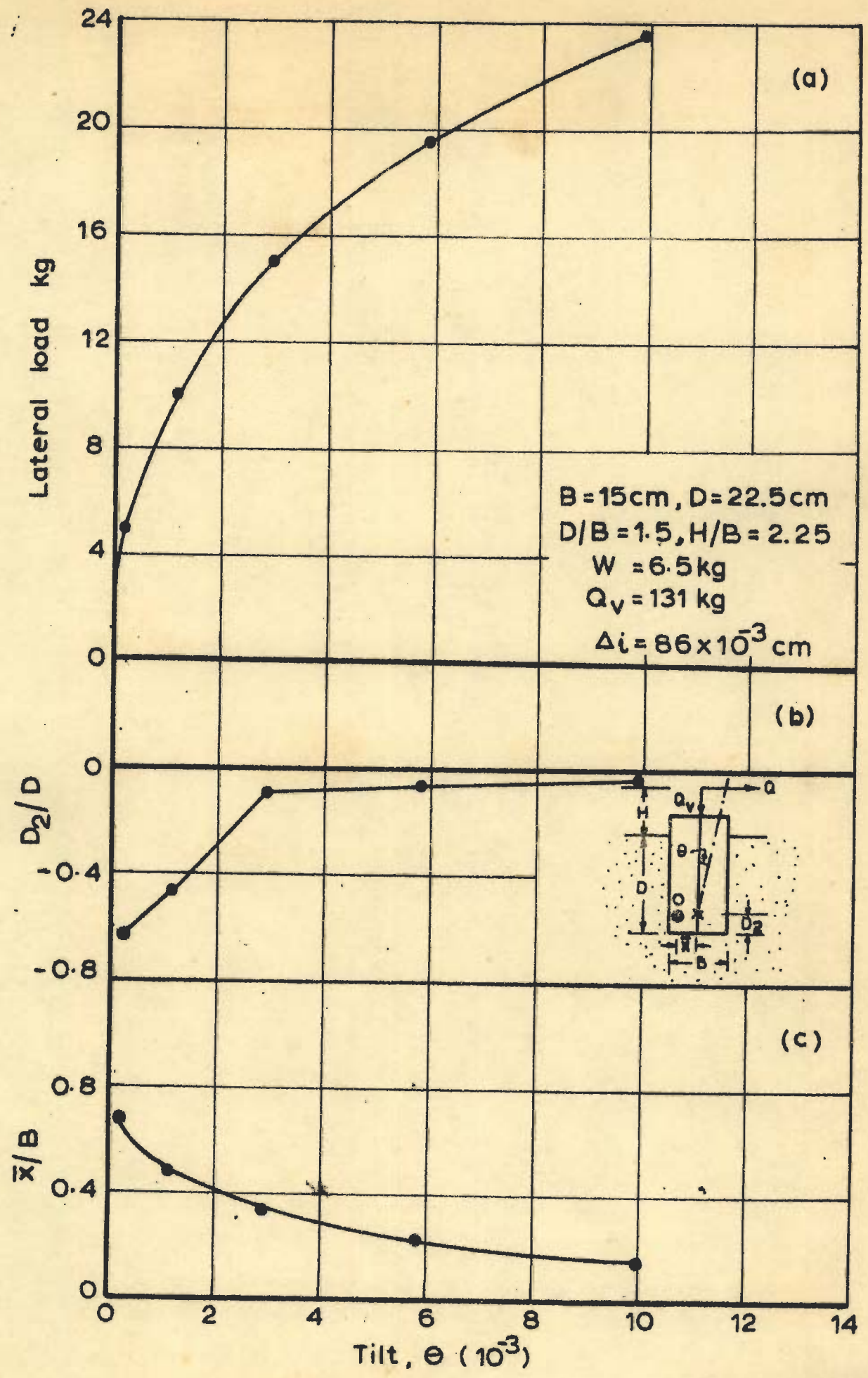
FIG. 46 _ LATERAL LOAD, D_2/D AND $\bar{x}/B$ VS TILT
(Test No. 1)
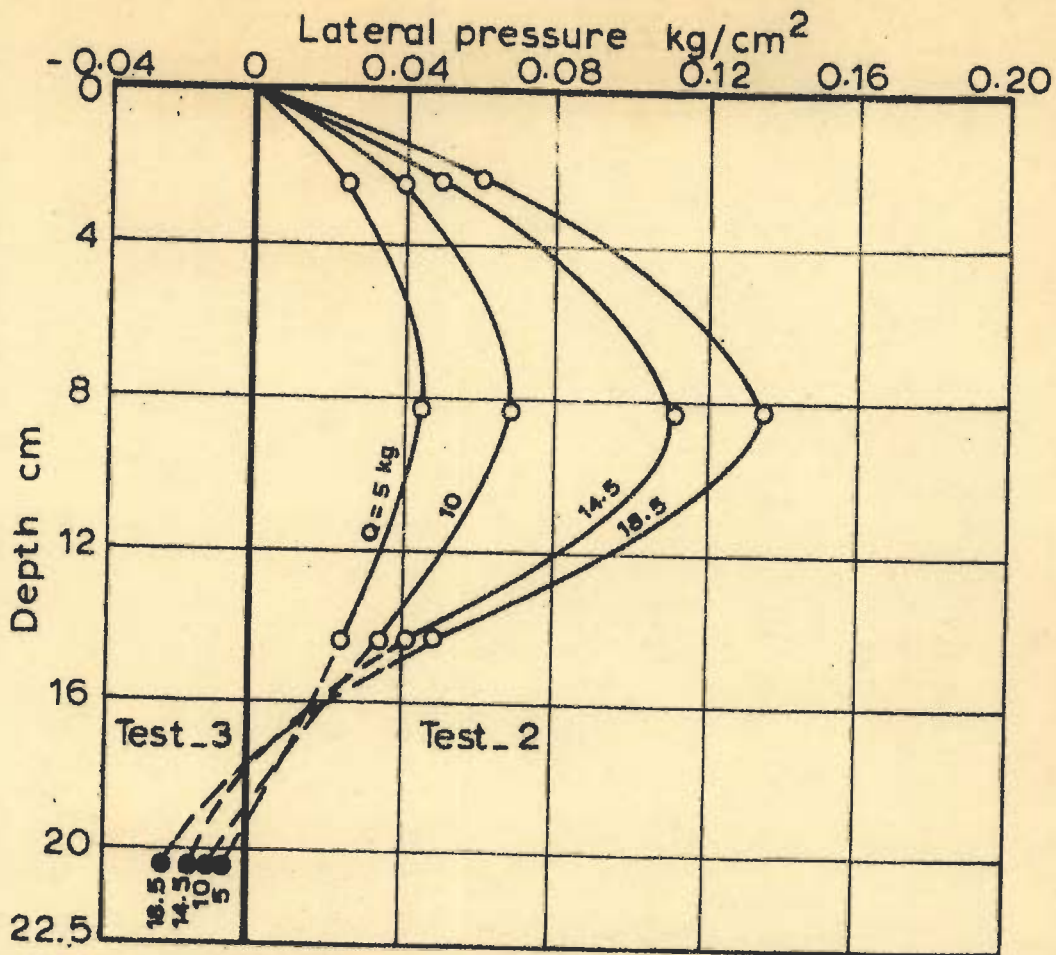
a – Pressure distribution on front and rear face vertical axis
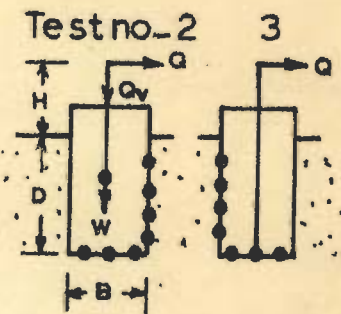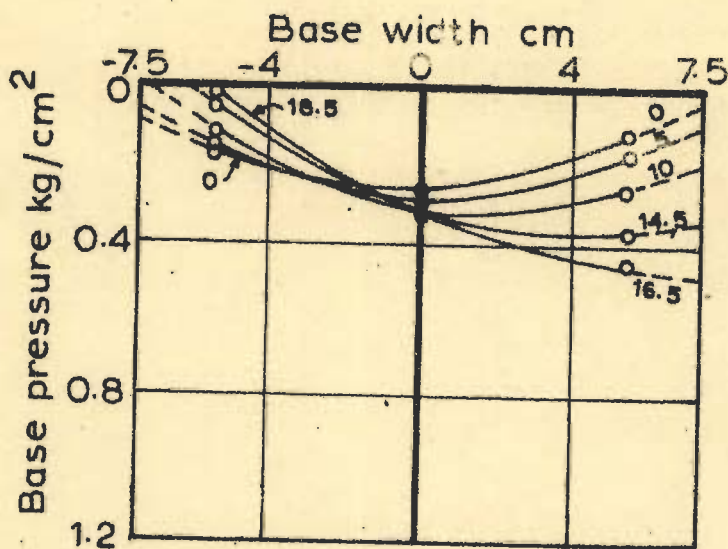
b – Pressure distribution on centroidal axis of the base

Test no_2   3

B = 15 cm, D = 22.5 cm
D/B = 1.5, H/B = 3
W = 6.5 kg
Q_v = 131 kg

FIG. 47 – PRESSURE DISTRIBUTION ON FACES AND BASE
(Test nos 2 & 3)
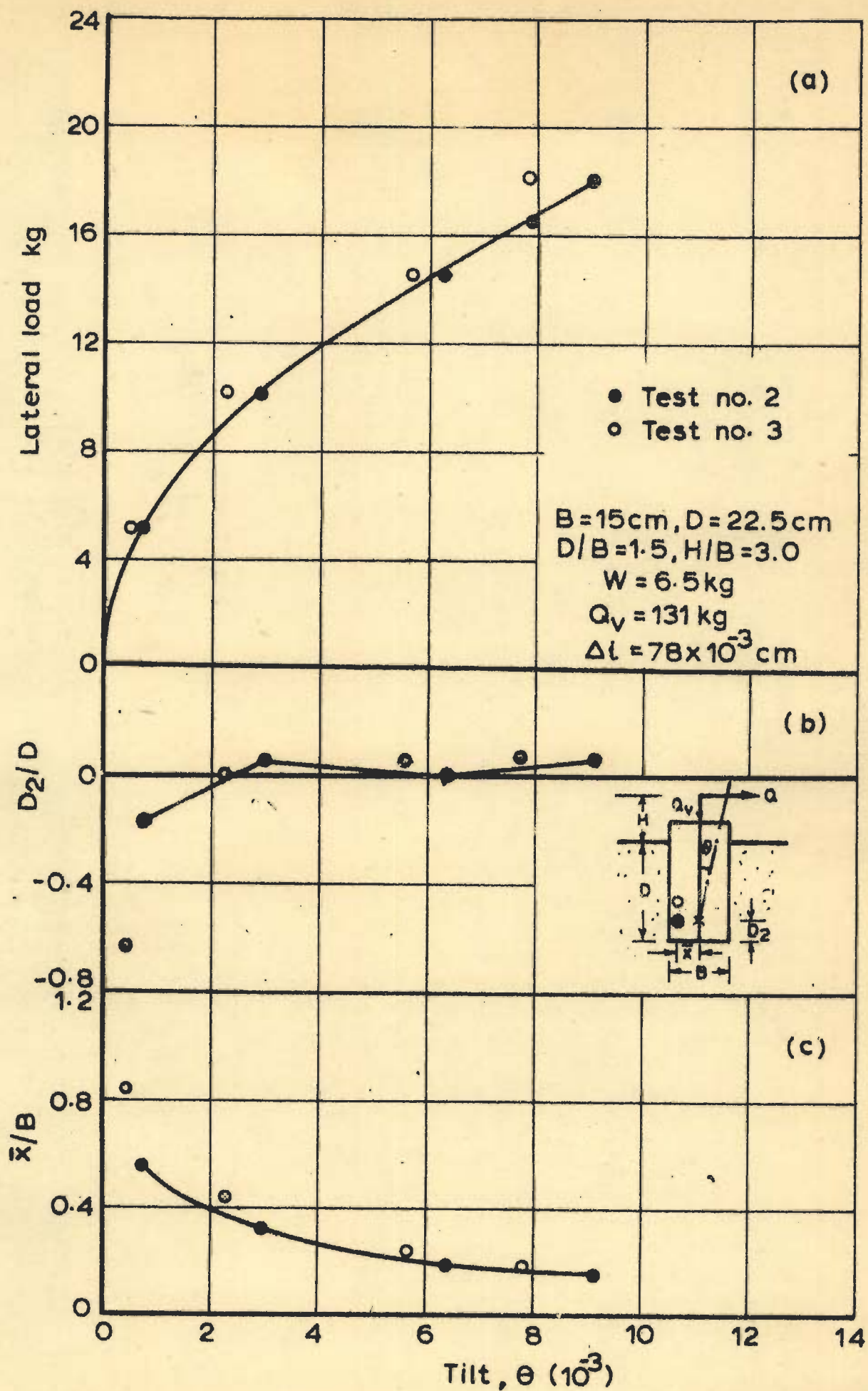
FIG. 48 _ LATERAL LOAD, D_2/D AND $\bar{x}/B$ VS TILT
(Test No. 2 and 3)
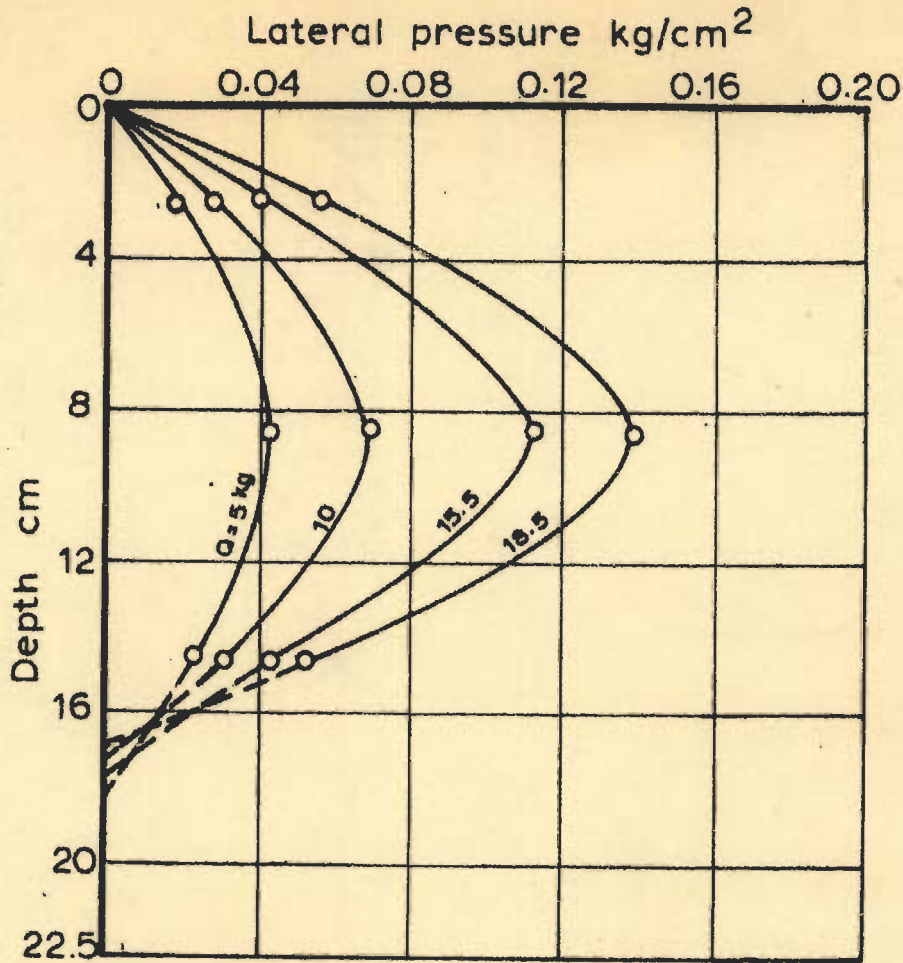
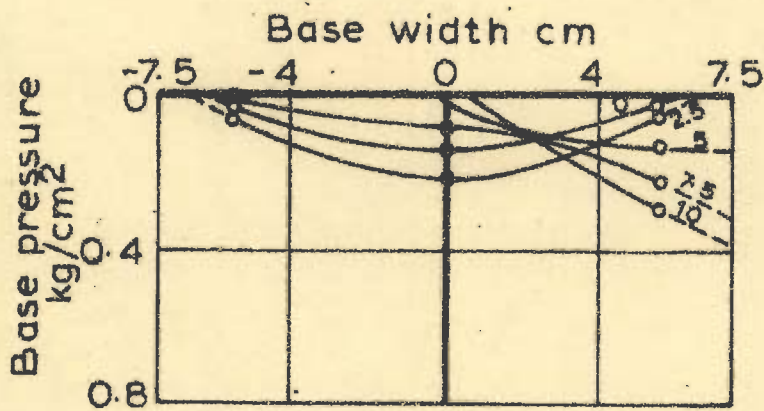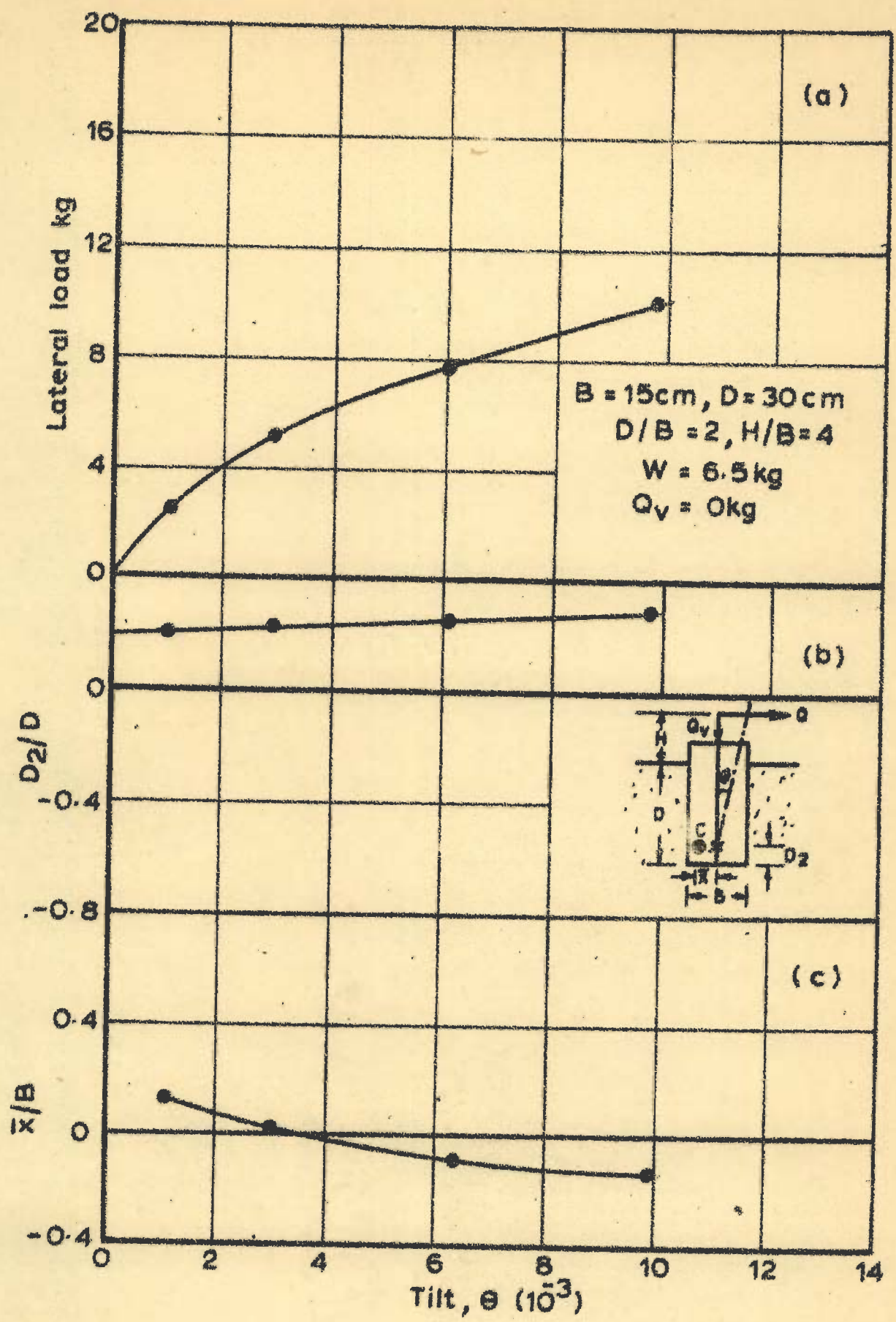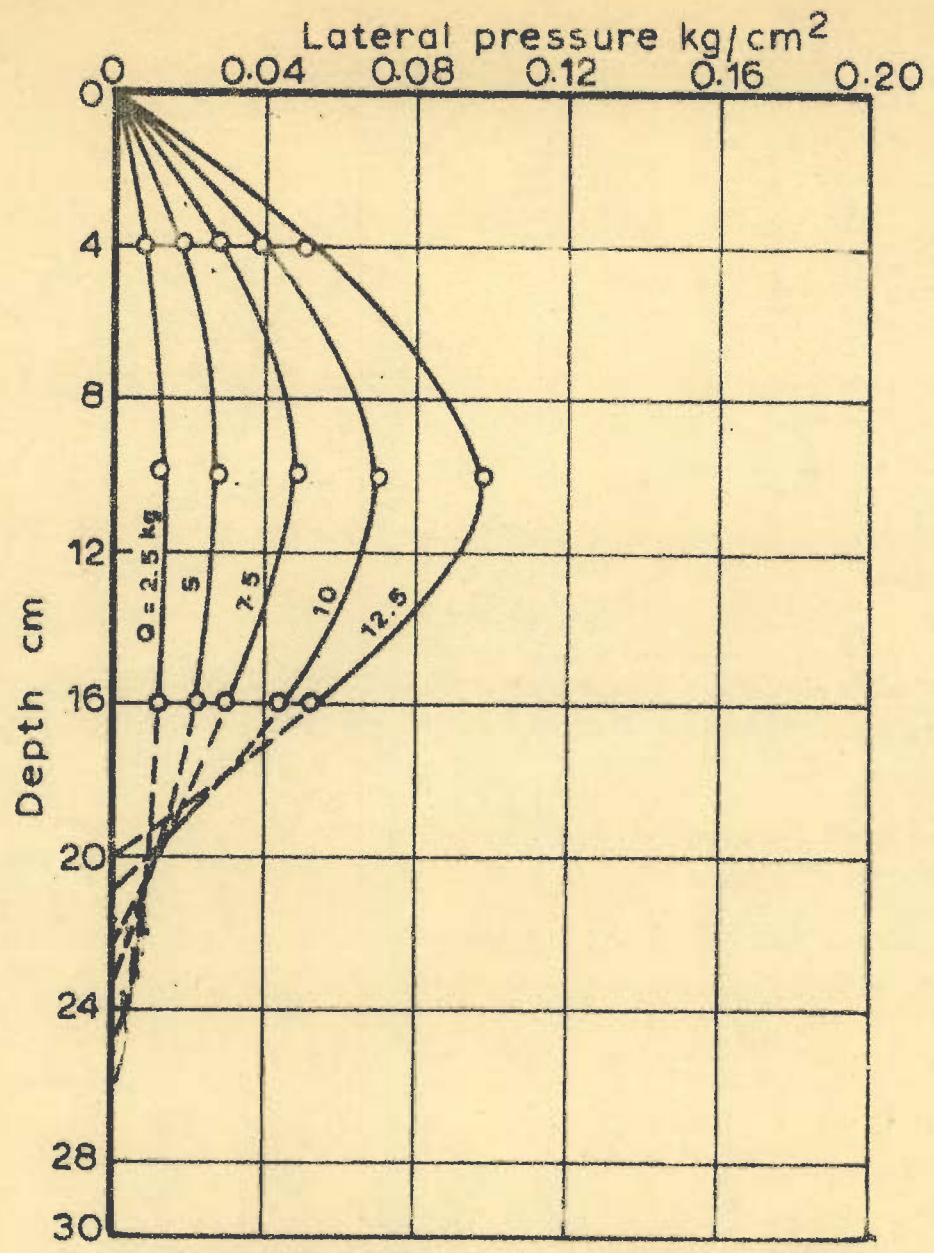a _ Pressure distribution on front face vertical axis
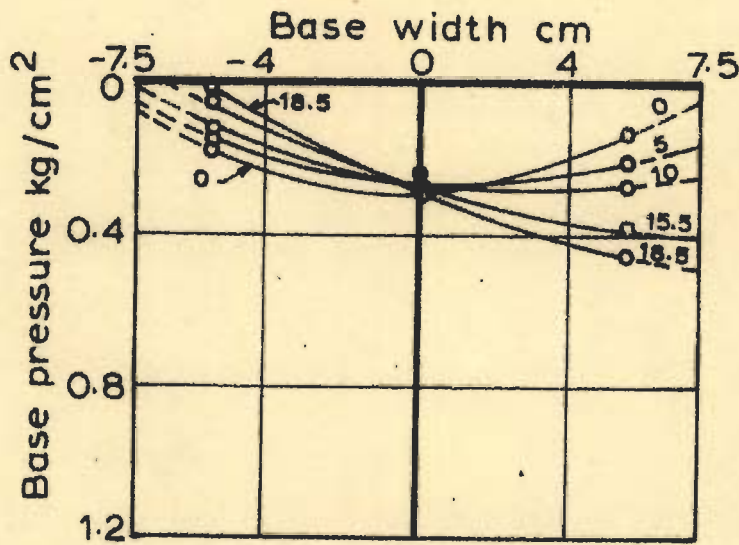
b _ Pressure distribution on centroidal axis of the base
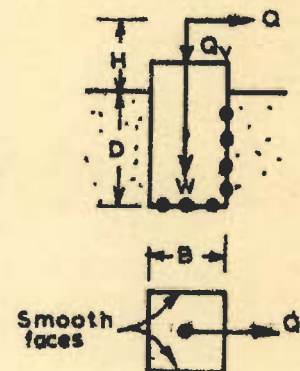
$B = 15\,cm,\ D = 22.5\,cm$
$D/B = 1.5,\ H/B = 2.25$
$W = 6.5\,kg$
$Q_v = 131\,kg$

FIG. 49 _ PRESSURE DISTRIBUTION ON FACE AND BASE
(Test no. 4)

227
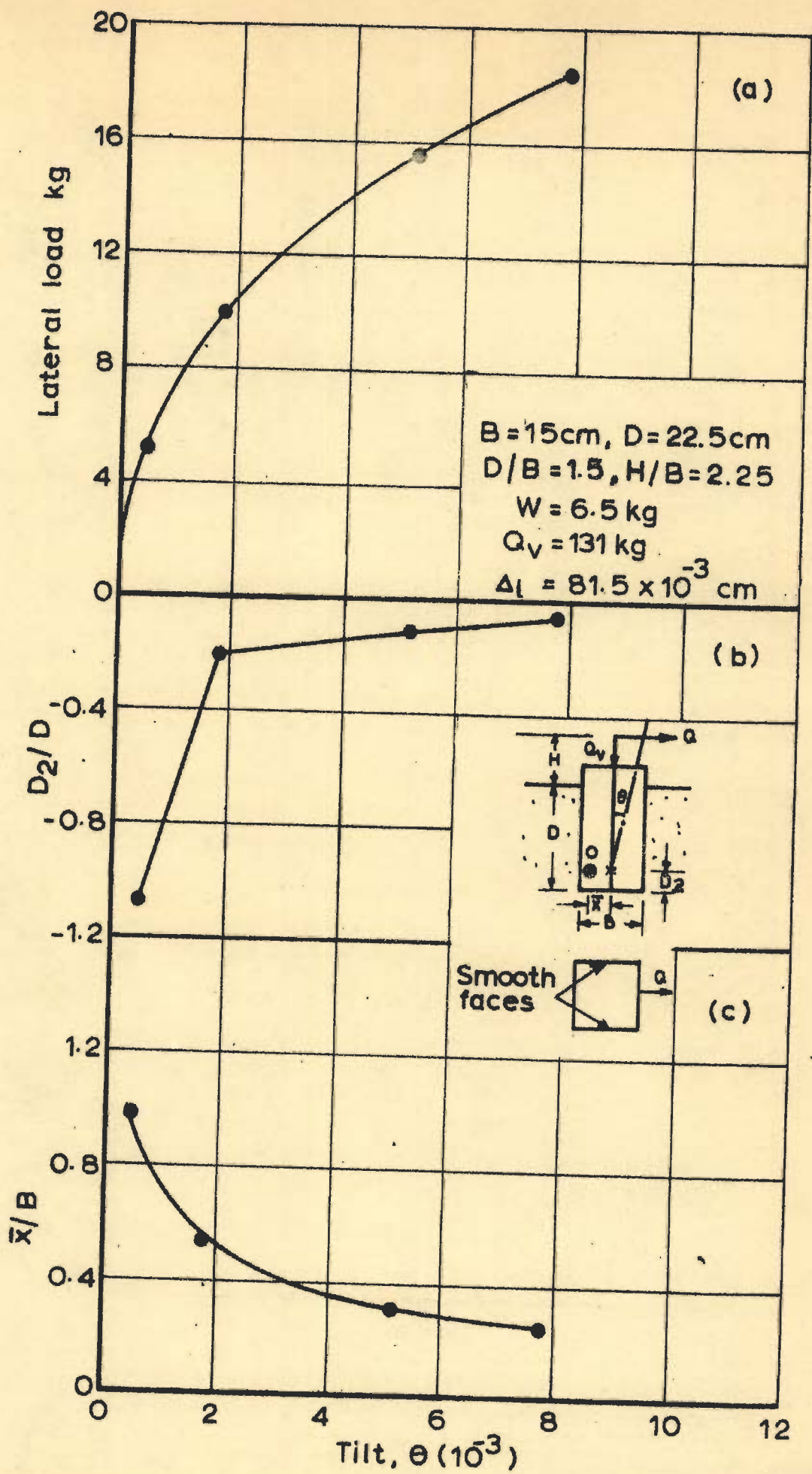
FIG. 50 — LATERAL LOAD, D_2/D AND $\bar{x}/B$ VS TILT
(Test No. 4)

Base width cm

7.5 4 0 4 7.5

Base pressure kg/cm²

0

0.4

0.8

1.2

a_Pressure ditribution on centoidal axis of the base

B = 15 cm, D = 22.5 cm
D/B = 1.5, H/B = 2.25
W = 6.5 kg
Q_V = 131 kg
$\Delta \ell$ = 91.5 × 10⁻³ cm

Lateral load kg

16

12

8

4

0

$-D_2/D$

0

-0.4

-0.8

$\bar{x}/B$

0.8

0.4

0

All face smooth

Tilt, θ (10³)

0 2 4 6 8 10 12 14
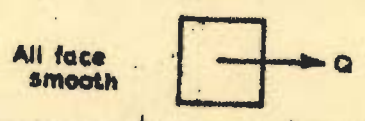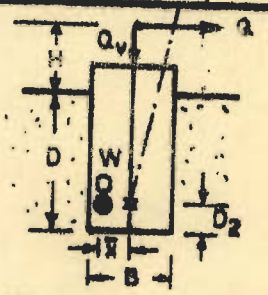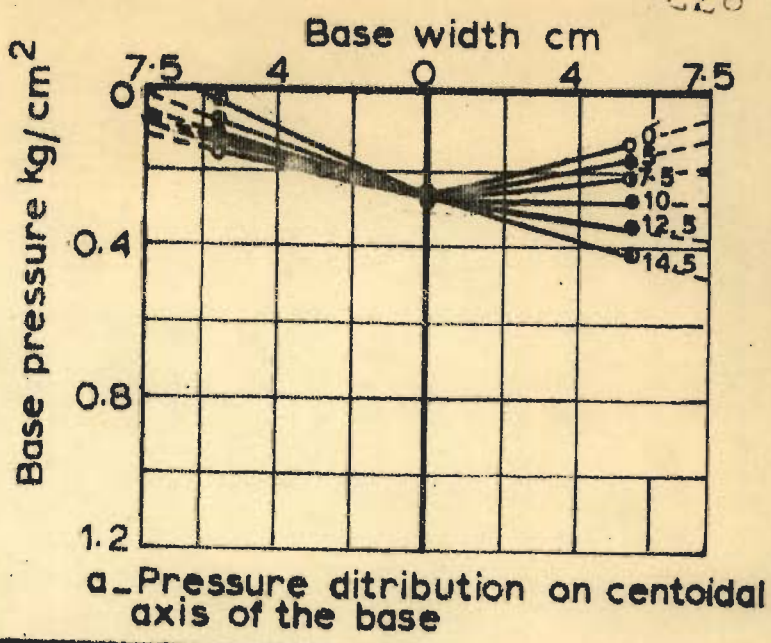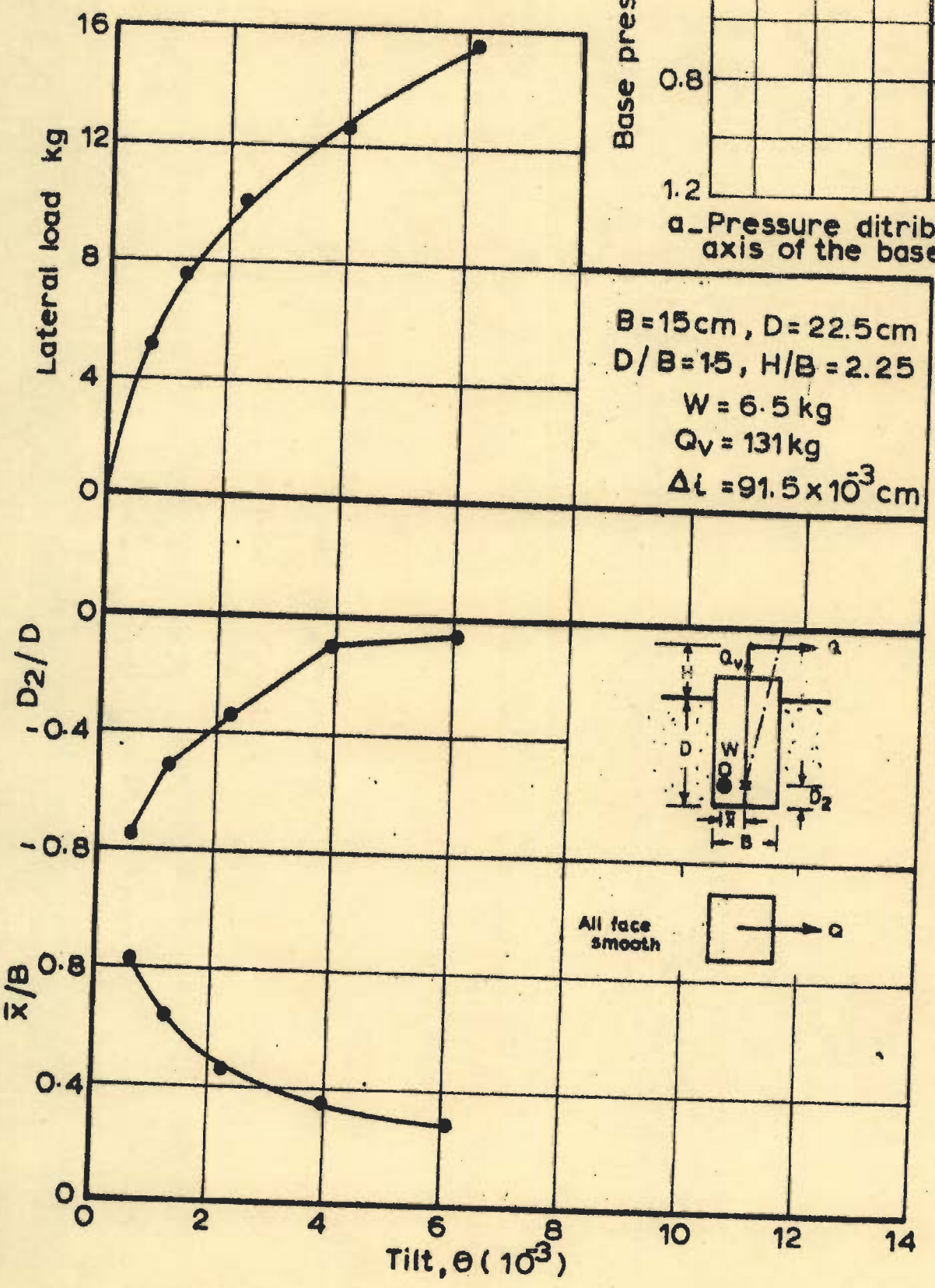
FIG. 51 _ PRESSURE DISTRIBUTION ON BASE AND LATERAL LOAD, D_2/D, $\bar{x}/B$ VS TILT (Test No 5)

Lateral pressure kg/cm^2

0.04   0.08   0.12   0.16   0.20

Depth cm

0·5 kg   10   14.5   18.5   20.5

a_ Pressure distribution on front face vertical axis

Base width cm

-7.5   -4   0   4   7.5

Base pressure kg/cm^2

20.5   20.5   10   14.5   18.5   20.5
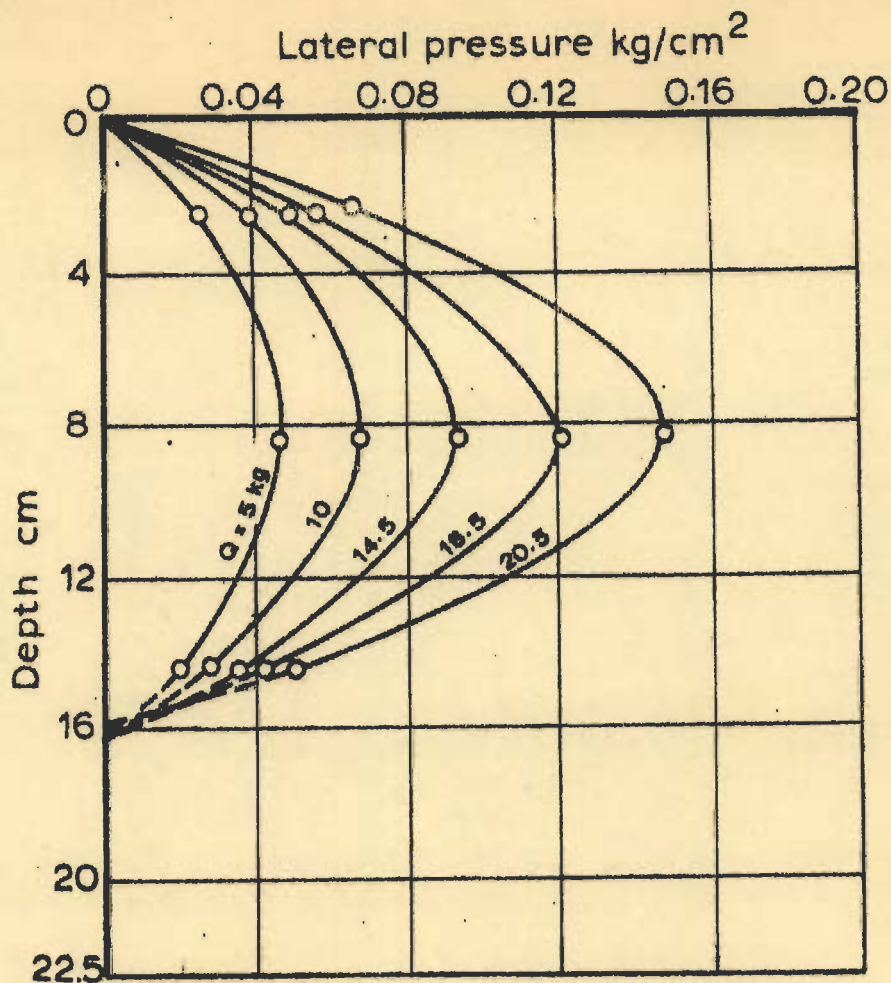
b_ Pressure distribution on centroidal axis of the base
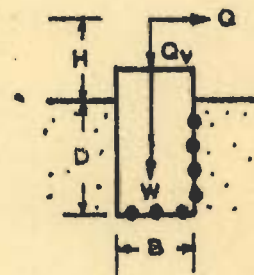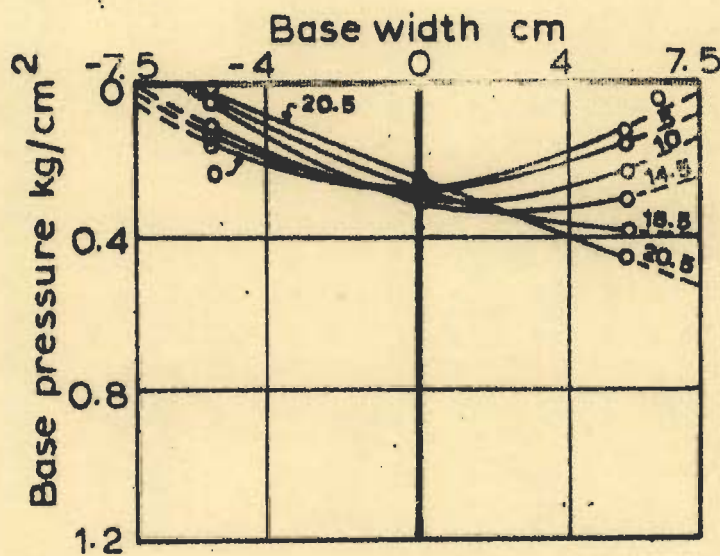
B = 15 cm, D = 22.5 cm
D/B = 1·5, H/B = 2.25
W = 6.5 kg
Q_V = 101 kg

FIG. 52 _ PRESSURE DISTRIBUTION ON FACE AND BASE
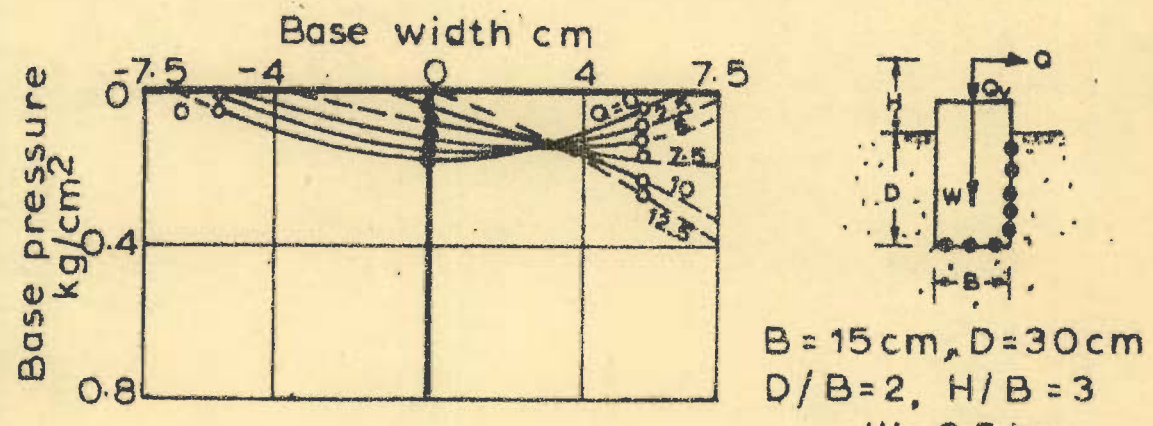(Test no. 6)
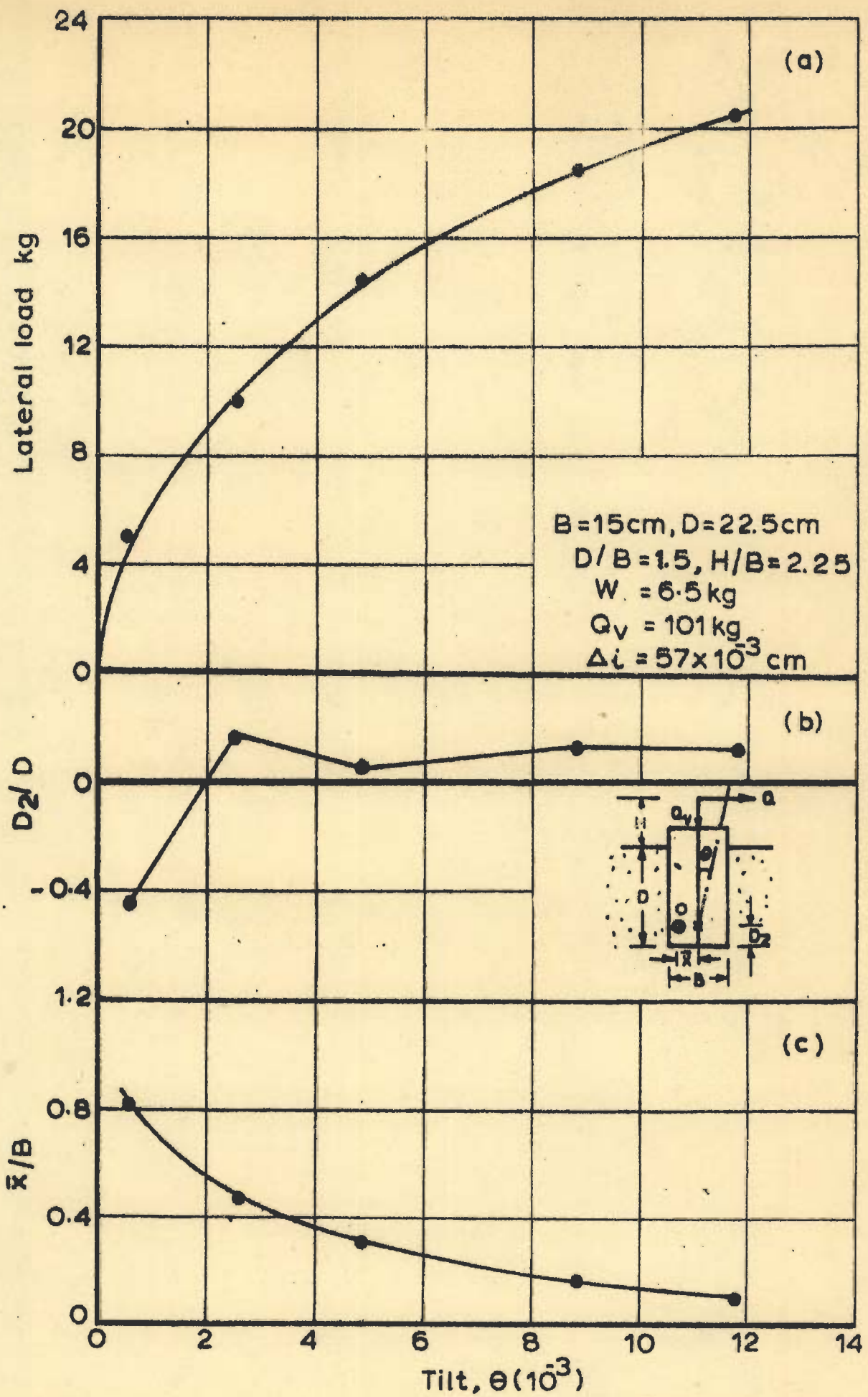
FIG. 53 _ LATERAL LOAD, D_2/D AND $\bar{x}/B$ VS TILT
(Test No. 6)
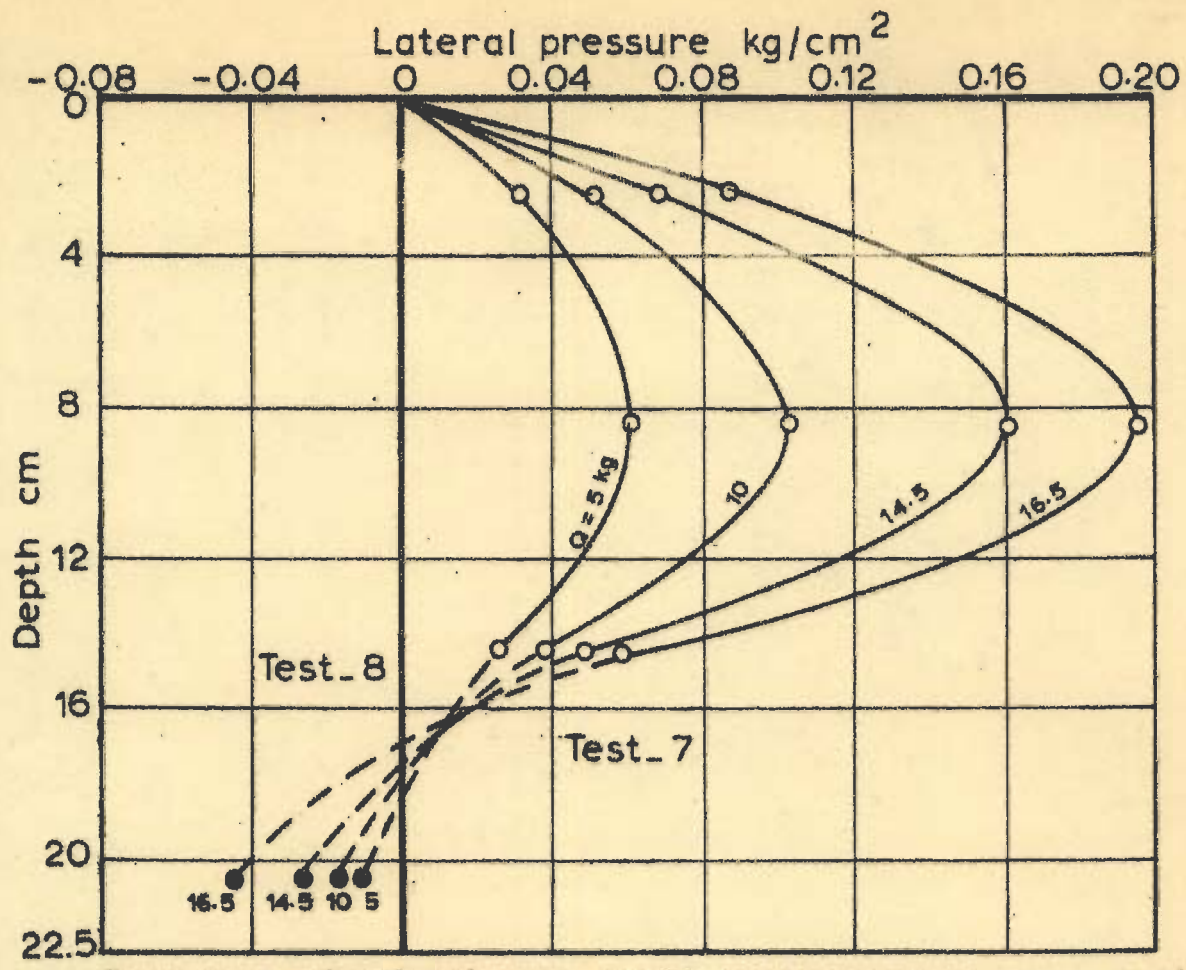
a _ Pressure distribution on front face and rear face vertical axis

b _ Pressure distribution on centroidal axis of the base

B = 15 cm, D = 22.5 cm
D/B = 1.5, H/B = 3.0
W = 6.5 kg
Q_v = 101 kg
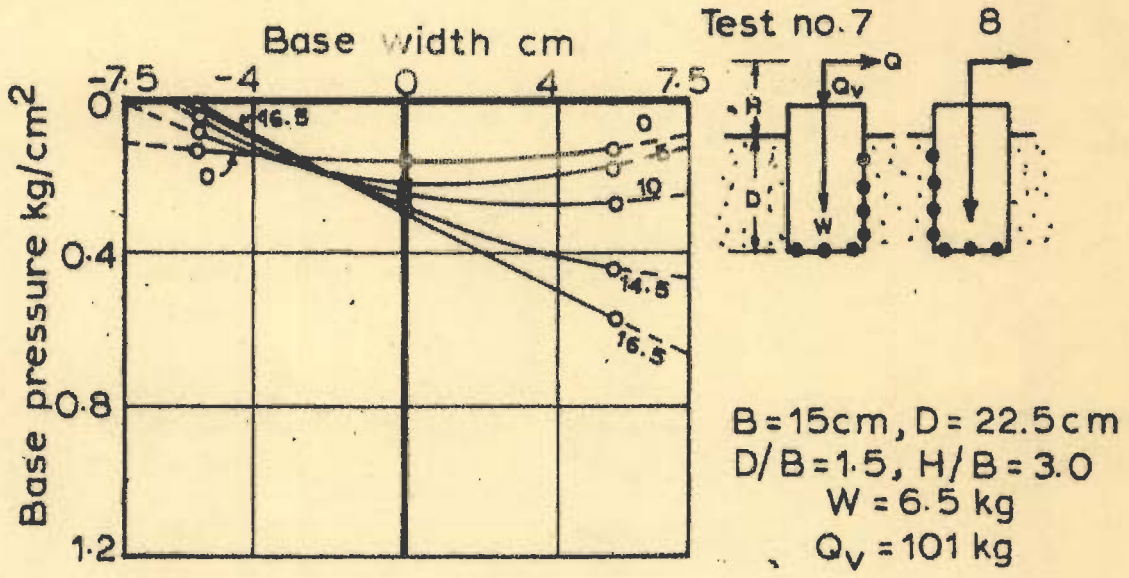
FIG. 54 _ PRESSURE DISTRIBUTION ON FACES AND BASE
(Test nos 7 & 8.)
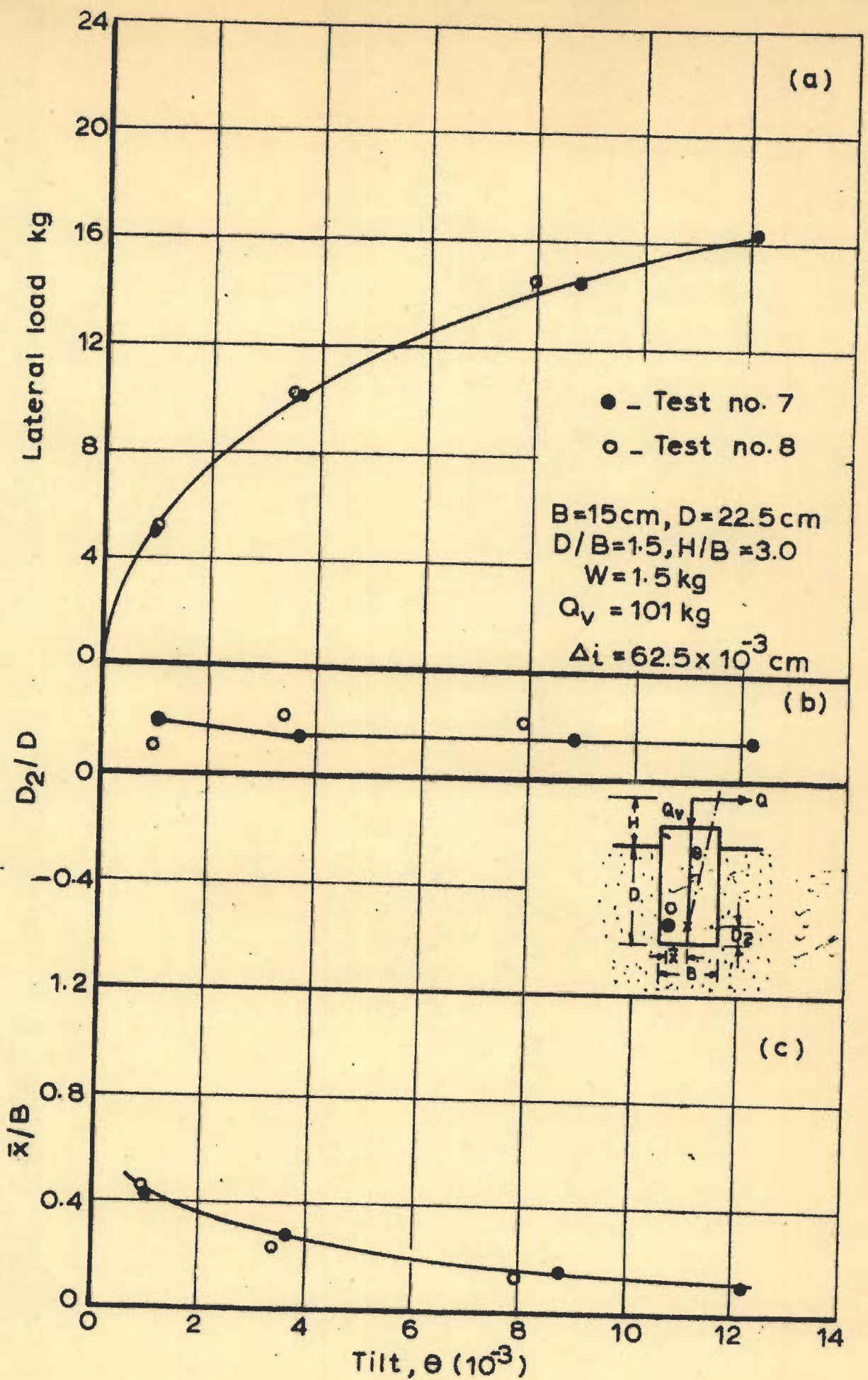
FIG. 55 _ LATERAL LOAD, D_2/D AND $\bar{x}/B$ VS TILT
(Test No. 7 and 8)
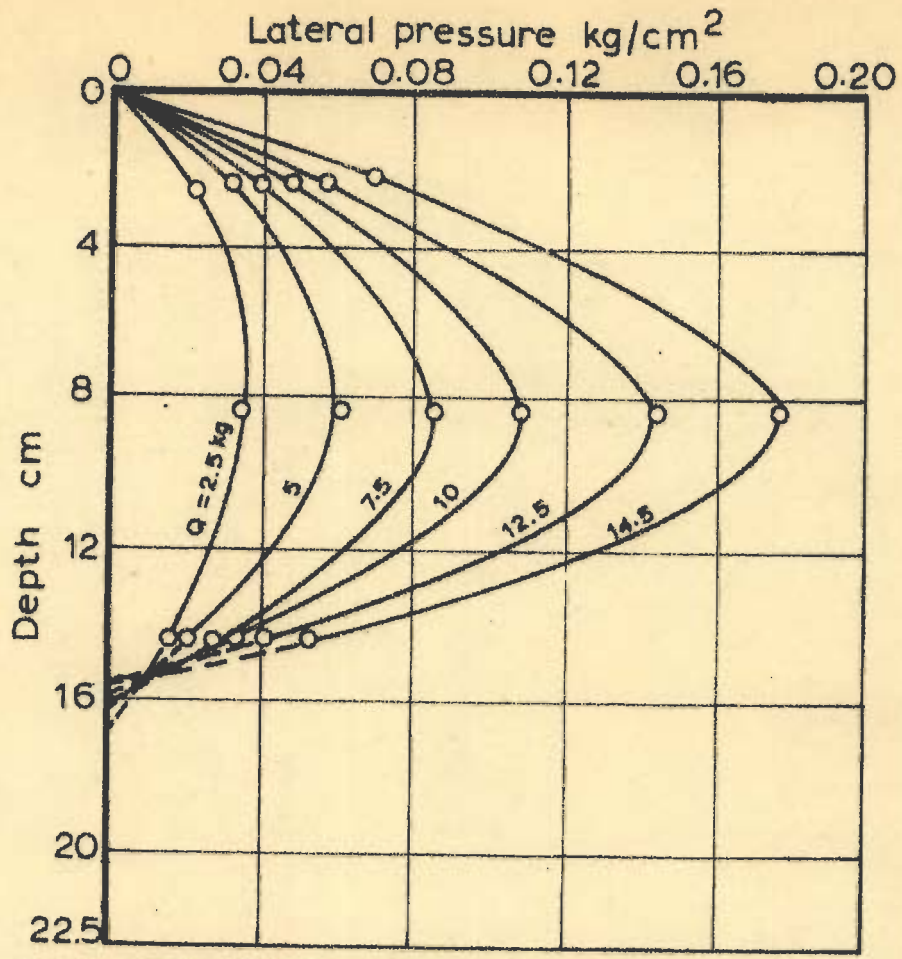
Lateral pressure kg/cm²

a_Pressure distribution on front face vertical axis
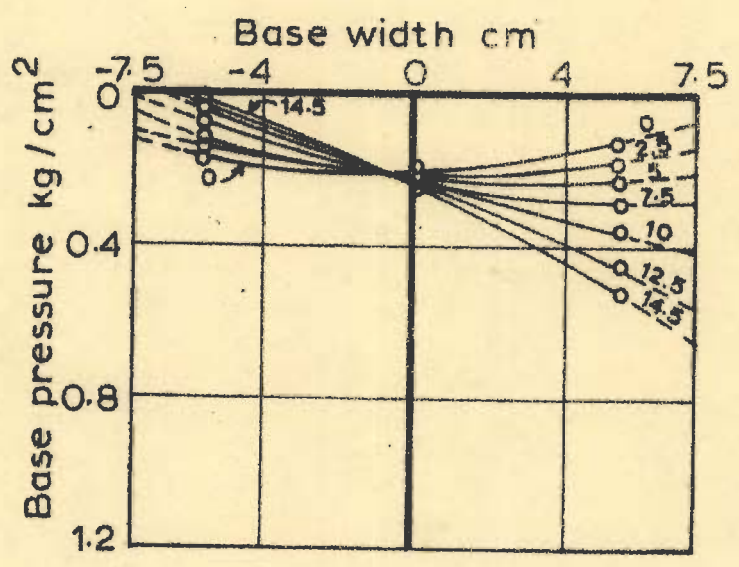
b_Pressure distribution on centroidal axis of the base
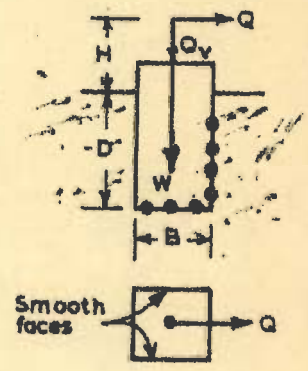
B = 15cm, D = 22.5 cm
D/B = 1.5, H/B = 3
W = 6.5 kg
Q_v = 101 kg

FIG. 56 _ PRESSURE DISTRIBUTION ON FACE AND BASE
(Test no. 9)
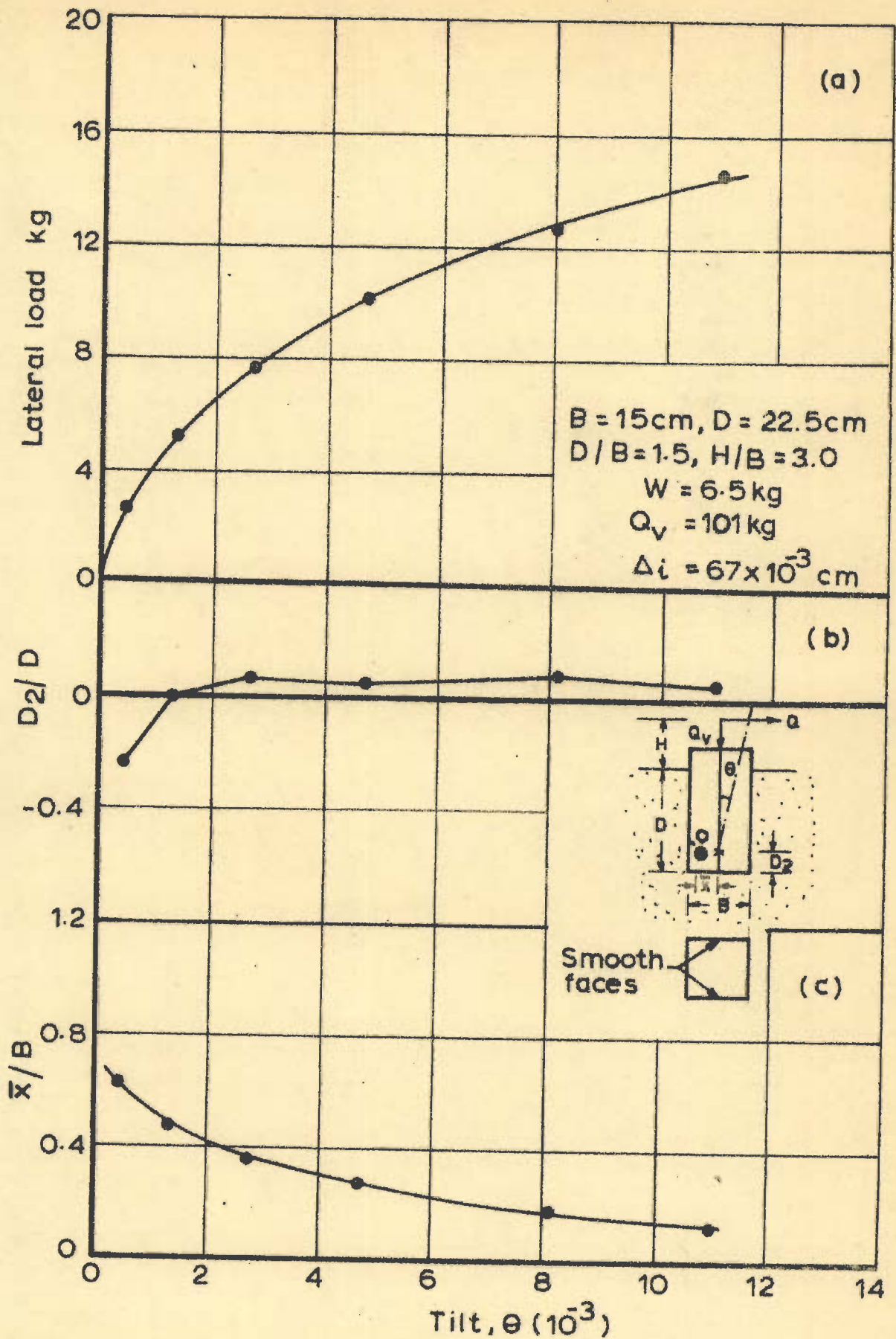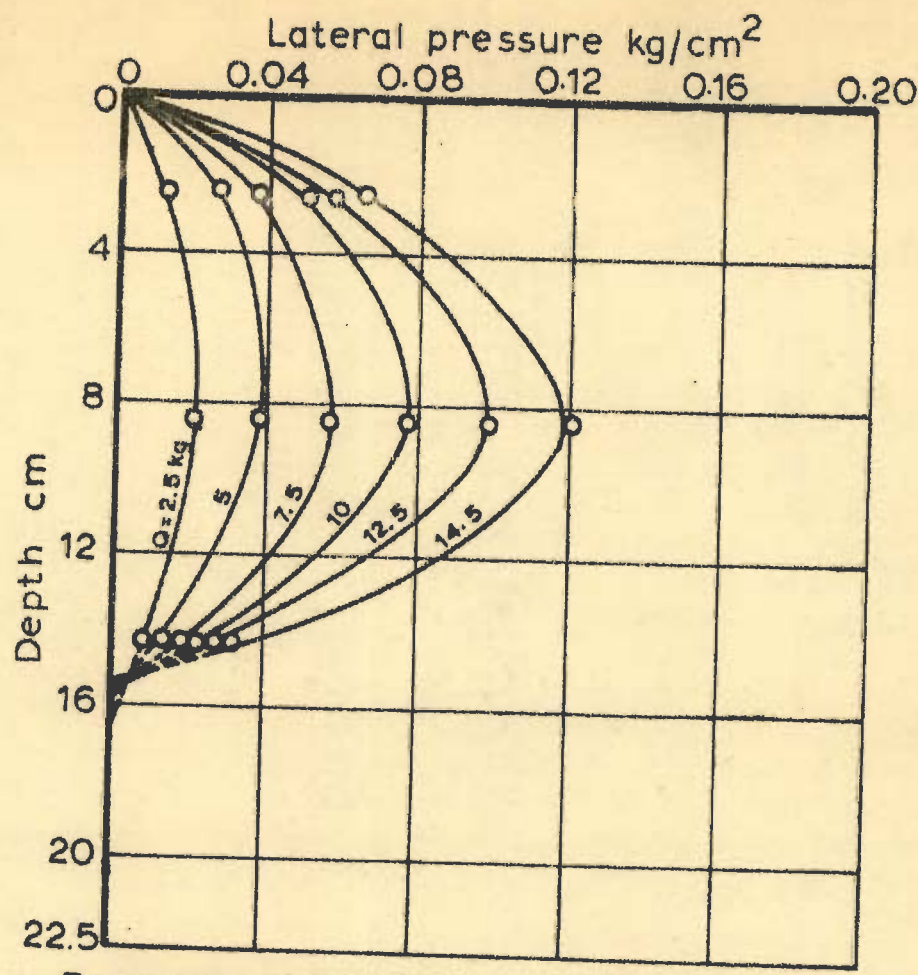
B = 15cm, D = 22.5cm
D/B = 1.5, H/B = 3.0
W = 6.5 kg
Q_V = 101 kg
Δi = 67 × 10^{-3} cm

FIG. 57 — LATERAL LOAD, D_2/D AND $\bar{x}/B$ VS TILT
(Test No. 9)

Lateral pressure kg/cm²

a‑ Pressure distribution on front face vertical axis

Base width cm
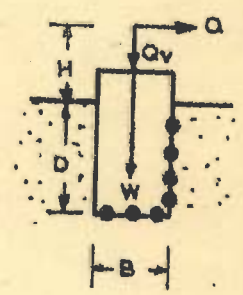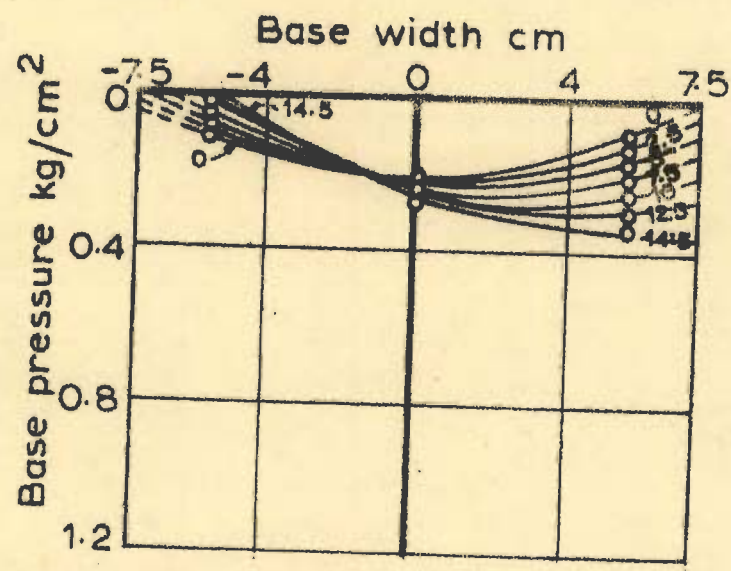
b‑ Pressure distribution on centroidal axis of the base

B = 15 cm, D = 22.5 cm
D/B = 1.5, H/B = 2.25
W = 6.5 kg
Q_V = 51 kg

FIG. 58 ‑ PRESSURE DISTRIBUTION ON FACE AND BASE
(Test no. 10)

FIG. 59 — LATERAL LOAD, D_2/D AND $\bar{x}/B$ VS TILT
(Test No.10)

Lateral pressure kg/cm^2

a - **Pressure distribution on front face vertical axis**

Depth cm

$Q = 5$ kg

10

14.5

18.5

20.5

Base width cm

Base pressure kg/cm2

20.5

$Q = 0$

5

10

14.5

18.5

20.5

b - **Pressure distribution on centroidal axis of the base**

B = 15 cm, D = 30 cm

D/B = 2 , H/B = 4

W = 6.5 kg

Q_V = 131 kg

FIG. 60 _ PRESSURE DISTRIBUTION ON FACE AND BASE
(Test no. 11)

(a)

B = 15cm, D = 30 cm
D/ B = 2, H/B = 4
W = 6.5 kg
Q_v = 131 kg
Δi = 70 x 10³cm

(b)

(c)

FIG. 61 _ LATERAL LOAD D_2/D AND $\bar{x}/B$ VS TILT
(Test no. 12)

Lateral pressure kg/cm²

a – Pressure distribution on front face vertical axis

Base width cm

b – Pressure distribution on centroidal axis of the base

B = 15 cm, D = 30 cm
D/B = 2, H/B = 3
W = 6.5 kg
Q_v = 131 kg

FIG. 62 – PRESSURE DISTRIBUTION ON FACE AND BASE
(Test no. 12)

FIG. 63 — LATERAL LOAD, D_2/D AND $\bar{x}/B$ VS TILT
(Test no. 11)

Lateral pressure kg/cm²

a – Pressure distribution on front face vertical axis

Base width cm
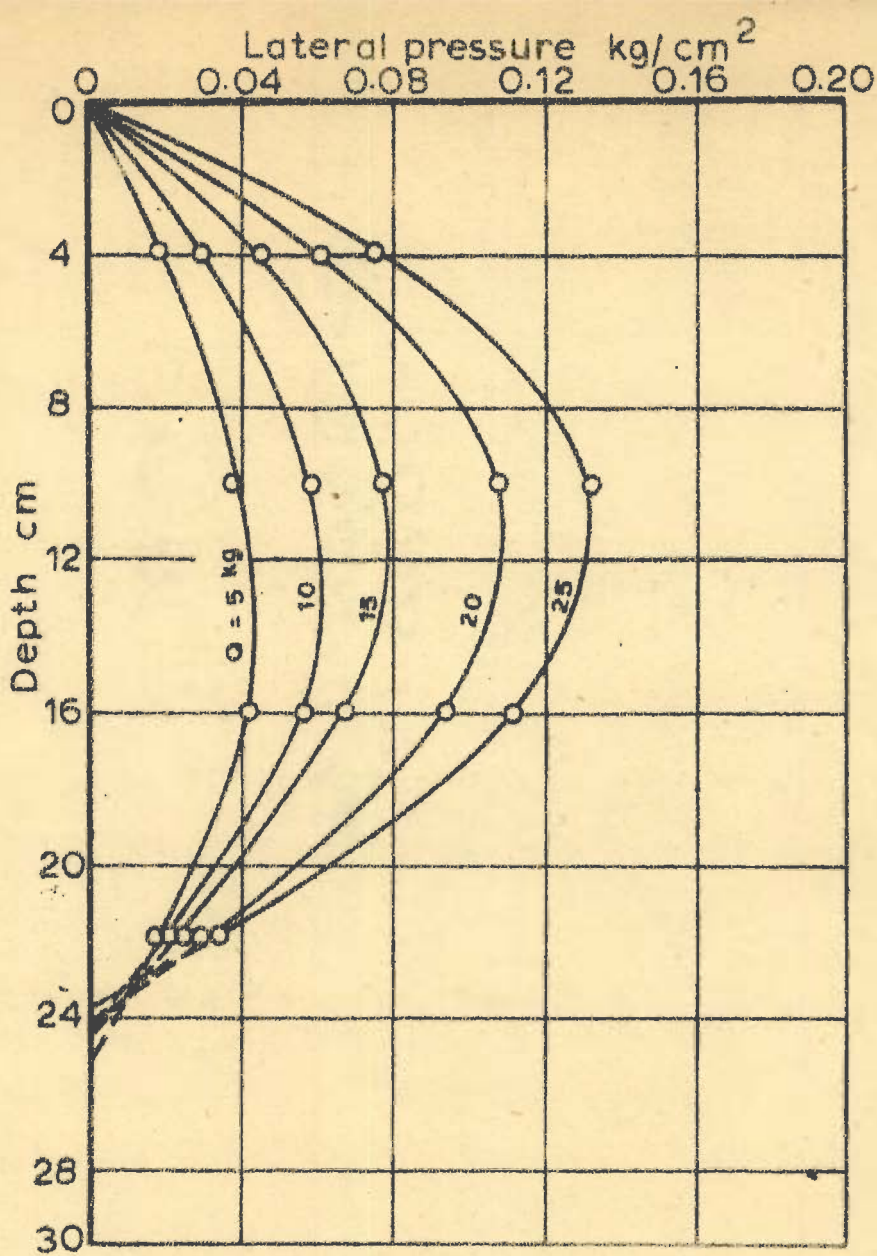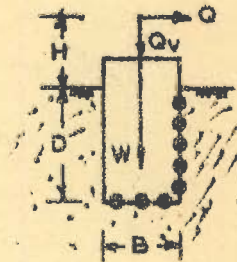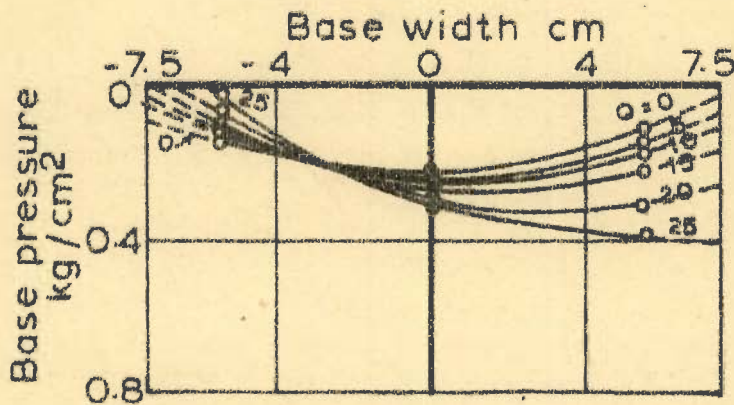
B = 15 cm, D = 30 cm
D/B = 2, H/B = 2
W = 6.5 kg
Q_V = 131 kg

b – Pressure distribution on centroidal axis of the base

FIG. 64 – PRESSURE   DISTRIBUTION ON FACE AND BASE
(Test no. 13)

(a)

Lateral load kg

$B = 15$ cm, $D = 30$ cm
$D/B = 2$, $H/B = 2$
$W = 6.5$ kg
$Q_V = 131$ kg
$\Delta i = 56 \times 10^{-3}$ cm

(b)

D_2/D

(c)

$\bar{x}/B$

Tilt, θ (10^{3})
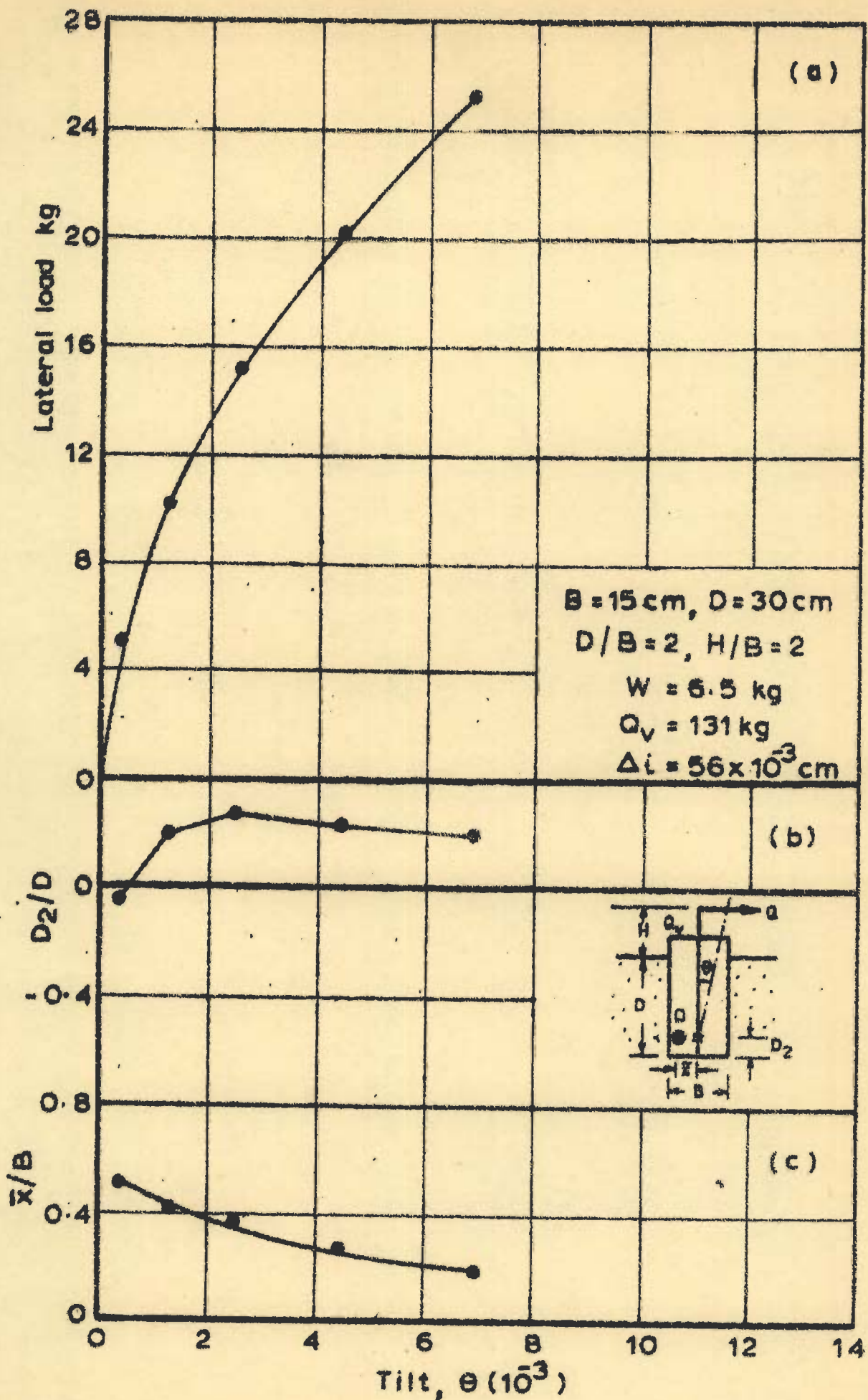
FIG. 65 _ LATERAL LOAD D_2/D AND $\bar{x}/B$ VS TILT
(Test no. 13)
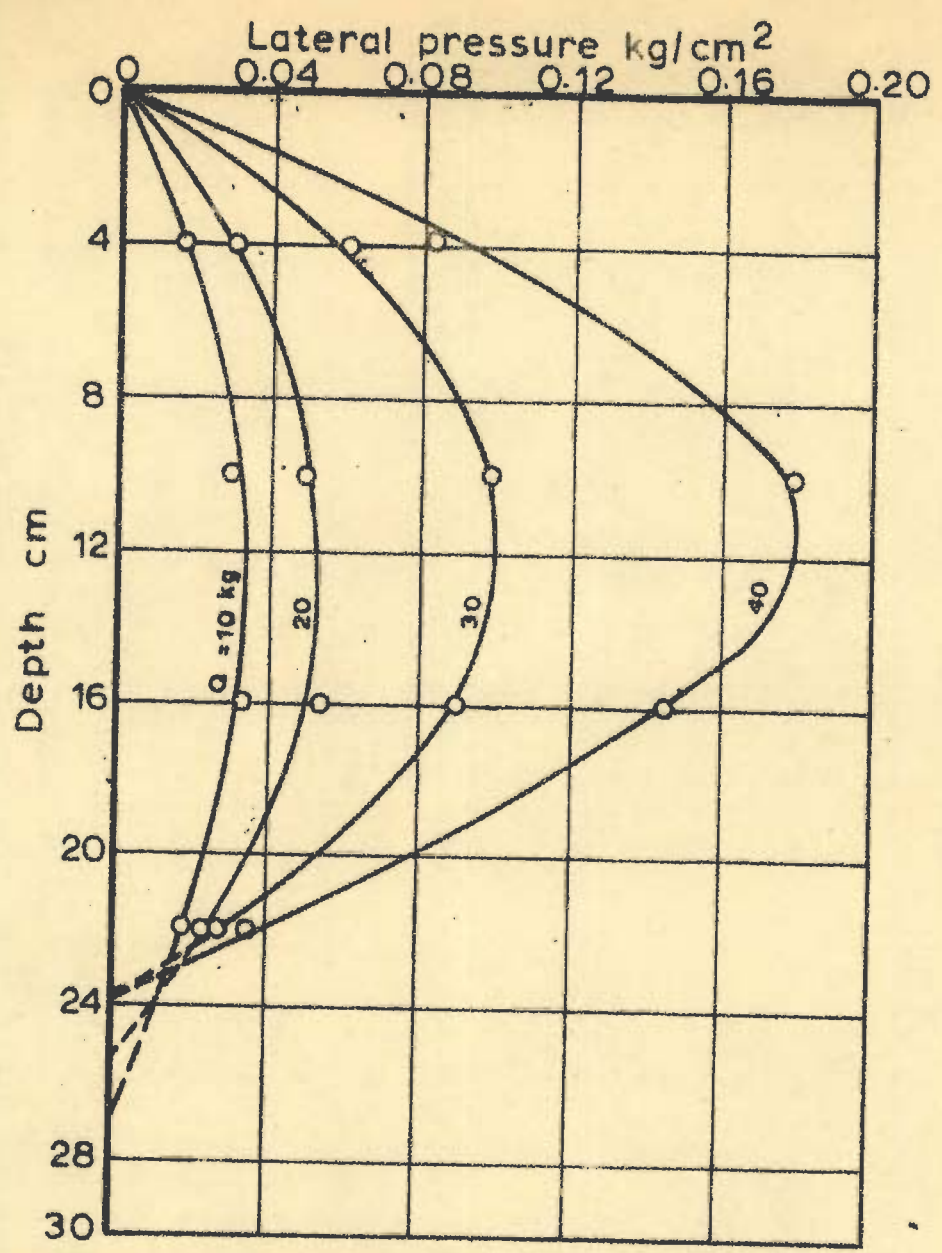
13

a. Pressure distribution on front face vertical axis
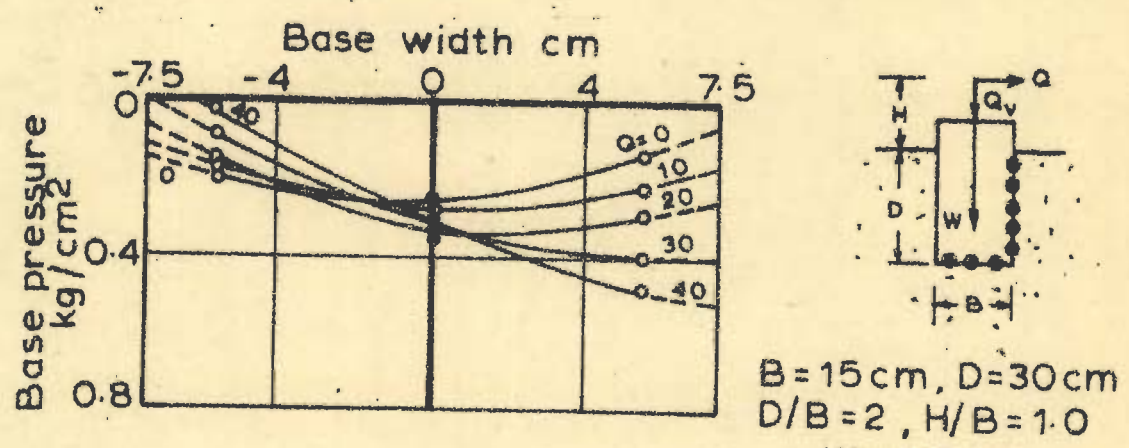
b. Pressure distribution on centroidal axis of the base

B = 15 cm, D = 30 cm
D/B = 2 , H/B = 1.0
W = 6.5 kg
Qᵥ = 131 kg

FIG. 66 _ PRESSURE DISTRIBUTION ON FACE AND BASE
(Test no. 14)

B = 15 cm, D = 30 cm
D/B = 2 H/B = 1.0
W = 6.5 kg
Q_v = 131 kg
Δ_i = 57 x 10^{-3} cm
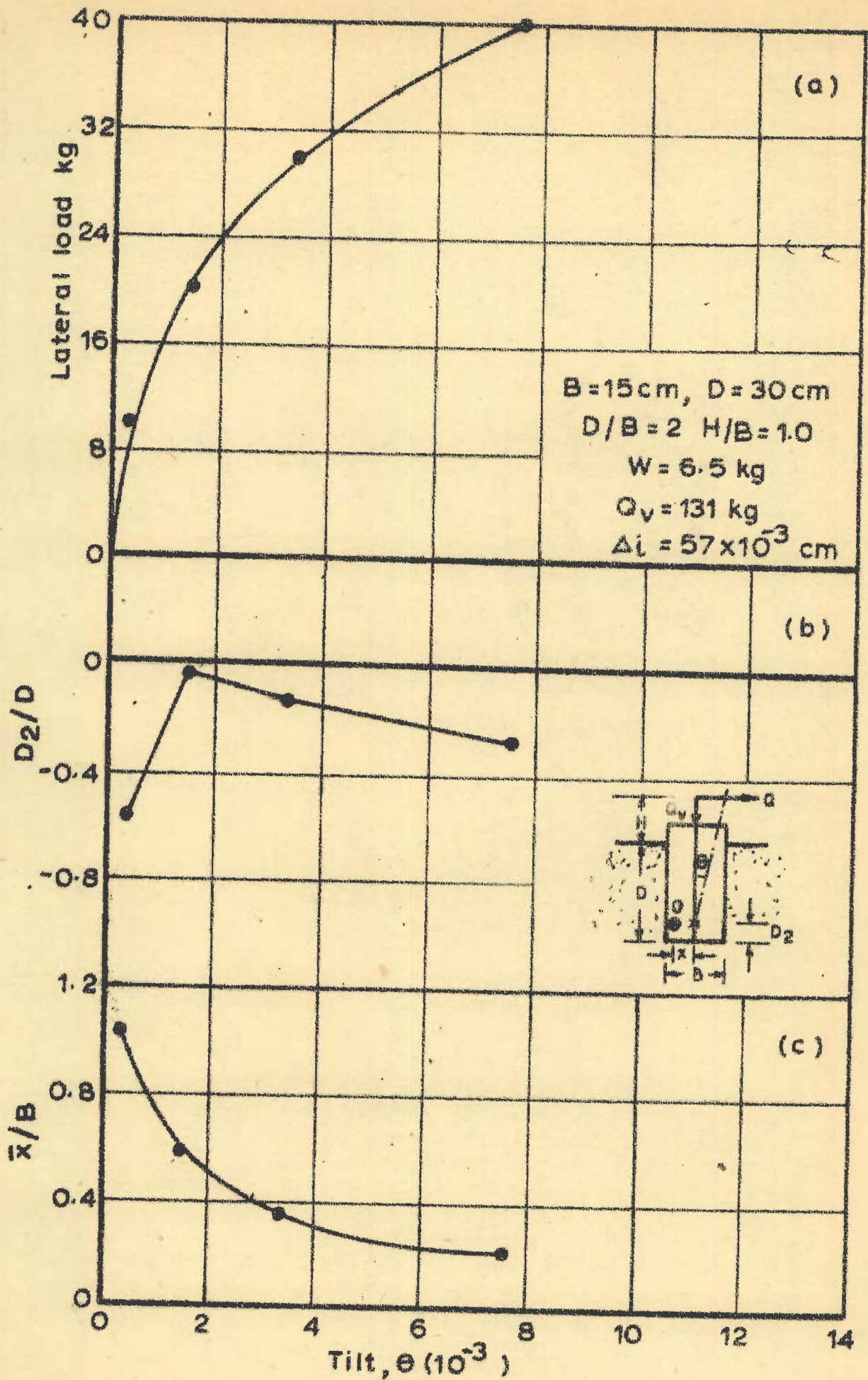
FIG. 67 _ LATERAL LOAD, D_2/D AND $\bar{x}/B$ VS TILT
(Test no. 14)
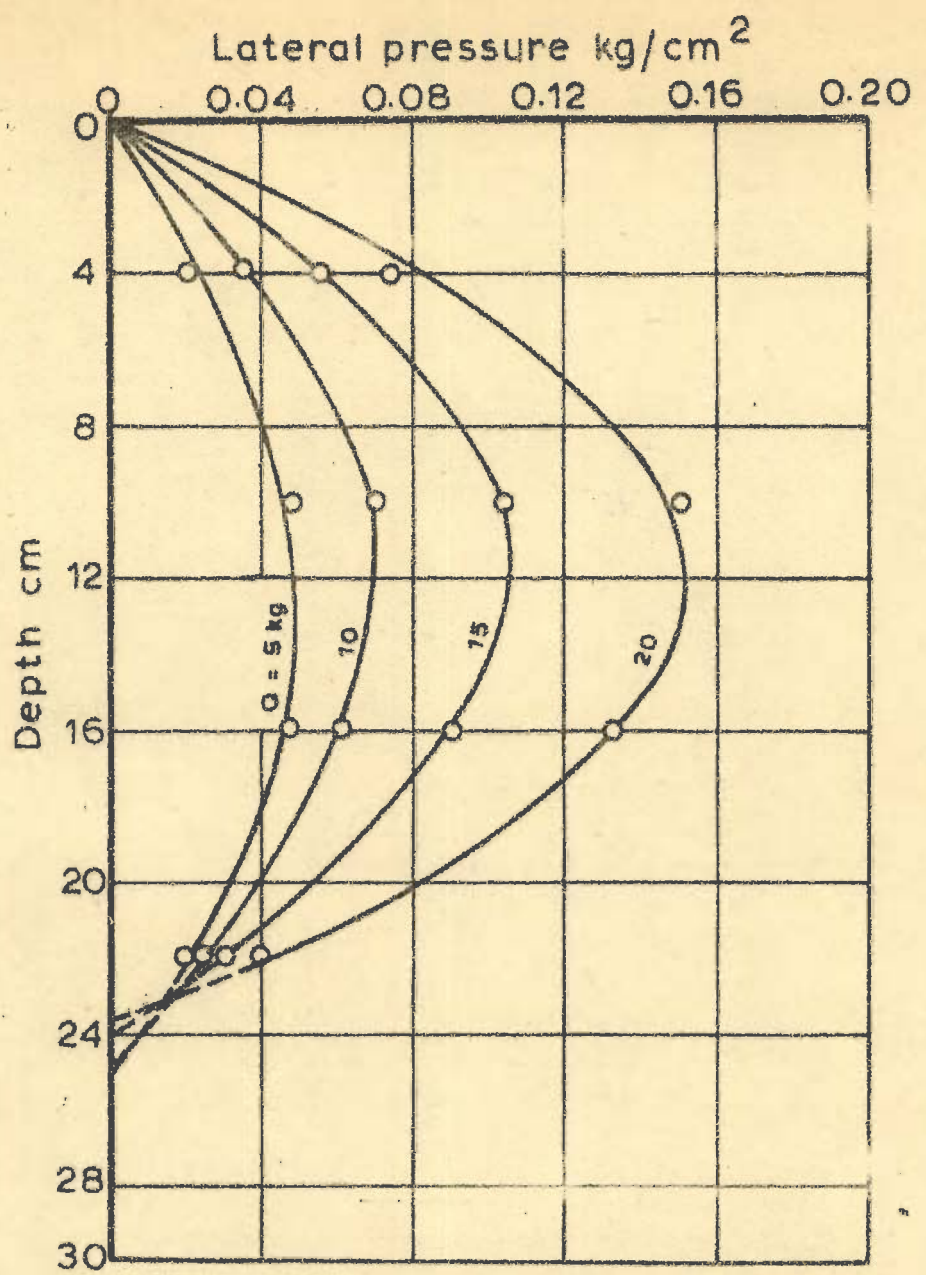
a_ Pressure distribution on front face vertical axis
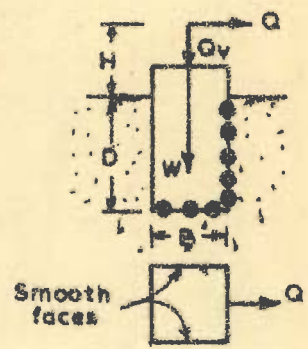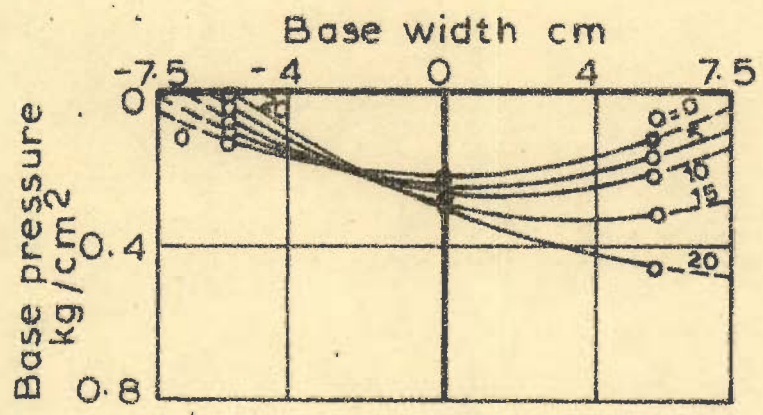
b_ Pressure distribution on centroidal axis of the base

B = 15 cm, D = 30 cm
D/B = 2 , H/B = 3
W = 6.5 kg
Q_V = 131 kg

FIG. 68 _ PRESSURE DISTRIBUTION ON FACE AND BASE
(Test no. 15)

(a)

B = 15 cm, D = 30 cm

D/B = 2, H/B = 3

W = 6.5 kg

Q_v = 131 kg

Δl = 85.5 x 10^{-3} cm

Lateral load kg

D_2/D

$\bar{x}/B$

Smooth faces

Tilt, Θ (10^{-3})

FIG. 69 _ LATERAL LOAD, D_2/D AND $\bar{x}/B$ VS TILT
(Test no. 15)

Base width cm

Base pressure g/cm²

a _ Pressure distribution on
centroidal axis of the base

(b)

Lateral load kg

B=15cm, D=30cm
D/B=2, H/B=3
W = 6.5 kg
Q_v = 131 kg
Δi = 92.5 × 10⁻³ cm

(c)

D_2/D

(d)

$\bar{x}/B$

Tilt, θ (10⁻³)
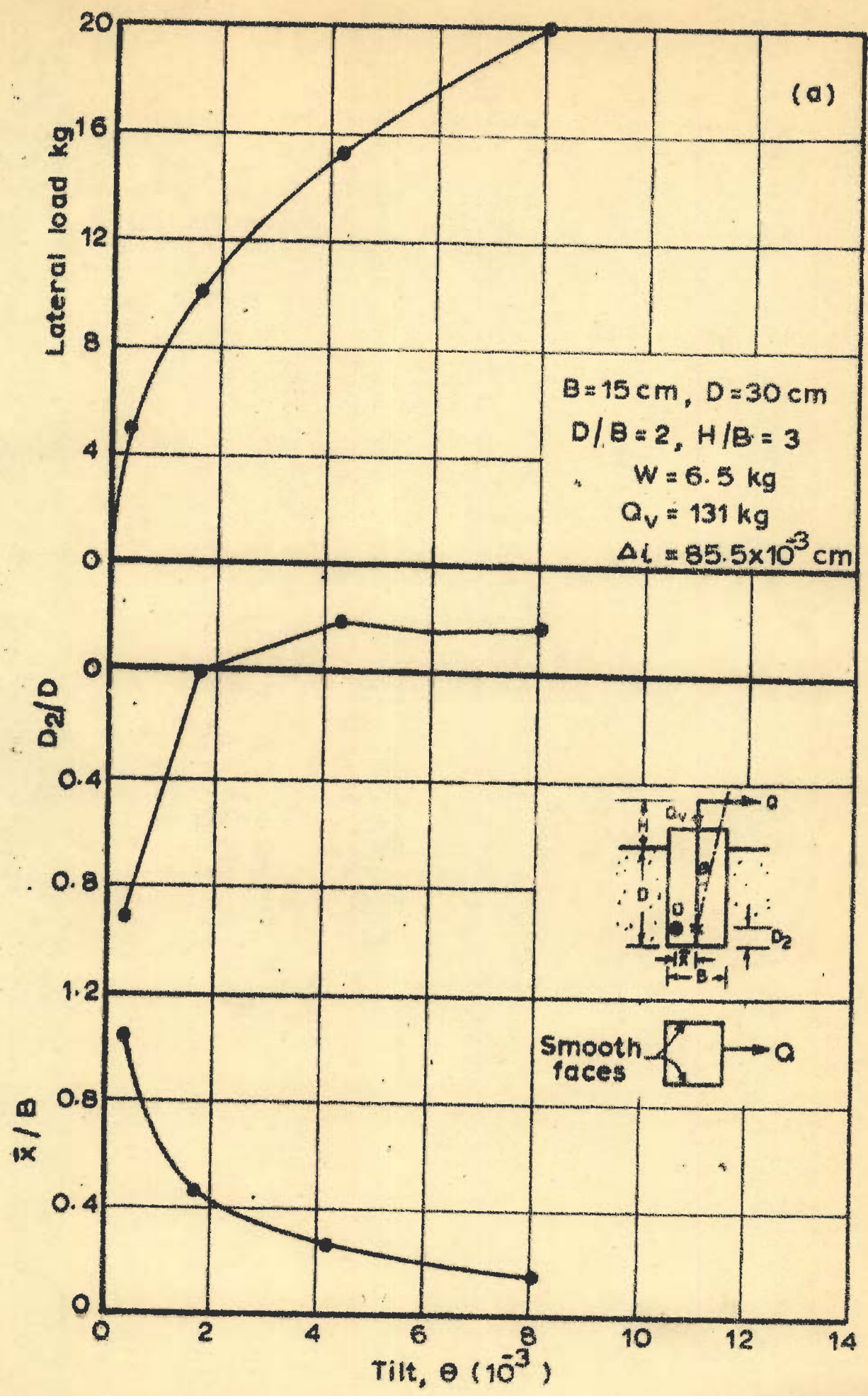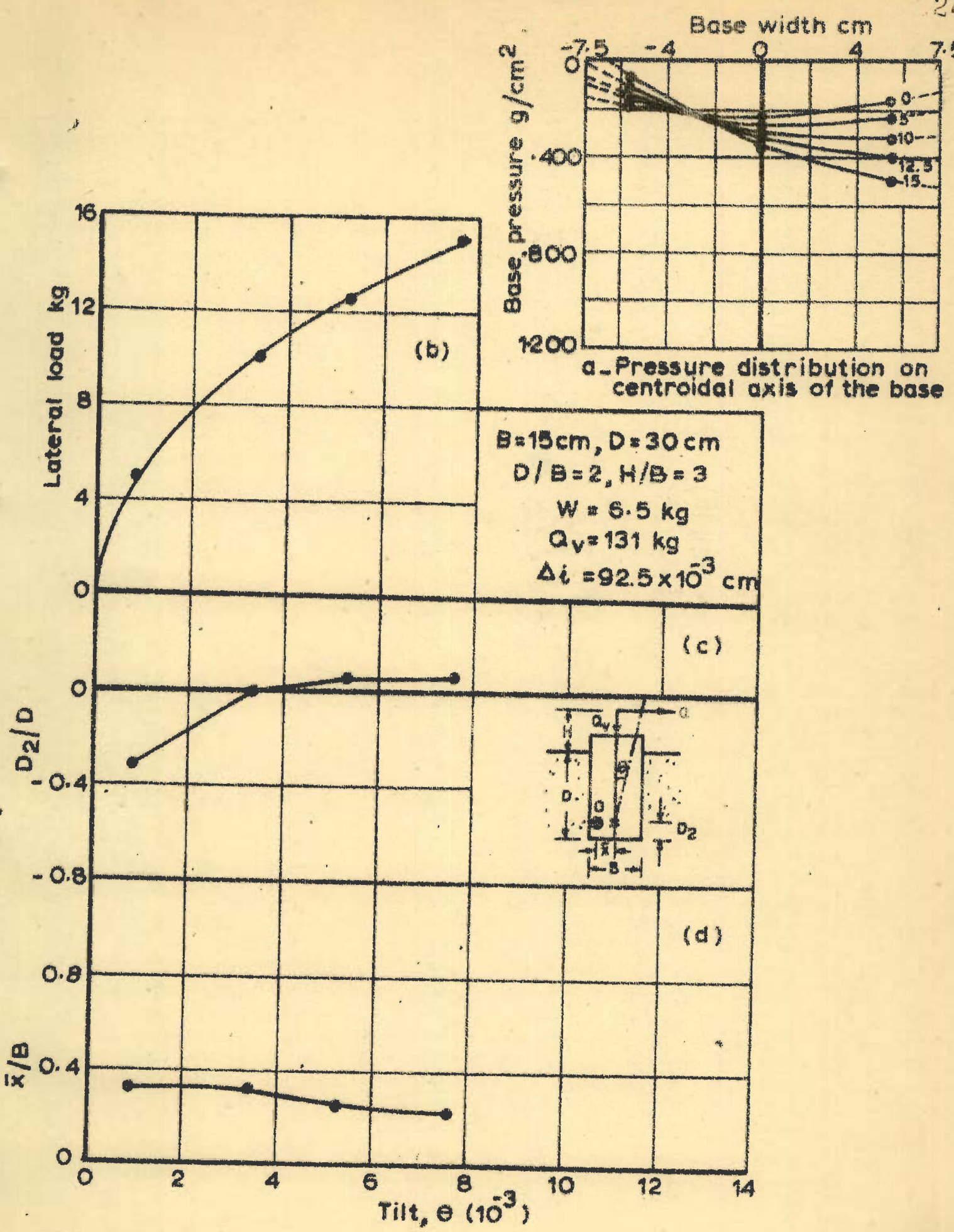
FIG. 70 _ BASE PRESSURES AND LATERAL LOAD, D_2/D
AND $\bar{x}/B$ VS TILT (Test no. 16)
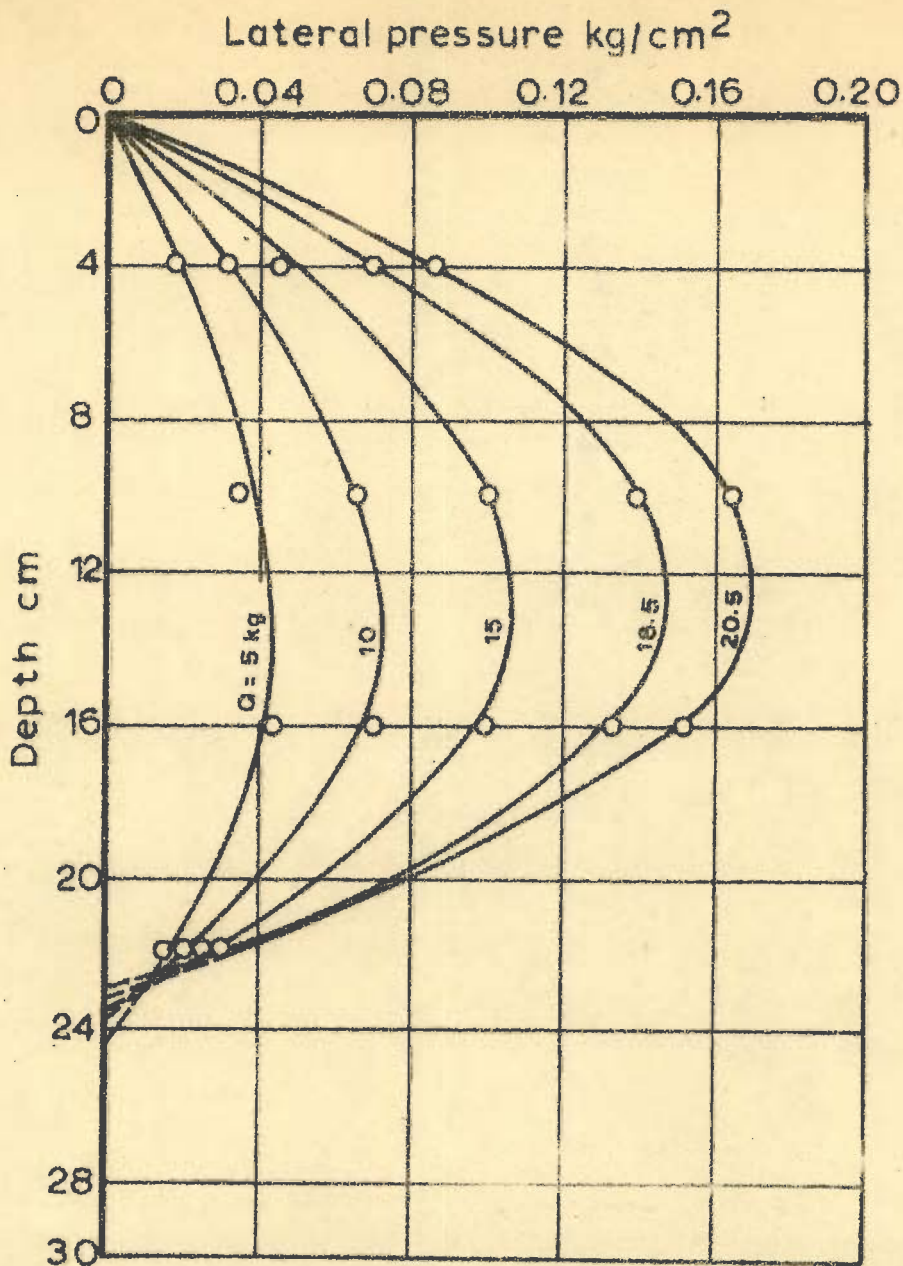
Lateral pressure kg/cm²

Depth cm

a – Pressure distribution on front face vertical axis

Base width cm

Base pressure kg/cm2
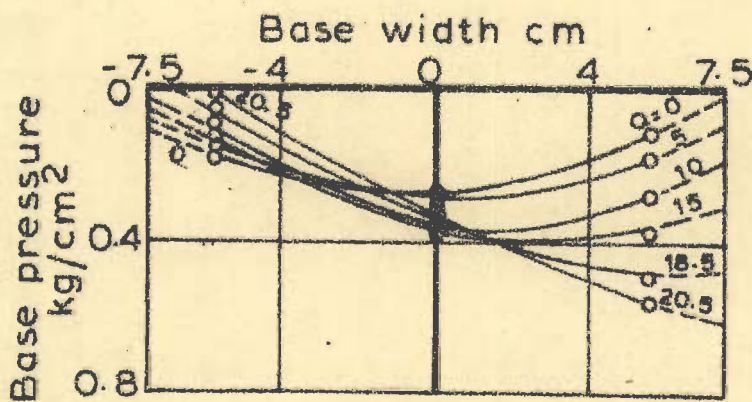
b – Pressure distribution on centroidal axis of the base
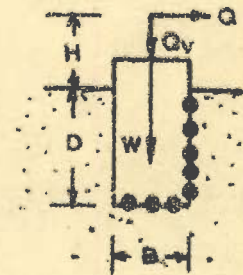
B = 15 cm, D = 30 cm
D/B = 2, H/B = 4
W = 6.5 kg
Q = 101 kg

FIG. 71 – PRESSURE DISTRIBUTION ON FACE AND BASE
(Test no. 17)
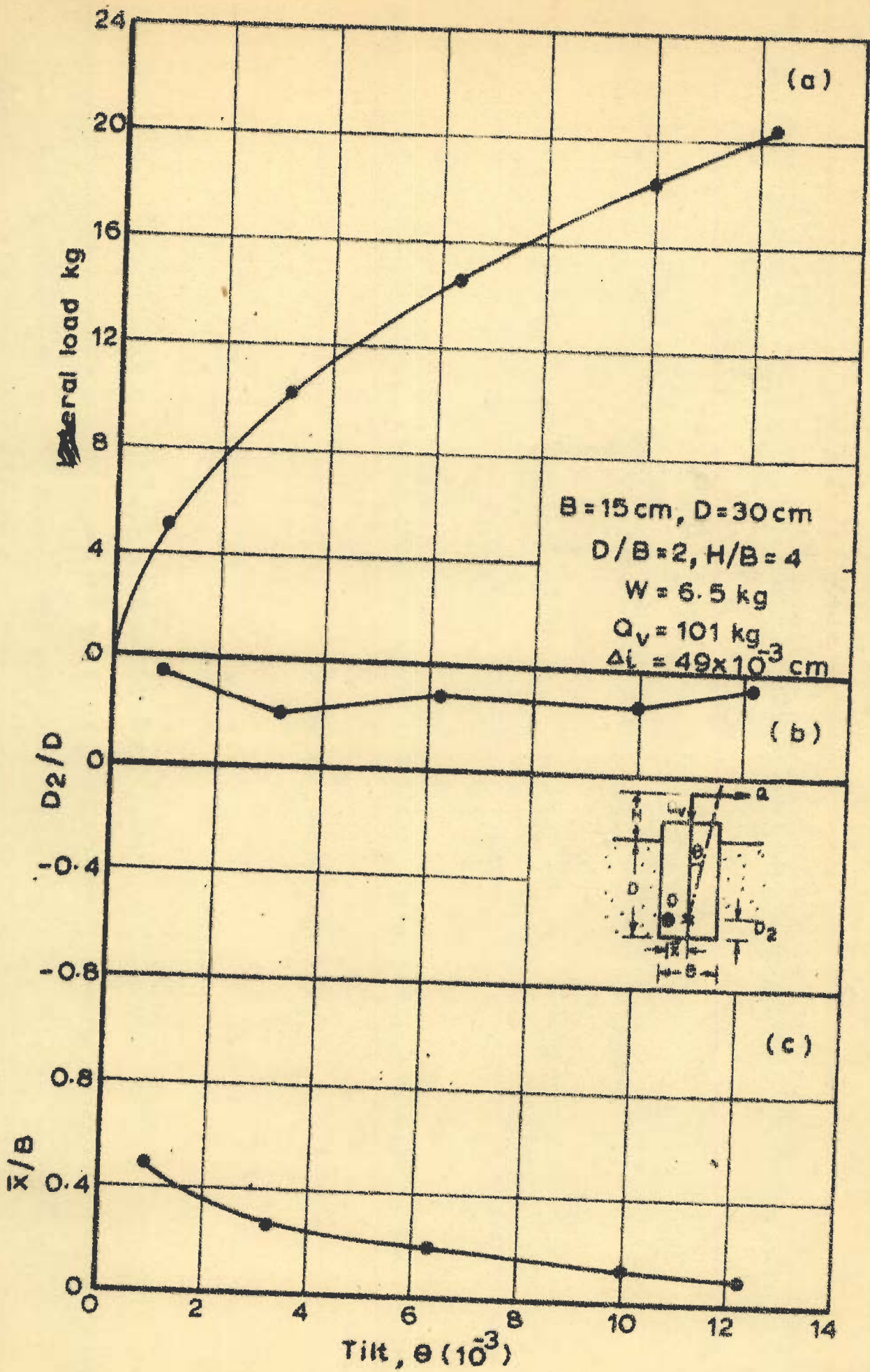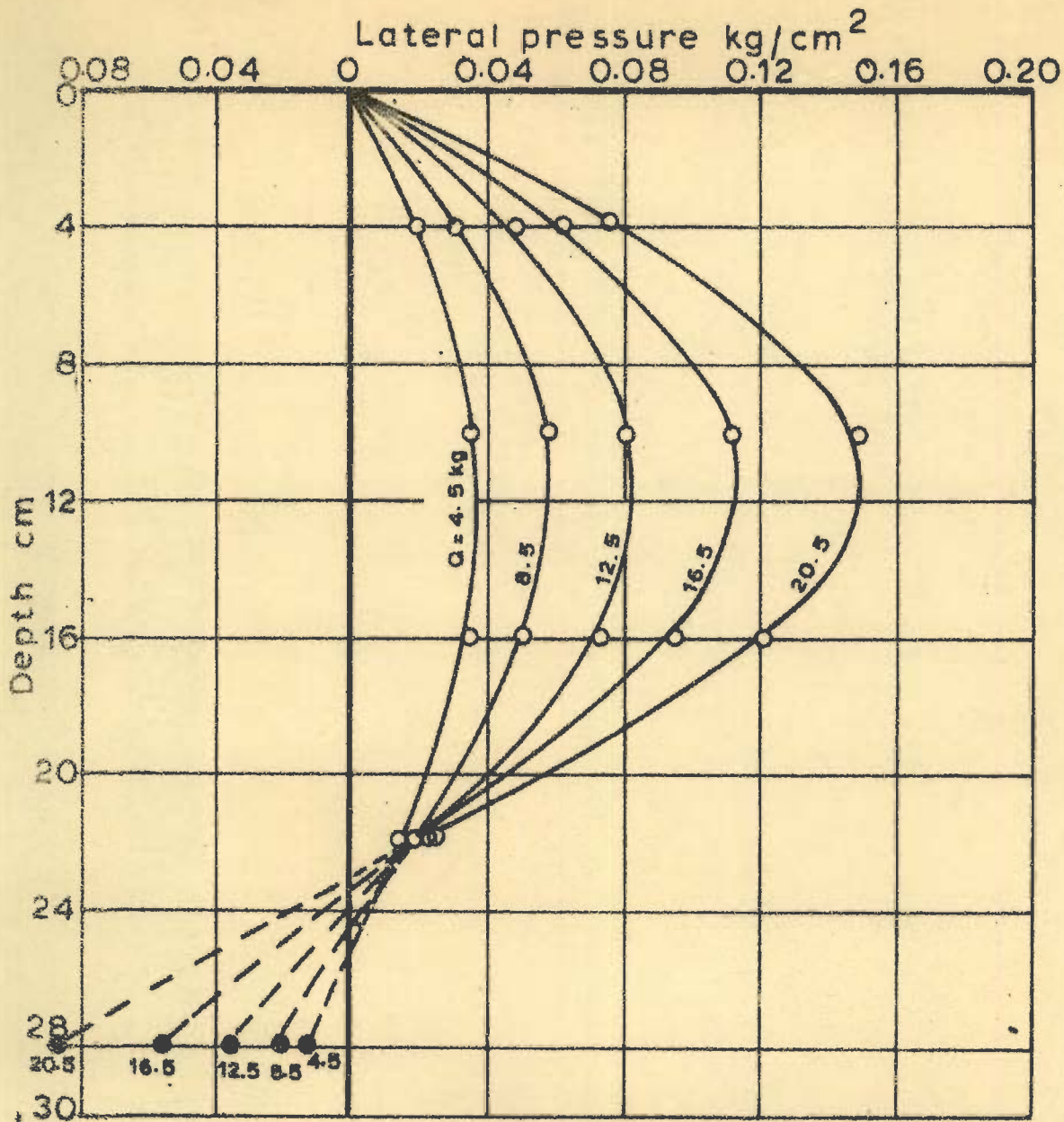
(a)

(b)

(c)

$B = 15\,cm,\ D = 30\,cm$

$D/B = 2,\ H/B = 4$

$W = 6.5\,kg$

$Q_v = 101\,kg$

$\Delta L = 49 \times 10^{-3}\,cm$

FIG. 72 _ LATERAL LOAD, D_2/D AND $\bar{x}/B$ VS TILT
(Test no. 17)

Lateral pressure kg/cm²

a – Pressure distribution on front face and rear face vertical axis
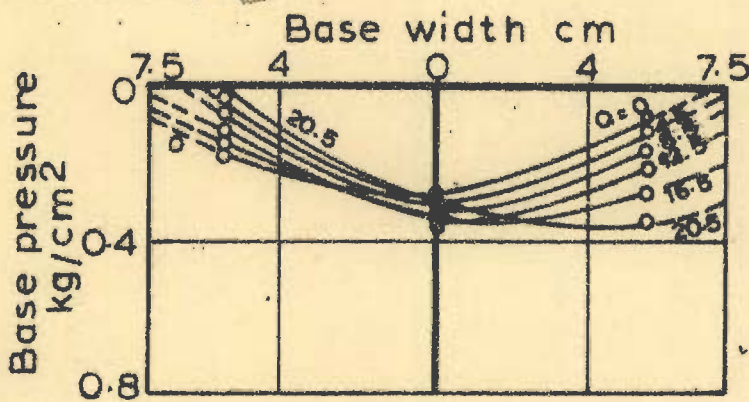
b – Pressure distribution on centroidal axis of the base
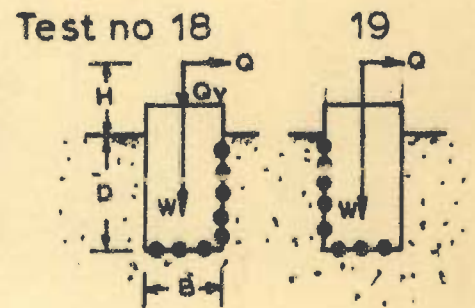
Test no 18   19

B = 15 cm, D = 30 cm
D/B = 2, H/D = 3
W = 6.5 kg
Q_v = 101 kg

FIG. 73 – PRESSURE DISTRIBUTION ON FACE AND BASE
(Test no. 18 and 19)
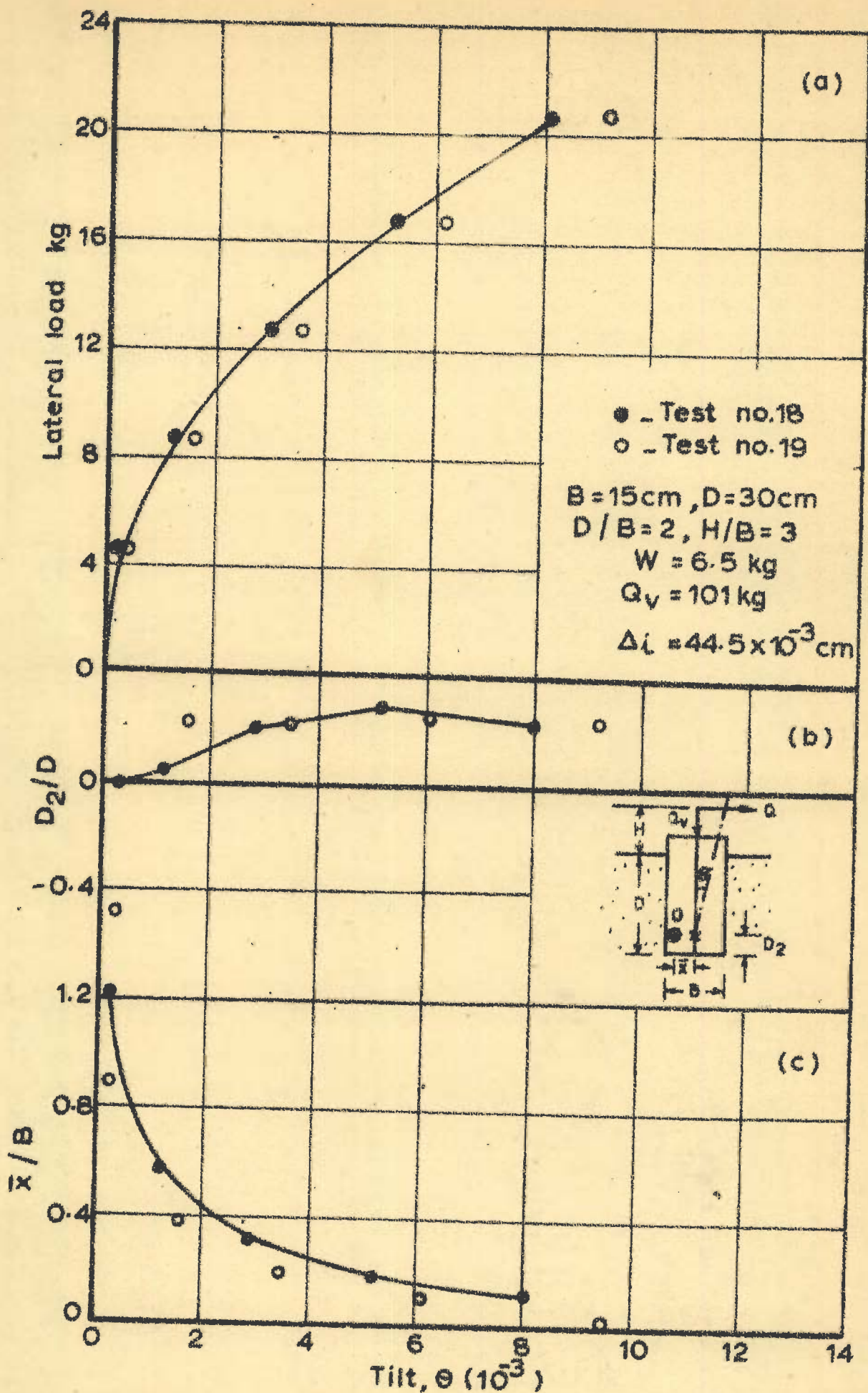
FIG. 74 _ LATERAL LOAD D₂/D AND x̄/B VS TILT
(Test no. 18 & 19)
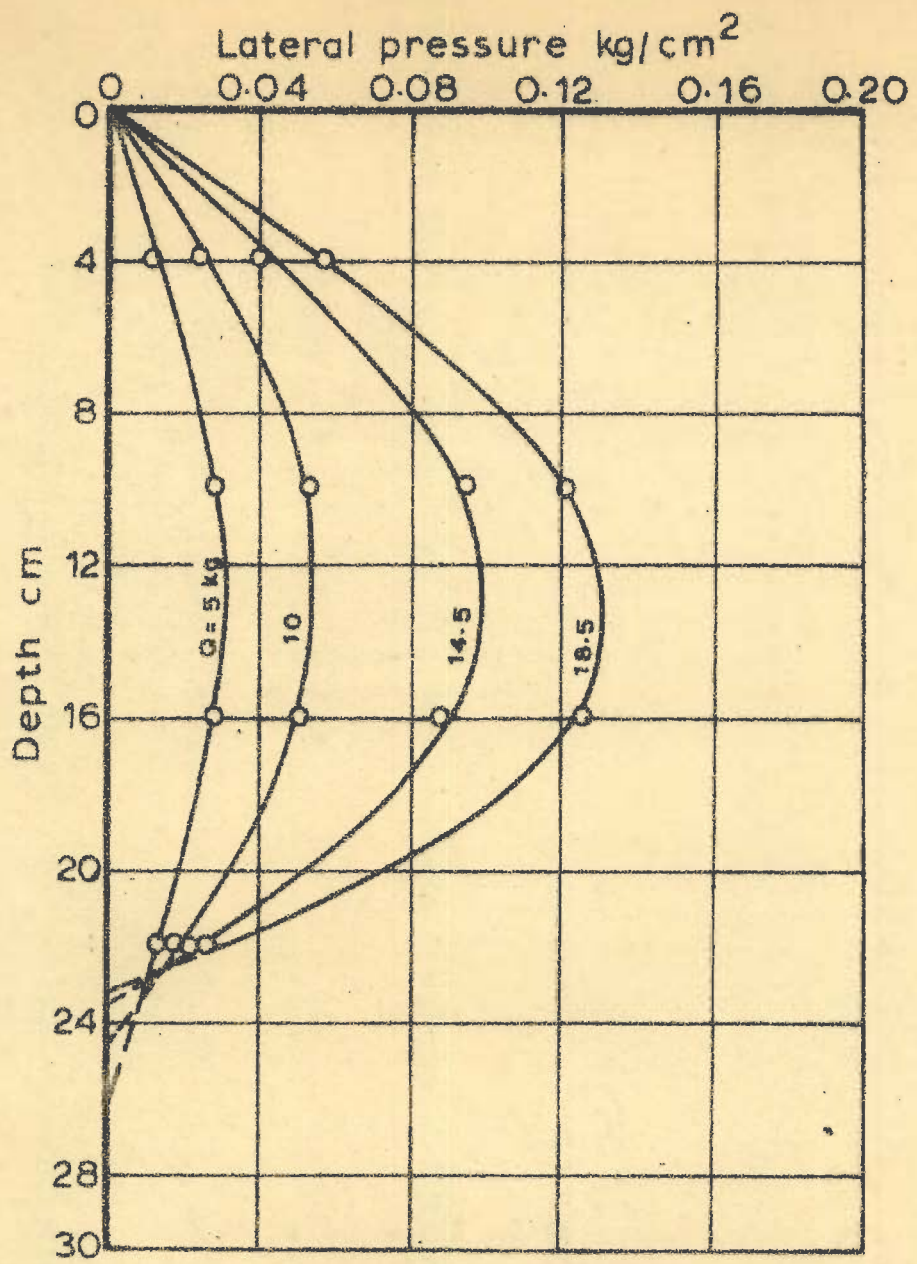
Lateral pressure kg/cm²

a _ Pressure distribution on front face vertical axis
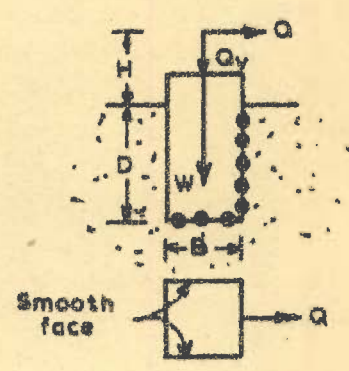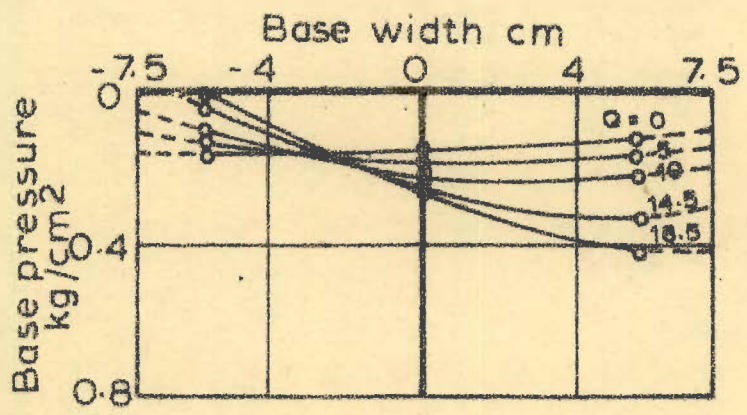
b _ Pressure distribution on centroidal axis of the base

B = 15 cm, D = 30 cm
D/B = 2 , H/B = 3
W = 6.5 kg
Q_V = 101 kg

FIG. 75 _ PRESSURE DISTRIBUTION ON FACE AND BASE
(Test no. 20)
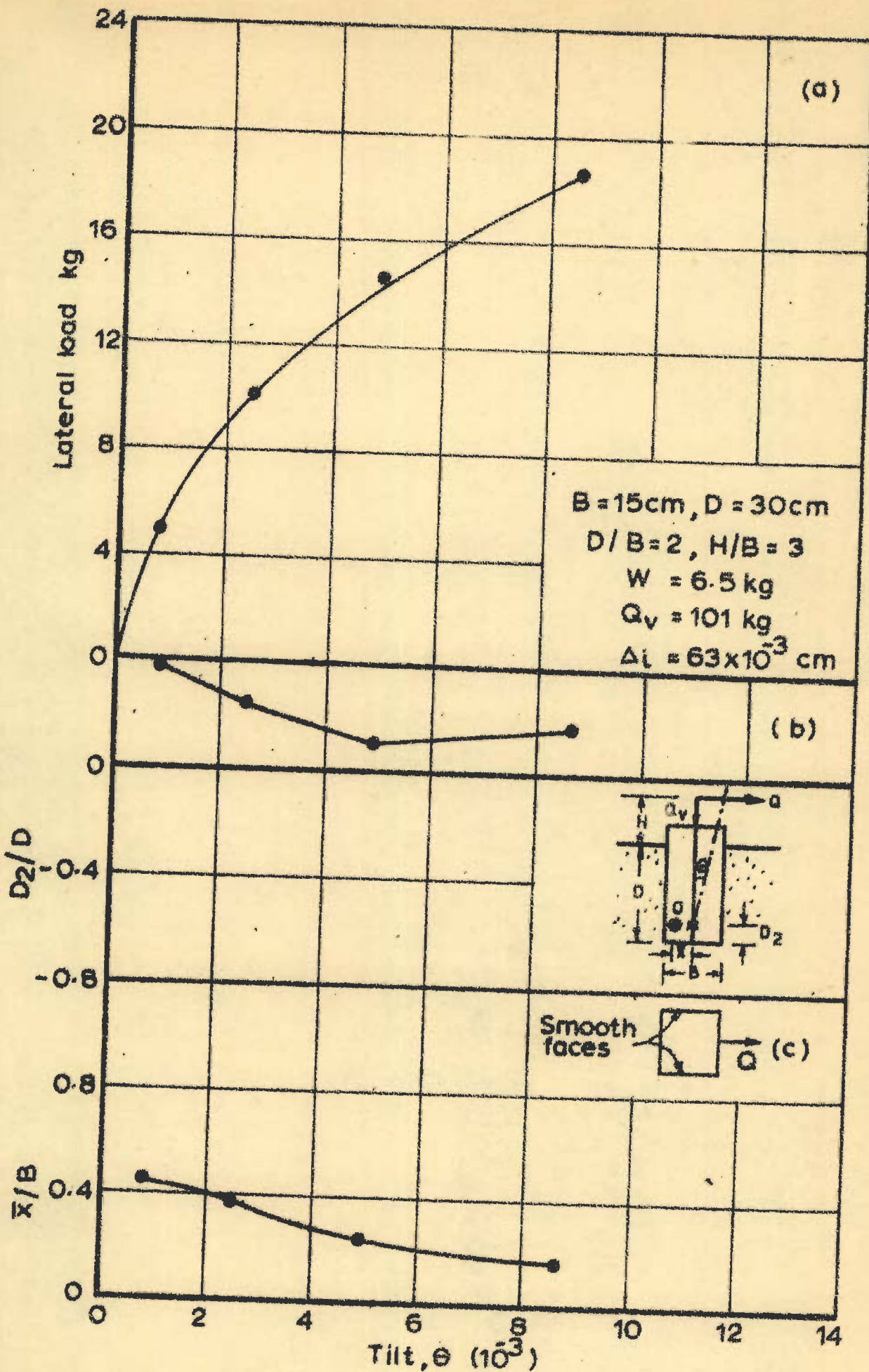
FIG. 76 — LATERAL LOAD, D_2/D, $\bar{x}/B$ VS TILT (Test no. 20)
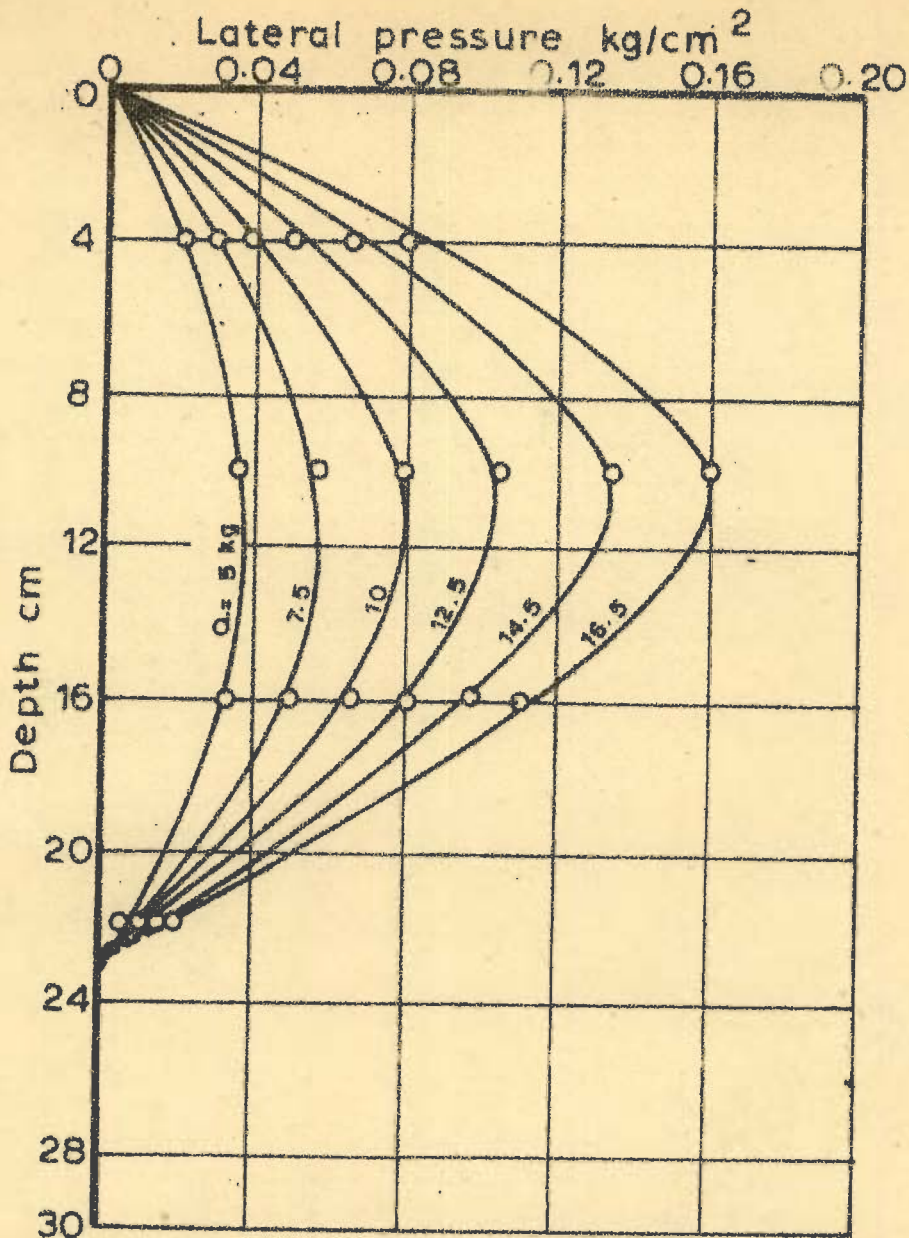
a — Pressure distribution on front face vertical axis
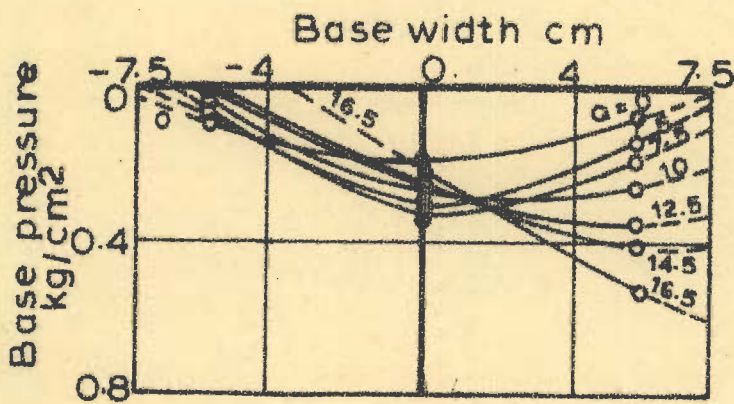
b — Pressure distribution on centroidal axis of the base
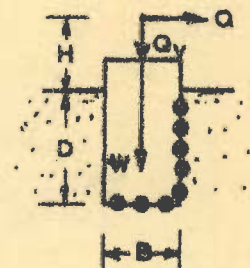
B = 15 cm , D = 30 cm
D/B = 2 , H/B = 4
W = 6.5 kg
Q_V = 51 kg

FIG. 77 — PRESSURE DISTRIBUTION ON FACES AND BASE
(Test no. 22)

FIG. 78 _ LATERAL LOAD, D_2/D AND $\bar{x}/B$ VS TILT
(Test no. 22)

B = 15 cm ; D = 30 cm
D/B = 2 , H/B = 3
W = 6.5 kg
Q_v = 51 kg
Δi = 18.75 $\times 10^{-3}$ cm
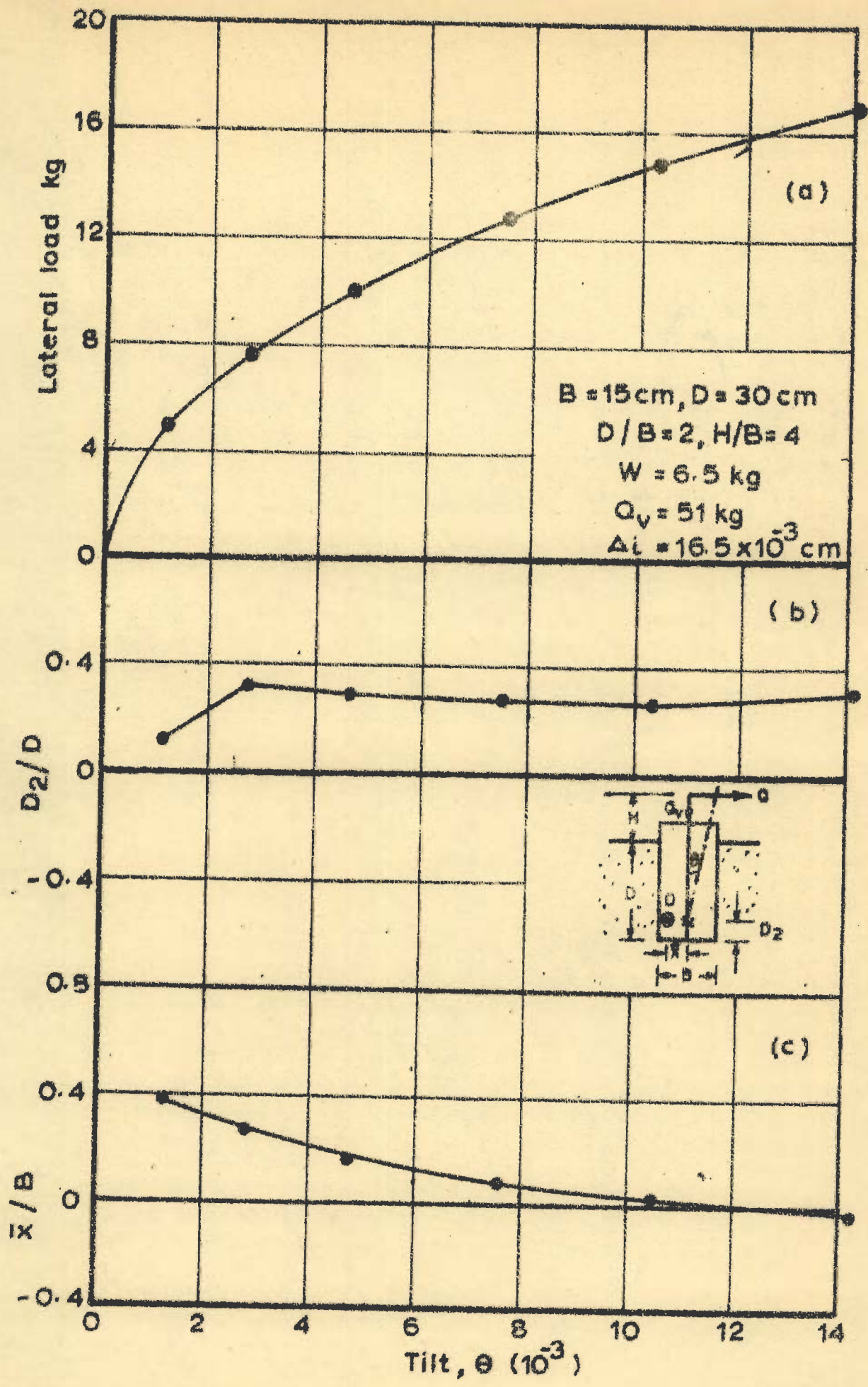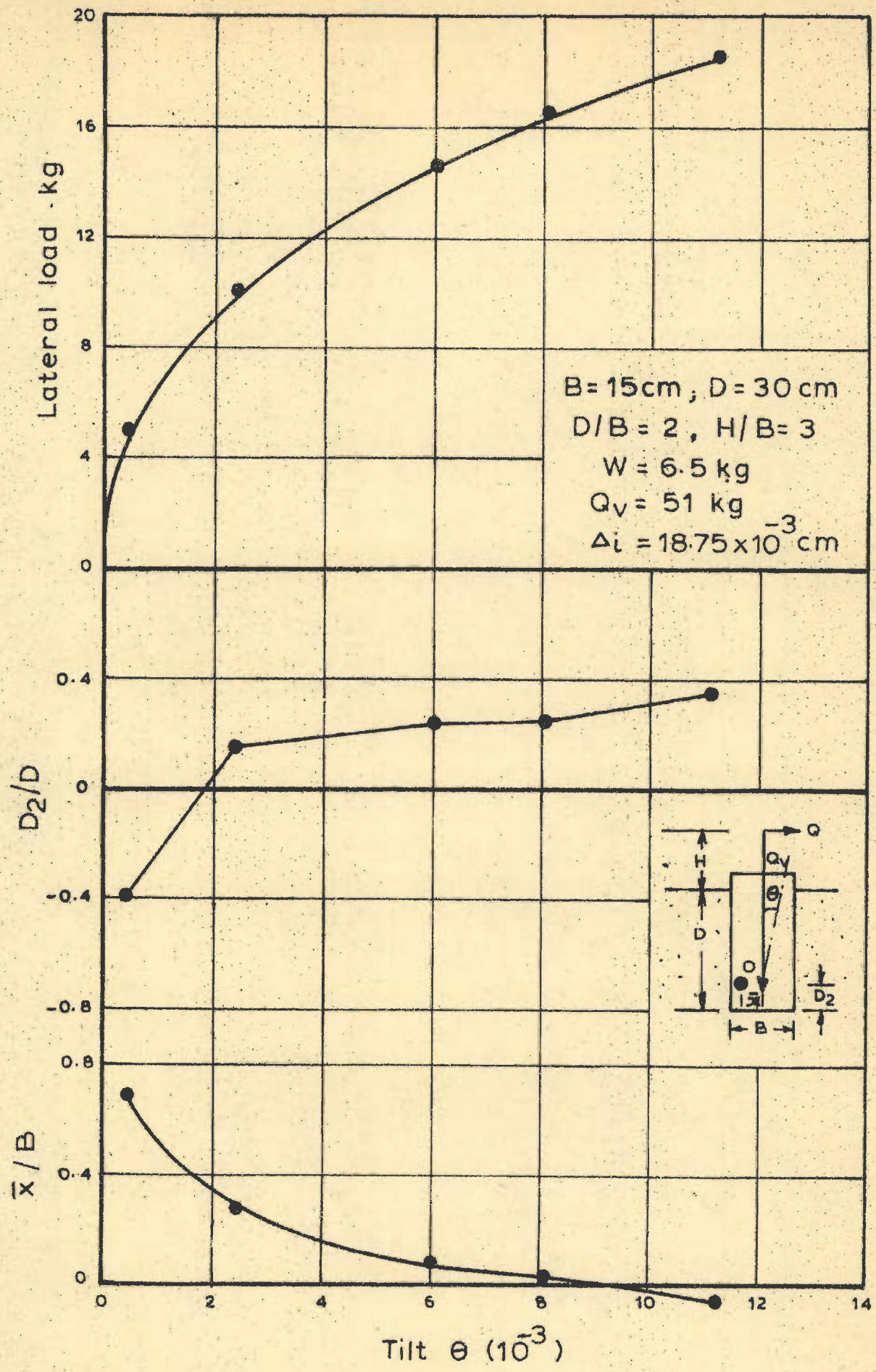
FIG. 79 _ LATERAL LOAD D_2/D AND $\bar{x}/B$ VS TILT
(Test no. 23)

a _ Pressure distribution on front face vertical axis
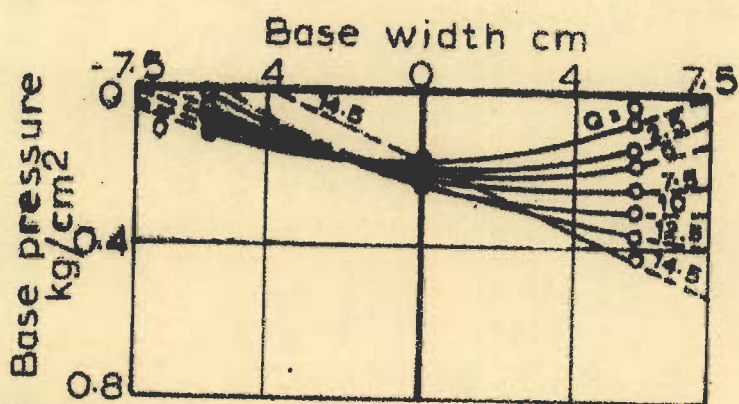
b _ Pressure distribution on centroidal axis of the base
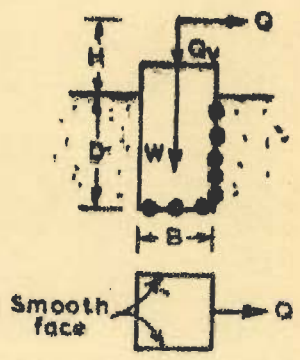
B = 10 cm, D = 30 cm
D/B = 2 , H/B = 3
W = 6.5 kg
Q_v = 51 kg

FIG. 80 _ PRESSURE DISTRIBUTION ON FACE AND BASE (Test no. 24)
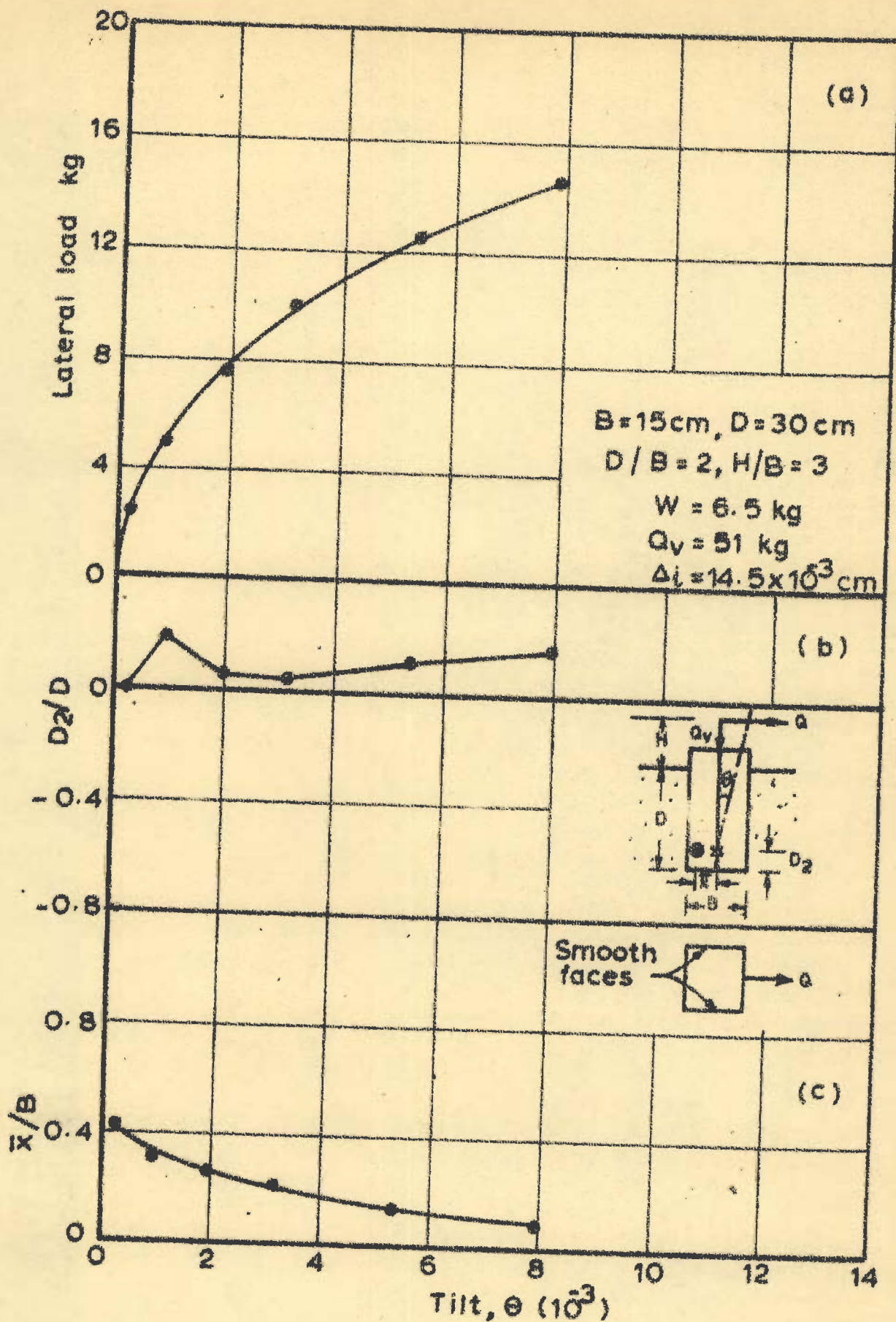
FIG. 81 — LATERAL LOAD, D_2/D AND $\bar{x}/B$ VS TILT
(Test no. 24)

a_Pressure distribution on centroidal axis of the base (Test no. 25)

B=15cm , D=30cm
D/B=2 , H/B=3
W=6.5 kg
Q_V= 51 kg
A_L = 22.5×10^{-3} cm

• Test no. 25
○ Test no. 26

(b)

(c)

(d)
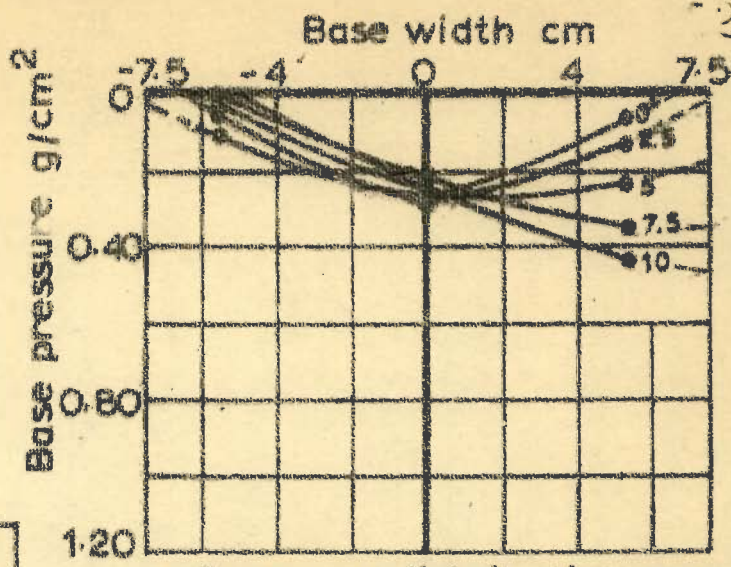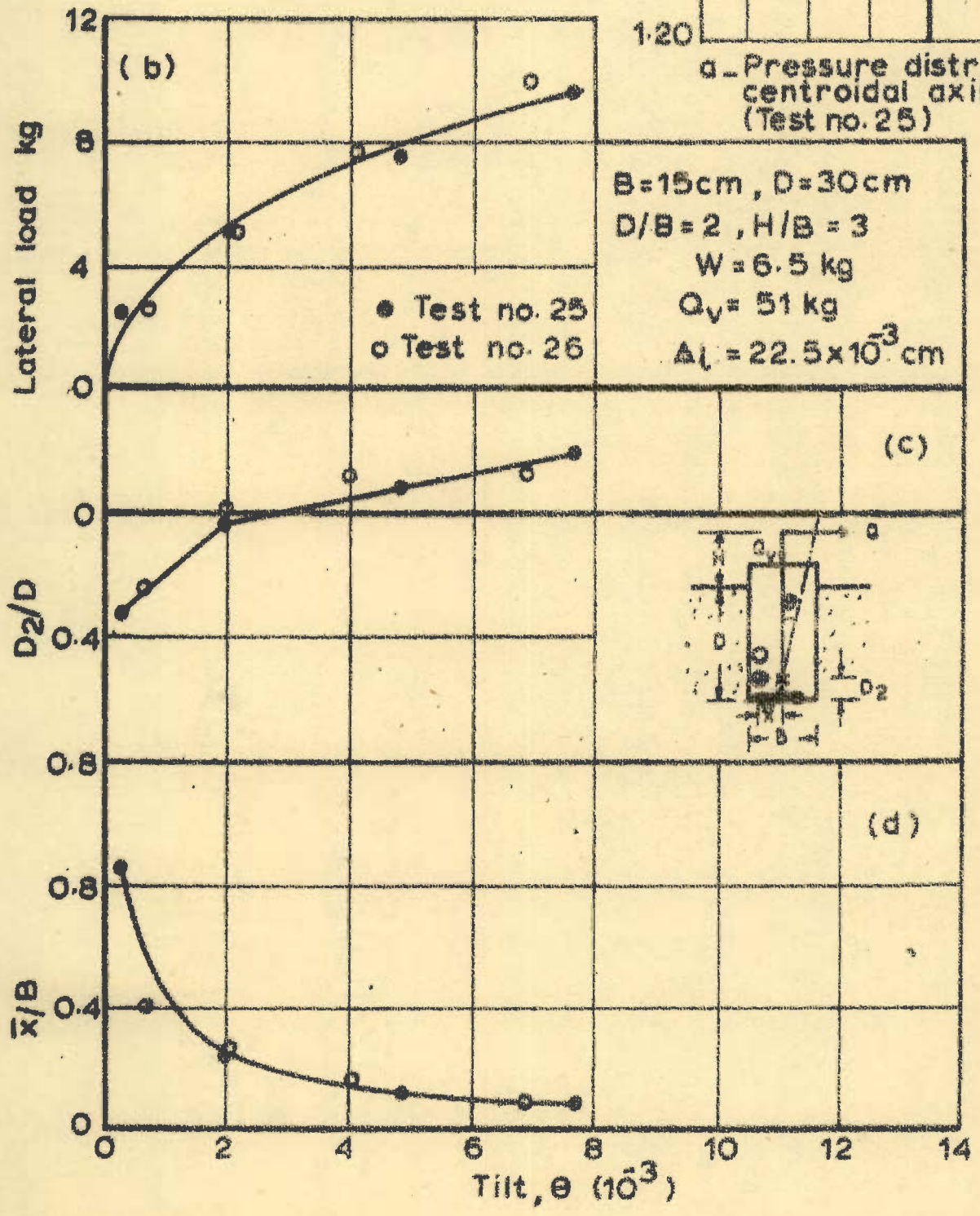
FIG. 6.2 _ BASE PRESSURES AND LATERAL LOAD, D_2/D, $\bar{x}$/B VS TILT (Test no. 25 & 26)

a_ Pressure distribution on front face vertical axis
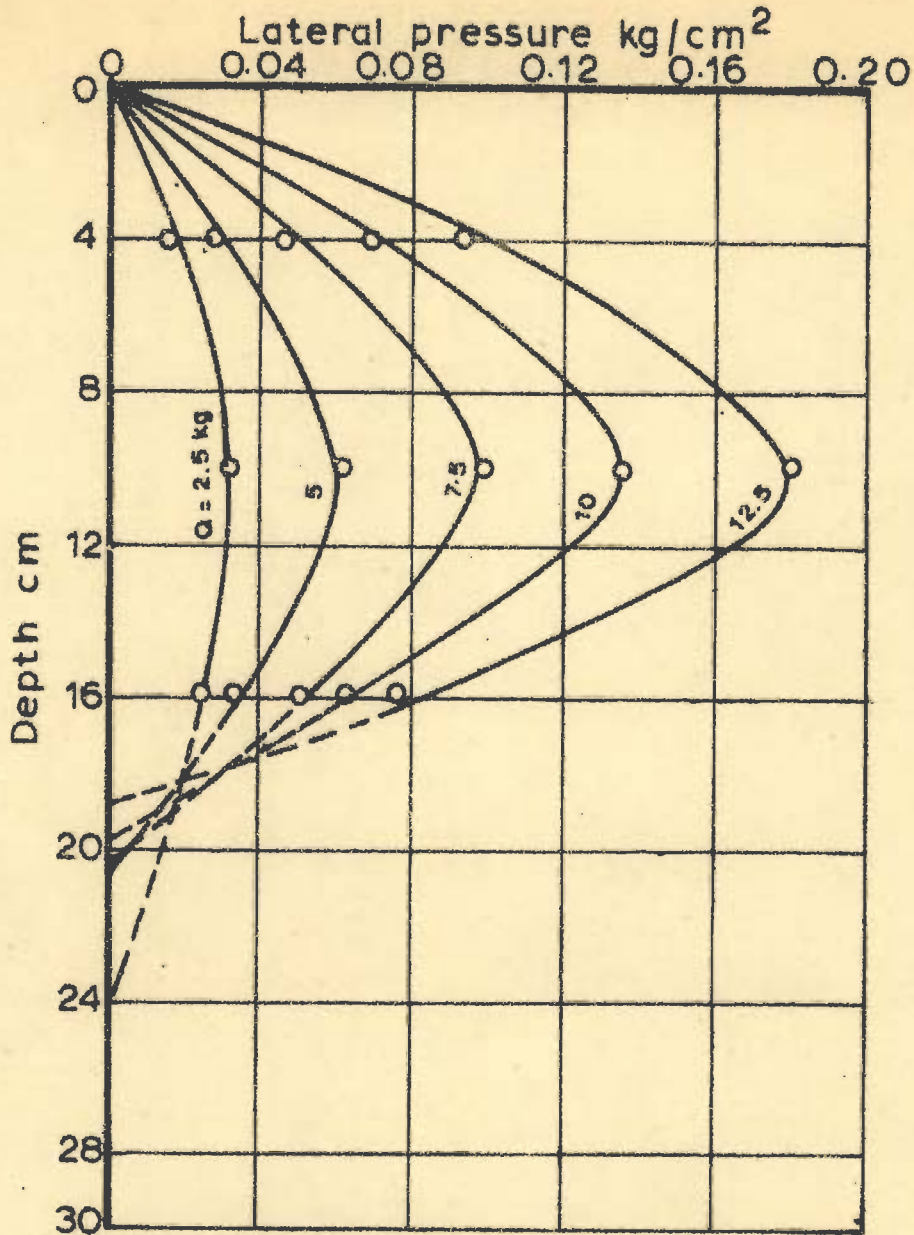
b_ Pressure distribution on centroidal axis of the base
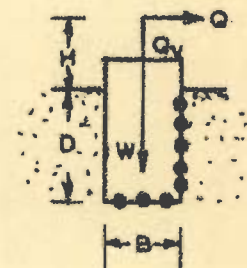
B = 15cm, D = 30cm
D/B = 2 , H/B = 4
W = 6.5 kg
Qv = 0

FIG. 83 _ PRESSURE DISTRIBUTION ON FACE AND BASE
(Test no. 27)

FIG. 84 _ LATERAL LOAD, D$_2$/D AND x̄/B VS TILT
(Test no. 27)

a — Pressure distribution on front face vertical axis

b — Pressure distribution on centroidal axis of the base

B = 15 cm, D = 30 cm
D/B = 2, H/B = 3
W = 6.5 kg
Q_V = 0 kg

FIG. 85 — PRESSURE DISTRIBUTION ON FACE AND BASE
(Test no. 28)

B = 15 cm, D = 30 cm
D/B = 2, H/B = 3
W = 6.5 kg
Q_V = 0 kg
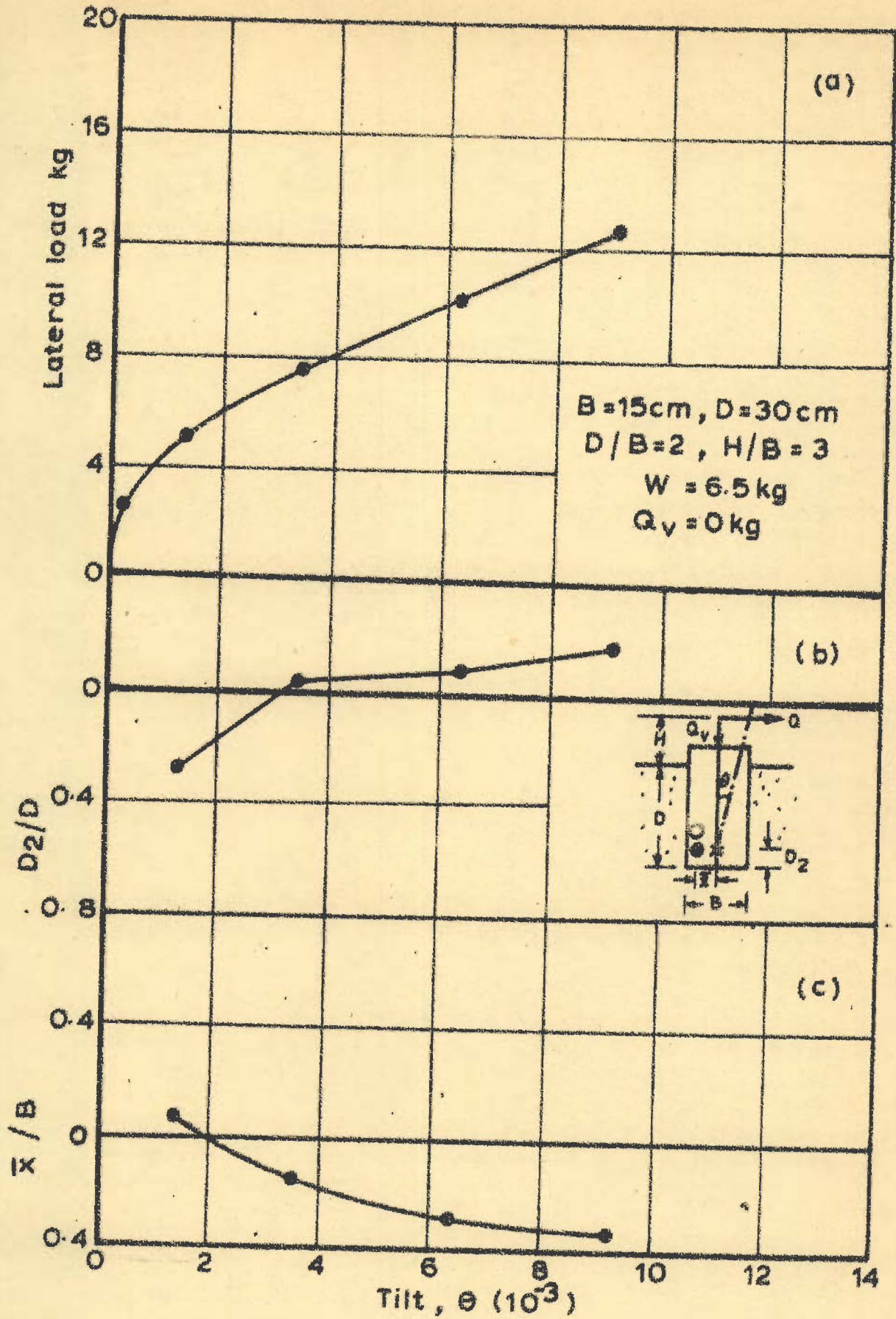
FIG. 86 — LATERAL LOAD, D_2/D AND $\bar{x}/B$ VS TILT
(Test no. 28)
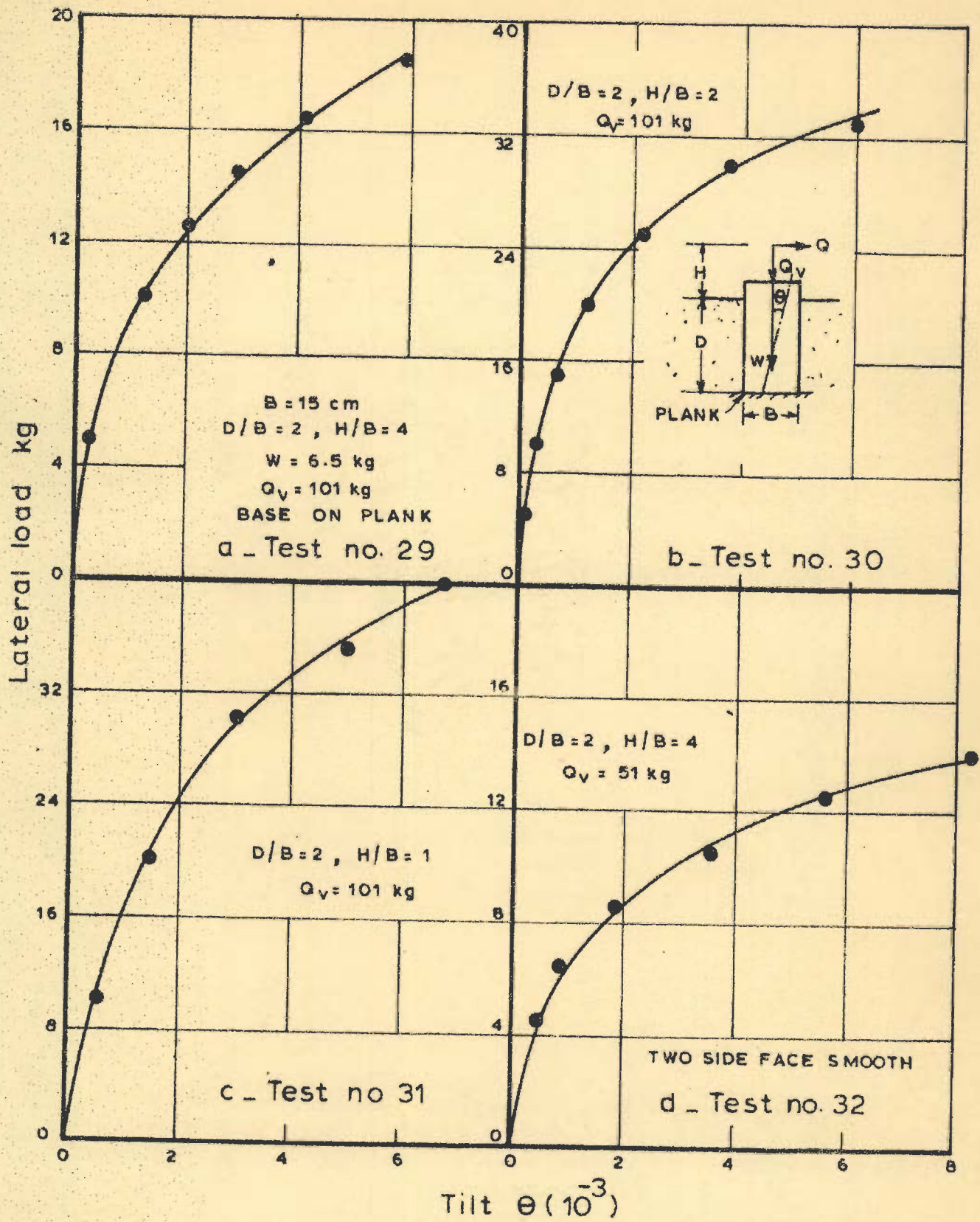
FIG.87-LATERAL LOAD VS TILT (Test no. 29 to 32)
(15 cm WELL ON PLANK)
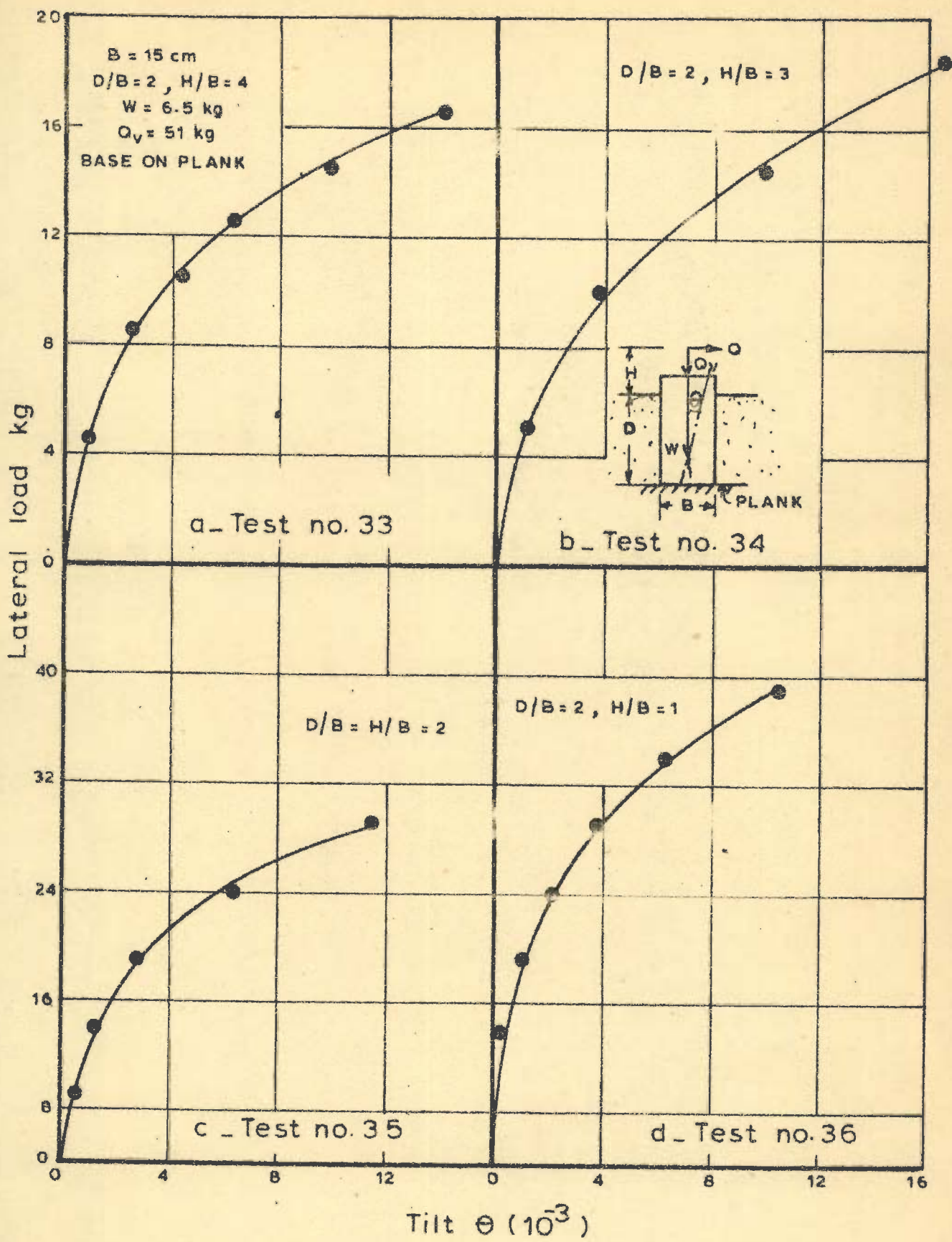
FIG. 88 _ LATERAL LOAD VS TILT (Test nos 33 to 36)
15 cm WELL ON PLANK
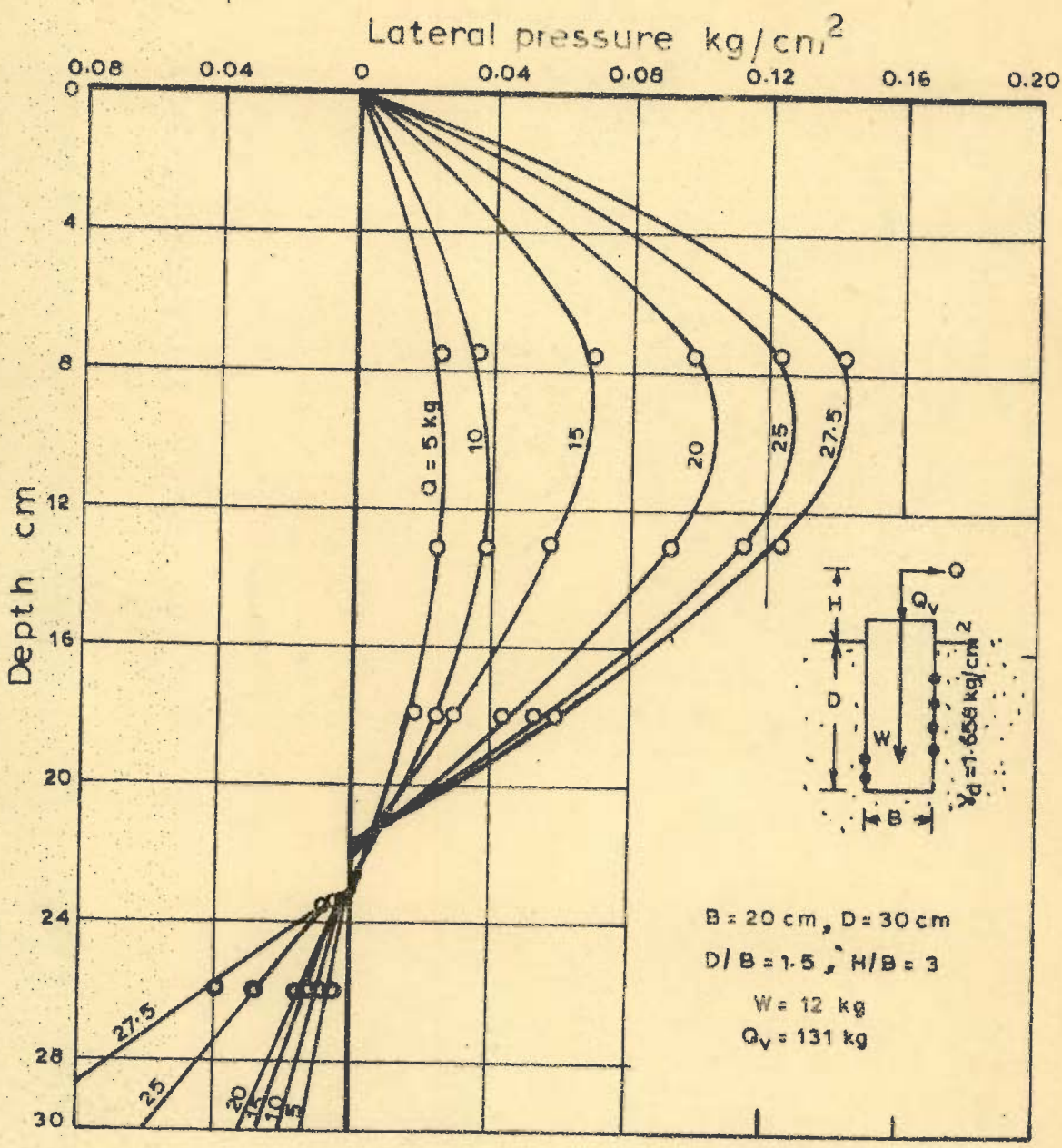
FIG. 89 — PRESSURE DISTRIBUTION ON FRONT AND REAR FACES FOR 20 cm WELL (Test no. 37)
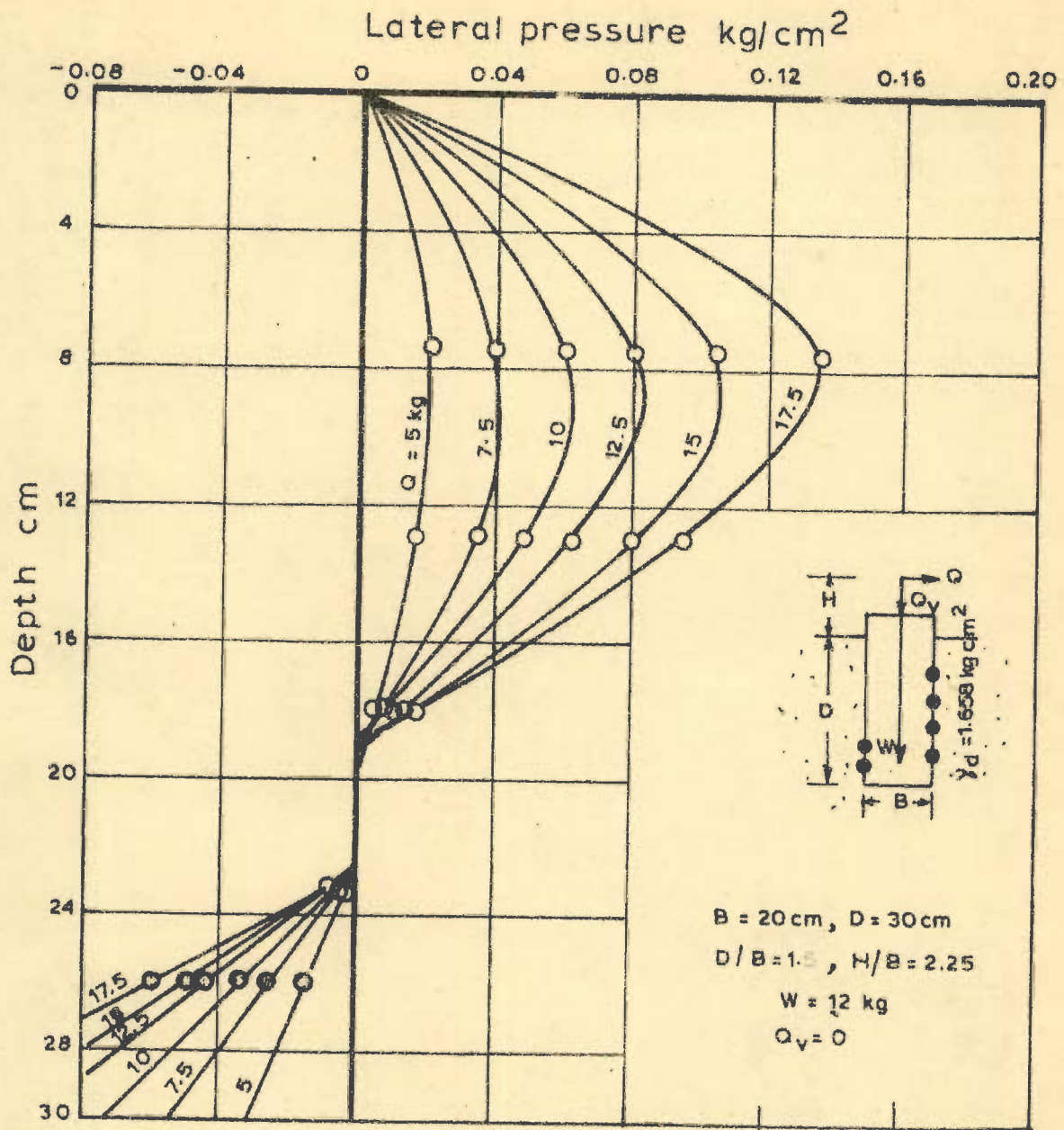
FIG. 90 _ PRESSURE DISTRIBUTION ON FRONT AND
REAR FACES FOR 20cm WELL (Test no. 40)

a_ Test no. 37 — B = 20 cm, D/B = 1.5, H/B = 2.25, Q_V = 131 kg

b_ Test no. 38 — B = 20 cm, D/B = 1.5, H/B = 2.25, Q_V = 131 kg, SIDE FACES SMOOTH

c_ Test no. 39 — B = 20 cm, D/B = 1.5, H/B = 2.25, Q_V = 131 kg, ALL FACES SMOOTH

d_ Test no. 40 — D/B = 1.5, H/B = 2.25, Q_V = 0 kg

e_ Test no. 41 — D/B = 2, H/B = 4, Q_V = 131 kg

f_ Test no. 42 — D/B = 2, H/B = 2, Q_V = 131 kg

g_ Test no. 43 — D/B = 2, H/B = 4, Q_V = 0

h_ Test no. 44 — D/B = 2, H/B = 4, Q_V = 0, SIDE FACES SMOOTH

i_ Test no. 45 — D/B = 2, H/B = 2, Q_V = 0

Lateral load kg

Tilt θ (10^{-3})
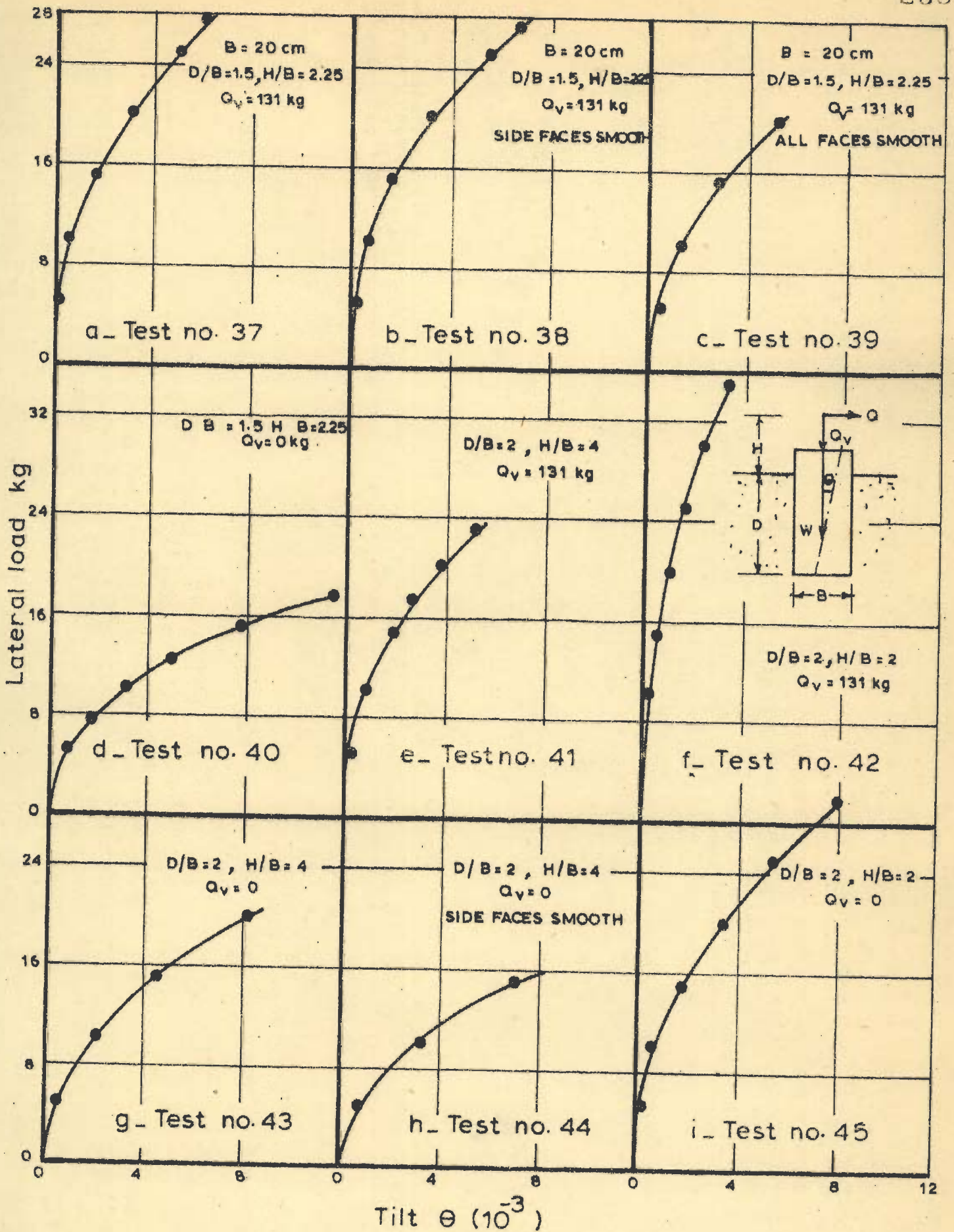
FIG. 91_ LATERAL LOAD VS TILT (Test no 37 to 45)
ON 20 cm WOODEN WELL
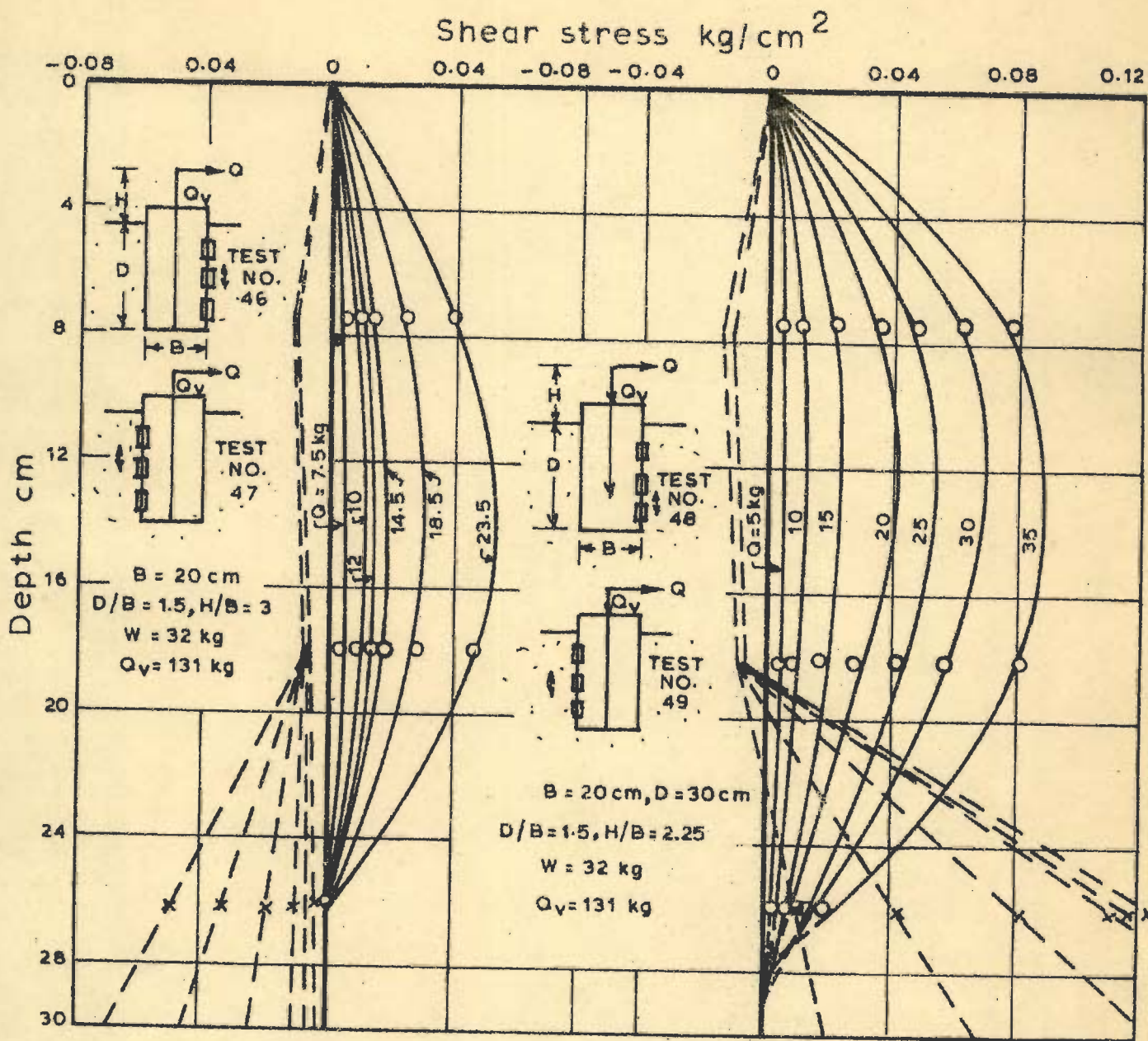
FIG. 92

FIG. 93

FRICTION ON FRONT AND REAR FACES

Shear stress kg/cm²

Depth cm

TEST NO. 50

B = 20 cm
D/B = 1·5, H/B = 3
W = 32 kg
Q = 56 kg

TEST NO. 51

B = 20 cm
D/B = 1·5, H/B = 2.25
W = 32 kg
Qv = 0 kg

TEST NO. 52

B = 20 cm
D/B = 1.5 H/B = 2.25
W = 32 kg
Qv = 0

FIG. 94

FIG. 95

FIG. 96

FRICTION ON FRONT FACE

a_Friction on side face

Displacement mm x 10^{-2}

Shear stress kg/cm2

B = 20cm, D = 30cm
D/B = 1.5, H/B = 3
W = 32 kg
Q_V = 131 kg
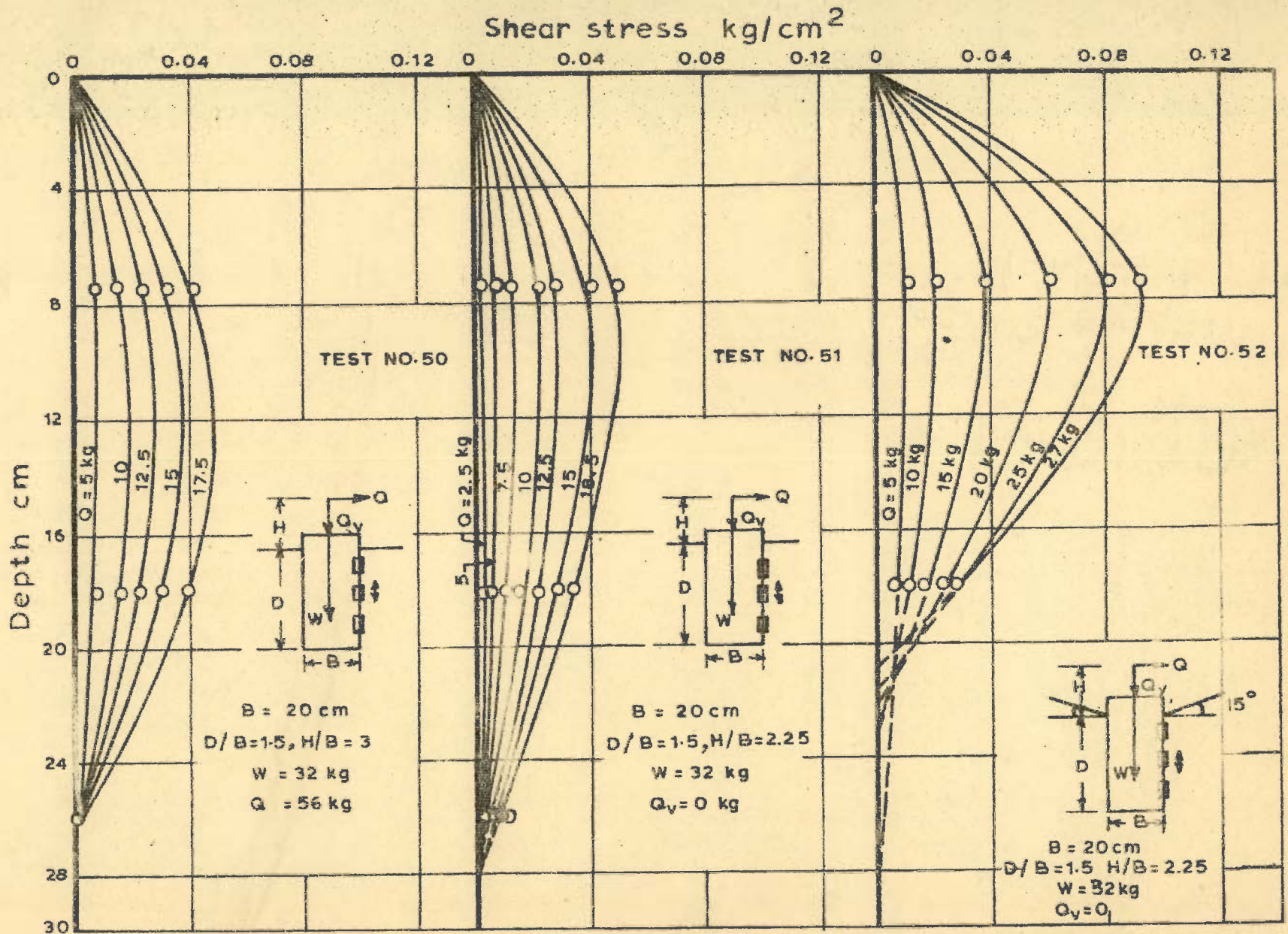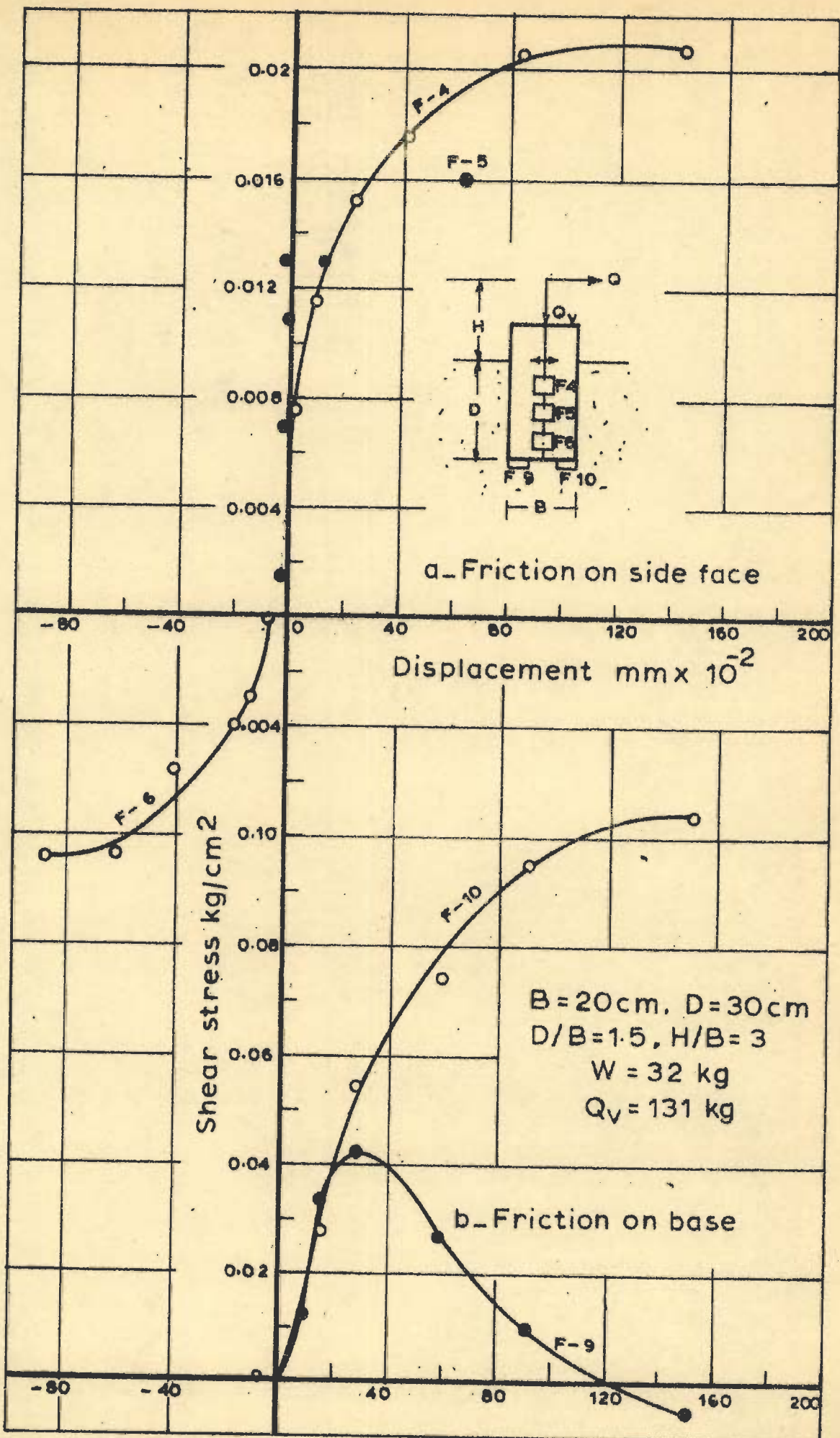
b_Friction on base

FIG. 97_ MOBILIZATION OF FRICTION ON SIDE FACE AND BASE (Test no. 53)

a_ Friction on side face

B = 20 cm, D = 30 cm
D/B = 1.5, H/B = 2.25
W = 32 kg
Q_V = 131 kg

b_ Friction on base

Shear stress kg./cm²

Displacement mm x 10²
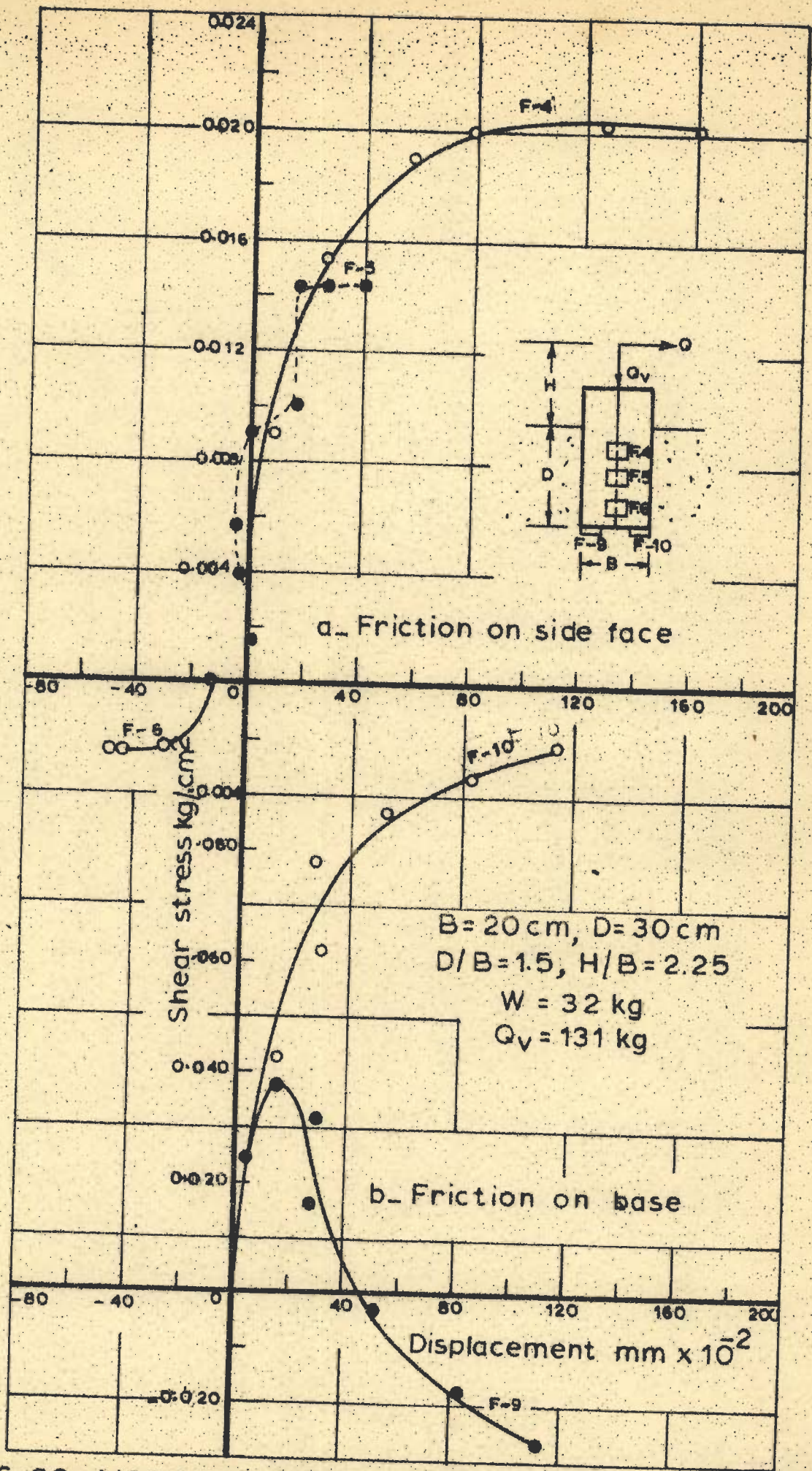
FIG. 98 _ MOBILIZATION OF FRICTION ON SIDE FACE
AND BASE (Test no. 54)

a_ Friction on side face

Displacement mm x 10^{-2}

B = 20cm, D = 30 cm
D/B = 1·5, H/B = 3
W = 32 kg
Q$_V$ = 56 kg

Shear stress kg/cm^2
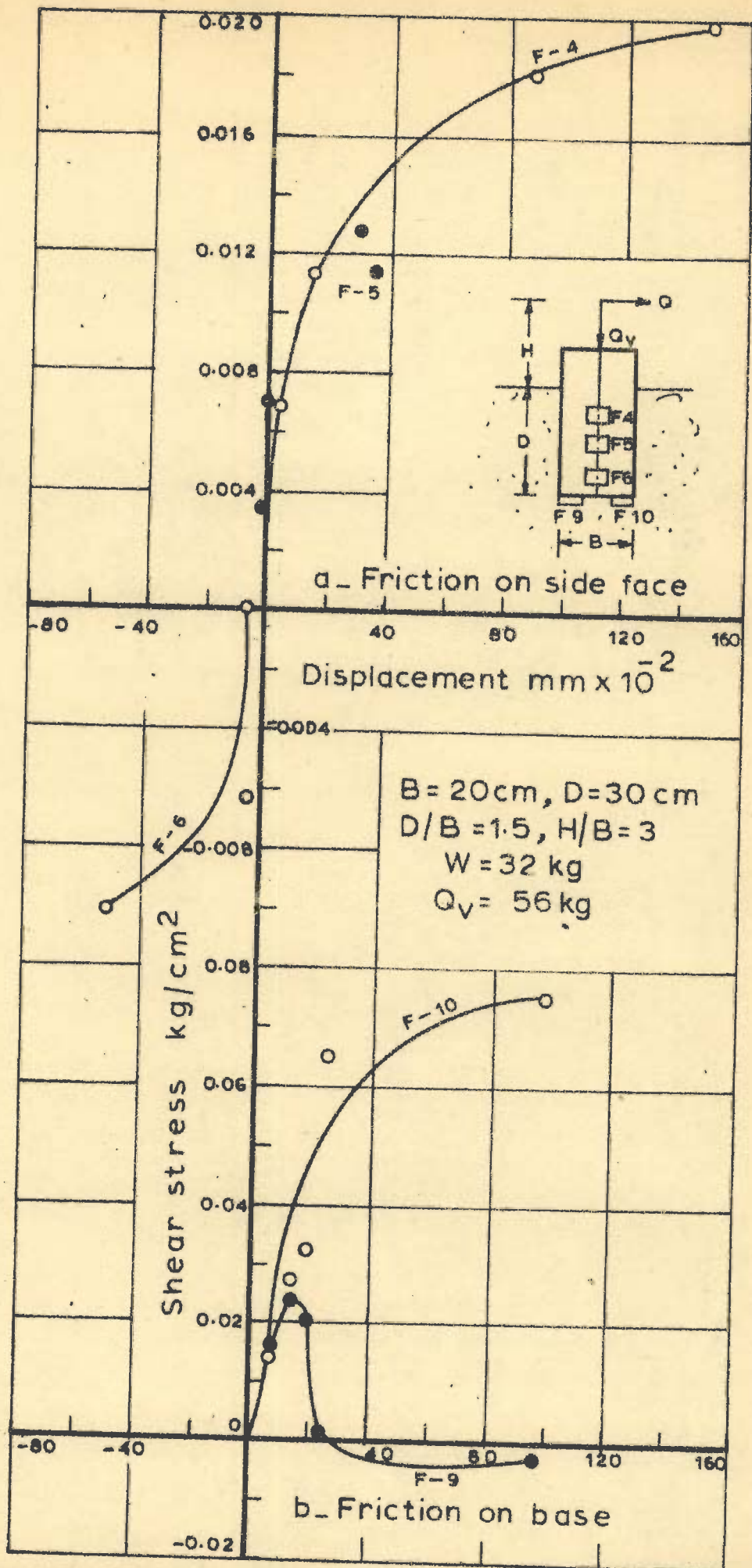
b_ Friction on base

FIG. 99 _ MOBILIZATION OF FRICTION ON SIDE FACE
AND BASE (Test no. 55)
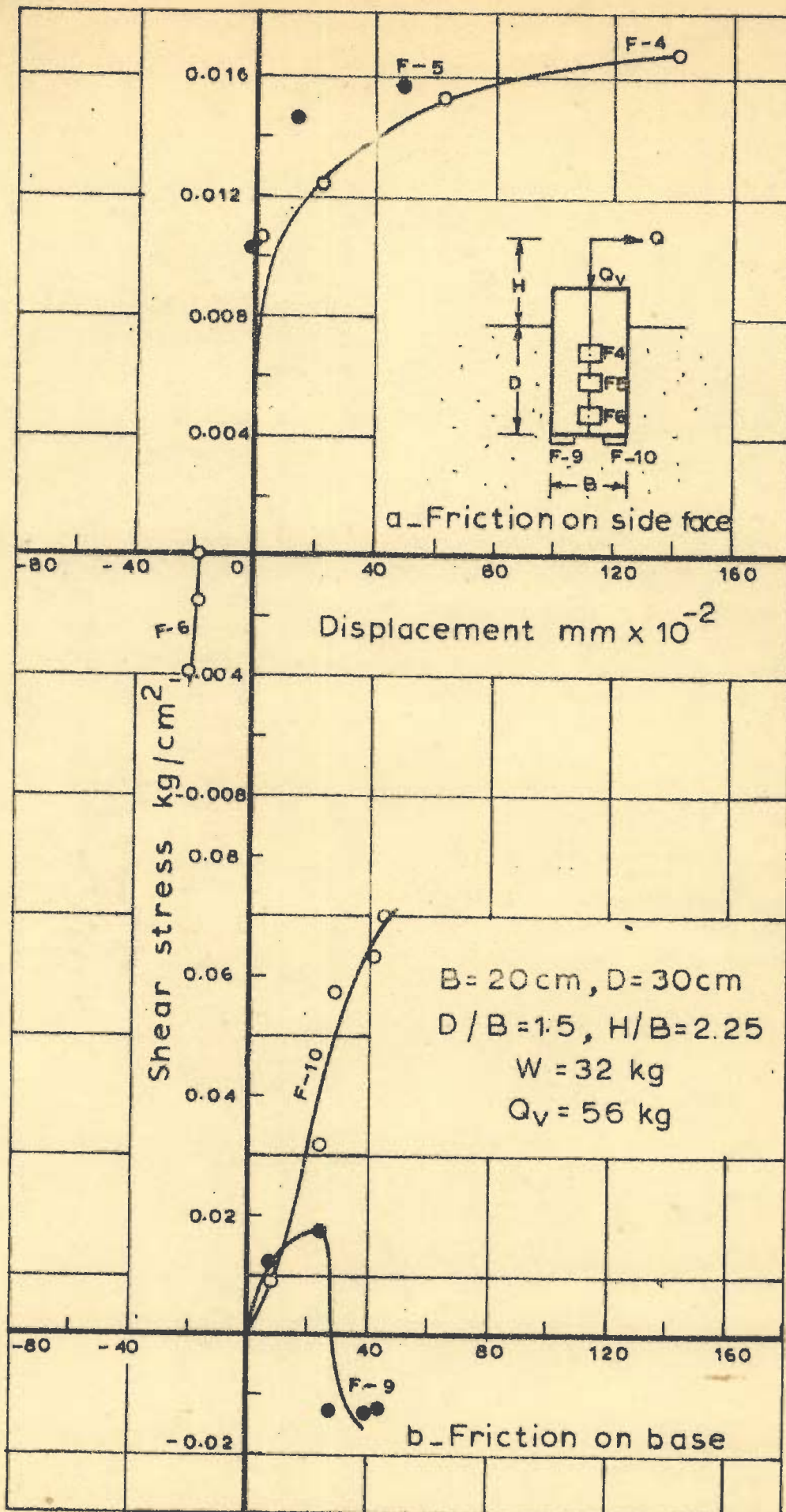
FIG. 100 – MOBILIZATION OF FRICTION ON SIDE FACE AND BASE (Test no. 56)
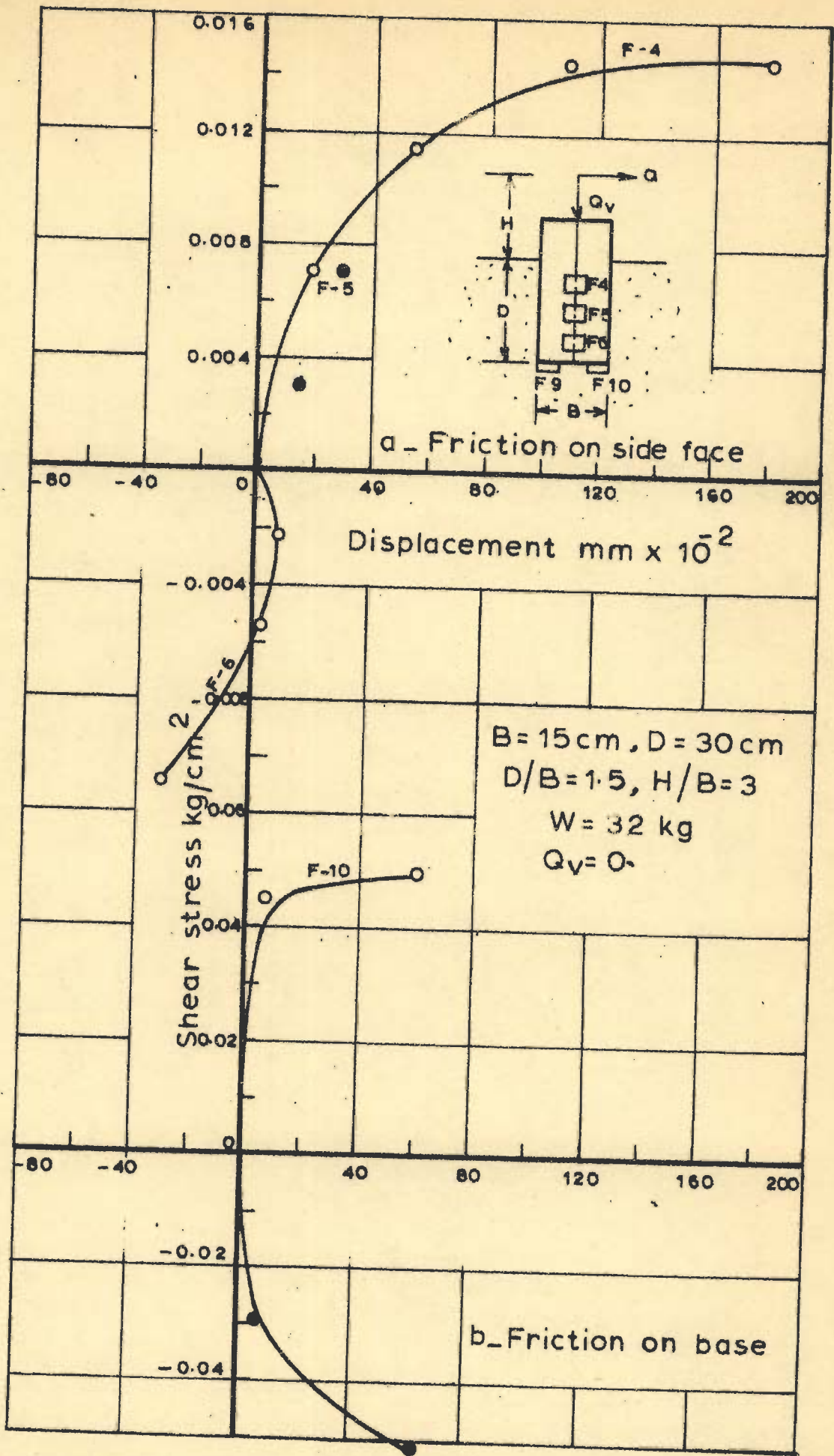
FIG. 101_MOBILIZATION OF FRICTION ON SIDE FACE AND BASE
(Test no. 57)
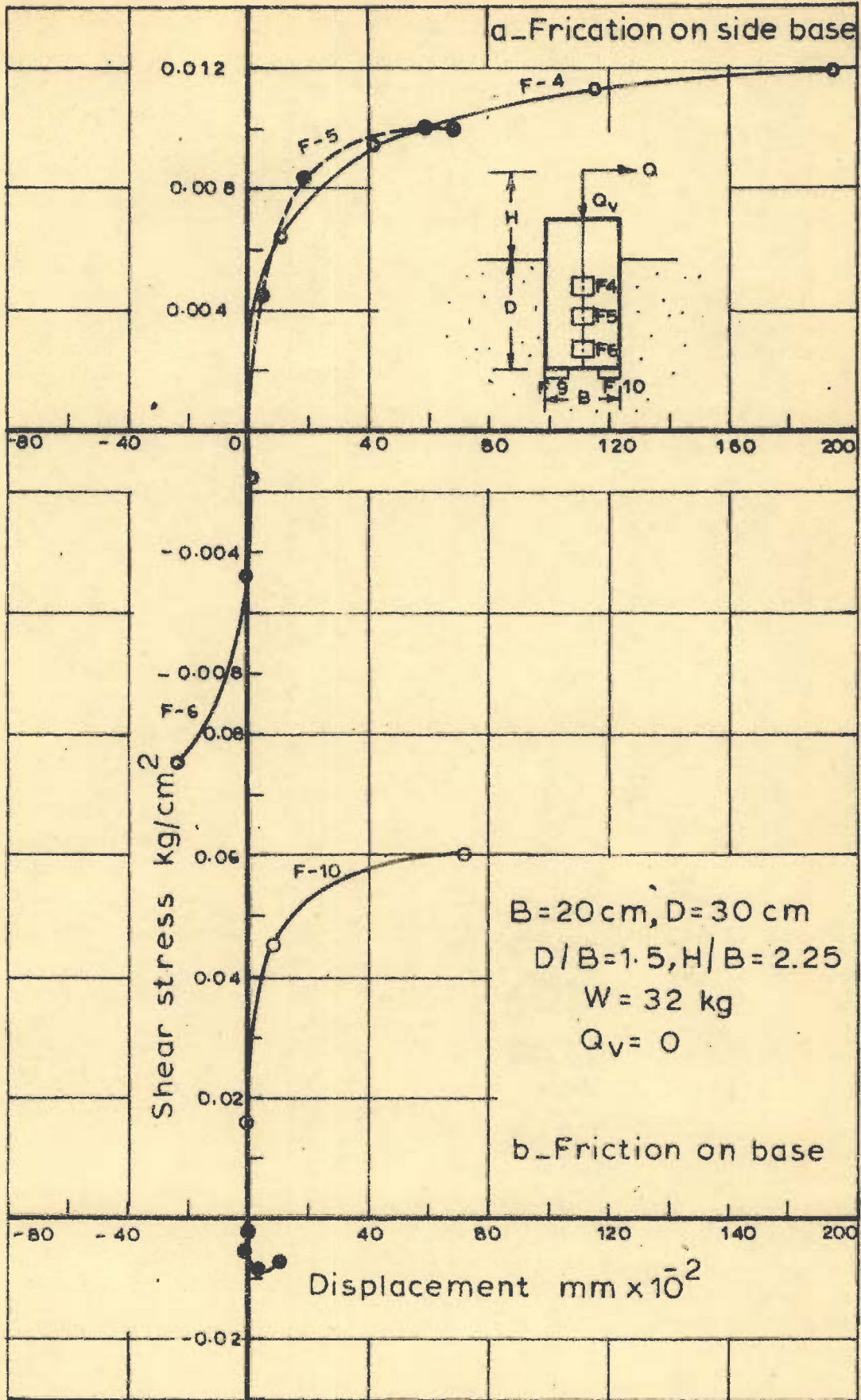
FIG.102 _ MOBILIZATION OF FRICTION ON SIDE FACE AND
BASE (Test no. 58)

CYCLIC LOAD TEST

B = 15 cm
D/B = 2, H/B = 3
W = 6.5 kg
Q_V = 131 kg
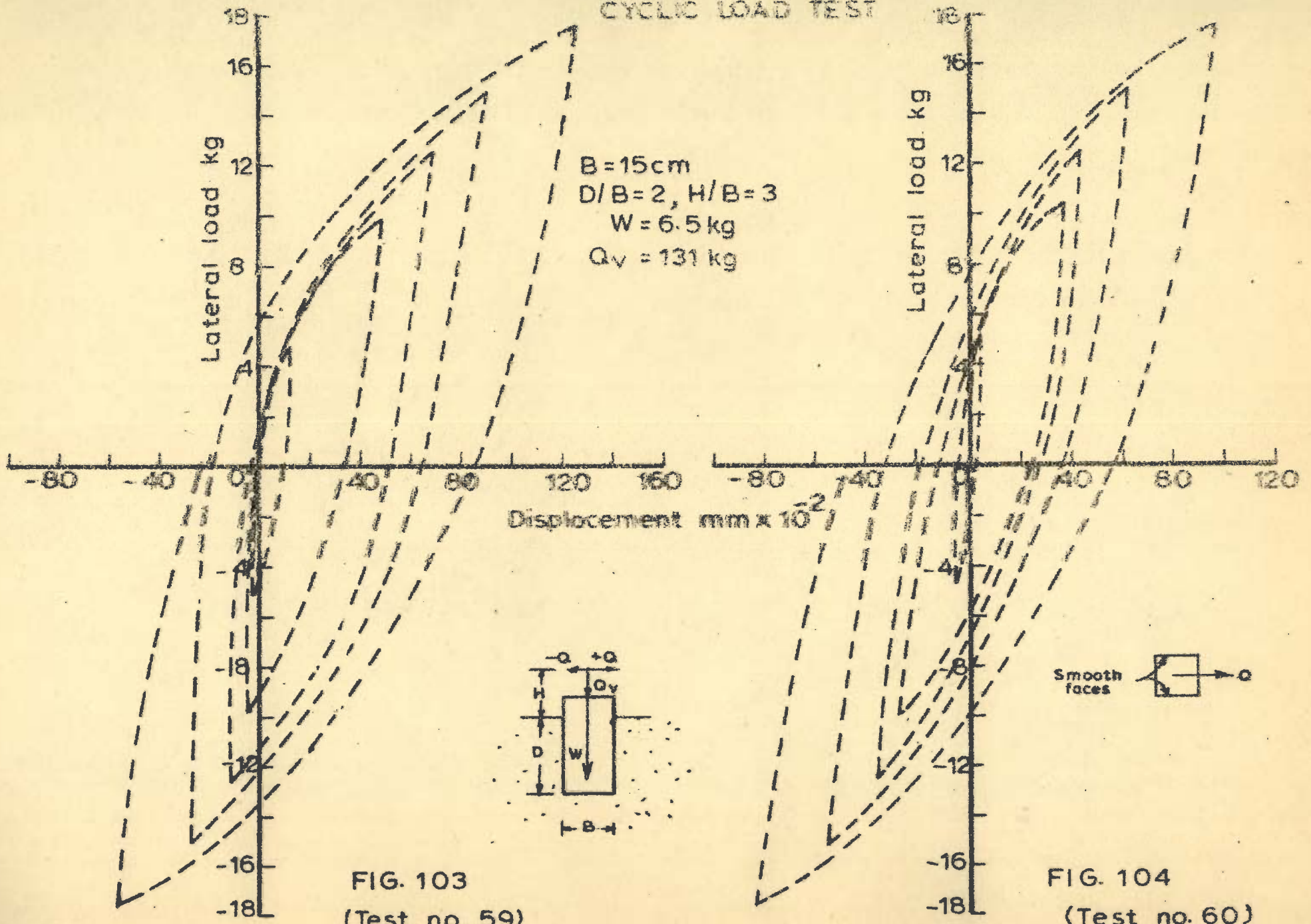
FIG. 103
(Test no. 59)

FIG. 104
(Test no. 60)

LATERAL LOAD VS DISPLACEMENT

CYCLIC LOAD TEST

All faces smooth
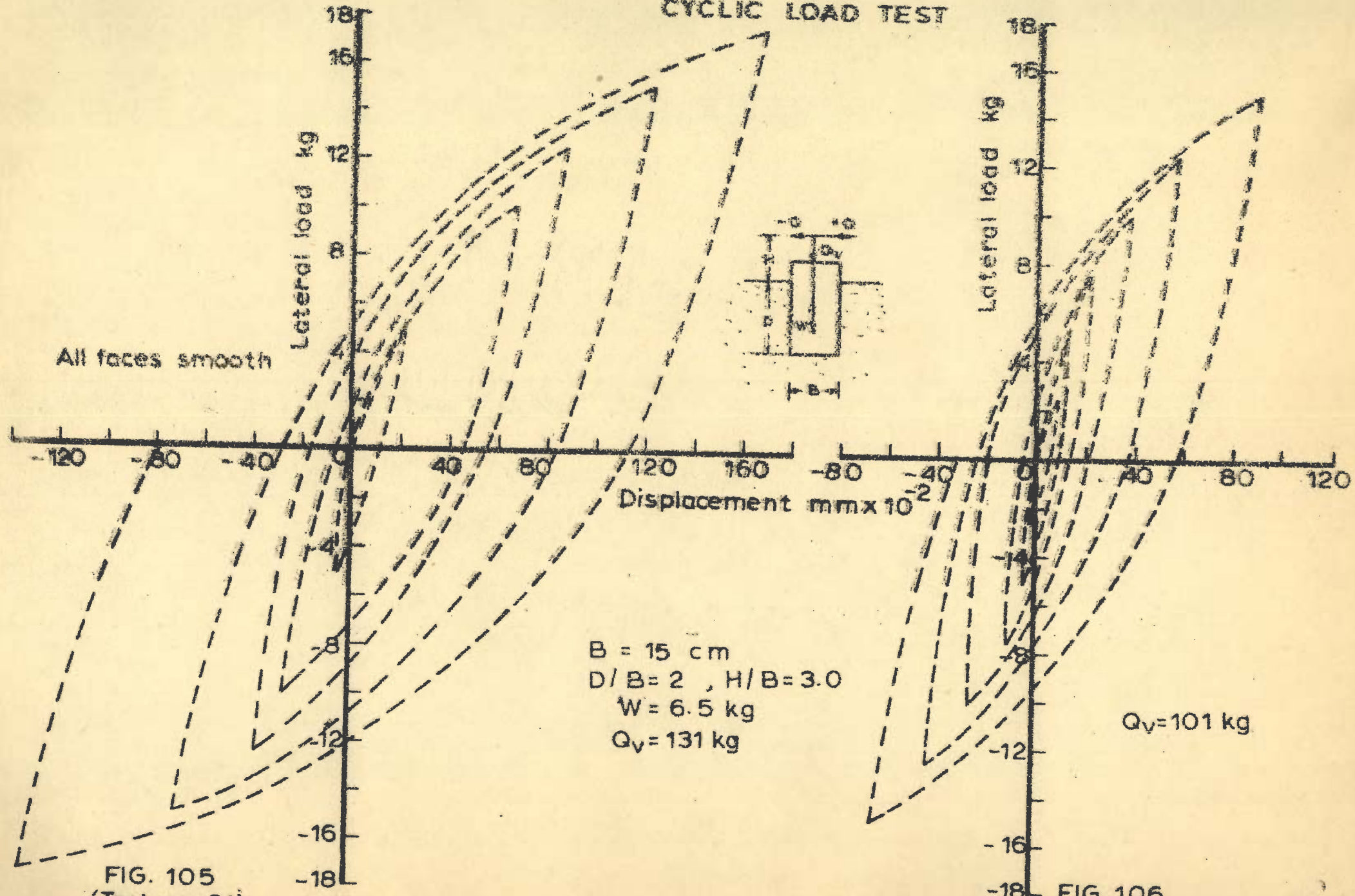
B = 15 cm
D/B = 2 , H/B = 3.0
W = 6.5 kg
Q_V = 131 kg

Q_V = 101 kg

FIG. 105
(Test no. 61)

FIG. 106
(Test no. 62)

LATERAL LOAD VS DISPLACEMENT
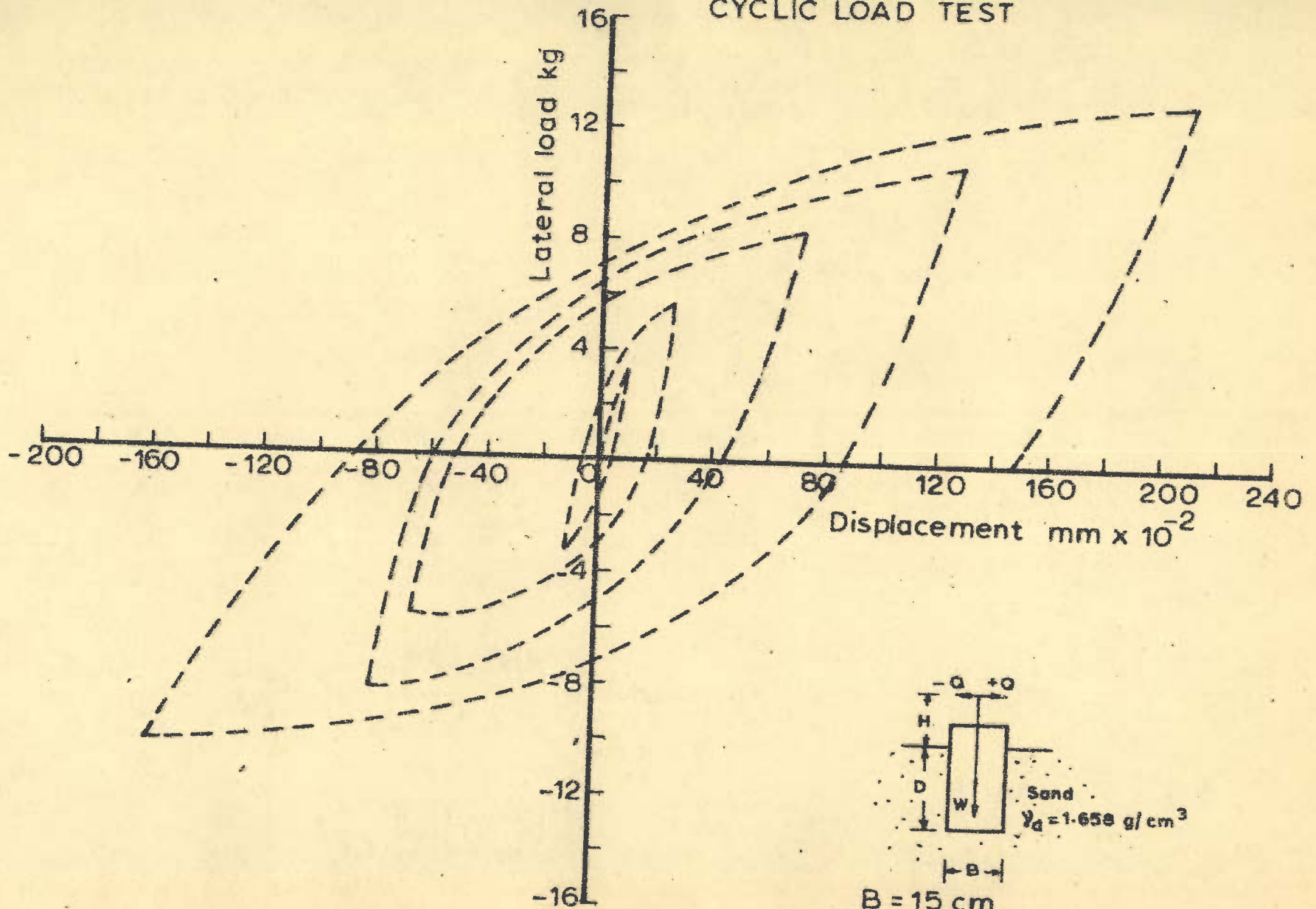
CYCLIC LOAD TEST

FIG. 107_ LATERAL LOAD VS DISPLACEMENT
(Test no. 63)

B = 15 cm
D/B = 2 , H/B = 3
W = 6.5 kg
Q_V = 0 kg

CYCLIC LOAD TEST
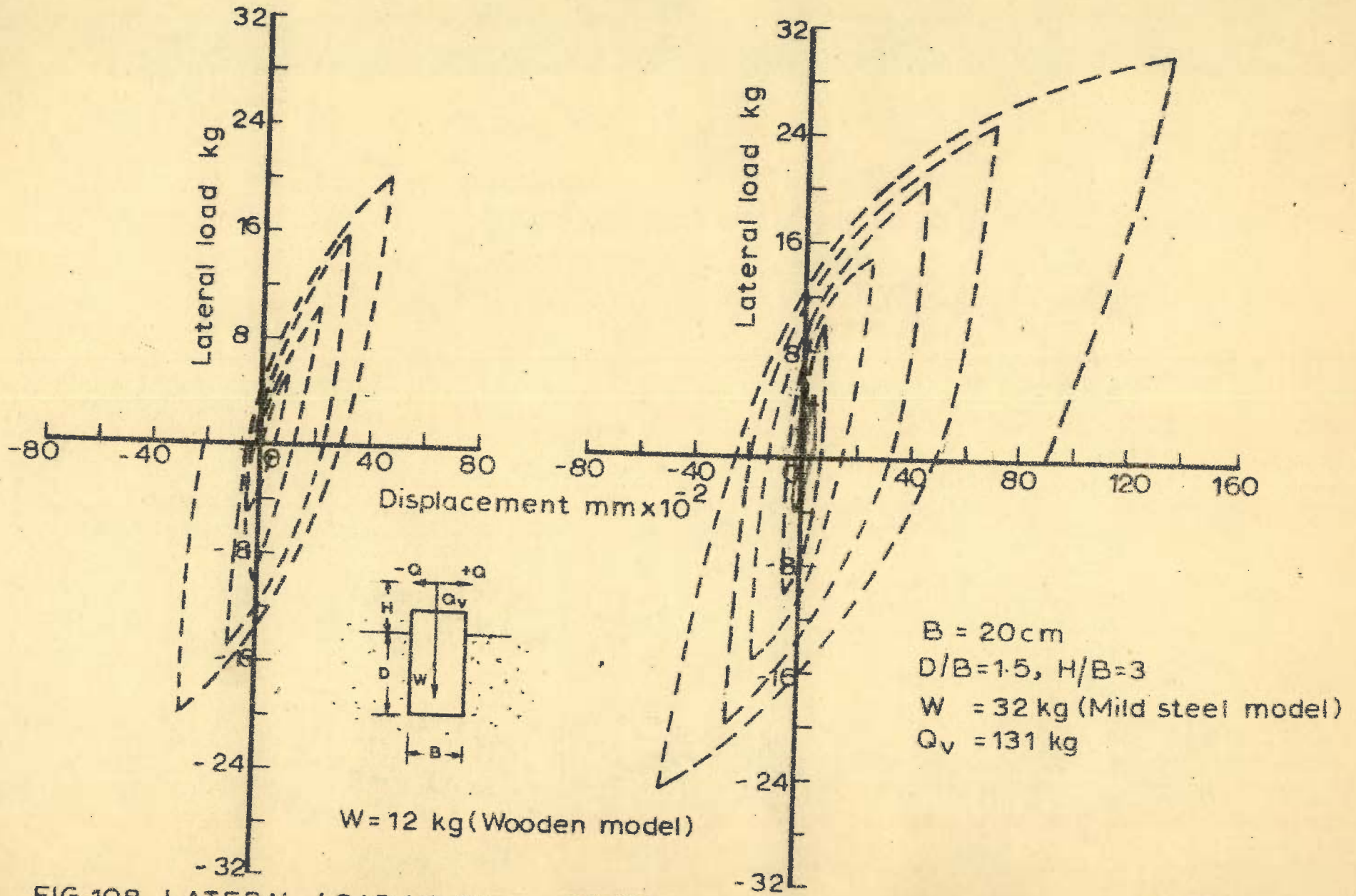
FIG. 108_ LATERAL LOAD VS DISPLACEMENT
(Test no. 64)

FIG. 109_ LATERAL LOAD VS DISPLACEMENT
(Test no. 65)

W = 12 kg (Wooden model)

B = 20cm
D/B = 1·5, H/B = 3
W = 32 kg (Mild steel model)
Q_v = 131 kg

Test no. 66
$Q_V = 156$ kg
FIG. 110

Test no. 67

$B = 20$ cm
$D/B = 1.5, H/B = 3$
$W = 32$ kg

$Q_V = 131$ kg

FIG. 111

Test no. 68
$Q_V = 55$ kg

FIG. 112

Lateral load kg

Displacement mm x10⁻²
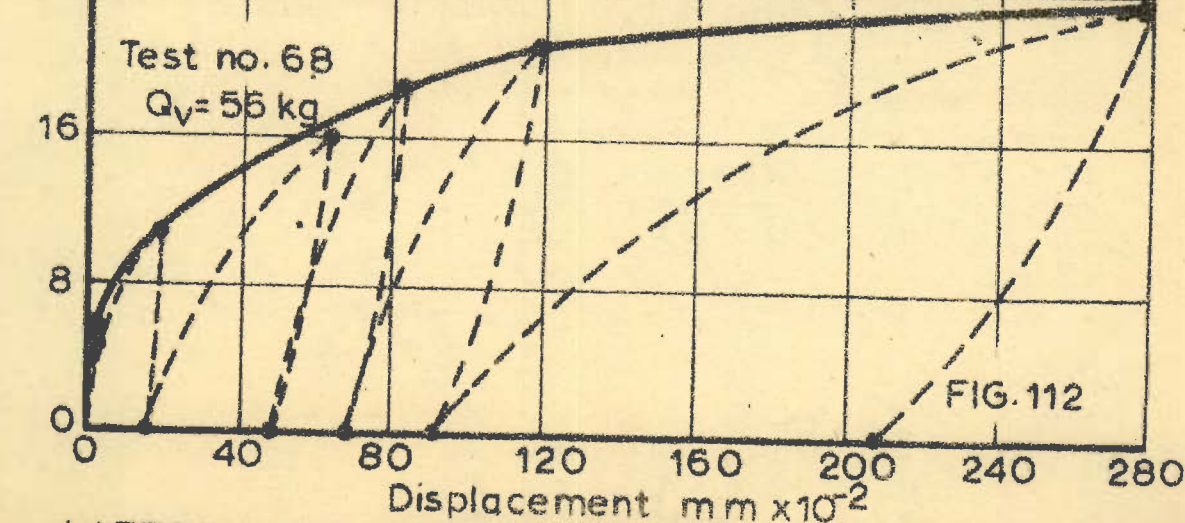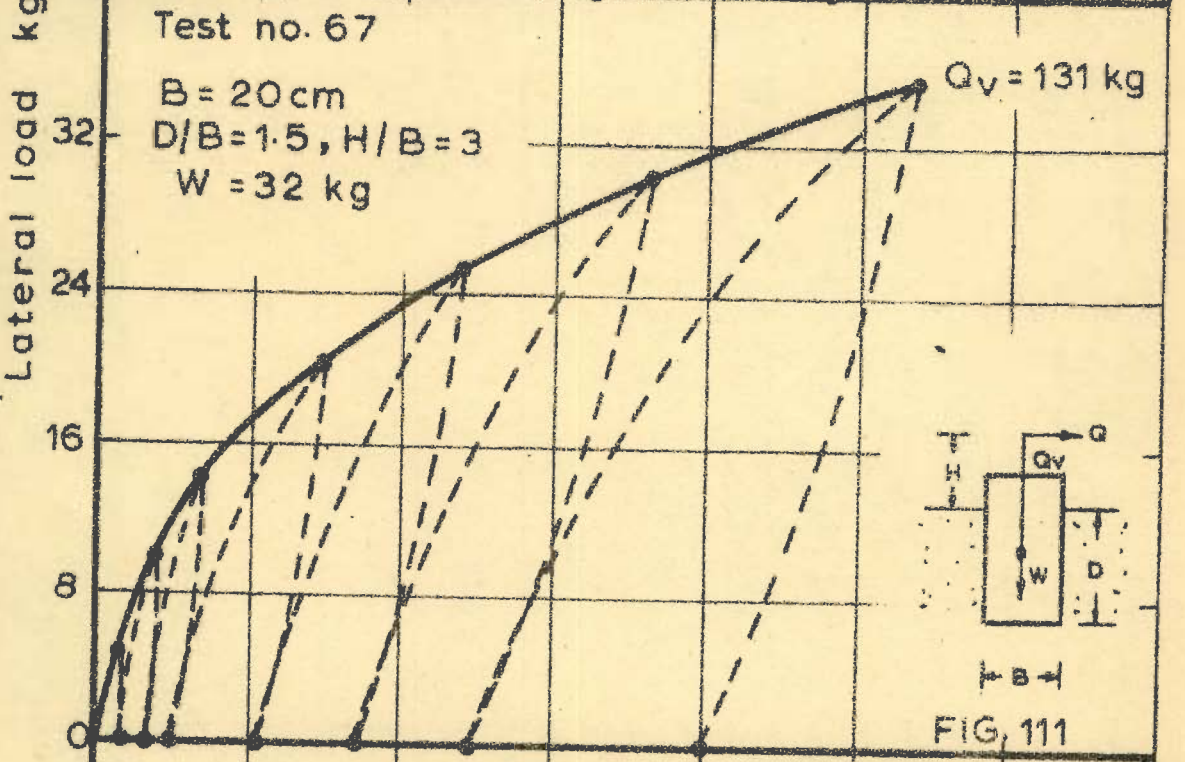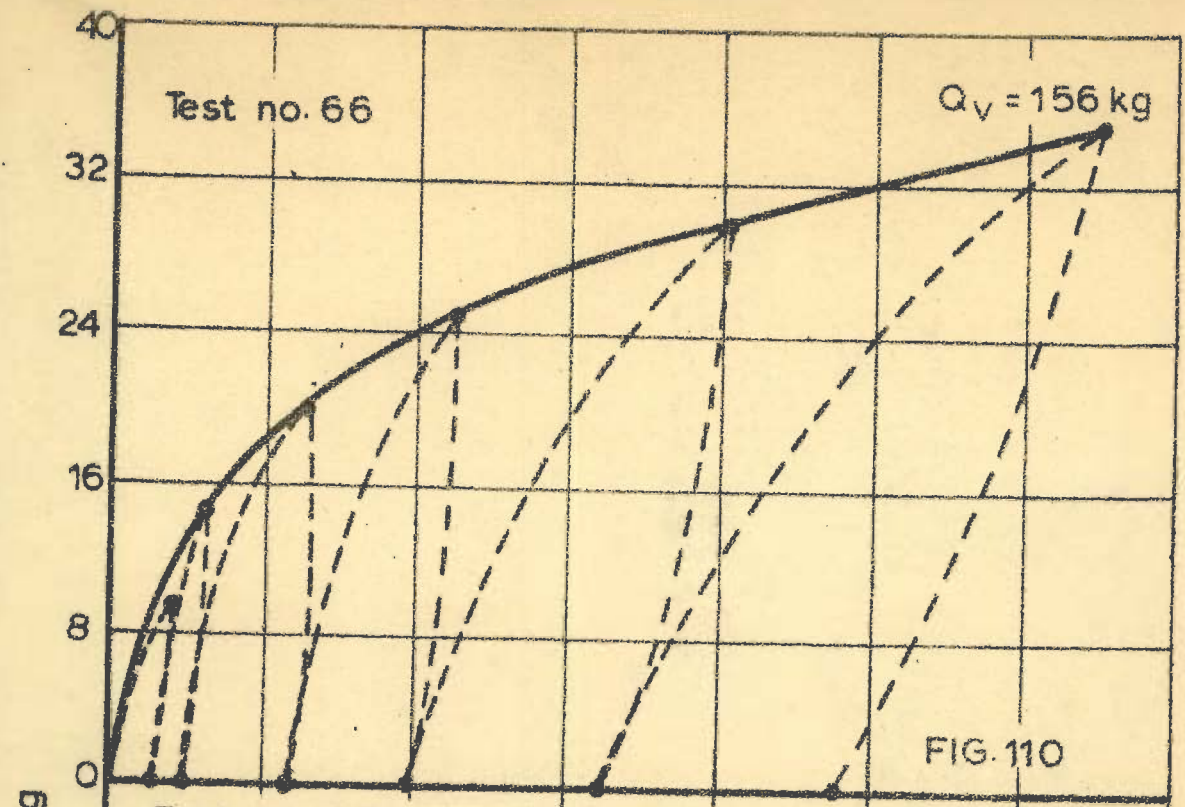
LATERAL LOAD VS DISPLACEMENT REPETITIVE LOAD TESTS

$Q_V = 101$ kg, $D/B = 1.5$

a_ Test no. 69

$Q_V = 51$ kg, $D/B = 1.5$

b _ Test no. 70

1.25 cm

0.1 sec

$Q_V = 0$ kg, $D/B = 1.5$

c _ Test no.71

$Q_V = 101$ kg, $D/B = 1.5$

All face smooth

d _ Test no. 72

$Q_V = 51$ kg, $D/B = 1.5$

All face smooth

e_ Test no. 73

$Q_V = 0$ kg, $D/B = 1.5$

All faces smooth

f_ Test no. 74

$Q_V = 131$ kg, $D/B = 2$

g_ Test no.75

$Q_V = 101$ kg, $D/B = 2$

All faces smooth

h_ Test no. 76

$Q_V = 51$ kg, $D/B = 2$

i_ Test no.77

All faces smooth

$Q_V = 0$ kg, $D/B = 2$

j_ Test no.78
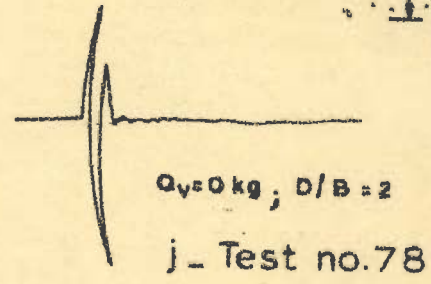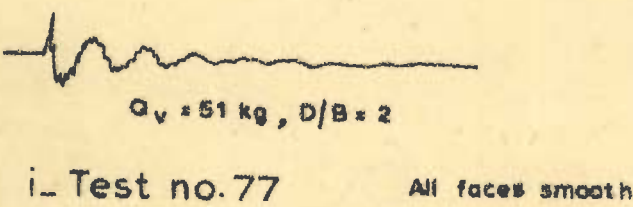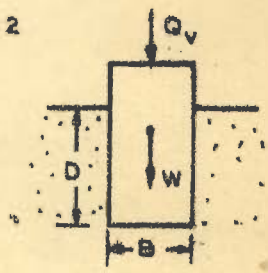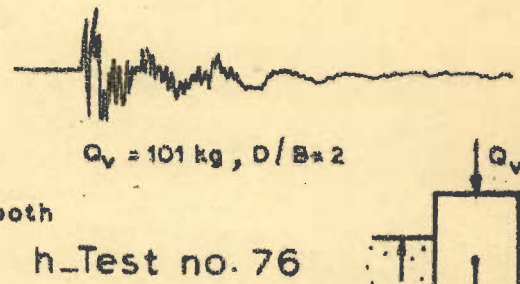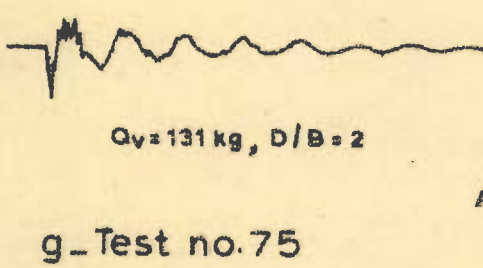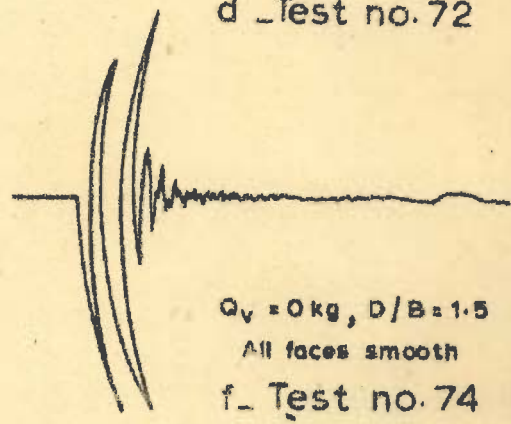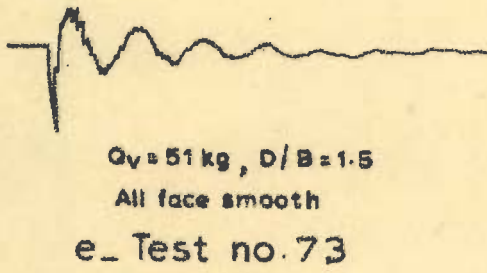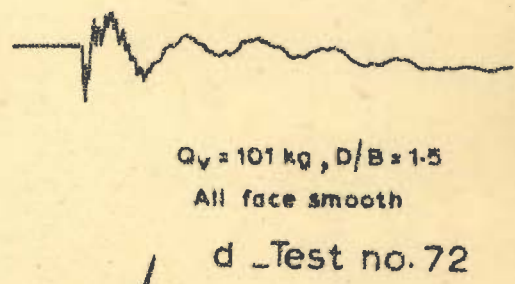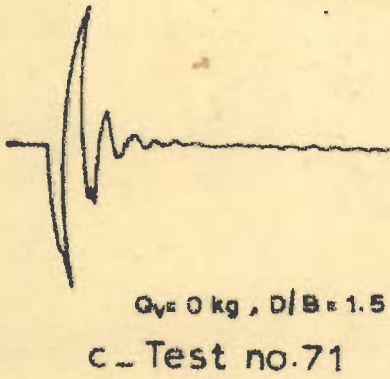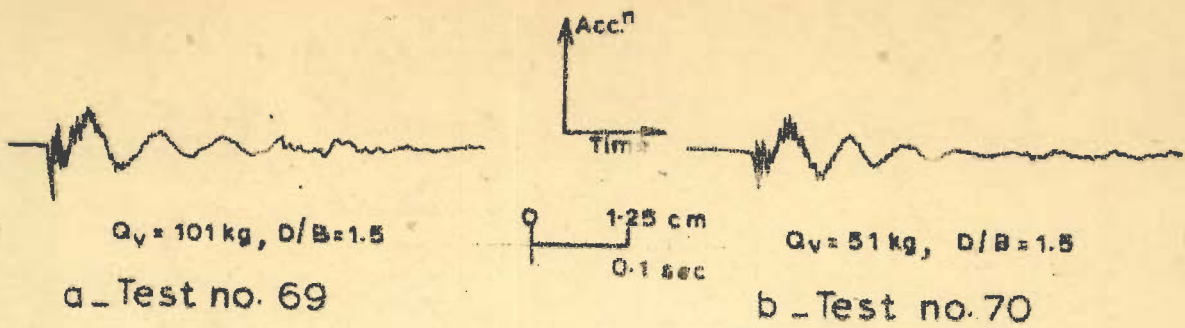
FIG.113 _ FREE VIBRATION RECORDS (Acceleration vs time)
of 15 cm well model

a _ For 15 cm wooden well

(B)

B = 15 cm , D = 30 cm

All faces rough

(A)

B = 15 cm   D = 22.5 cm

B = 15 cm   D = 30 cm   All faces smooth
                              (C)

b _ For 20 cm wells

Q_v

D

Sand
$\gamma_d = 1.658 \ g/cm^3$

W

Gap

B

Mild steel model   (G)

All face rough   (F)

B = 20 cm, D = 30 cm

B = 20 cm, D = 40 cm   Wooden model

B = 20 cm, D = 30 cm   (D)

B = 20 cm, D = 30 cm   Wooden model (All faces smooth)
                        (E)

Vertical load kg

Vertical displacement mm
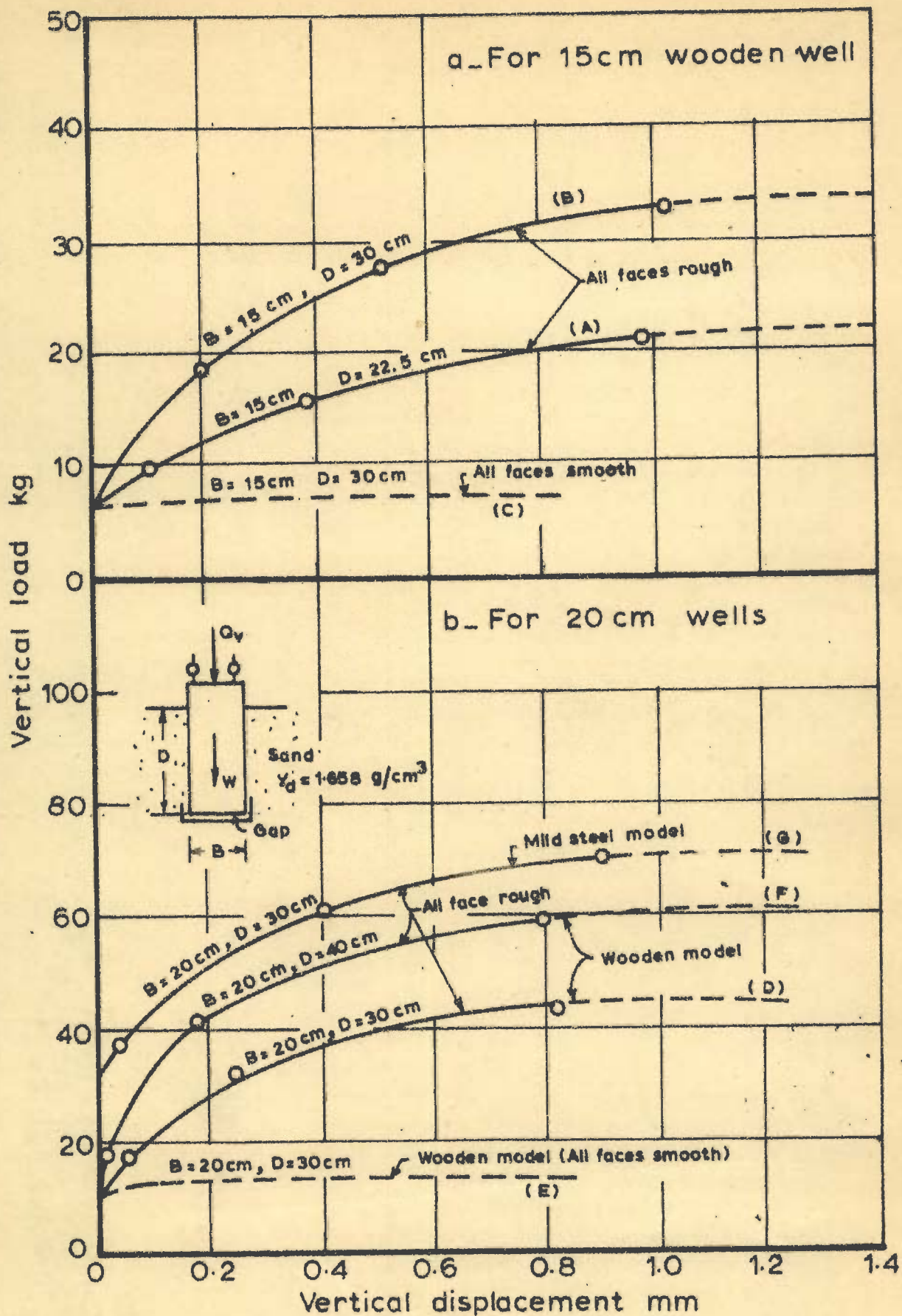
FIG. 114 _ VERTICAL LOAD VS DISPLACEMENT-SKIN FRICTION
TEST (Test nos 101 to 107)
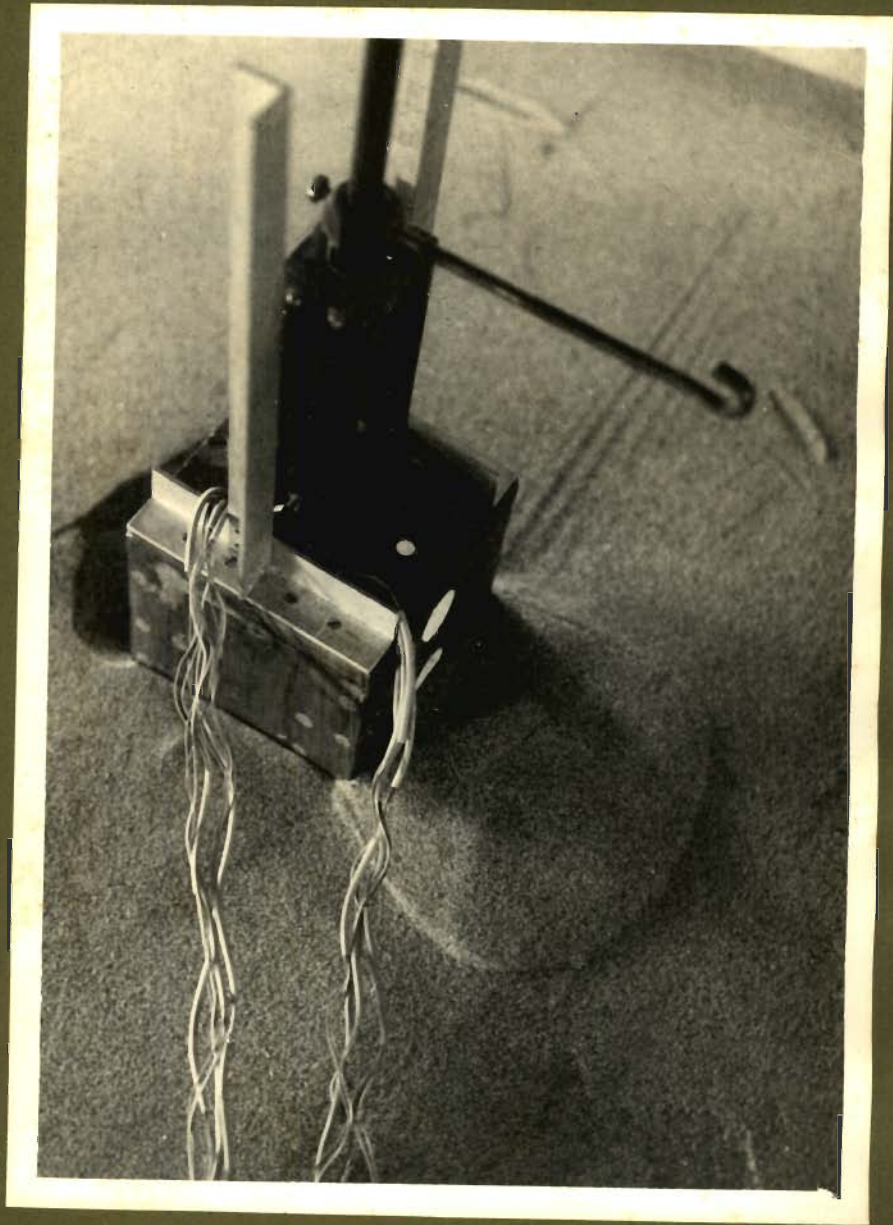
FIG.115-Failure Outcrop Test No. 111
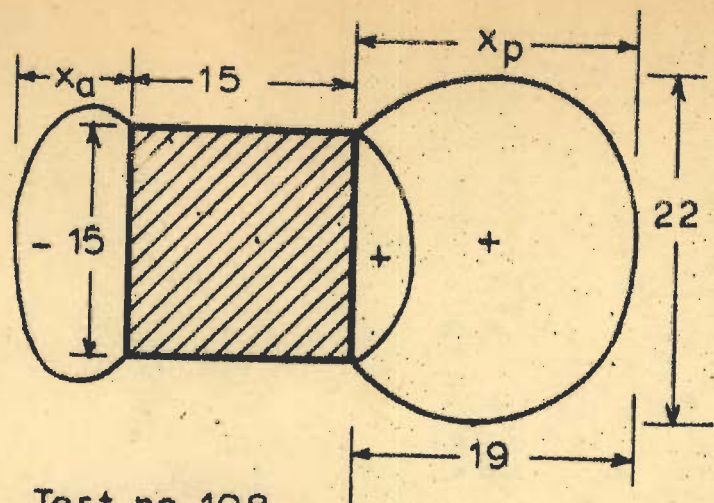
a _ Test no. 108

B = 15 cm
D/B = 2, H/B = 2
W = 6.5 kg
Q_V = 0 kg
$Q_{Failure}$ = 21 kg
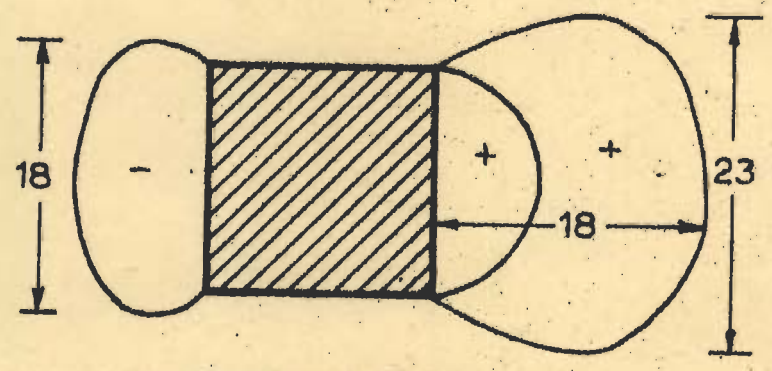
b _ Test no. 109

B = 15 cm
D/B = 2, H/B = 1
W = 6.5 kg
Q_V = 0 kg
$Q_{Failure}$ = 28.50 kg

Base on plank
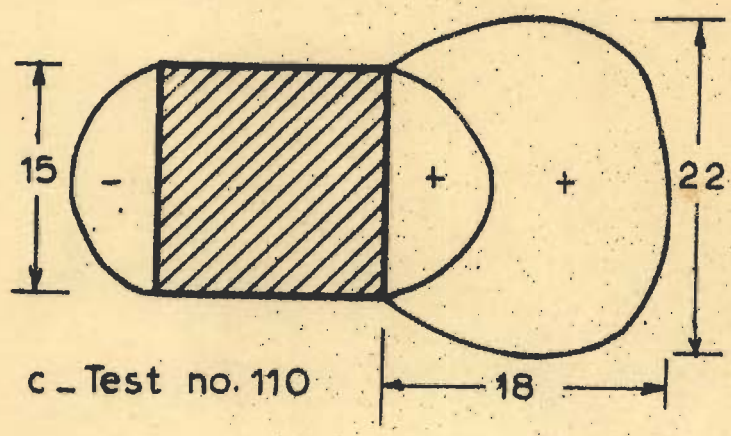
c _ Test no. 110

B = 15 cm
D/B = 1.5, H/B = 1.5
W = 6.5 kg
Q_V = 0 kg
$Q_{Failure}$ = 16.75 kg
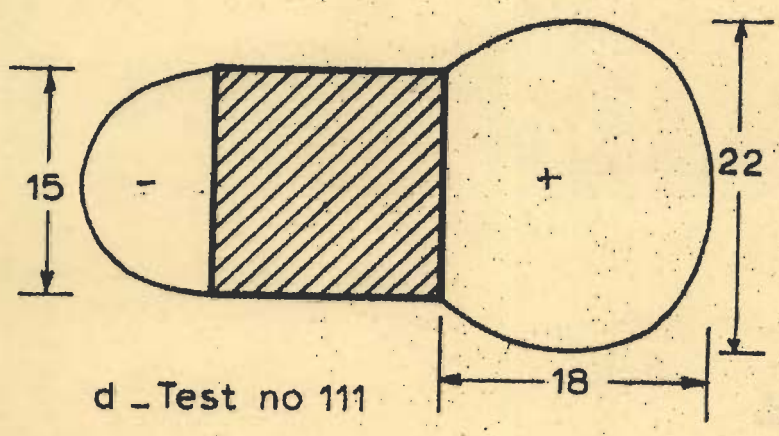
d _ Test no 111

B = 15 cm
D/B = 2, D/B = 1
W = 6.5 kg
Q_V = 56 kg
$Q_{Failure}$ = 43 kg

Base on plank

Direction of loading

FIG. 116 _ FAILURE OUTCROPS AT GROUND LEVEL (Test nos 108 to 111)
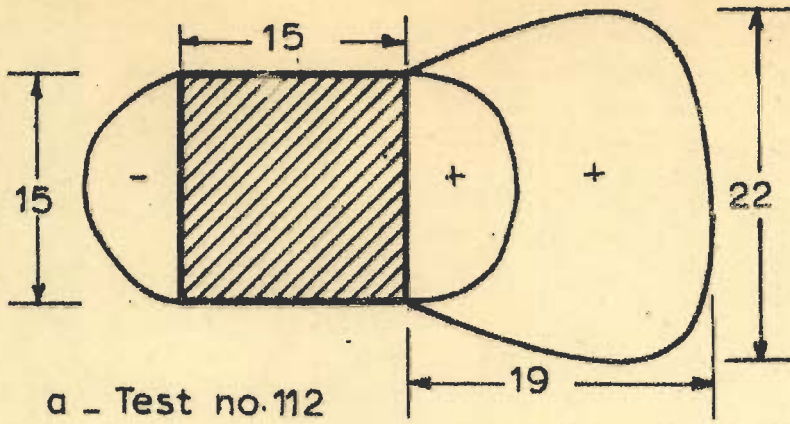
a _ Test no. 112

B = 15 cm
D/B = 2, H/B = 3
W = 6.5 kg
Q_V = 0 kg
Q Failure = 13.5 kg
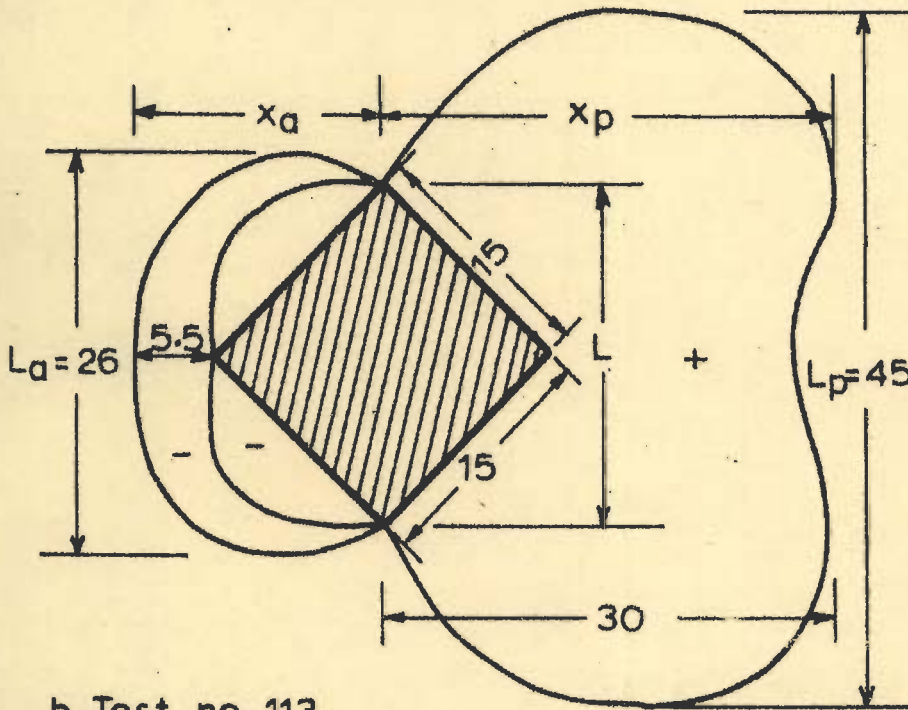
b_Test no. 113

B = 15 cm
D/B = 2, H/B = 3
W = 6.5 kg
Q_V = 0 kg
Q Failure = 14.5 kg
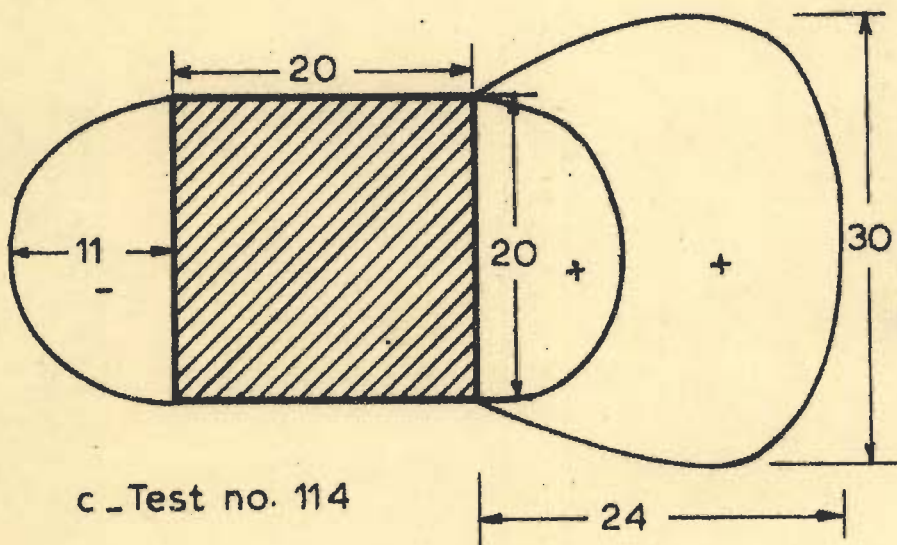
c _ Test no. 114

B = 20 cm
D/B = 1.5, H/B = 2.25
W = 32 kg (Mild steel model)
Q_V = 0 kg
Q Failure = 33 kg
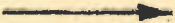
Direction of loading

FIG. 117 _ FAILURE OUTCROPS AT GROUND LEVEL (Test nos 112 to 114)

B = 20 cm
D/B = 1.5, H/B = 2.25
W = 32 kg
Q_V = 131 kg
$Q_{Failure}$ = 44.5 kg

(Mild steel model)

a _ Test no. 115

B = 20 cm
D/B = 1.5, H/B = 2.25
W = 32 kg
Q_V = 0 kg
$Q_{Failure}$ = 32 kg

(Mild steel model)

b _ Test no. 116

B = 20 cm
D/B = 1.5, H/B = 2.25
W = 32 kg
Q_V = 0 kg
$Q_{Failure}$ = 38 kg

(Mild steel model)

Ground sloping 15° with horizontal

Direction of loading
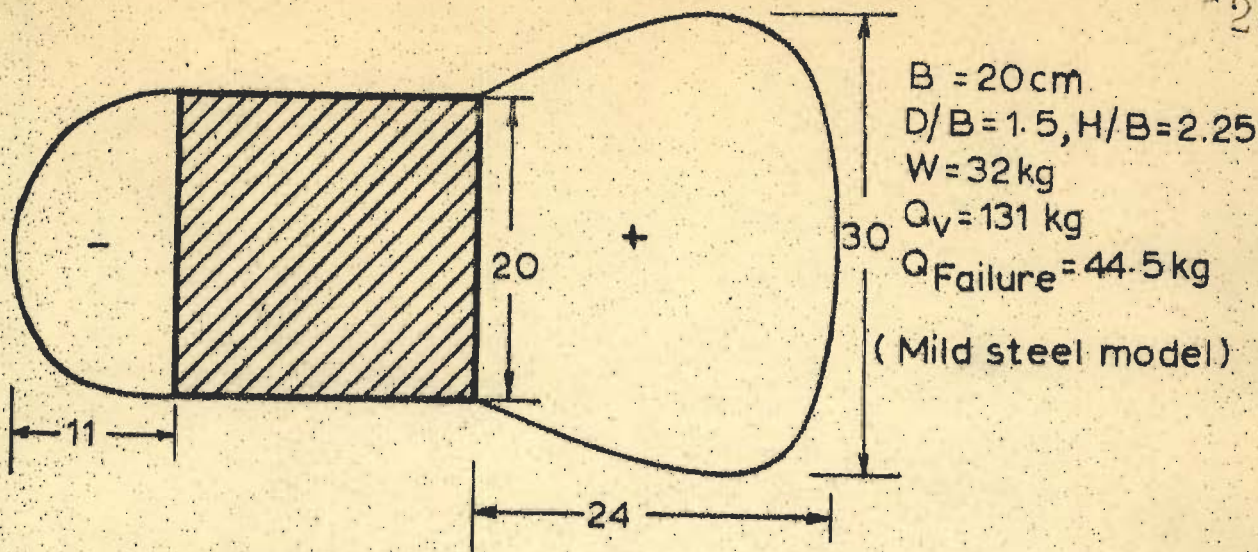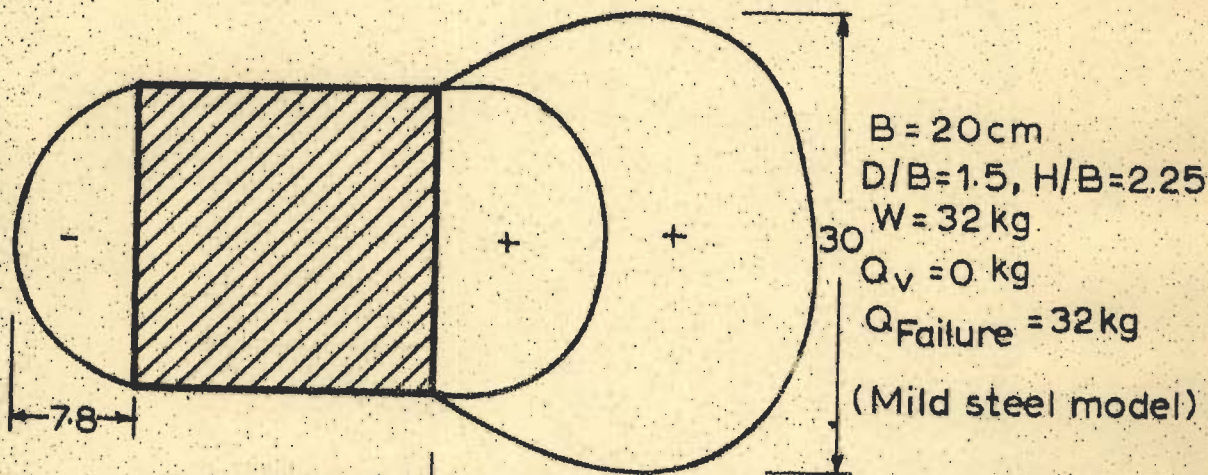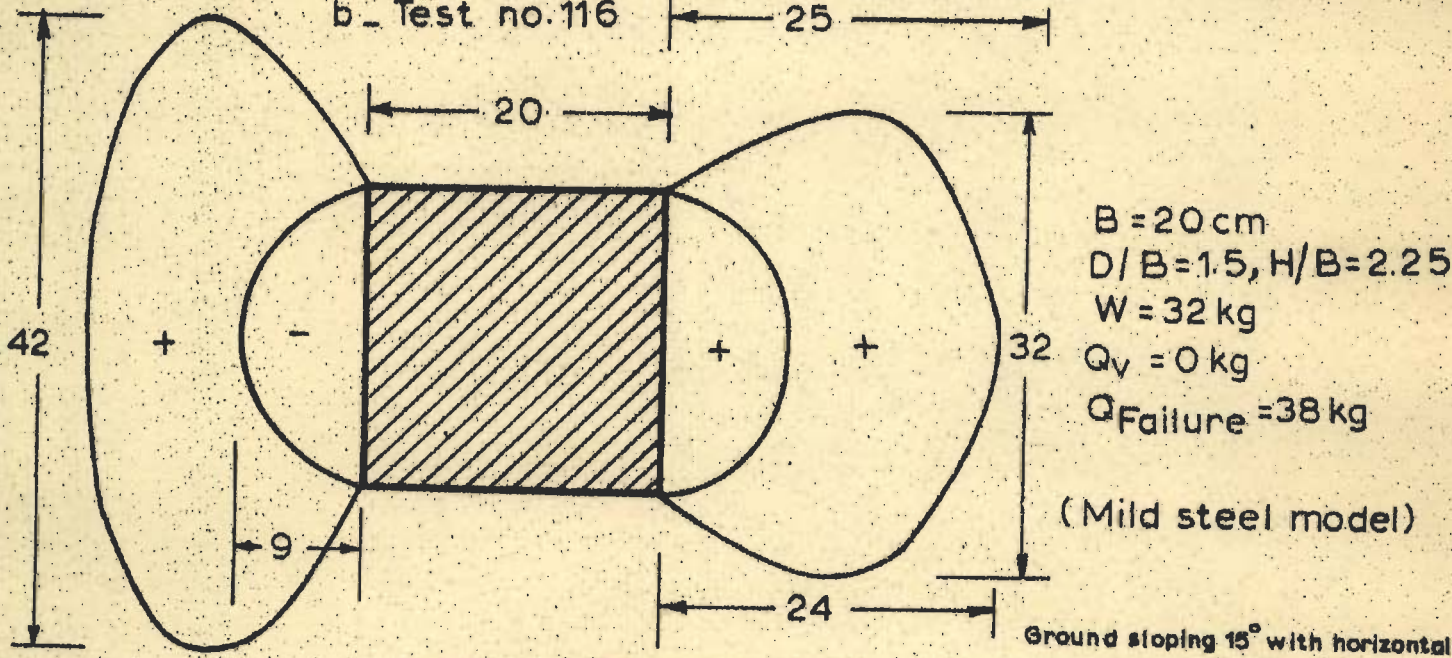
Test no. 117

FIG. 118 _ FAILURE OUTCROPS AT GROUND LEVEL (Test nos. 115 to 117)

Base pressure T/m²

Settlement mm x 10⁻²

ASSUMED LINEAR RELATIONSHIP

LOADING

UNLOADING

DIAL GAUGE

$Q_v = 2.25, 4.5, 6.75$ T
G.L.

2.25

DRY SOIL (SM)

W

W = 6.5 Tonnes

1.5m

1.5m
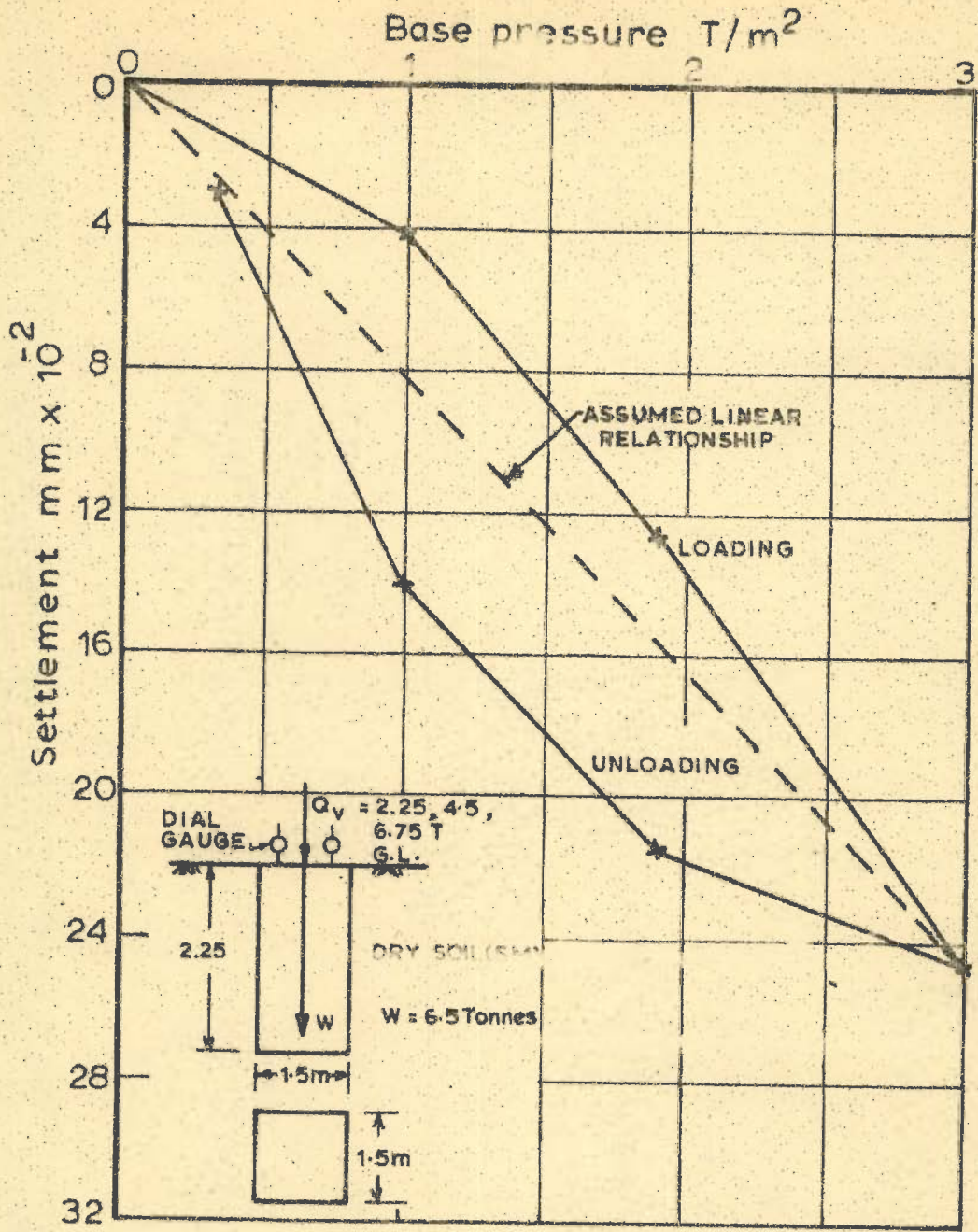
FIG. 119 - VERTICAL LOAD VS SETTLEMENT CURVE
FOR FIELD MODEL (Test no. 118)
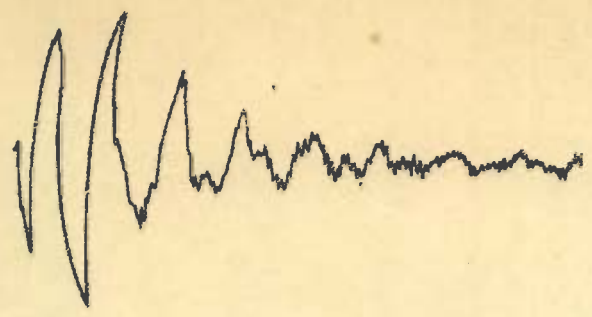
a – Test no.119
GROUND CONDITION – NATURAL
$Q_v = 0$
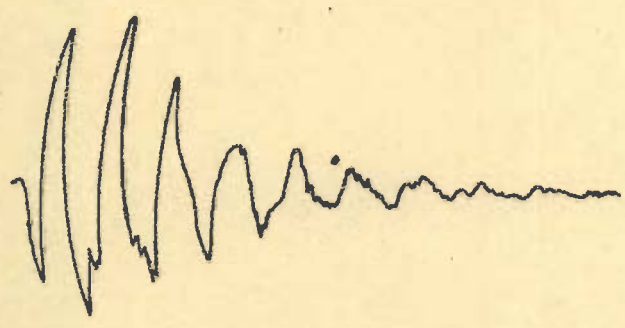
b – Test no.120
GROUND CONDITION – NATURAL
$Q = 2.25$ tonne
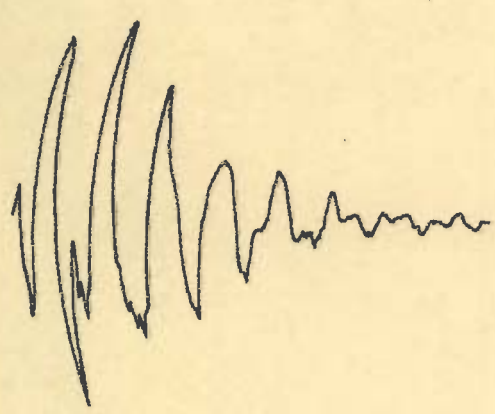
c – Test no.121
GROUND CONDITION – NATURAL
$Q_v = 4.25$ tonne
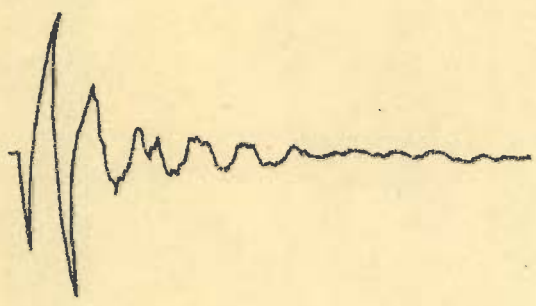
d – Test no.122
GROUND CONDITION – SATURATED
$Q_v = 4.25$ tonne

ACC^n

O TIME
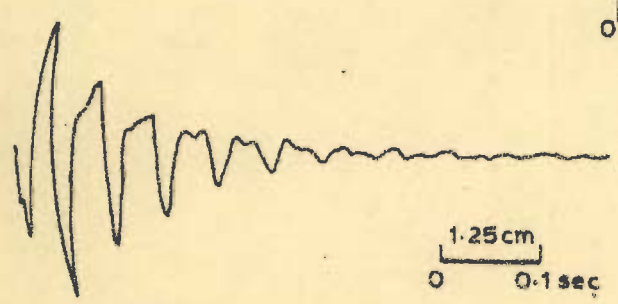
e – Test no.123
GROUND CONDITION – SATURATED
$Q_v = 2.25$ tonne
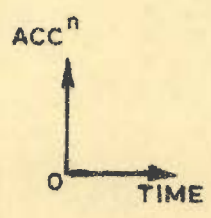
1.25 cm
O   0.1 sec

FIG. 120 – FREE VIBRATION RECORDS OF FIELD
MODEL (Test no. 119 to 123)
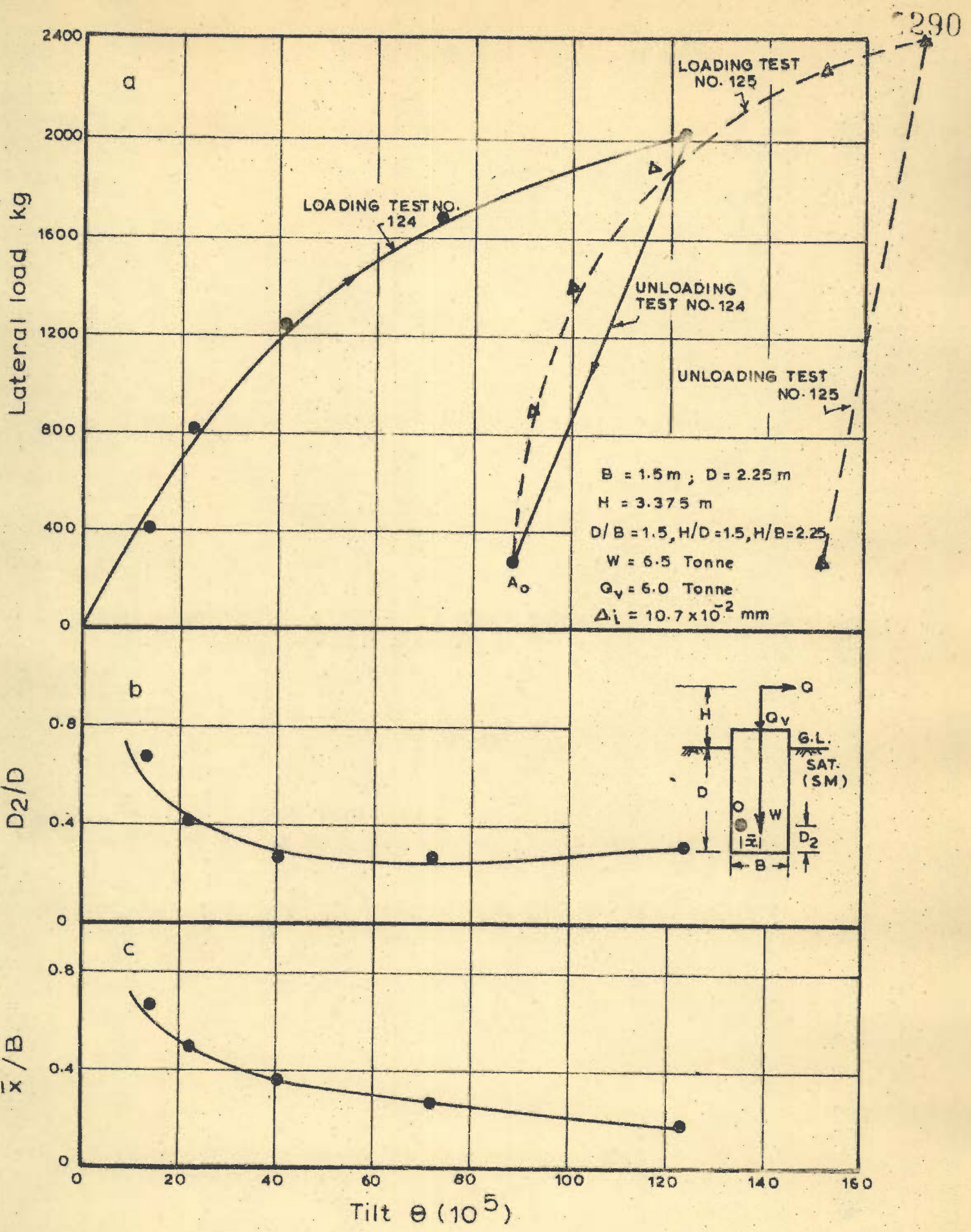
FIG. 121 _ LATERAL LOAD, D_2/D, $\bar{x}/B$ VS TILT OF FIELD
WELL MODEL (Test no. 124)
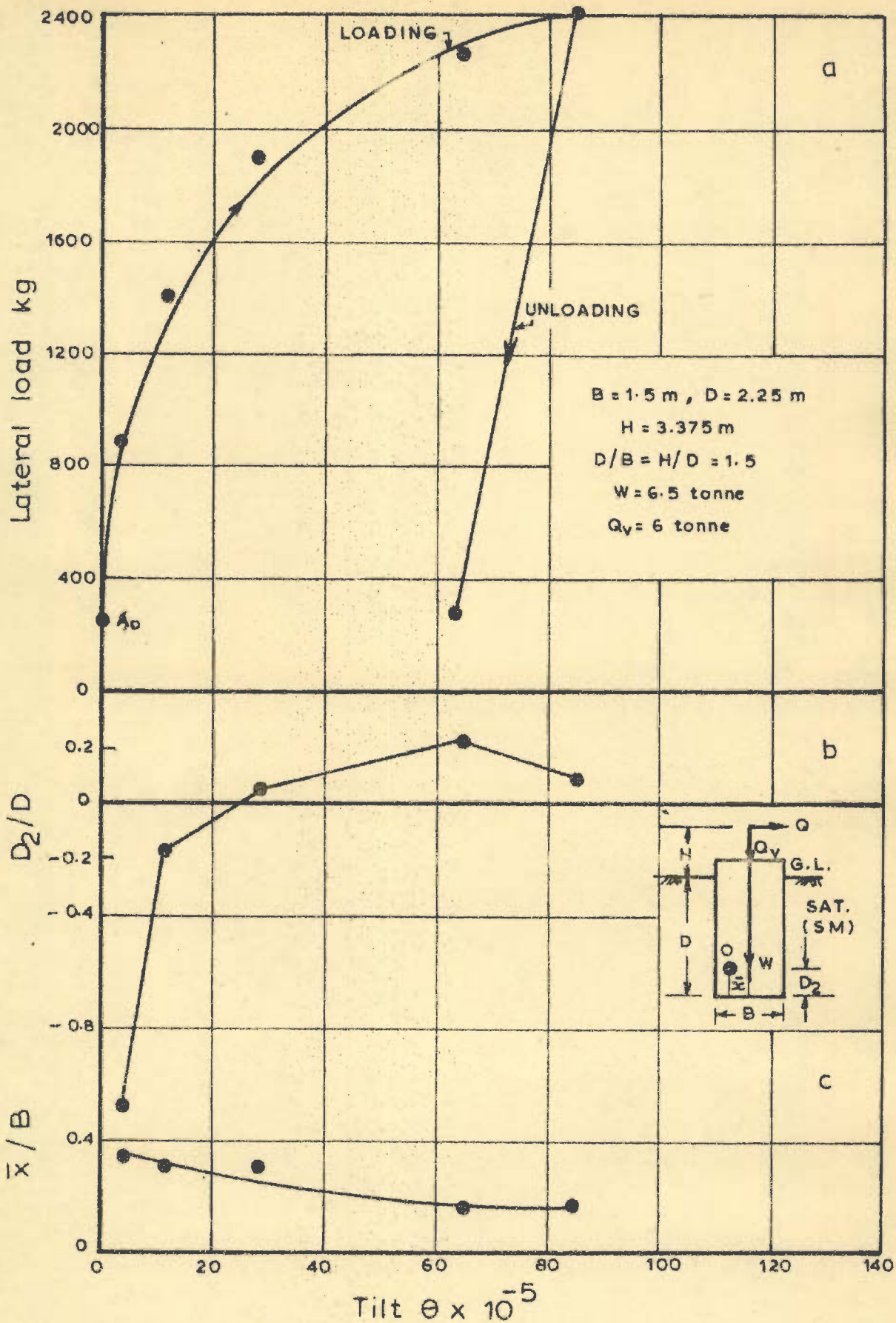
FIG. 122 _ LATERAL LOAD D2/D AND x̄/B VS TILT
(Test no. 125)

Lateral pressure kg/cm²

REAR FACE

Depth cm

FRONT FACE

B X B = 1.5 m x 1.5 m
D/B = 1.5 , H/B = 2.25
W = 6.5 tonne
Q_V = 6 tonne
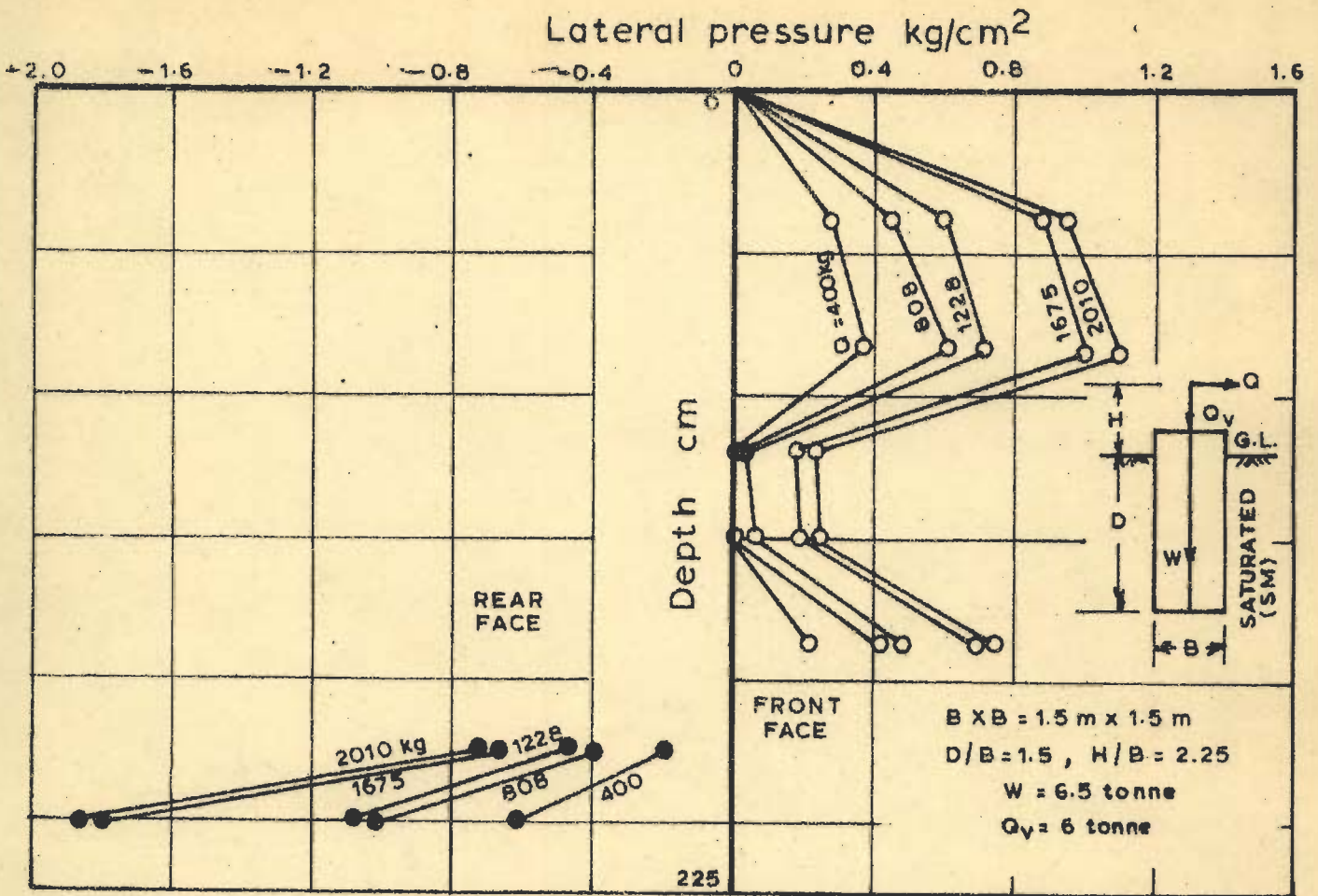
a_ Lateral pressure distribution along vertical axis of front and rear face

Base width cm

Base pressure kg/cm²
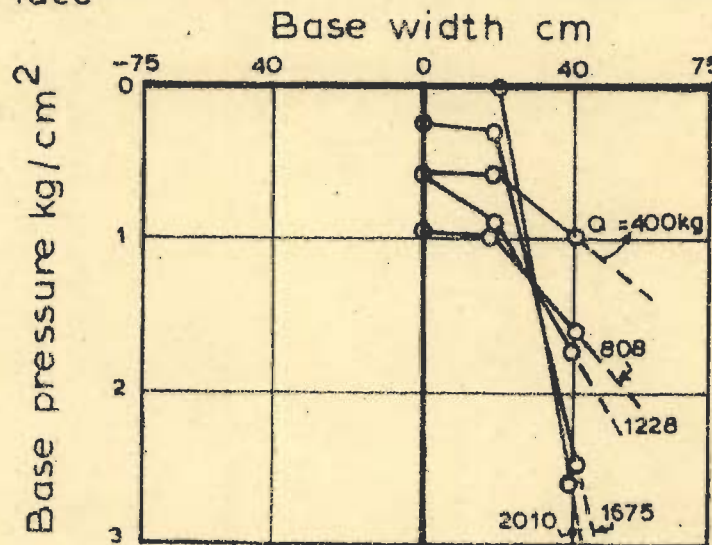
b_ Pressure distribution along the centroidal axis of the base

FIG. 123_ PRESSURE DISTRIBUTION ON FACES AND BASE OF FIELD MODEL WELL (Test no 124)

Face width cm

-75   P-12 P-11 P-10   +75

Face width cm

-75   P-8   P-7   P-6   +75

Pressure kg/cm²

a _ ALONG PRESSURE CELLS P-12, P-11,
P-10 ON FRONT FACE (35cm BELOW
G.L.)

b _ ALONG PRESSURE CELLS P-8, P-7,
P-6 ON FRONT FACE (100cm BELOW
G.L.)

Face width cm

-75   S-7   S-8   S-9   +75

Q = 400 kg

808
1228

1675

2010

c _ ALONG PRESSURE CELLS S-7,
S-8, S-9 ON REAR FACE
(205 cm BELOW G.L.)

Base length cm

-75   S-6   S-5   S-3   +75

d _ ALONG PRESSURE CELLS S-6 S-5
S-3 ON BASE
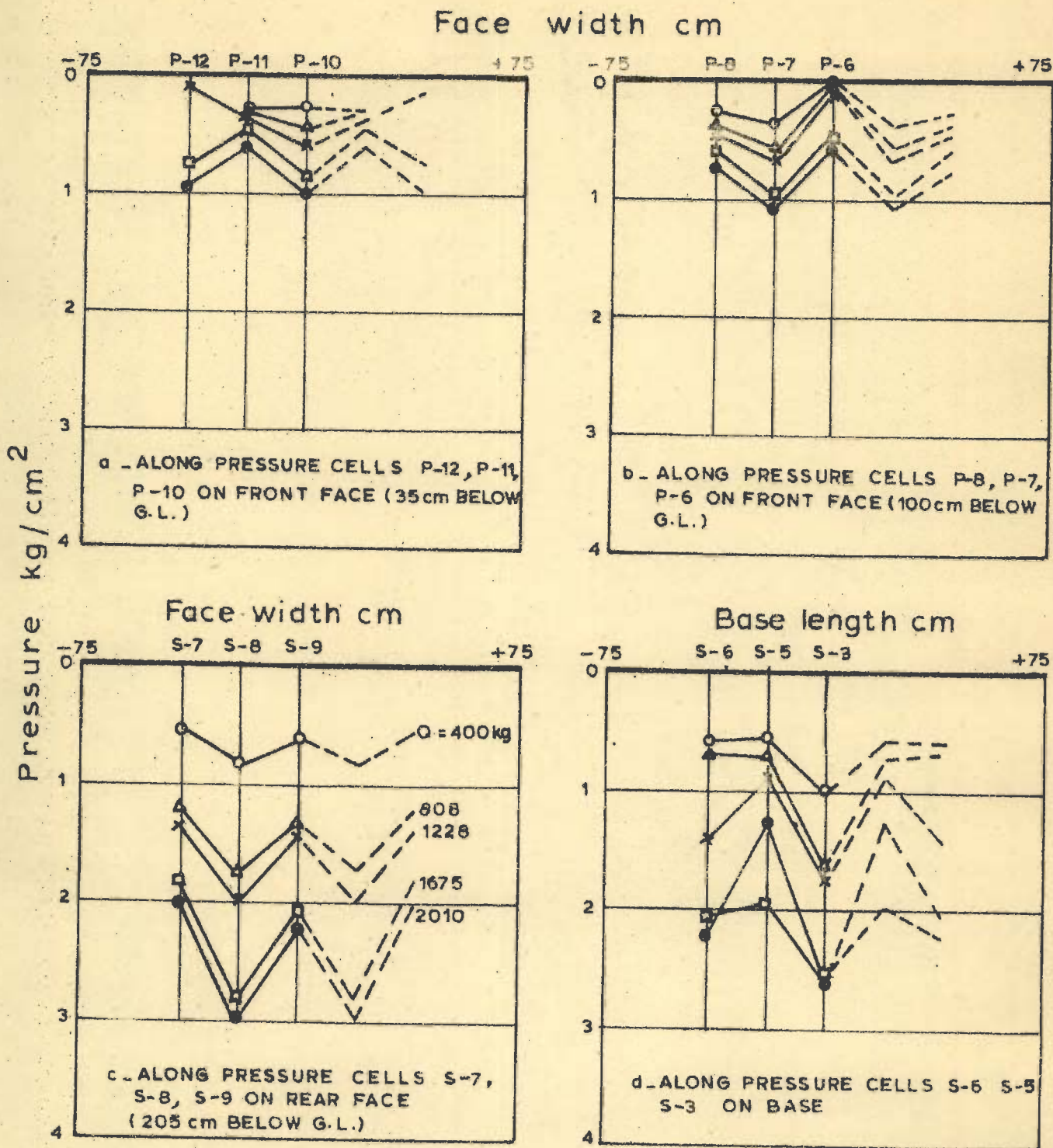
FIG. 124 _ PRESSURE DISTRIBUTION ON FACES AND BASE
OF FIELD WELL MODEL (Test no. 125)
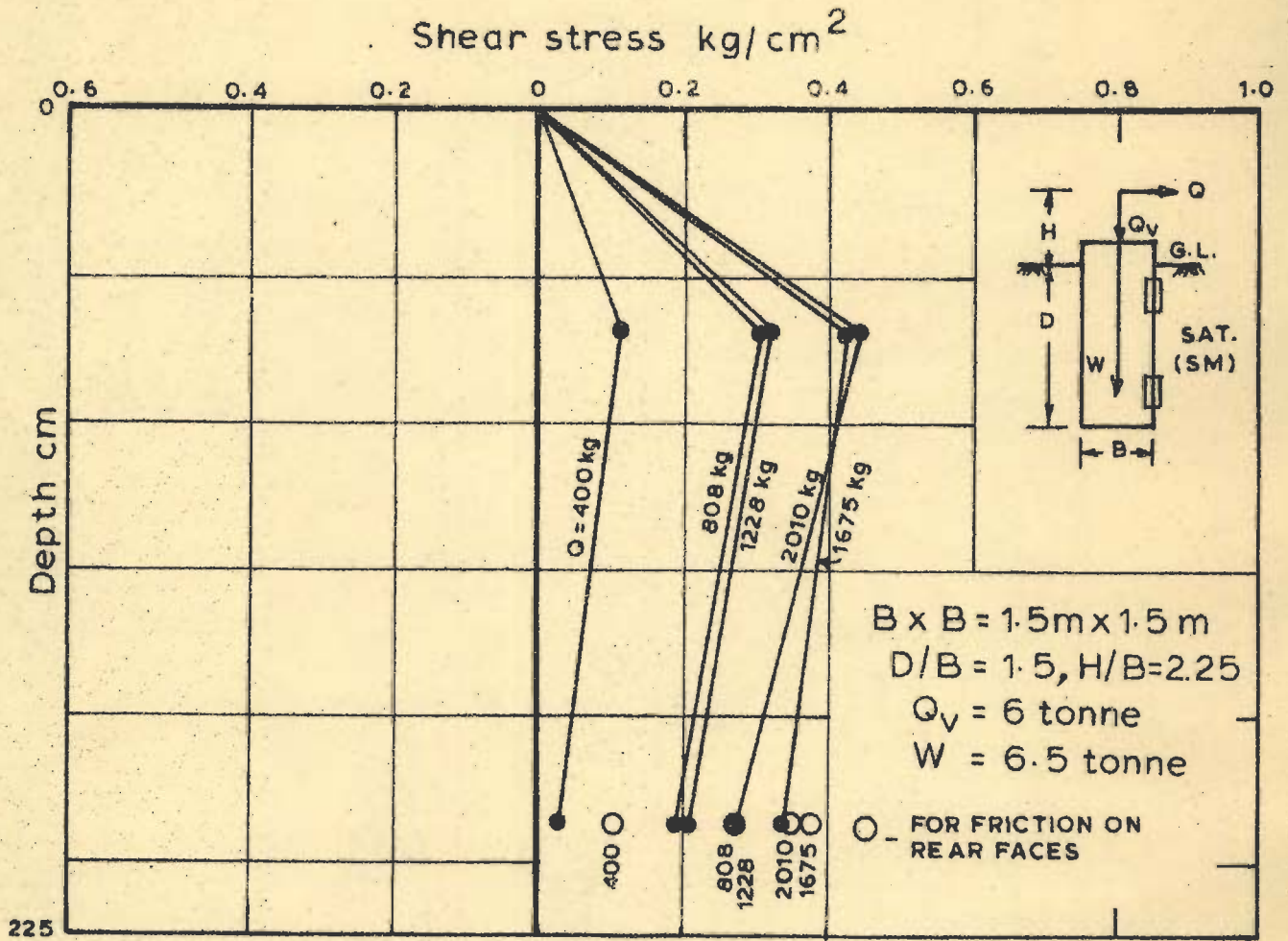
FIG. 12 5 _ FRICTION ON FRONT AND REAR FACES OF FIELD
MODEL (Test no. 124)

The figure consists of six plots (a)–(f) of Lateral load (kg) versus Tilt θ (10^{-3}).

(a) $Q_v = 131\ kg$ (FIG. 46a); 101 (53a); 51 (59a). $B = 15\ cm$, $D/B = 1.5$, $H/B = 2.25$

(b) $Q_v = 131\ kg$ (FIG. 48a); 101 (55a). $D/B = 1.5$, $H/B = 3.0$

(c) $Q_v = 131\ kg$ (FIG. 63a); 101 (74a); 51 (79a); 0 (86a). $D/B = 2$, $H/B = 3$

(d) $Q_v = 131\ kg$ (FIG. 61a); 101 (72a); 51 (78a); 0 (84a). $D/B = 2$, $H/B = 4$

(e) $Q_v = 101\ kg$ (FIG. 89b); $Q_v = 51\ kg$ (90c). $D/B = 2$, $H/B = 2$ BASE ON PLANK

(f) $Q = 101\ kg$ (FIG. 89a); 51 (90a). $D/B = 2$, $H/B = 4$ BASE ON PLANK
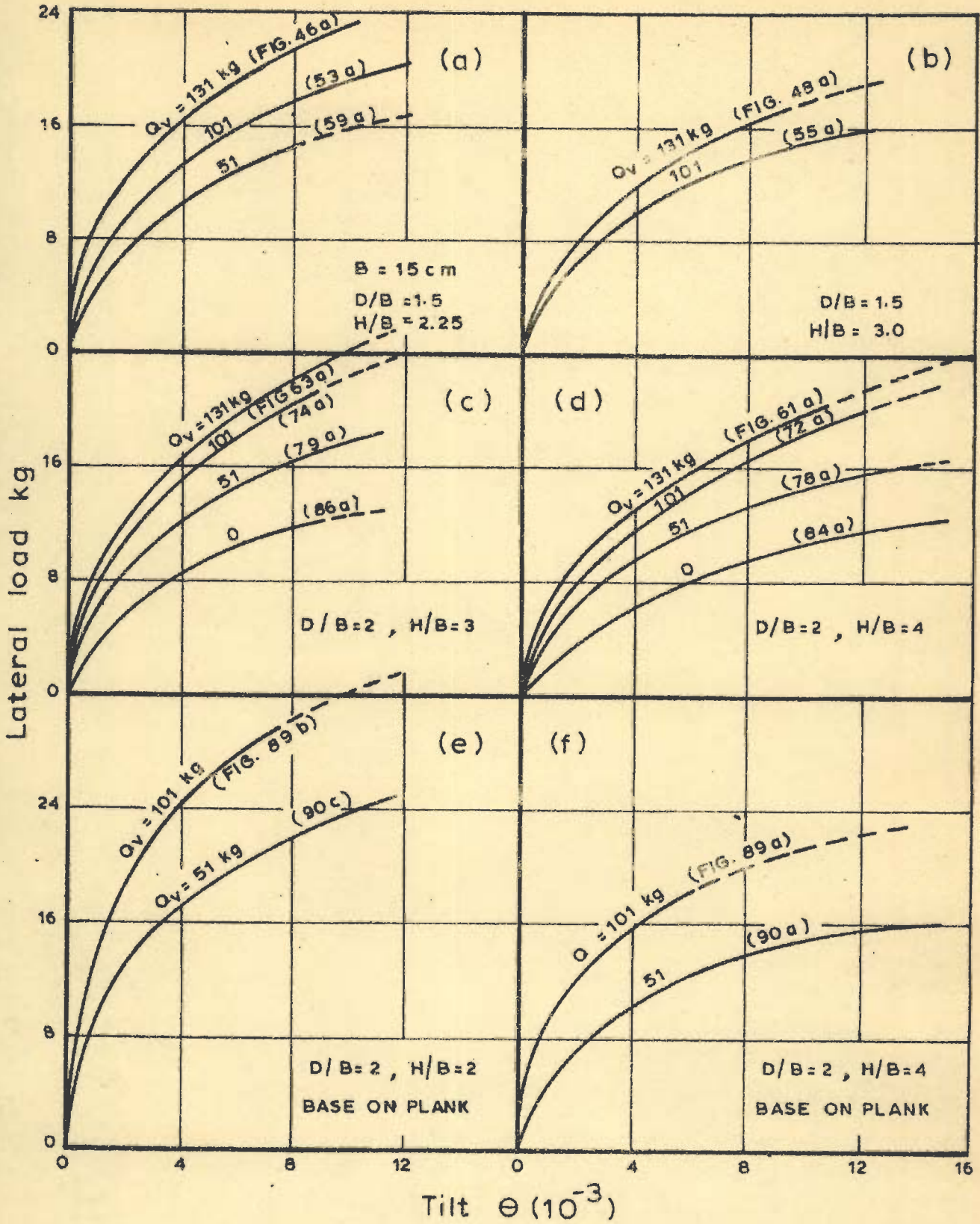
FIG. 126 _ EFFECT OF VERTICAL LOAD
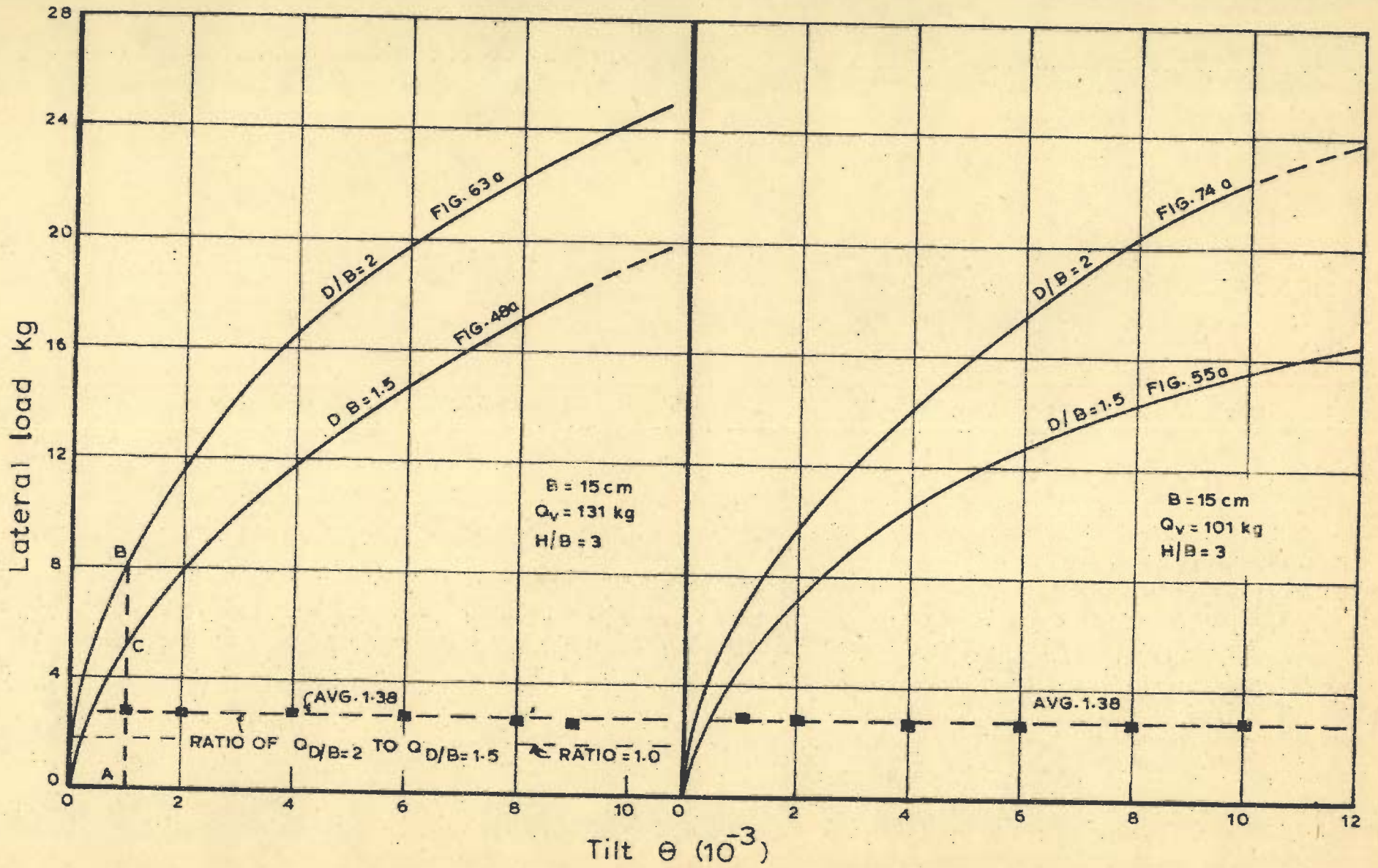
FIG. 127 - EFFECT OF DEPTH OF EMBEDMENT
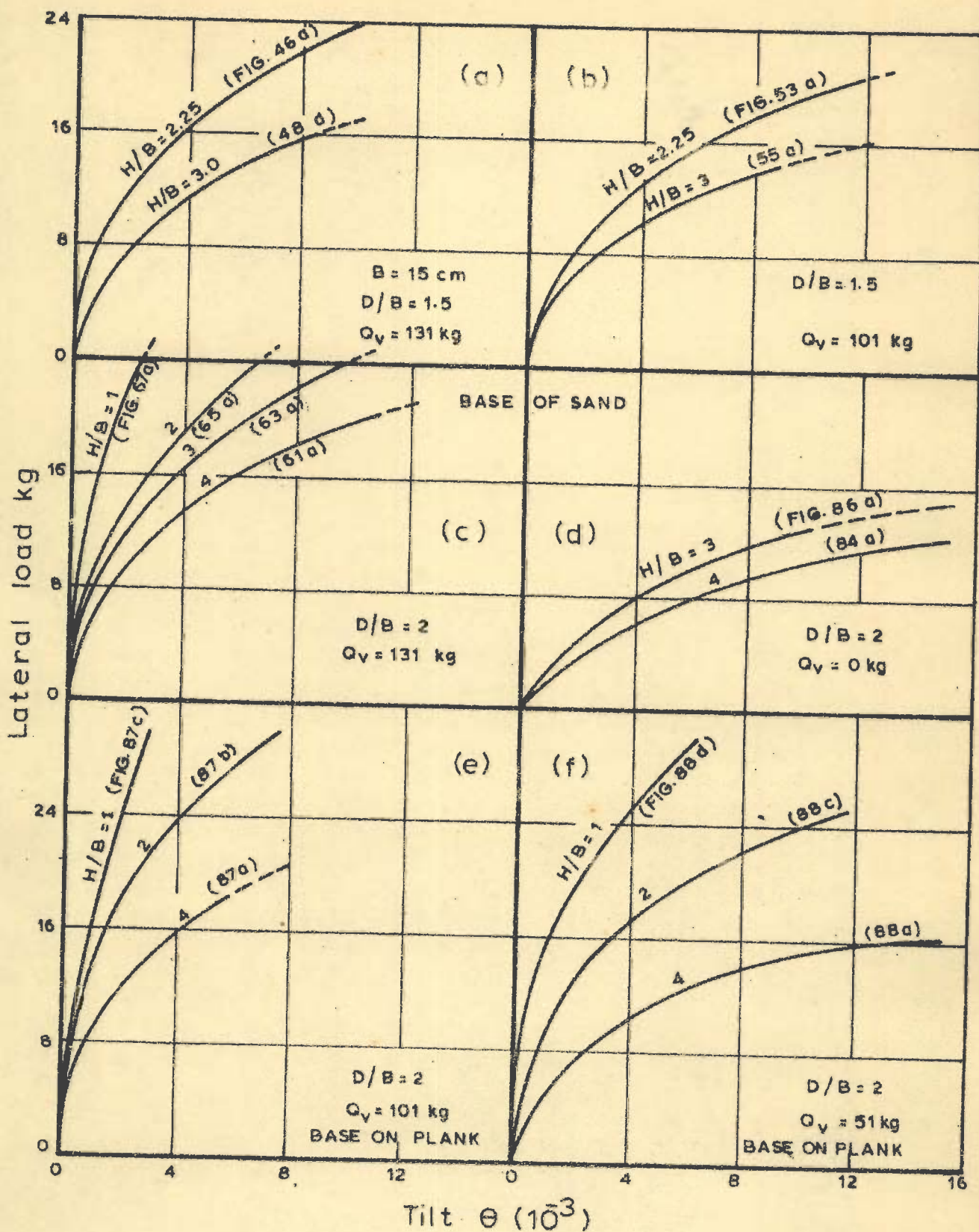
FIG. 128 _ EFFECT OF POSITION OF LATERAL LOAD
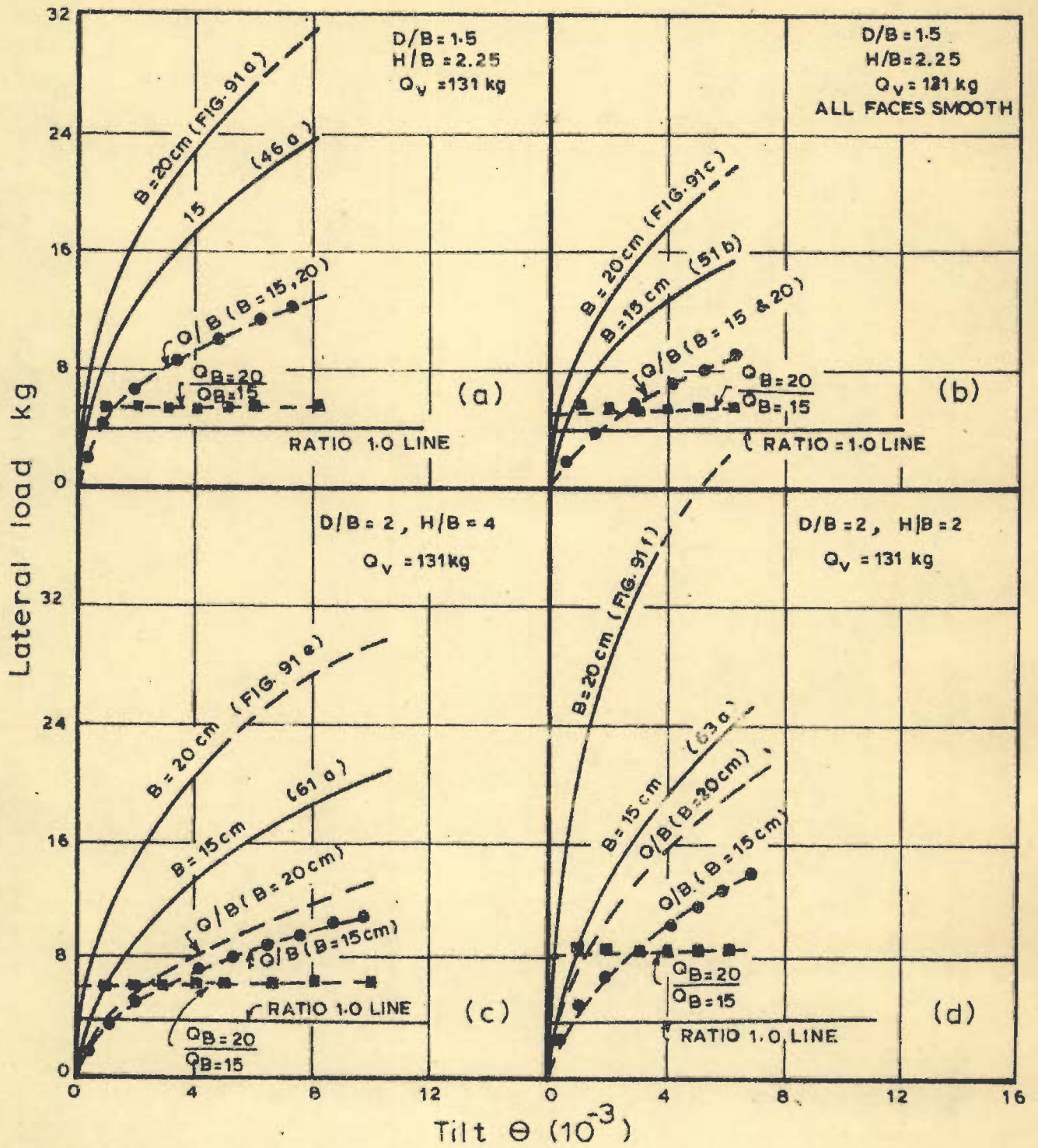
FIG. 129 _ EFFECT OF SIZE OF BASE
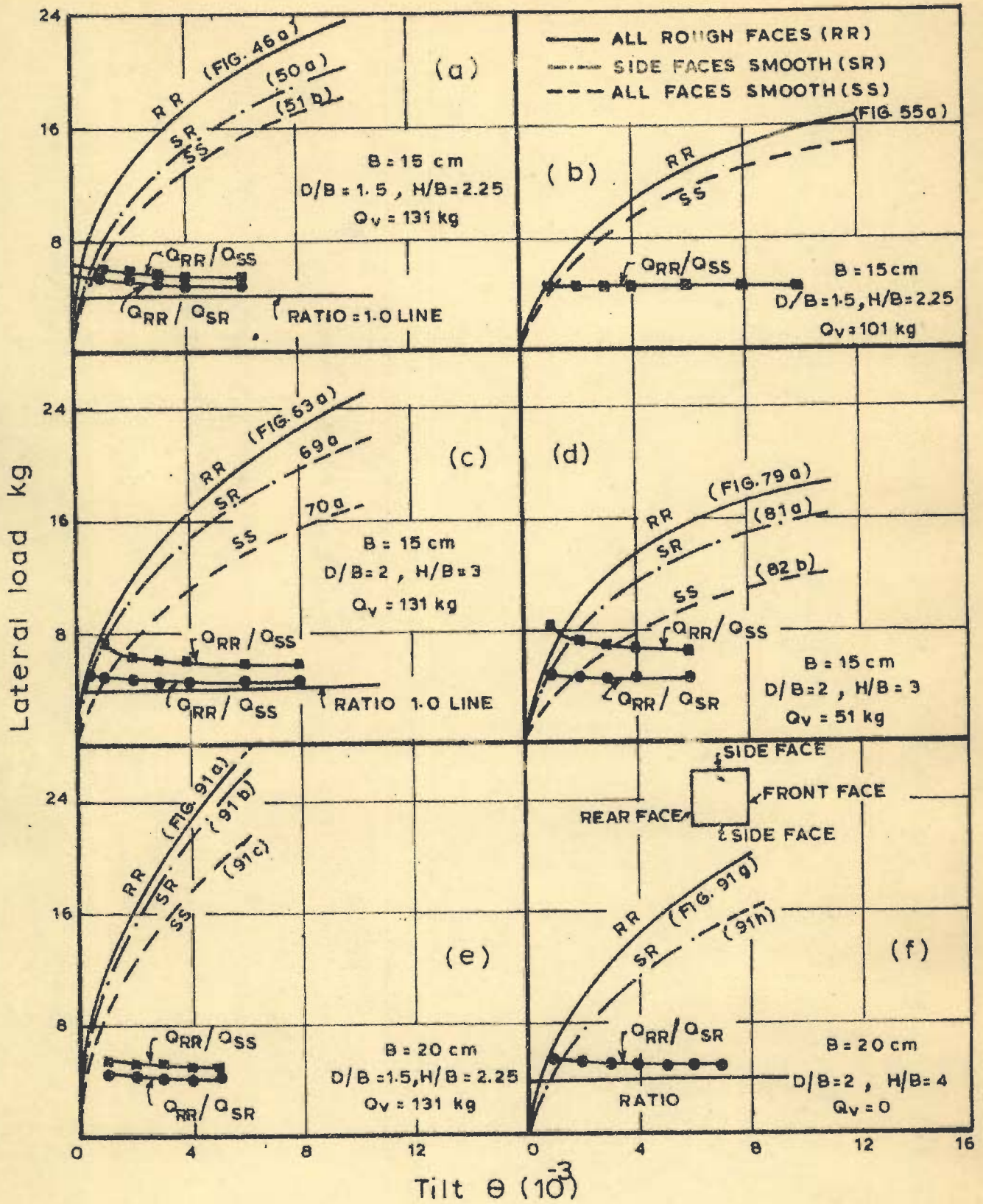
FIG. 130 _ EFFECT OF FRICTION
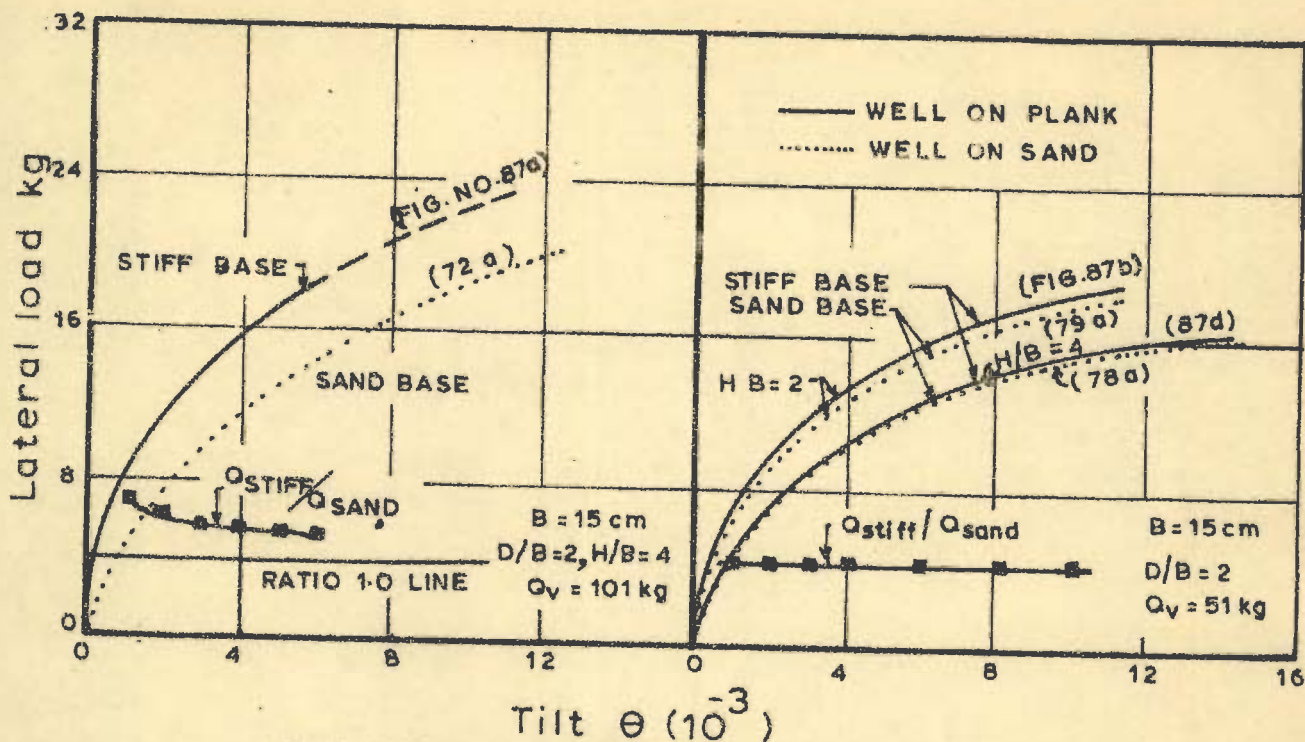
FIG.131 _ EFFECT OF BASE STIFFNESS
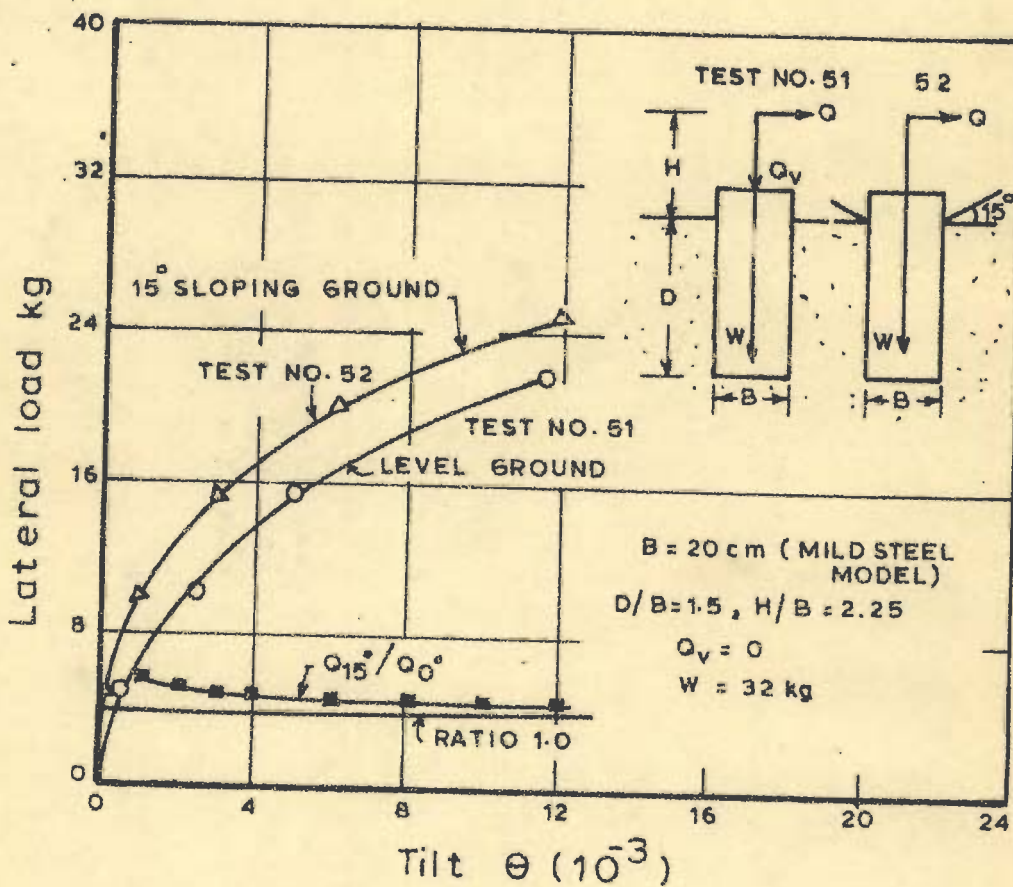
FIG. 132 _ EFFECT OF SHAPE OF SCOUR PIT
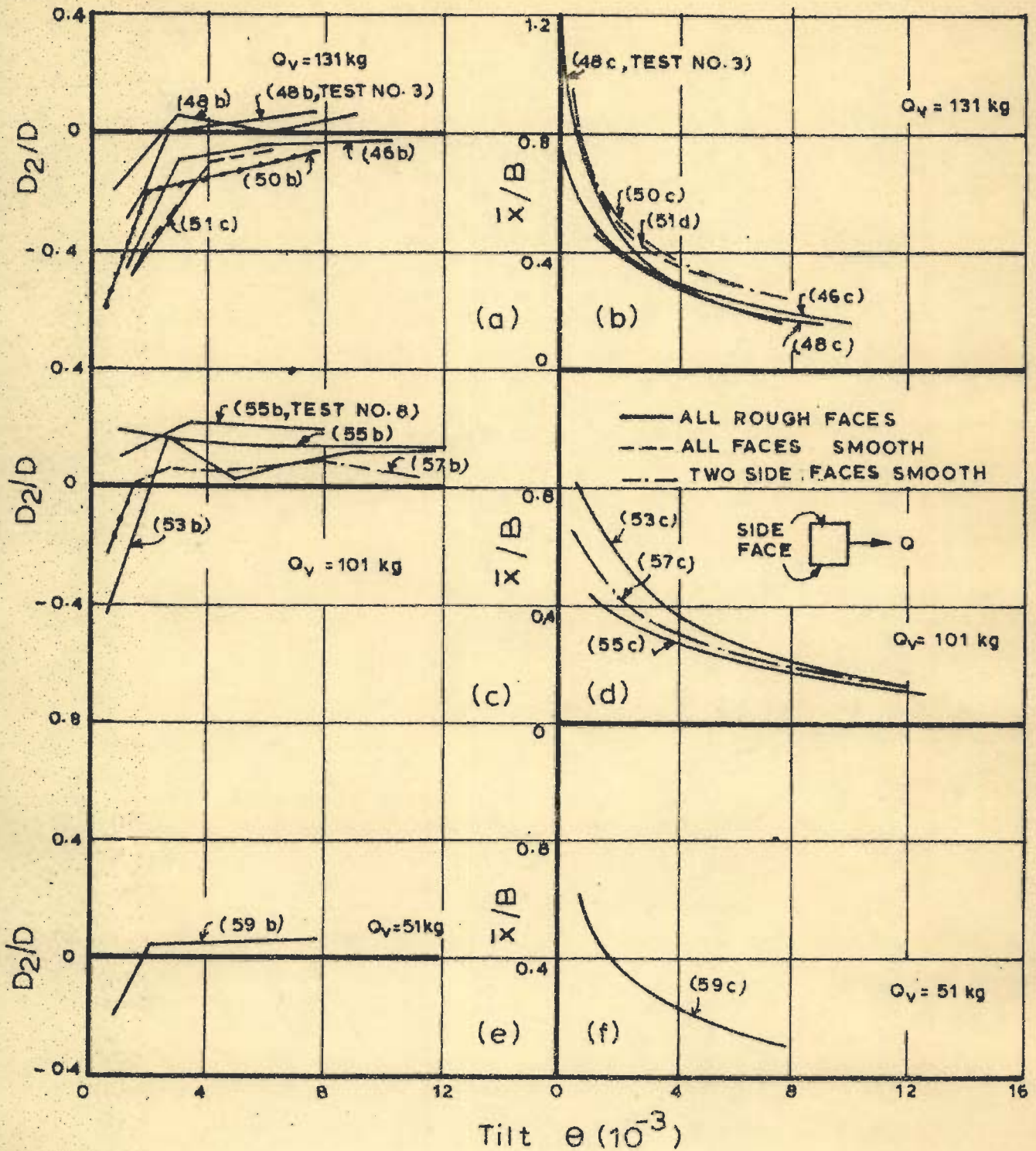
FIG. 133 _ INSTANTANEOUS POINTS OF ROTATION FOR 15 cm
WELL WITH D = 22.5 cm (Test no. 1 to 10)
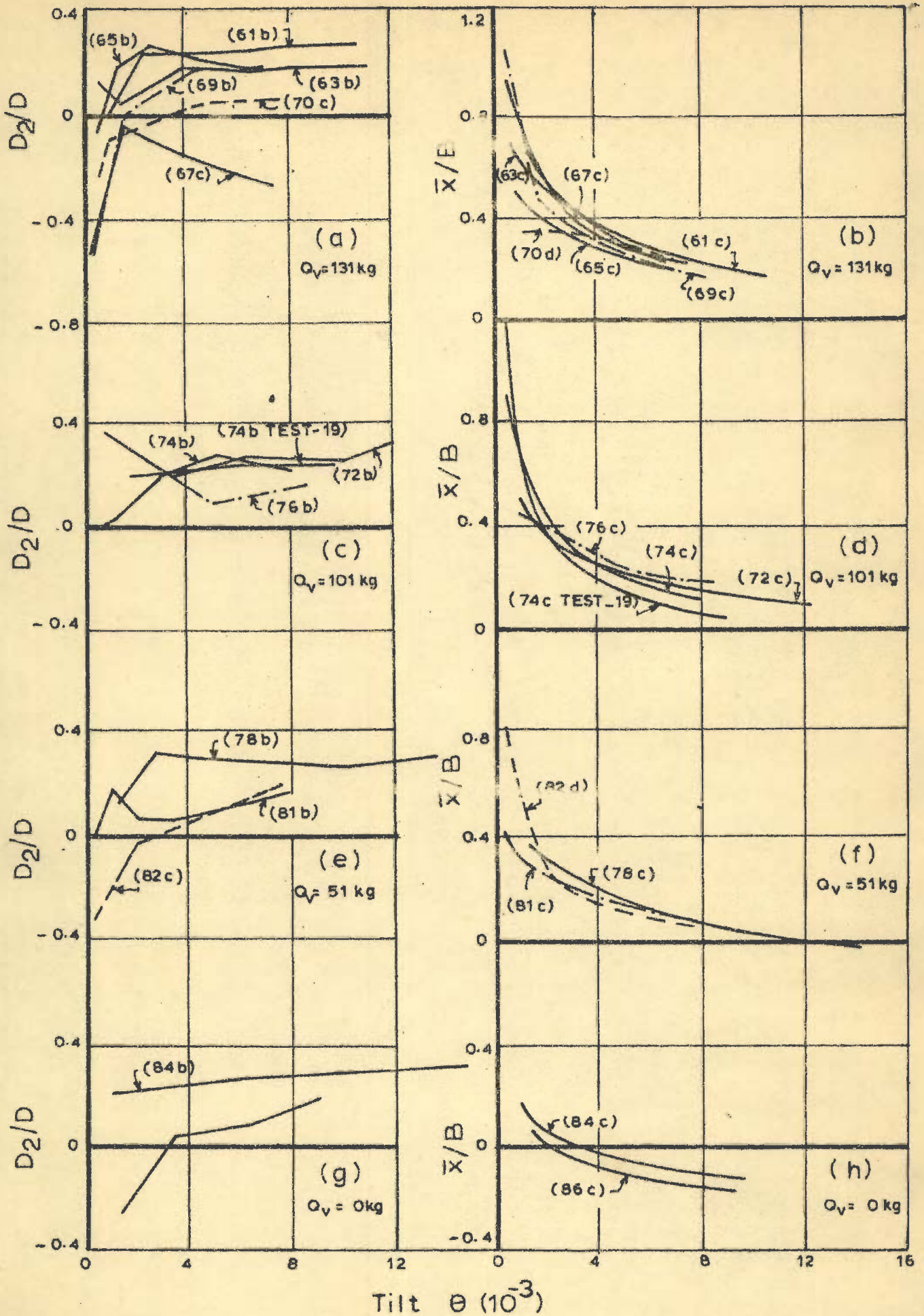
FIG. 134 _ INSTANTANEOUS POINTS OF ROTATION FOR 15cm
WELL WITH D = 30cm (Test no. 11 to 28)
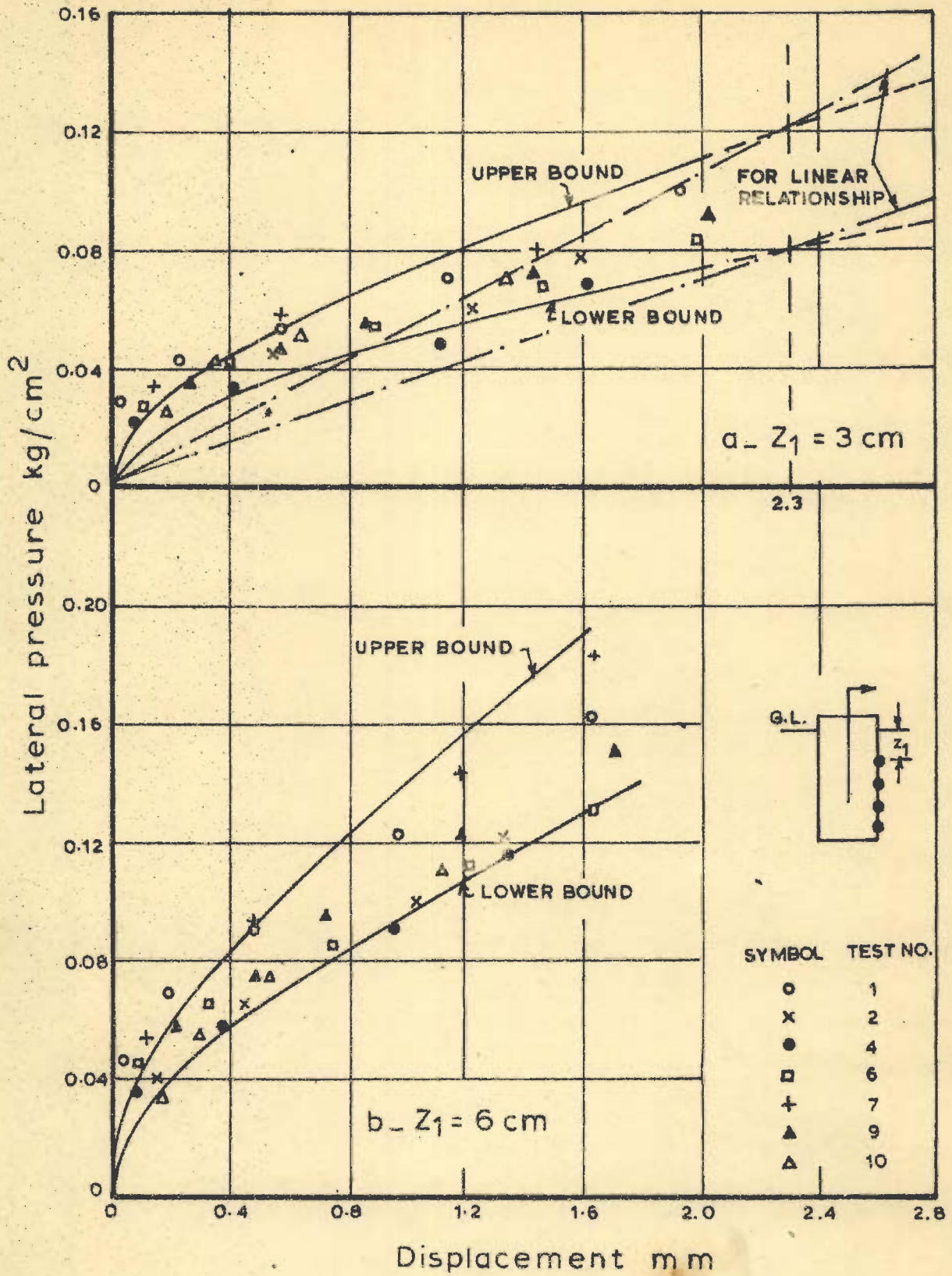
FIG. 135 _ p VS y PLOTS FROM LATERAL PRESSURE
DIAGRAMS (Test no. 1 to 10)

a _ p vs y PLOTS FROM LATRAL PRESSURE DIAGRAM (TEST NO. 1 to 10)

b_ k_h vs z_1 PLOTS FROM FIG. 137a ,b AND 138 a
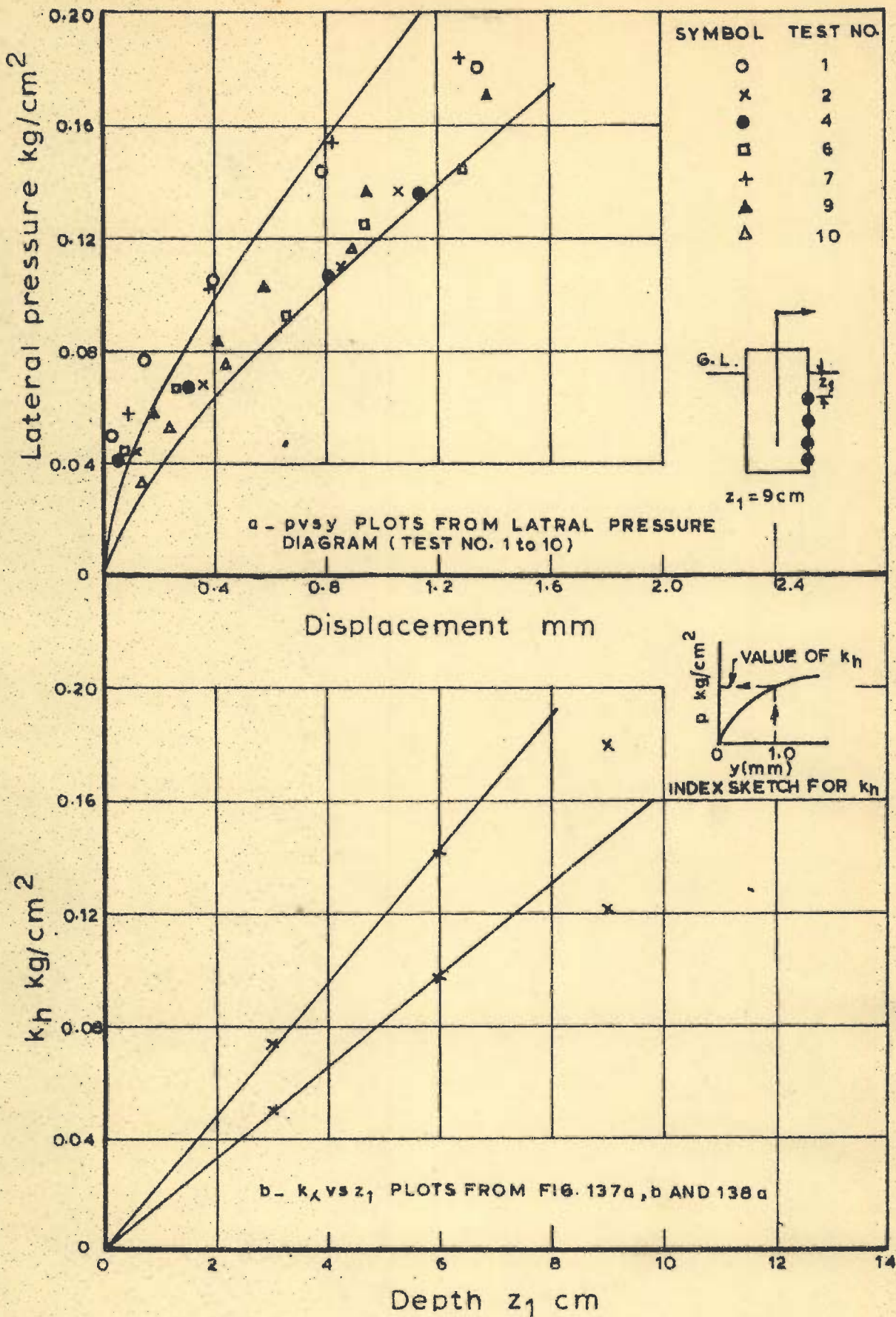
FIG. 136 _ p VS y AND k_h vs z PLOTS (Test no. 1 to 10)
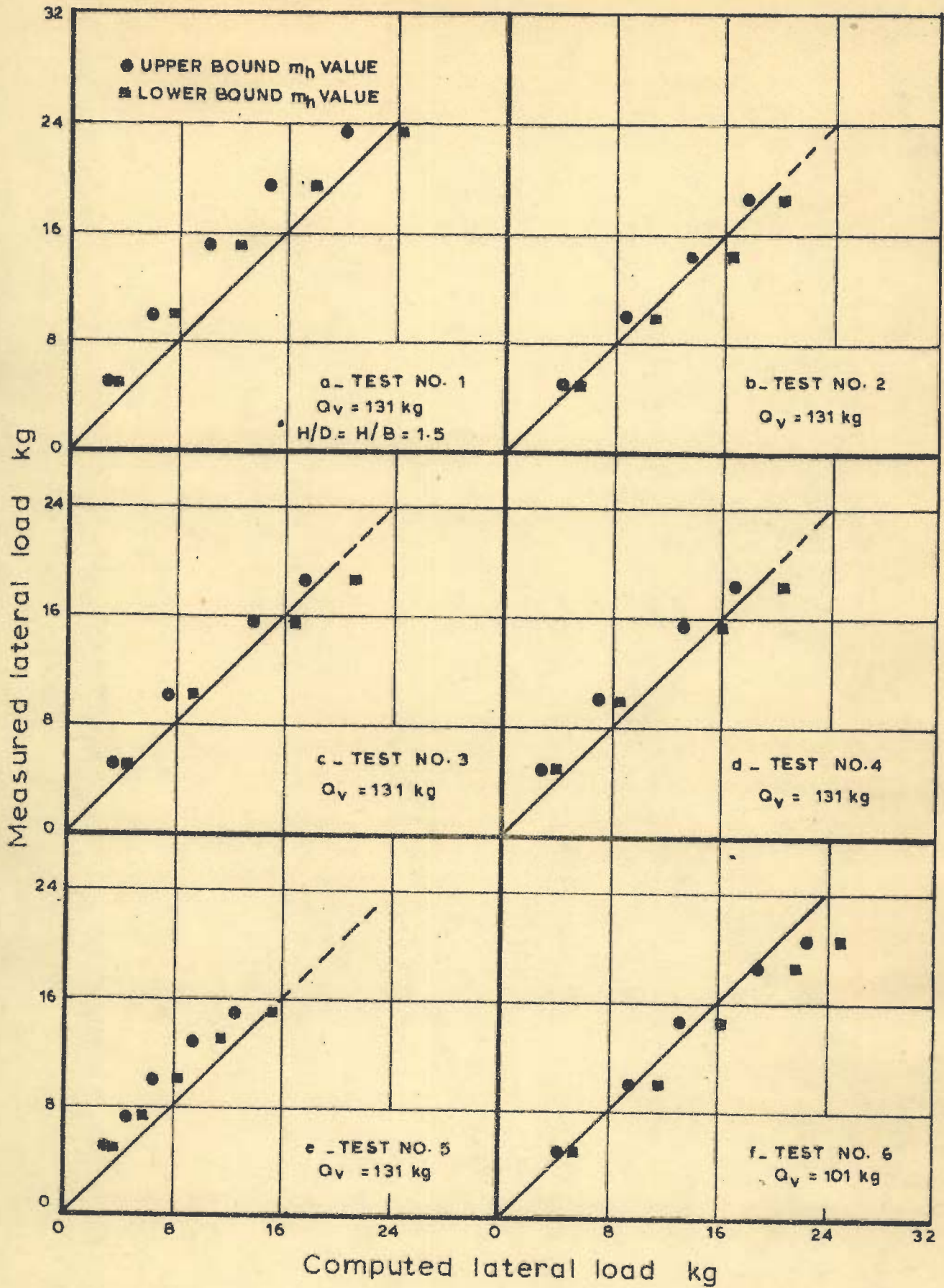
FIG. 137 _ MEASURED AND COMPUTED LATERAL LOADS
(Test no. 1 to 6)
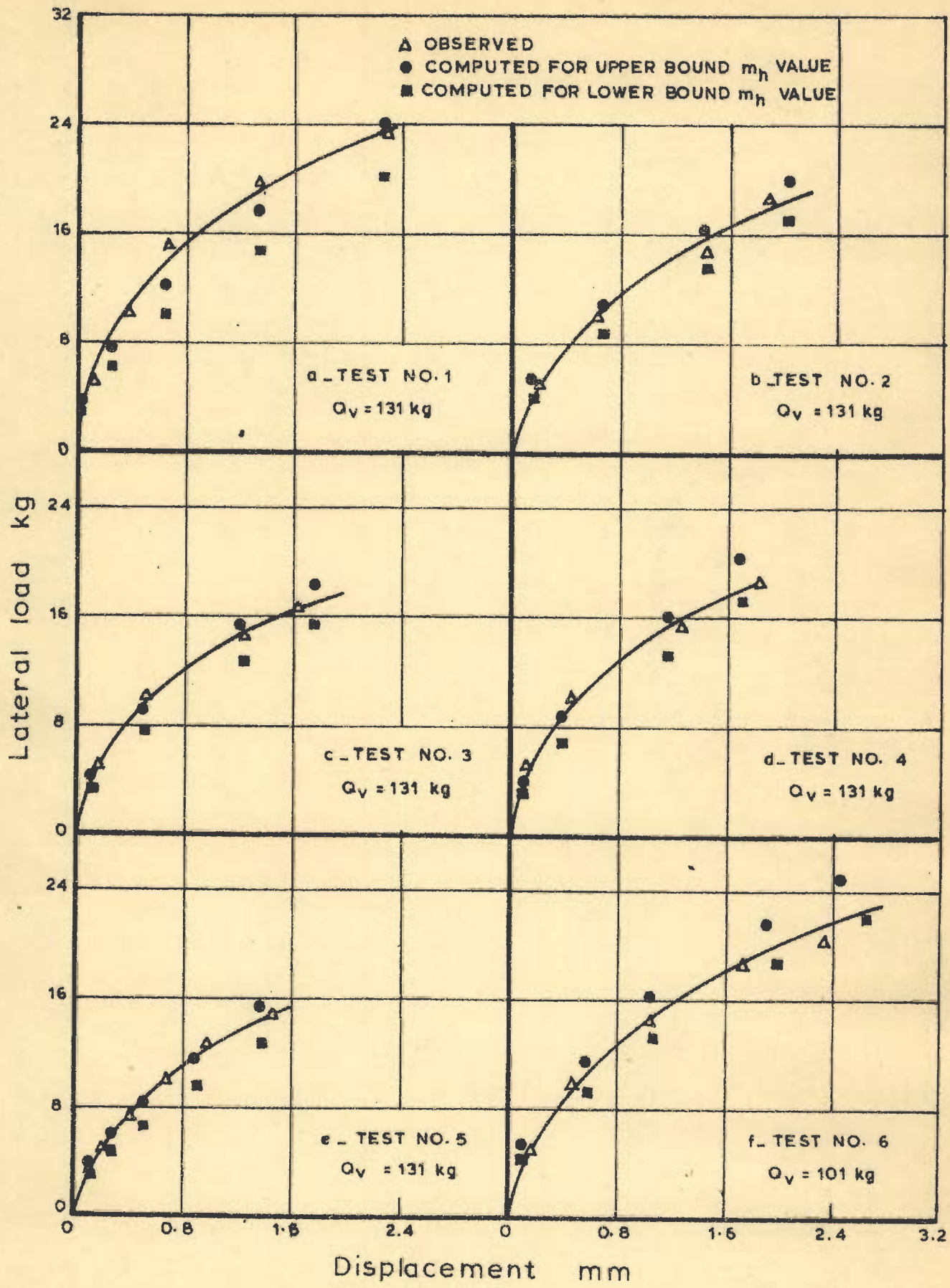
FIG. 138 _ MEASURED AND COMPUTED LATERAL LOAD VS
DISPLACEMENTS AT GROUND LEVEL
(Test no. 1 to 6)
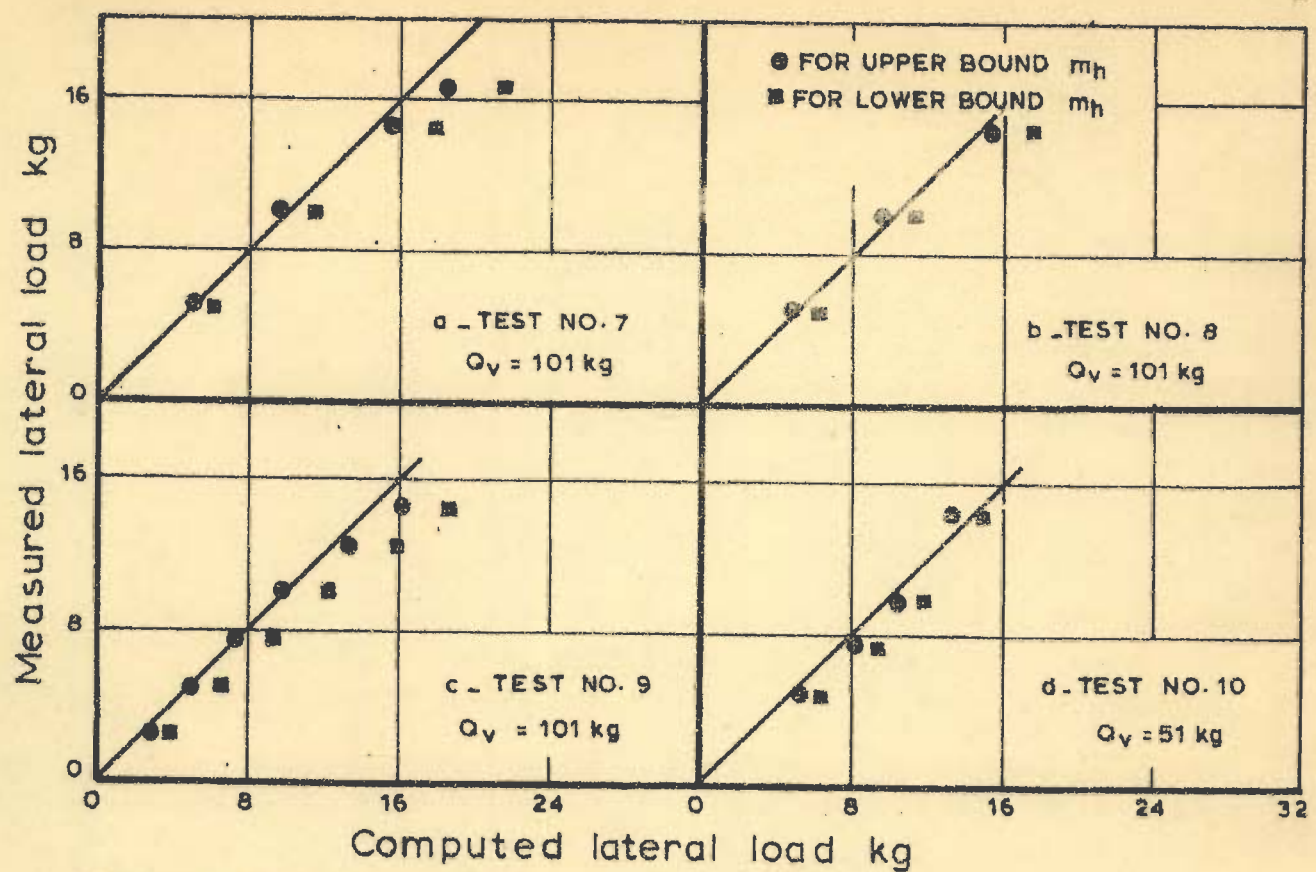
FIG.139_ MEASURED AND COMPUTED LATERAL LOADS
(Test no. 7 to 10)
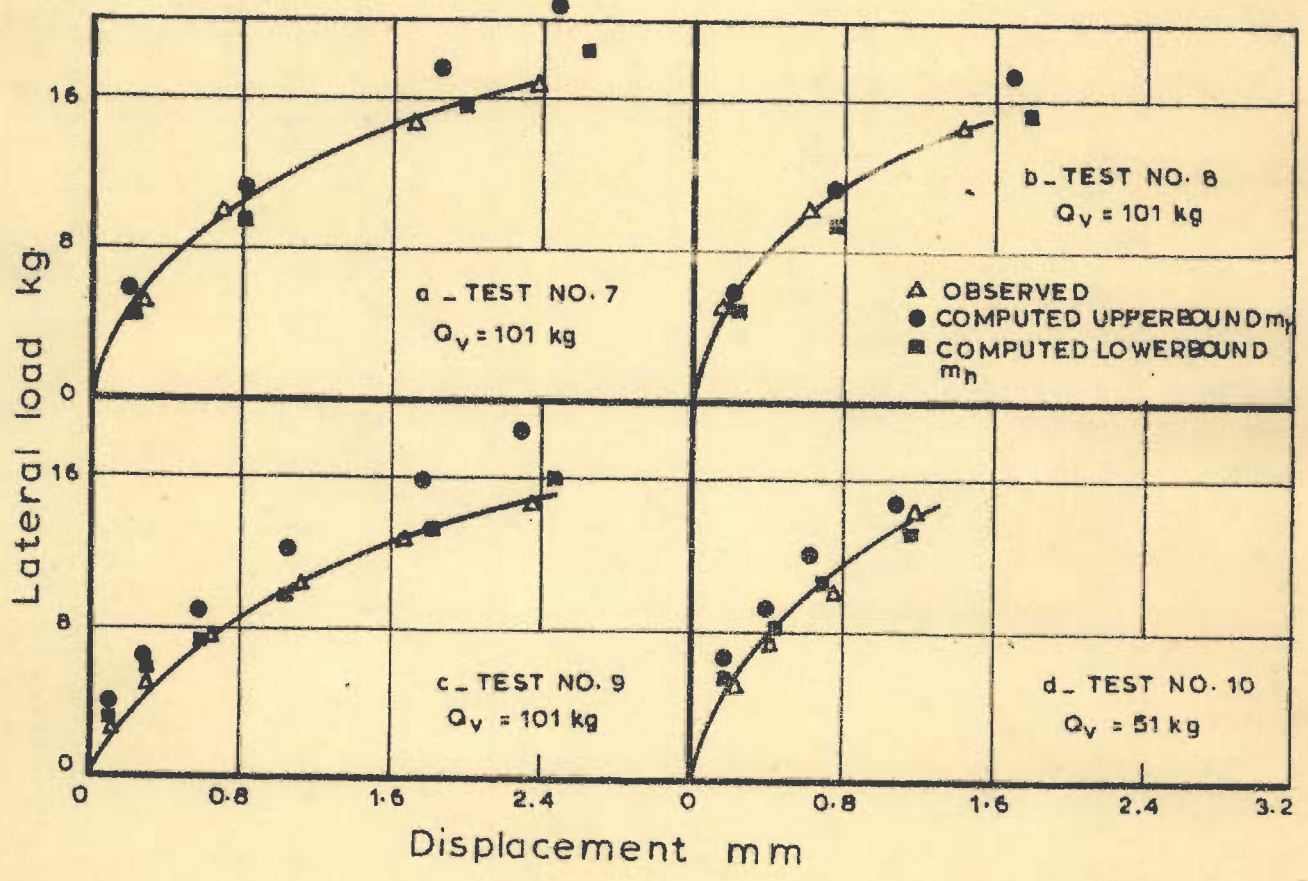
FIG. 140 _ MEASURED AND COMPUTED LATERAL LOAD
VS DISPLACEMENT AT GROUND LEVEL
(Test no. 7 to 10)
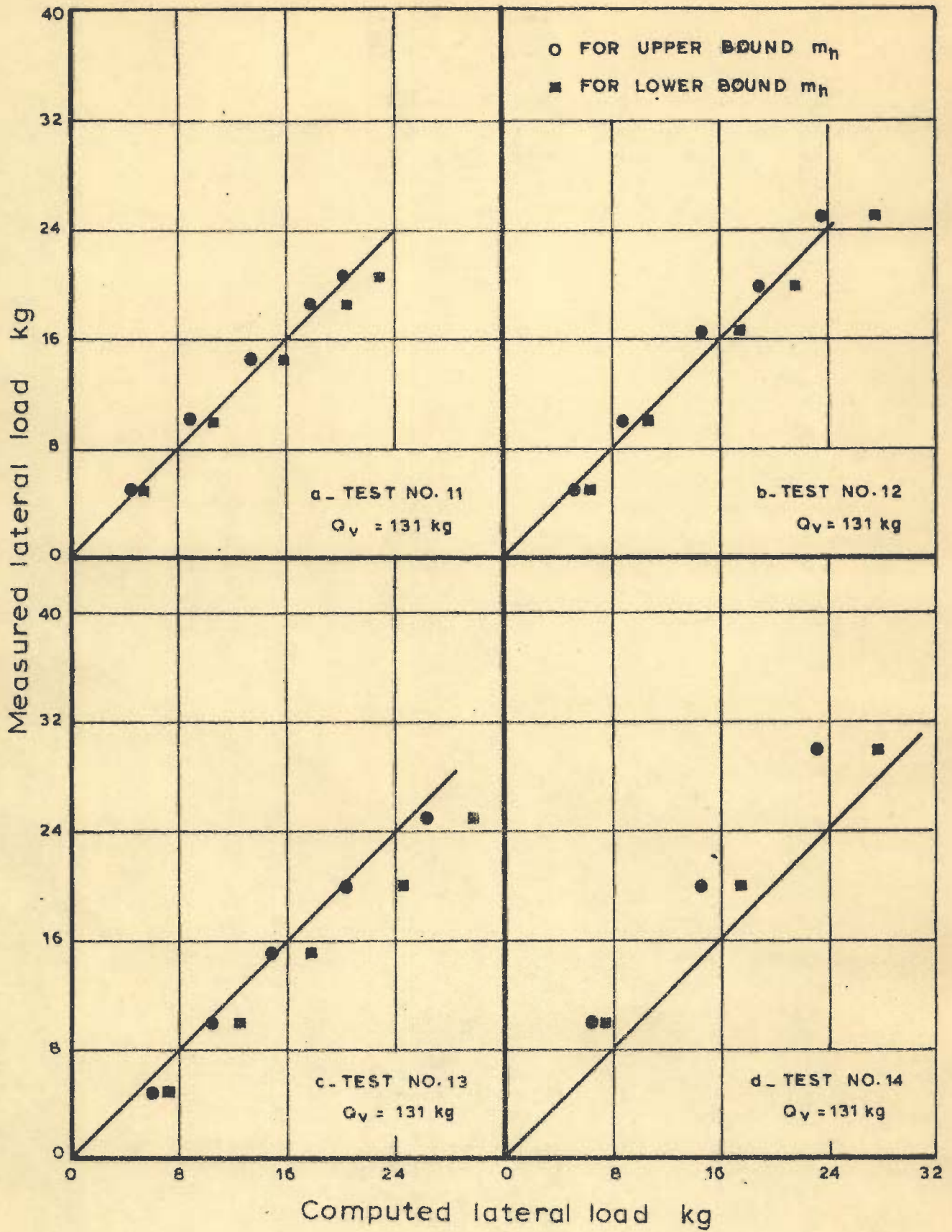
FIG. 141 _ MEASURED AND COMPUTED LATERAL LOADS
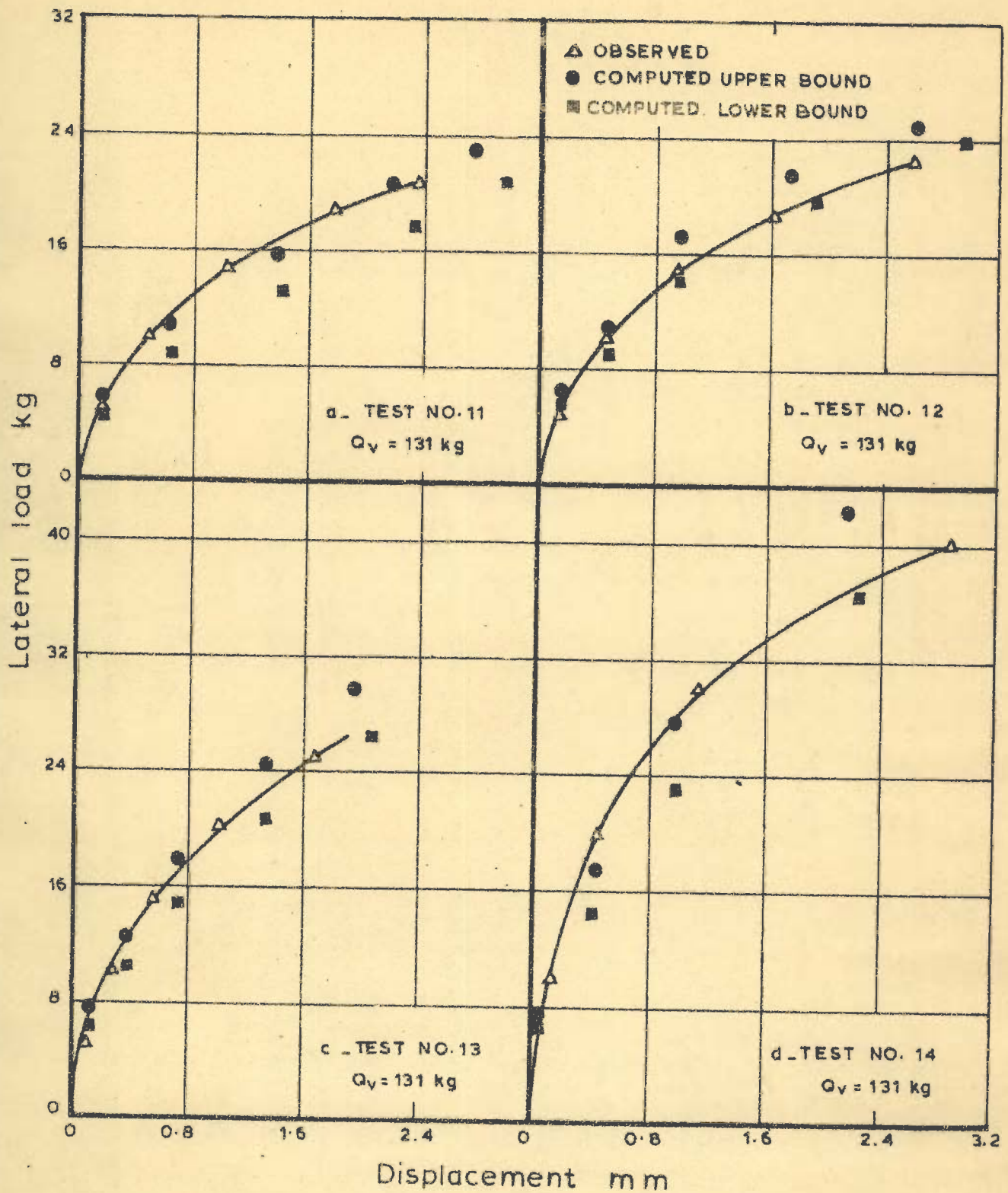(Test no. 11 to 13)

FIG.142 _ MEASURED AND COMPUTED LATERAL LOAD VS DISPLACEMENT AT GROUND LEVEL (Test no 11 to 14)
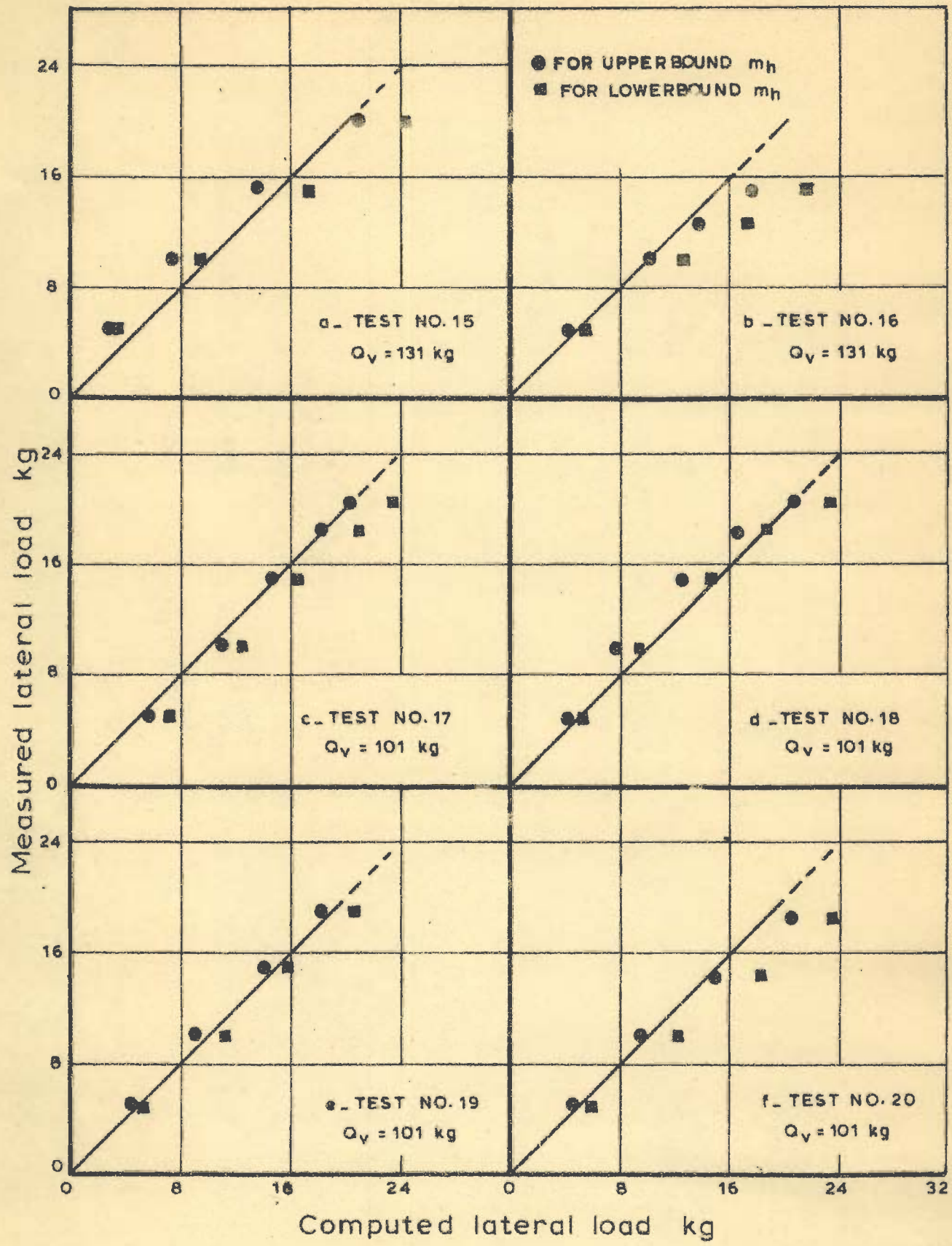
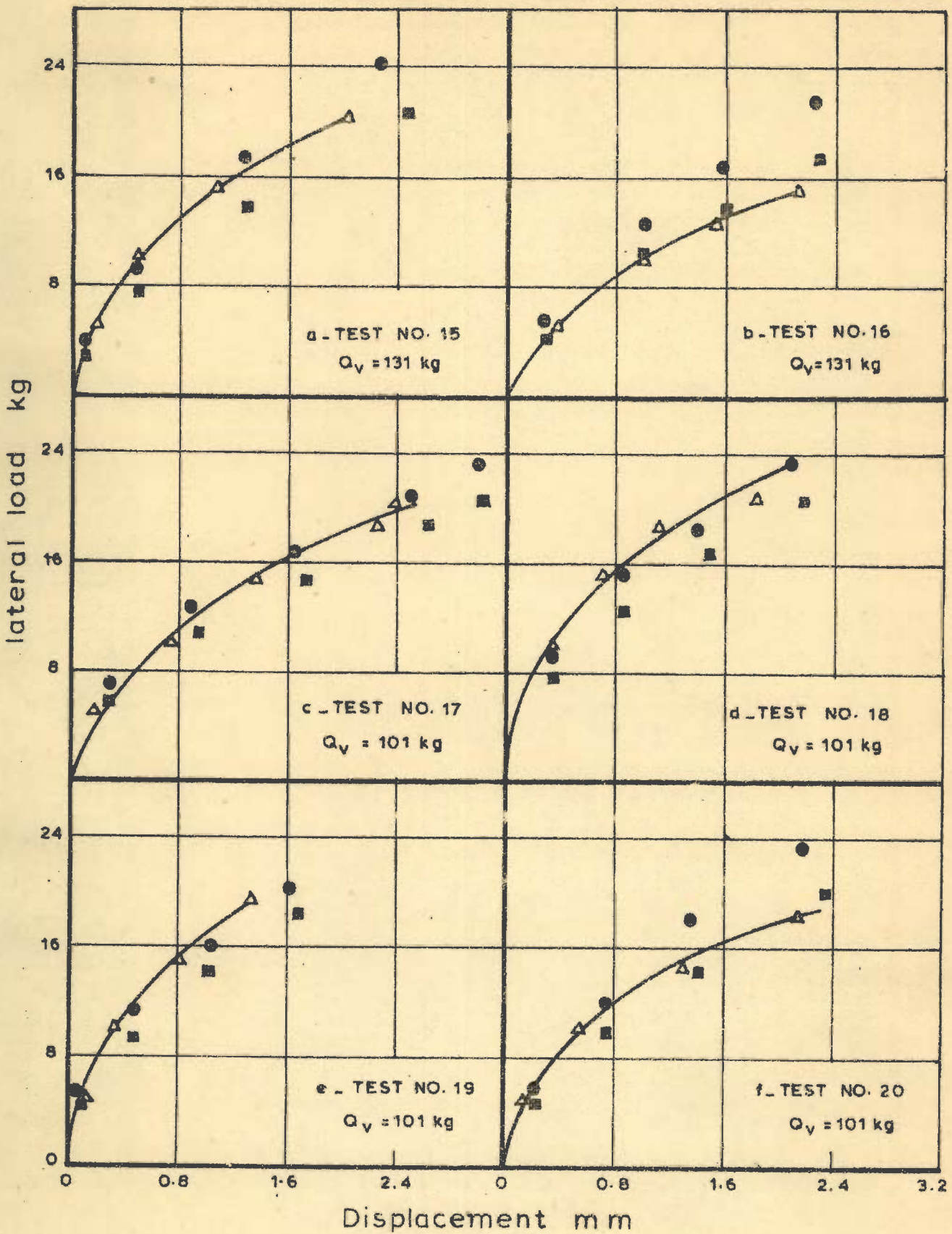FIG. 143 _ MEASURED AND COMPUTED LATERAL LOADS
(Test no. 15 to 20)

FIG. 144_ MEASURED AND COMPUTED LATERAL LOAD VS
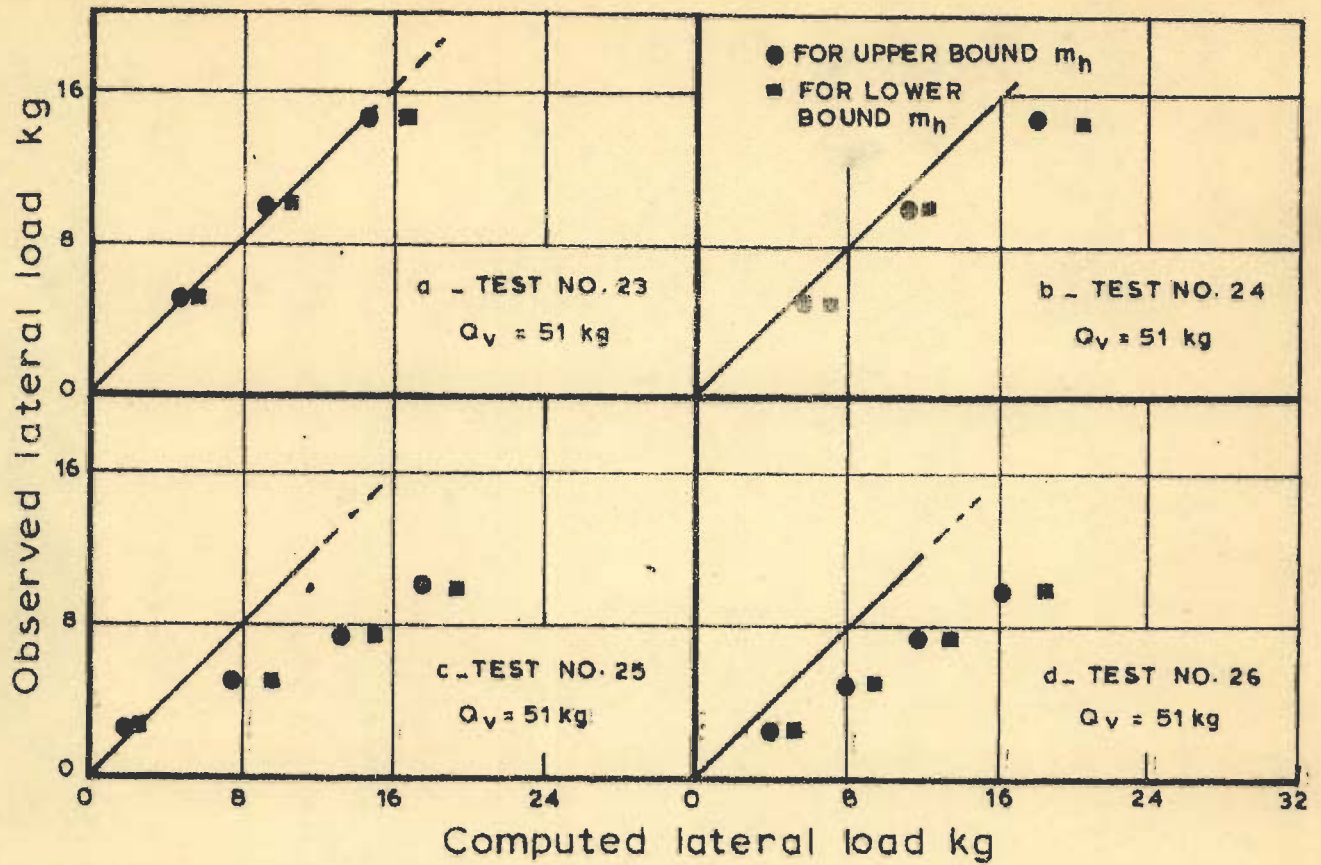DISPLACEMENT AT GROUND LEVEL(Test no.15 to 20)

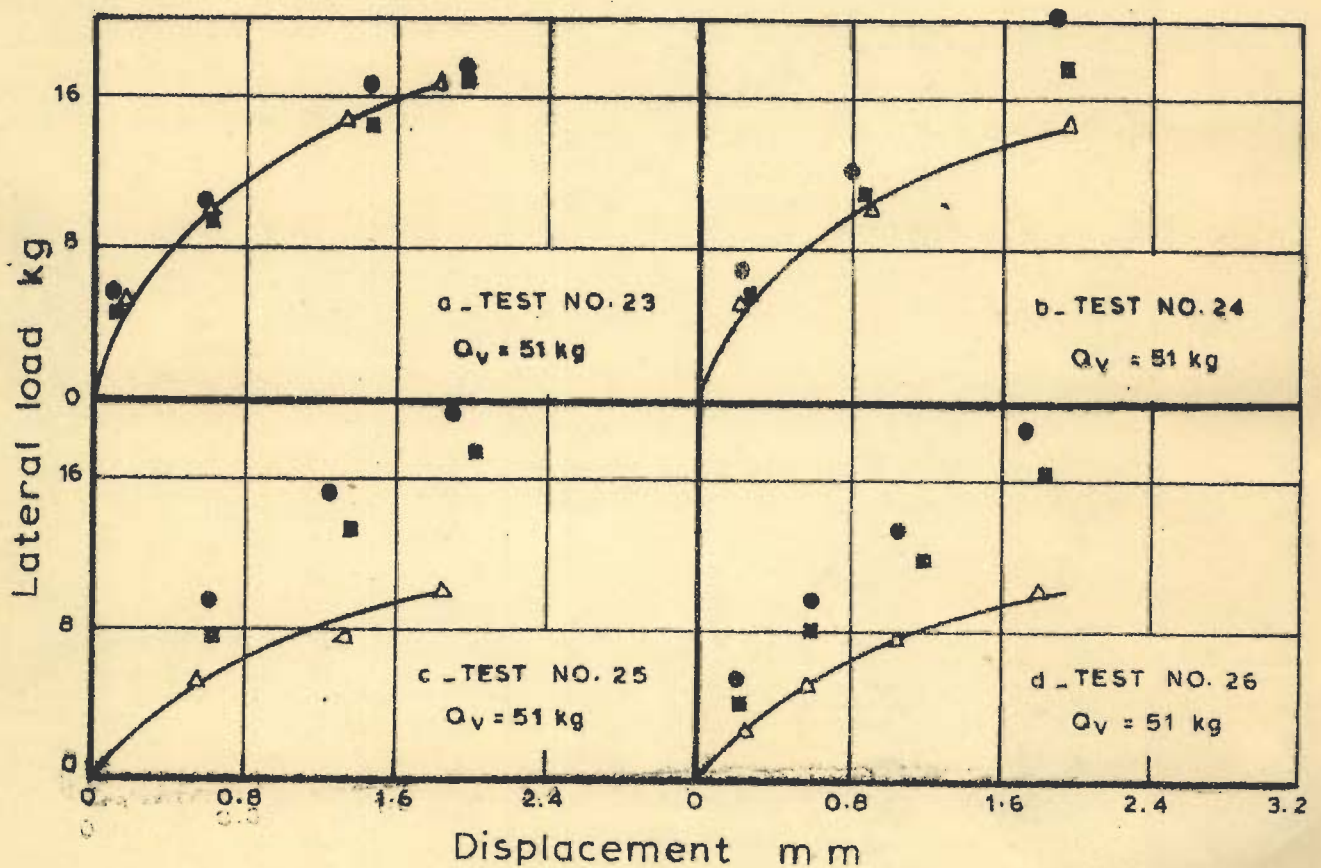FIG. 145 _ MEASURED AND COMPUTED LATERAL LOADS
(Test no. 23 to 26)

FIG. 146 _ MEASURED AND COMPUTED LATERAL LOAD VS
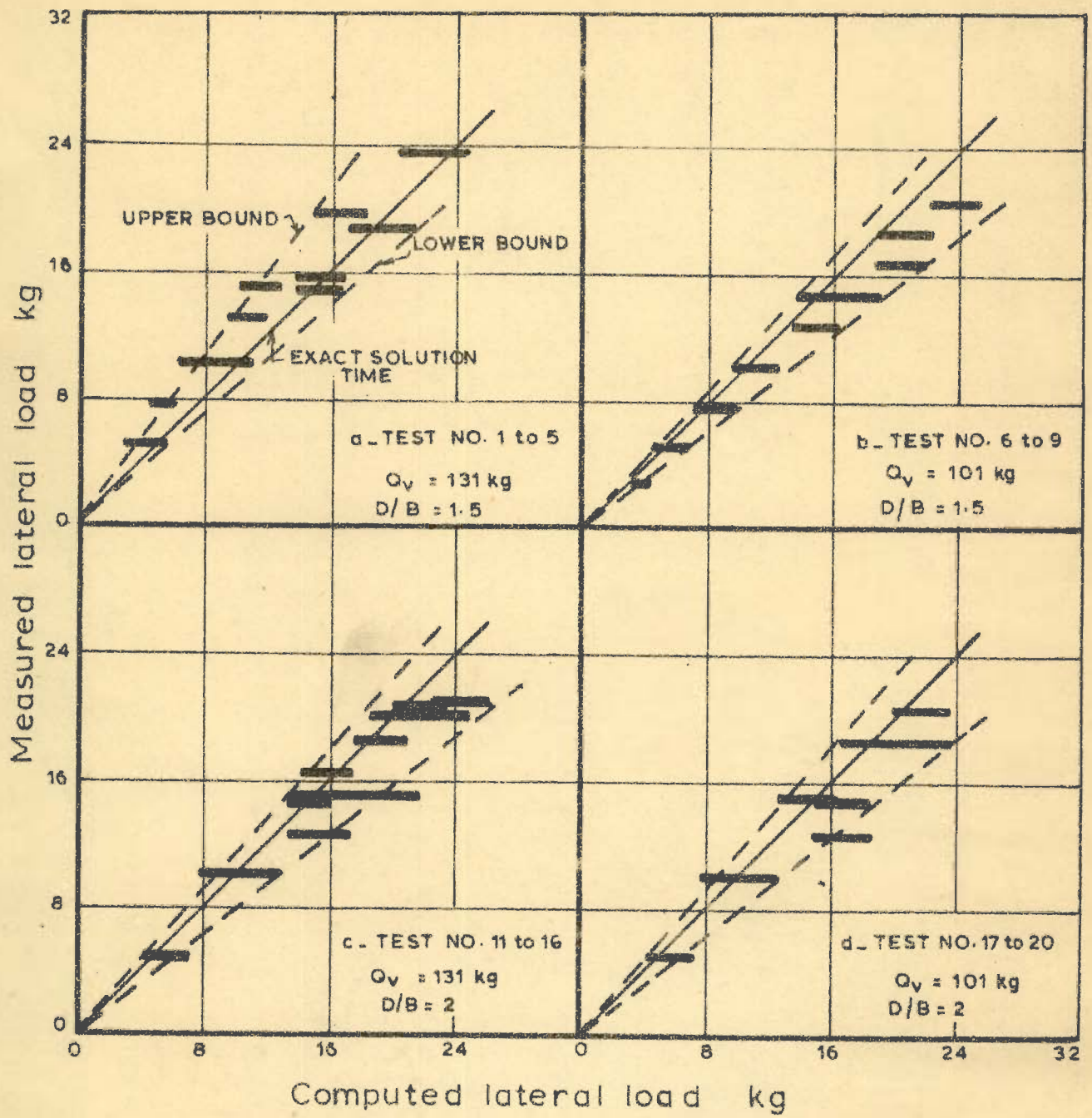DISPLACEMENT AT GROUND LEVEL (Test no. 23 to 26)

FIG. 147_ GENERAL TREND OF MEASURED VS COMPUTED LATERAL LOADS
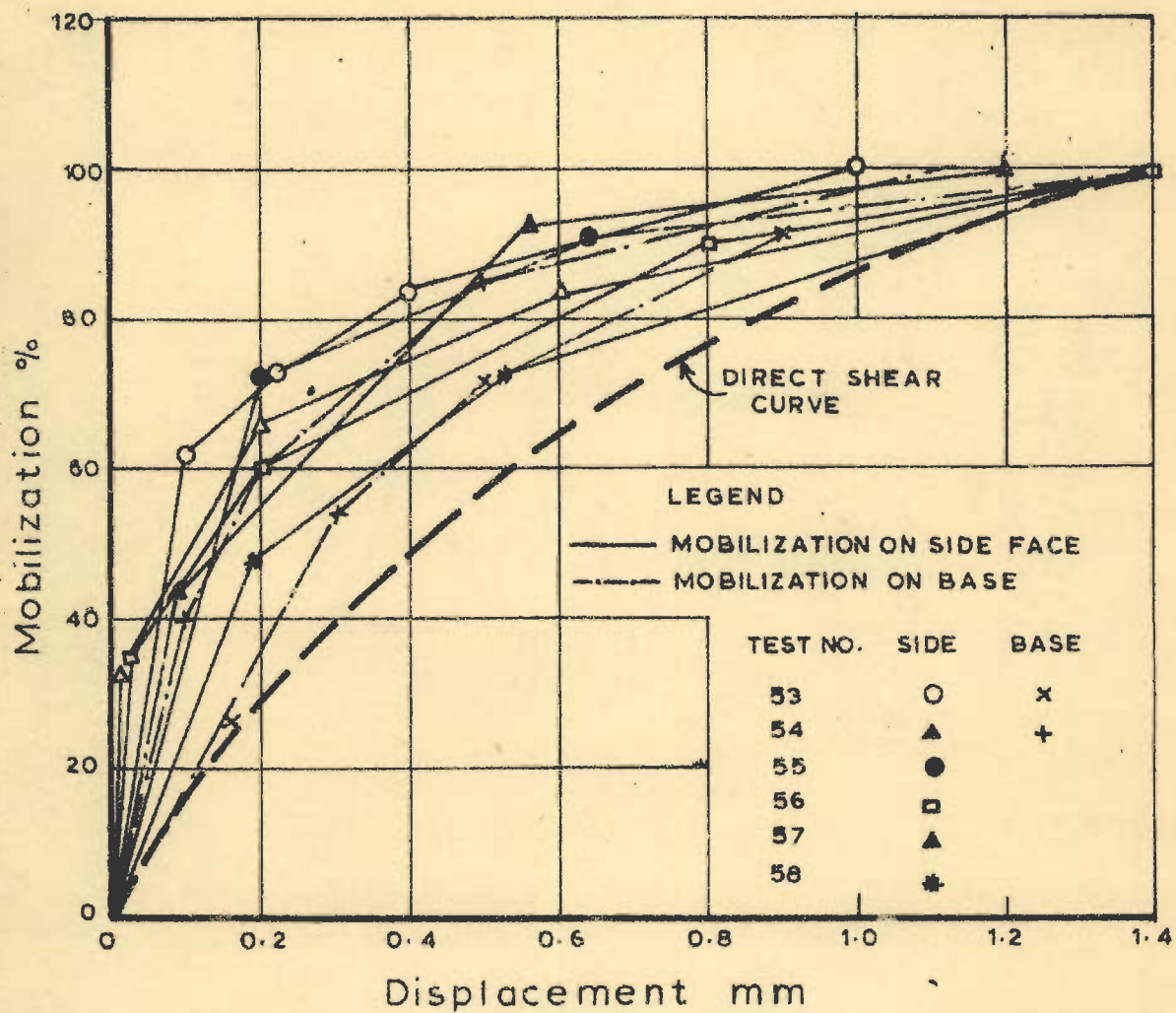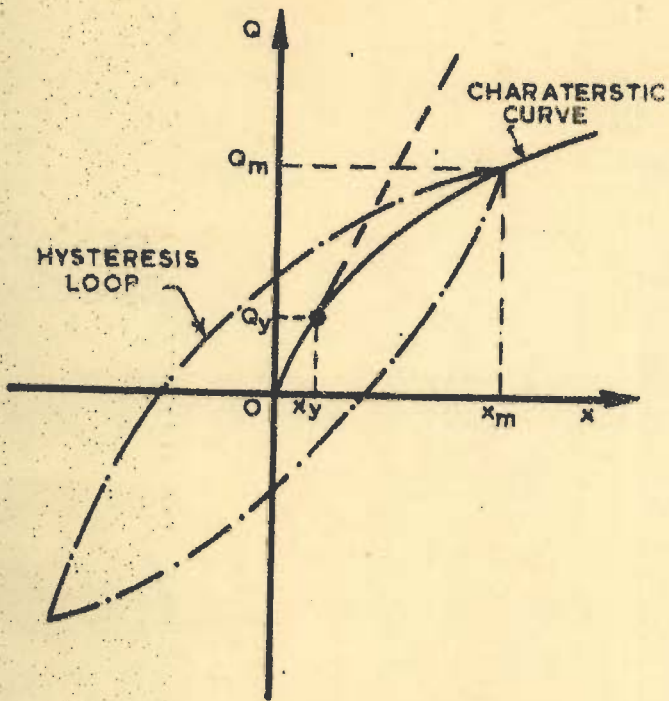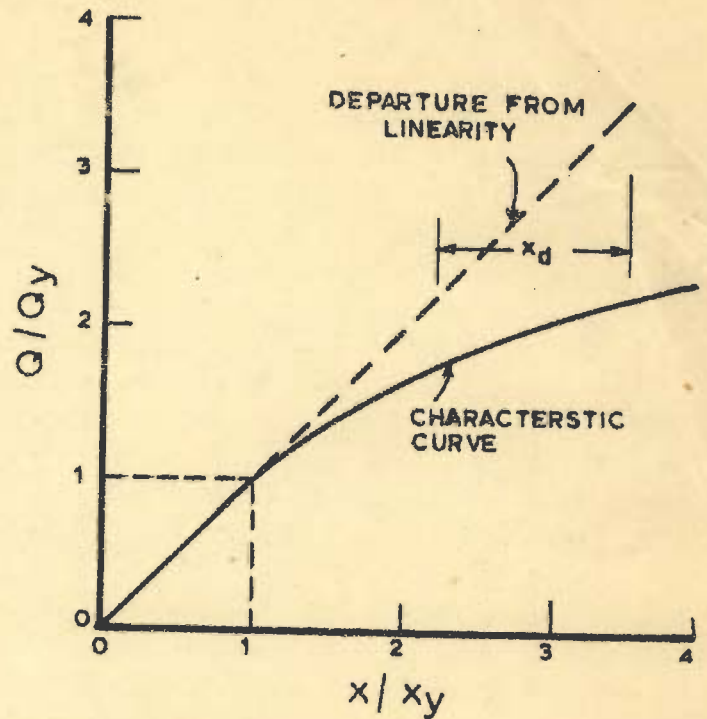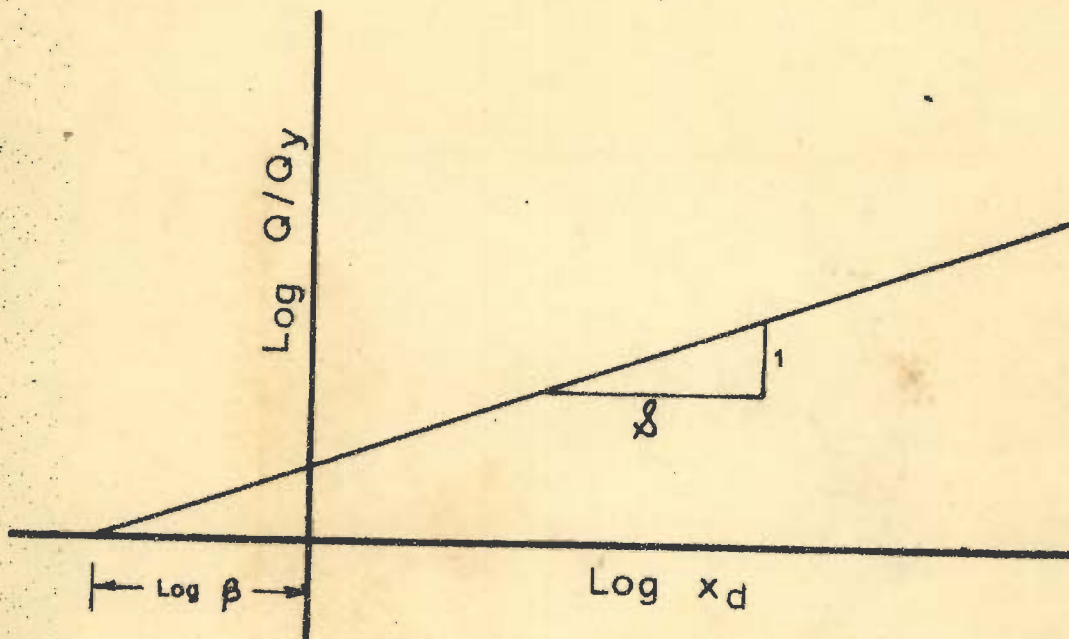
FIG. 148_ MOBILIZATION OF FRICTION IN 20 cm WELL
MODEL (Test no 53 to 58)

a _ A hysteretic system

b _ Departure from linearity

c _ Plot of Q/Qy vs departure

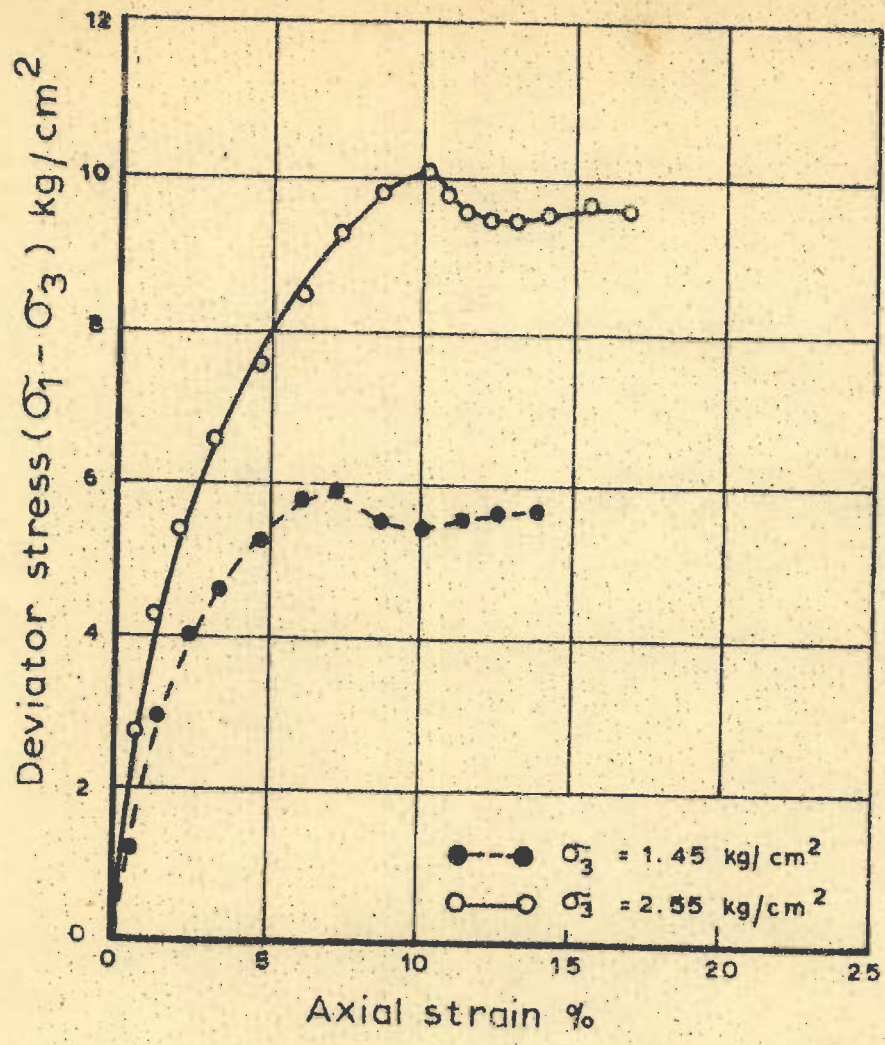FIG. 149 _ METHOD OF FINDING β AND δ OF A HYSTERETIC SYSTEM

FIG. I-A _ TRIAXIAL STRESS STRAIN CURVE
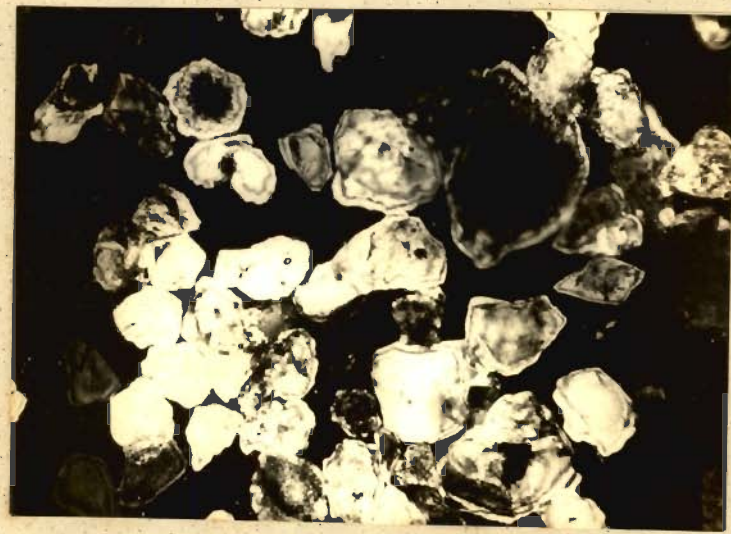RANIPUR-SAND

FIG. I- B _ GRAIN SHAPE AND SIZE RAINPUR
SAND
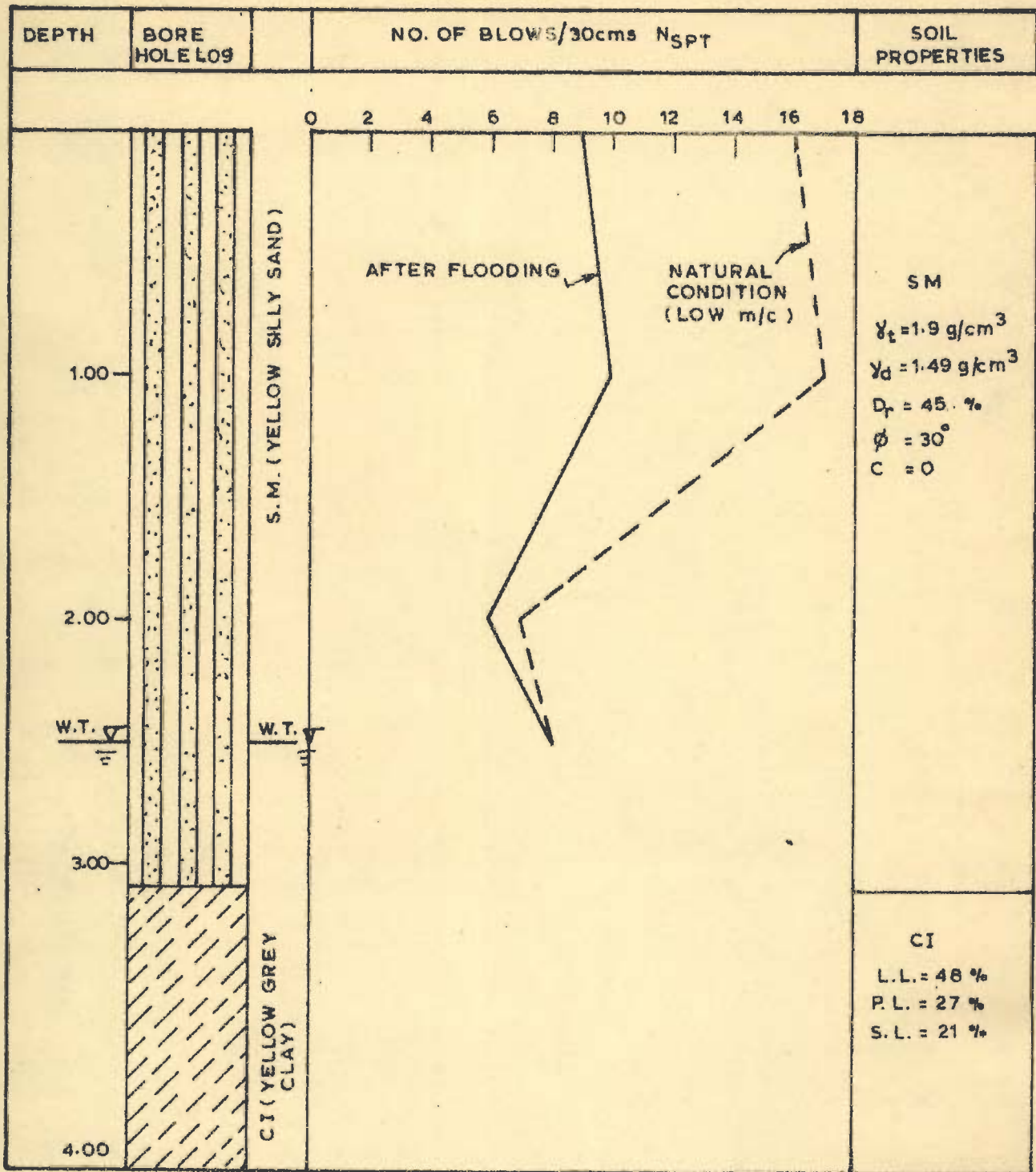
FIG. I-C _ SOIL EXPLORATION DATA FIELD TEST SITE

APPENDIX I

EXAMPLE OF COMPUTATION OF LATERAL LOAD

Data of Test No. 6, Table 4 p.171 and Figs 53 a,b and c has been used

The available data is

From Table 4, p. 171.

$$B = 15 \text{ cm}, \quad L = 15 \text{ cm}, \quad D = 22.5 \text{ cm}, \quad H = 33.75 \text{ cm},$$

$$Q_v = 101 \text{ kg}, \quad W = 6.5 \text{ kg} \text{ and } \gamma = 1.658 \text{ g/cm}^3$$

From p. 189

$$Q_s = 21 \text{ kg}$$

From p. 189

$$K_o = 1.265$$

From p.129

$$\mu_1 = 0.66, \quad \mu_2 = 0.66$$

From p. 125

$$m_h \text{ (lower bound)} = 0.0568, \text{ kg-cm units}$$

and m_h (upper bound) = 0.0781, kg-cm units

From p. 125

$$r = 0.55, \quad n = 1 \text{ and from p. 131, } r' = 1$$

From Fig. 53b, p. 230

$$\Delta_i = 57 \times 10^{-3} \text{ cm for } Q_v = 101 \text{ kg}$$

Observed values of θ, $\bar{x}$ and D_2 for various levels of lateral loads Q given below are from Figs. 53a, b and c. Procedure for computing lateral loads for observation number 4 only will be explained step by step since this includes both

Observation No.	Q (kg)	θ 10^{-3} rad.	$\bar{x}$ (cm)	D_2 (cm)
1	5	0.529	0.82B	-0.466D
2	10	2.59	0.475B	-0.178D
3	14.5	4.89	0.317B	0.045D
4	18.5	8.90	0.18B	0.129D
5	20.5	11.71	0.113B	0.111D

the situations of base friction of $\alpha < 1$ and $\alpha = 1$.

Step 1

Let $D_2 = 0$

Step 2 : Calculating R_B from Eqn. 24

From Eqn. 24, we get

$$R_B = W_B - (F_1 \pm F_2 + 2F_3) \qquad \ldots (24a)$$

(i)   Evaluation of W_B

Substituting $Q_v = 101$ kg and $W = 6.5$ kg, in Eqn. 3

$$W_B = Q_v + W \qquad \ldots (3)$$

We get $W_B = 107.5$ kg

(ii)   Evaluation of F_1

Substituting $\mu_1 = 0.66$, $L = 15$ cm, $\theta = 8.90 \times 10^{-3}$ rad.
$D = 22.5$ cm, $r = 0.55$, $n = 1$, and $D_1 = D - D_2 = 22.5$ cm and
the lower bound $m_h = 0.0568$ kg-cm units, in Eqn. 7.

We get $F_1 = 29.72$ kg

Similarly $F_1 = 40.87$ kg for upper bound
m_h of 0.0781 kg cm units.

(iii) Evaluation of F_2

In Eqn. 11,

$$N_2 = \int_o^{D_2/D_1} (1+\psi)^n \psi^r \, d\psi$$

as $D_2 = 0$, therefore N_2 will be zero

and so, $F_2 = 0$ for both m_h values

(iv) Evaluation of F_3

Substituting $\mu_1 = 0.66$, $K_o = 1.265$, $\gamma = 1.658$ g/cm³,

$B = 15$ cm and $D = 22.5$ cm in Eqn. 13.

We get $F_3 = 10.5$ kg

(v) Evaluation of R_B

Calculating the value of R_B by substituting values of F_1, F_2 and F_3, in Eqn. 24a, we get

$$R_B = 67.28 \text{ kg for } m_h = 0.0568 \text{ (lower bound)}$$

and $\quad R_B = 56.13$ kg for $m_h = 0.0781$ (upper bound)

Step 3 : Computing k_v from Eqn. 20

From Eqn. 20, we have

$$k_v = R_B \div \frac{B.L}{6} \left[(\Delta_i + x_1\theta)^{r'} + 4(\Delta_i + \bar{x}\theta)^{r'} + (\Delta_i + x_2\theta)^{r'} \right] \quad \ldots (20a)$$

Substituting, $R_B = 67.28$ kg (for $m_h = 0.0568$, , lower bound)

$B = L = 15$ cm $\qquad \Delta_i = 57 \times 10^{-3}$ cm $\qquad$, $r' = 1$

$\bar{x} = 0.18 \times B = 2.7$ cm $\qquad \bar{x}_1 = \bar{x} + B/2 = 10.2$ cm

$x_2 = \bar{x} - B/2 = -4.8$ cm $\qquad \theta = 8.90 \times 10^{-3}$ radians $\qquad$, in the

above equation.

we get $k_v = 3.69$ kg/cm³ (for $m_h = 0.0568$, lower bound)

Hence modified, $k_v = k_v' = 2.3 \times 3.69$

$$= 8.48 \text{ kg/cm}^3$$

Similarly $k_v' = 7.08$ kg/cm³ for ($m_h = 0.0781$, upper bound)

Step 4 : Computing the value of Q from Eqn. 26

From Eqn. 25, we have

$$F_B = (P_1 - P_2 + 2F_4 - 2F_5) - Q \qquad \dots (25a)$$

Substituting first $M_{FB} = F_B \cdot D$ and $M_o = Q.H$ in Eqn. 26 and next substituting the value of F_B from Eqn. 25a,
We get

$$Q = -M_{P1} + M_{P2} + M_{F1} \mp M_{F2} - 2M_{F4} + 2M_{F5}$$

$$+ M_{RB} + (P_1 - P_2 + 2F_4 - 2F_5).D \div (H+D) \qquad \dots (26a)$$

Evaluation of P_1, M_{P1}

Substituting $L = 15$ cm, m_h (Lower Bound)

$\theta = 8.9 \times 10^{-3}$ rad., $D_1 = D = 22.5$ cm, $n = 1$, $r = 0.55$
in Eqn. 5c, we get

$P_1 = 61.92$ kg

and from Eqn. 6b, $M_{P1} = 570.90$ kg-cm, for m_h (lower bound),

also, $P_1 = 60.36$ kg

Similarly, $M_{P1} = 784.90$ kg-cm, for m_h (upper bound)

Evaluation of P_2 and M_{P2}

Value of P_2 and M_{P2} will be zero in both the cases since the the quantity H_2 and N_3 in Eqns 9b and 10b respectively will be zero for $D_2 = 0$.

Evaluation of F_1 and M_{F1}

Substituting $B = 15$ cm and $F_1 = 29.72$ kg from step 2, in Eqn. 8

$\qquad M_{F1} = 222.93$ kg-cm for m_h (lower bound),

also, $F_1 = 40.87$ kg,

and $\quad M_{F1} = 306.53$ kg-cm for m_h (upper bound)

Evaluation of F_2 and M_{F2}

$\qquad M_{F2}$ from Eqn. 12 in both the cases will be zero since F_2 is zero

Evaluation of F_4 and M_{F4}

Substituting, $\mu_1 = 0.65$, $K_o = 1.26$, $\gamma = 1.658$ g/cm^3,

$\qquad B = 15$ cm and $D_1 = D = 22.5$ cm in Eqn. 14 and 15 respectvely we get,

$\qquad F_4 = 10.50$ kg,

and, $\quad M_{F4} = 157.5$ in both the cases.

Evaluation of F_5 and M_{F5}

From Eqn. 17 the value of M_{F5} will be zero since $D_1 = D$ for $D_2 = 0$ and the quantity $(D^3 - D_1^3)$ will reduce to zero.

Evaluation of F_B and M_{FB}

Substituting $\mu_2 = 0.65$ and $R_B = 65.12$ kg f.. in Eqn. 22 we get

$\qquad F_B = 55.54$ kg.

Now substituting $D = 22.5$ cm and value of F_B in Eqn. 23 we get

$\qquad M_{FB} = 1249.6$ kg-cm. for lower bound m_h value

Similarly $F_B = 72.42$ kg

and $\quad M_{FB} = 1629.6$ kg-cm for upper bound m_h value

Evaluation of M_{RB}

Substituting modified value of $k_v = 8.48$ kg/cm^3,

B = L = 15 cm, $\Delta_i = 57 \times 10^{-3}$ cm, $x_1 = 10.2$ cm

and $x_2 = -4.8$ cm from Step 3, in Eqn. 21.

We get

$M_{RB} = 318.66$ kg.cm for lower bound m_h value

Similarly by substituting modified $k_v = 7.08$ kg/cm^3 for upper bound m_h value we get

$M_{RB} = 265.86$ kg.cm

Evaluation of Q

Finally, substituting the values of M_{P1}, M_{P2}, M_{F1}, M_{F2}, M_{F4}, M_{F5}, M_{RB}, P_1, P_2, F_4, F_5, D and H in the equation 26a for evaluating Q, we get

$Q = 18.89$ kg for lower bound m_h value

and $Q = 22.39$ kg for upper bound m_h value.

Step 5: Checking mobilization factor α

Substituting values of P_1, P_2, F_4, F_5, Q and F_B in the following Eqn.

$$\alpha = \frac{(P_1 - P_2 + 2F_4 - 2F_5) - Q}{F_B}$$

we get

$\alpha = 0.83$ for lower bound m_h values

and,

$\alpha = 1.35$ for upper bound m_h values.

It is clearly seen that for lower bound m_h value since $\alpha = 0.83$. The condition that $-1 < \alpha < 1$ is satisfied hence Q = 18.89 kg

is the required value of lateral load.

However we see that for upper bound m_h value $\alpha = 1.35$. This violates the condition $-1 < \alpha < 1$. Hence $Q = 22.39$ for this case does not satisfy the physical condition at the base and so computations shall have to be made again with $D_2 > 0$ for obtain a value of Q against $\alpha = 1$.

If now for the upper bound values of m_h computations for observation No. 4 are made again step by step by taking different values of $D_2 > 0$, the following values will be obtained:

Assumed D_2 (cm)	....Computed Q (kg)	α
0.225	22.22	1.27
0.45	22.06	1.20
1.15		0.97

It is seen from the above table that α changes its value from 1.20 to 0.97 in the last two computations since $\alpha = 1$ lies between these two values the required Q will also lie between $Q = 22.06$ kg and 21.61 kg. The value of D_2 will also lies between 0.45 cm and 1.15cm. By linear interpolation

$$Q = 21.8 \text{ kg and } D_2 = 0.845 \text{ cm}$$

for $\alpha = 1$ which are the required values of Q and D_2 for $\theta = 8.9 \times 10^{-3}$ rad. for upper bound m_h values.

V I T A

Name
: SATISH CHANDRA SHARDA

Born
: 25th January, 1938, at Gwalior (Madhya Pradesh), India

Education
: Husband Memorial High School, AJMER, Rajasthan 1946-1952

Goverment College, AJMER, Rajasthan - 1952-1954

Indian Institute of Technology, KHARAGPUR, West Bengal - 1954-1958

University of Roorkee, Roorkee, Uttar Pradesh - 1960-1961

Degrees
: B. Tech. (Hons.), Civil Engineering - 1958

M.E. (Soils and Foundation), Civil Engineering- 1962

Experience
: Lecturer in Civil Engineering, Ajmer Polytechnic, Ajmer, Rajasthan - Sept., 1958-Aug. 1960

Assistant Engineer, Design and Planning, Rana Pratap Sagar, Kota Dams, Chambal Project, Kota, Rajasthan - Oct., 1961- Aug. 1964

Lecturer in Civil/Structural Engineering, Malviya Regional Engineering College, Jaipur, Rajasthan- Aug. 1964 - March 1967

Reader in Structural Engineering, Malviya Regional Engineering College, Jaipur, Rajasthan, April 1967 onwards

Professional Societies Membership
: 1. Indian Geotechnical Society, India

2. Indian Society of Earthquake Technology, India

Publications
: 1. Sharda, S.C., (1962), "Shearing Strentth of Cohesive Soil Due to Pore Pressure Dissipation", Earth and Rockfill Dams Symposium, Roorkee, India.

2. Sharda, S.C., (1965), "An Account of Chambal Valley Development Scheme Rajasthan", M.R. Engg. College Magazine, Jaipur, Rajasthan.

3. Sharda, S.C., (1968), "Harnessing the River Bias", M.R. Engg. College Magazine, Jaipur, Rajasthan.

4. Sharda, S.C., (1969), "Sampling and Testing of Soils", Institution of Engrs, Rajasthan Centre, Jaipur, Rajasthan.

5. Sharda, S.C., (1970), "Creep in Soils", M.R. Engg. College Magazine, Jaipur, Rajasthan.

6. Arya, A.S., and Sharda, S.C., (1974), "Lateral Load Resistance of Well Foundations" Bridge and Structural Engineer, Vol. 4, No. 3, Sept. 1974

7. Discussions in ASCE and I.N.S.SMFE (India)

Conferences and Seminars Attended

1. First Asian Regional Conference on Soil Mechanics and Foundation Engineering, New Delhi - India - 1961

2. Symposium on Earth and Rockfull Dams- Indian National Society of Soil Mechanics and Foundation Engineering, Talwara, Punjab, India - 1968

3. Forty-Ninth Annual Session- Institution of Engineers India, Jaipur, Rajasthan - 1969

4. Summer School in Rock Mechanics at Kuru- kshetra - 1970

5. Fourth Symposium on Earthquake Engineering, Roorkee, India - 1970

6. Symposium on Modern Trends in Civil Engineering, Roorkee, India - 1972

Field Experience

1. Design, Drawing, Estimating and Investigations of Masonry and Earth and Rockfill dams, and appertinance works including Power Houses, Tunnels etc. Rana Pratap Sagar and Kota Dams, Chambal Project Kota For three years.

2. Soil Investigation of sites for Civil Engineering Construction work at Jaipur.

Marital Status

Married to Uma in 1962
Archana - Daughter - 11 yrs
Apoorva - Son   - 4 yrs